JOURNAL OF RESEARCH

OF THE U.S. GEOLOGICAL SURVEY

SEPTEMBER–OCTOBER 1978
VOLUME 6, NUMBER 5

Scientific notes and summaries of investigations in geology, hydrology, and related fields

U.S. DEPARTMENT OF THE INTERIOR

UNITED STATES DEPARTMENT OF THE INTERIOR
CECIL D. ANDRUS, Secretary
GEOLOGICAL SURVEY
H. William Menard, Director

For sale by Superintendent of Documents, U.S. Government Printing Office, Washington, DC 20402. Annual subscription rate, $18.90 (plus $4.75 for foreign mailing). Make check or money order payable to Superintendent of Documents. Send all subscription inquiries and address changes to Superintendent of Documents at above address.

Purchase single copy ($3.15) from Branch of Distribution, U.S. Geological Survey, 1200 South Eads Street, Arlington, VA 22202. Make check or money order payable to U.S. Geological Survey.

Library of Congress Catalog-card No. 72-600241.

The Journal of Research is published every 2 months by the U.S. Geological Survey. It contains papers by members of the Geological Survey and their professional colleagues on geologic, hydrologic, topographic, and other scientific and technical subjects.

Correspondence and inquiries concerning the Journal (other than subscription inquiries and address changes) should be directed to Anna M. Orellana, Managing Editor, Journal of Research, Publications Division, U.S. Geological Survey, 321 National Center, Reston, VA 22092.

Papers for the Journal should be submitted through regular Division publication channels.

The Secretary of the Interior has determined that the publication of this periodical is necessary in the transaction of the public business required by law of this Department. Use of funds for printing this periodical has been approved by the Director of the Office of Management and Budget through June 30, 1980.

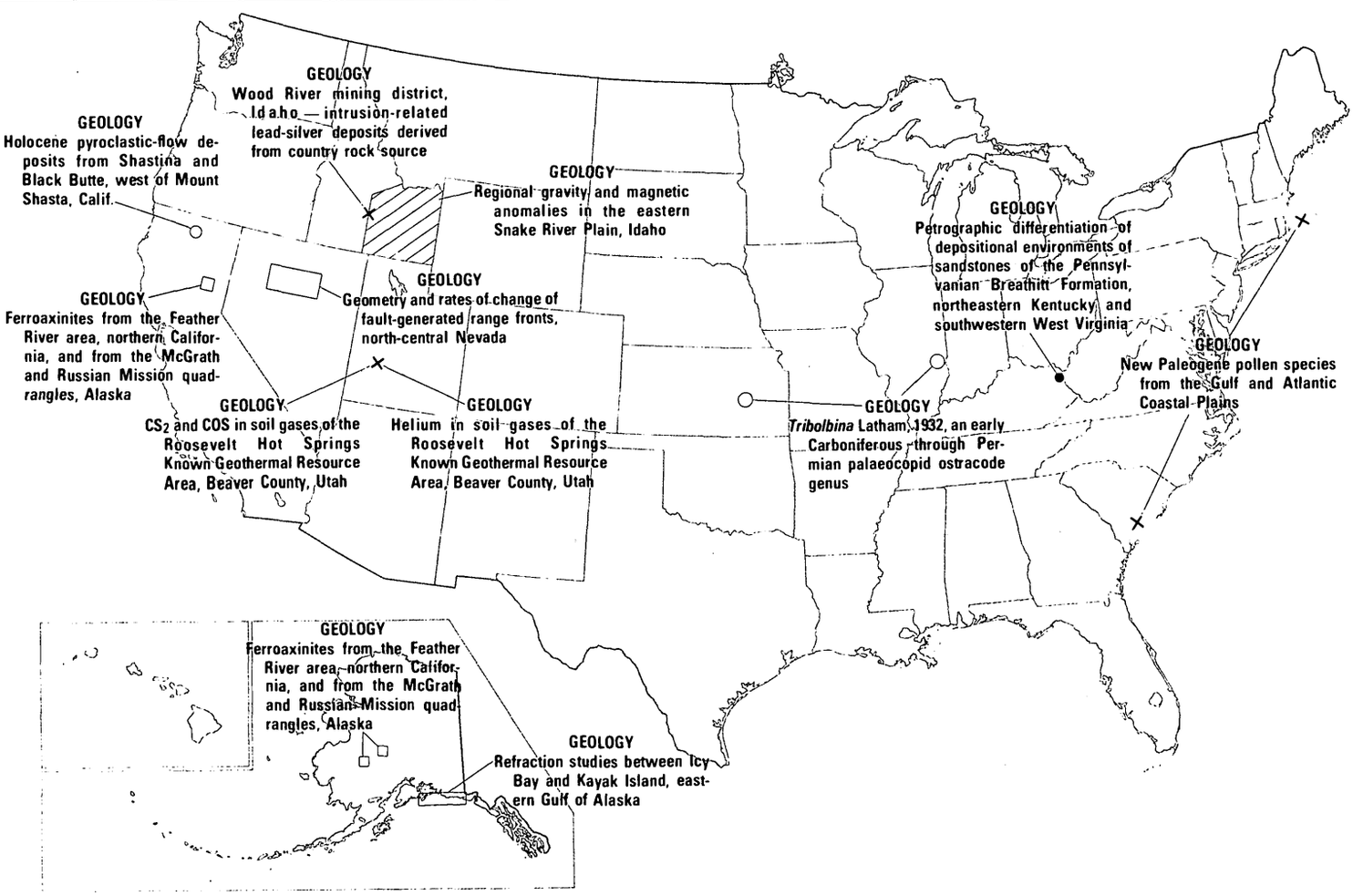

GEOGRAPHIC INDEX TO ARTICLES

See "Contents" for articles concerning areas outside the United States and articles without geographic orientation.

JOURNAL OF RESEARCH

of the

U.S. Geological Survey

Vol. 6, No. 5 Sept.–Oct. 1978

CONTENTS

SI UNITS AND U.S. CUSTOMARY EQUIVALENTS

[SI, International System of Units, a modernized metric system of measurement. All values have been rounded to four significant digits except 0.01 bar, which is the exact equivalent of 1 kPa. Use of hectare (ha) as as alternative name for square hectometer (hm^2) is restricted to measurement of land or water areas. Use of liter (L) as a special name for cubic decimeter (dm^3) is restricted to the measurement of liquids and gases; no prefix other than milli should be used with liter. Metric ton (t) as a name for megagram (Mg) should be restricted to commercial usage, and no prefixes should be used with it. Note that the style of meter^2 rather than square meter has been used for convenience in finding units in this table. Where the units are spelled out in text, Survey style is to use square meter]

SI unit		U.S. customary equivalent	
Length			
millimeter (mm)	=	0.039 37	inch (in)
meter (m)	=	3.281	feet (ft)
	=	1.094	yards (yd)
kilometer (km)	=	0.621 4	mile (mi)
	=	0.540 0	mile, nautical (nmi)
Area			
centimeter^2 (cm^2)	=	0.155 0	inch^2 (in^2)
meter^2 (m^2)	=	10.76	feet^2 (ft^2)
	=	1.196	yards^2 (yd^2)
	=	0.000 247 1	acre
hectometer^2 (hm^2)	=	2.471	acres
	=	0.003 861	section (640 acres or 1 mi^2)
kilometer^2 (km^2)	=	0.386 1	mile^2 (mi^2)
Volume			
centimeter^3 (cm^3)	=	0.061 02	inch^3 (in^3)
decimeter^3 (dm^3)	=	61.02	inches^3 (in^3)
	=	2.113	pints (pt)
	=	1.057	quarts (qt)
	=	0.264 2	gallon (gal)
	=	0.035 31	foot^3 (ft^3)
meter^3 (m^3)	=	35.31	feet^3 (ft^3)
	=	1.308	yards^3 (yd^3)
	=	264.2	gallons (gal)
	=	6.290	barrels (bbl) (petroleum, 1 bbl=42 gal)
	=	0.000 810 7	acre-foot (acre-ft)
hectometer^3 (hm^3)	=	810.7	acre-feet (acre-ft)
kilometer^3 (km^3)	=	0.239 9	mile^3 (mi^3)
Volume per unit time (includes flow)			
decimeter^3 per second (dm^3/s)	=	0.035 31	foot^3 per second (ft^3/s)
	=	2.119	feet^3 per minute (ft^3/min)
Volume per unit time (includes flow)—Continued			
decimeter^3 per second (dm^3/s)	=	15.85	gallons per minute (gal/min)
	=	543.4	barrels per day (bbl/d) (petroleum, 1 bbl=42 gal)
meter^3 per second (m^3/s)	=	35.31	feet^3 per second (ft^3/s)
	=	15 850	gallons per minute (gal/min)
Mass			
gram (g)	=	0.035 27	ounce avoirdupois (oz avdp)
kilogram (kg)	=	2.205	pounds avoirdupois (lb avdp)
megagram (Mg)	=	1.102	tons, short (2 000 lb)
	=	0.984 2	ton, long (2 240 lb)
Mass per unit volume (includes density)			
kilogram per meter^3 (kg/m^3)	=	0.062 43	pound per foot^3 (lb/ft^3)
Pressure			
kilopascal (kPa)	=	0.145 0	pound-force per inch^2 (lbf/in^2)
	=	0.009 869	atmosphere, standard (atm)
	=	0.01	bar
	=	0.296 1	inch of mercury at 60°F (in Hg)
Temperature			
temp kelvin (K)	=	[temp deg Fahrenheit (°F) + 459.67]/1.8	
temp deg Celsius (°C)	=	[temp deg Fahrenheit (°F) − 32]/1.8	

The policy of the "Journal of Research of the U.S. Geological Survey" is to use SI metric units of measurement except for the following circumstance:

When a paper describes either field equipment or laboratory apparatus dimensioned or calibrated in U.S. customary units and provides information on the physical features of the components and operational characteristics of the equipment or apparatus, then dual units may be used. For example, if a pressure gage is calibrated and available only in U.S. customary units of measure, then the gage may be described using SI units in the dominant position with the equivalent U.S. customary unit immediately following in parentheses. This also applies to the description of tubing, piping, vessels, and other items of field and laboratory equipment that normally are described in catalogs in U.S. customary dimensions.

S. M. LANG, *Metrics Coordinator,*
U.S. Geological Survey

Jour. Research U.S. Geol. Survey
Vol. 6, No. 5, Sept.-Oct. 1978, p. 553-562

REGIONAL GRAVITY AND MAGNETIC ANOMALIES IN THE EASTERN SNAKE RIVER PLAIN, IDAHO

By DON R. MABEY, Denver, Colo.

Abstract.—Over the eastern Snake River Plain, the Bouguer gravity anomaly and the magnetic intensity are, in general, high. In detail, both the gravity and the magnetic anomalies are a complex of highs and lows, in contrast to the simpler anomalies over the western Snake River Plain. The broad gravity high associated with the eastern Snake River Plain cannot be produced by a dense mass at shallow depth under the plain, but must be produced either by a deep feature under the plain or by a broader, shallower feature extending well beyond the plain. The high could be produced by a thinning of the crust under the plain by 4.5 to 7 kilometers. The data suggest that the Cenozoic rocks of the plain are underlain by rocks that have density and magnetization similar to the density and magnetization of the pre-Cenozoic rocks north and south of the plain. The data do not suggest rifting of the upper crust such as is inferred for the western Snake River Plain. The plain is in approximate isostatic equilibrium with adjoining regions to the north and south and thus contrasts with the adjoining areas where the basin-and-range topography is not in isostatic equilibrium. The local gravity anomalies on the plain are probably produced by variations in the thickness of Cenozoic rocks, but the wavelength of the anomalies is about twice that of the basin-and-range structural features in areas adjoining the plain. The gravity expression of basin-and-range structural features does not extend far onto the plain. Magnetic anomalies on the plain are produced by Cenozoic volcanic rocks.

The Snake River Plain extends across southern Idaho in an arc about 550 kilometers long (fig. 1). Although the plain is a continuous physiographic feature, the gravity and magnetic anomalies over its eastern and western parts are significantly different. The western Snake River Plain is characterized by large but relatively simple gravity and magnetic anomalies. The dominant Bouguer gravity anomaly over the western Snake River Plain is an elongate high cresting in a series of en echelon closures along the axis of the plain, and the gross magnetic anomaly is a high along the southwestern edge of the plain and a low along the northeastern edge. Together, these magnetic features suggest a thick layer of magnetic material underlying the western part of the plain, and the gravity anomaly requires a large positive mass anomaly in the crust. A model for the western Snake River Plain previously presented (Mabey, 1976) demonstrated that the gravity and magnetic anomalies can be produced by variations in the thickness and physical properties of the upper crust and that no contribution from the lower crust or the upper mantle is required. Although several models can satisfy the measured anomalies over the western Snake River Plain, the data seem to require a very thin or perhaps completely rifted upper crust with a large volume of dense magnetic rock (presumably basalt) high in the crust.

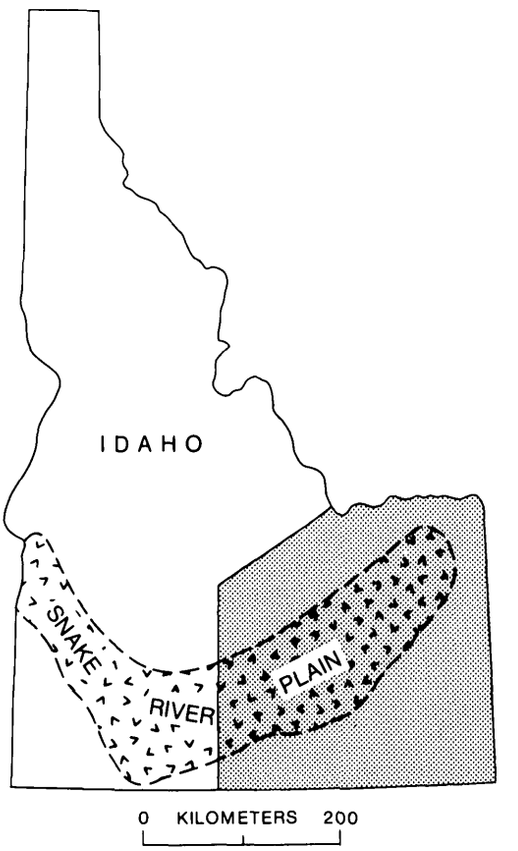

FIGURE 1.—Index map of Idaho showing Snake River Plain and area of study (stippled).

In contrast, the eastern Snake River Plain is an area of more complex gravity and magnetic anomalies. The amplitude of the regional Bouguer gravity high over the eastern plain is about half that over the western plain, and a series of highs and lows with differing trends are superimposed upon the regional high. The general level of magnetic intensity over the eastern plain is high, but the pattern is a complex of highs and lows. In this report, the gross features of the magnetic and gravity anomalies over the eastern Snake River Plain will be examined.

GRAVITY ANOMALIES

The regional Bouguer gravity map (fig. 2) illustrates the gravity high over the eastern Snake River Plain relative to the gravity features of the adjoining regions and also shows variations in patterns within the plain. In the area where the plain strikes approximately east, a pair of gravity highs are separated by a gravity low; these major gravity features trend approximately parallel to the axis of the plain. The northern of the two highs is an extension of the axial high that is the dominant gravity feature of the western Snake River Plain.

Where the Snake River Plain begins to trend northeast, major gravity features that trend northwest, approximately normal to the axis of the plain, are superimposed on the regional high centered over the plain. This pattern continues for about 90 km to the northeast. In the northeastern part of the plain, the trends of the gravity features are more arcuate.

Southeast and northwest of the eastern Snake River Plain, the dominant gravity anomalies are associated with basin-and-range structures; large lows are produced by low-density Cenozoic rocks that underlie the valleys. Individual gravity lows do not exceed about 70 km in length, and some are much shorter. In the area between Burley and Pocatello, the basin-and-range-type anomalies decrease in amplitude toward the edge of the Snake River Plain but apparently continue onto the plain as far as 15 km and then terminate abruptly. The single exception is the low in Arbon Valley south of the plain. Northward, this low swings to the northeast into the adjoining range and then turns northwest to continue across the plain to the Craters of the Moon (CM in fig. 2). Where this low crosses the southeastern edge of the plain the low is not coincident with the valley. These gravity data suggest that along this segment of the southeastern edge of the plain, the structural border of the plain is a few kilometers north of the physiographic edge of the plain and is deeply buried by the sedimentary and volcanic rocks of the plain that lap onto the north-plunging basin-and-range structural features.

For about 100 km east of Pocatello, the large gravity lows that occur in the major valleys terminate well south of the plain as does the major basin-and-range topography. Small relief structures that produce small gravity effects may extend to and across this segment of the border of the plain, but clearly the gravity expression of major basin-and-range structures does not. Farther east, the gravity low in Swan and Grand Valleys is not typical of anomalies associated with basin-and-range valleys. The valleys are very narrow, and the bounding gravity gradients extend into the adjoining ranges in a way that suggests that reverse faults may bound the valleys. Whatever the nature of this structure, the gravity expression terminates south of the border of the plain. A gravity low is produced by low-density sediments underlying Teton Valley to the northeast. Although Teton Valley is open to the north, the gravity low does not extend north of it.

Three basin-and-range valleys open onto the northwestern side of the eastern Snake River Plain. Large gravity lows occur in parts of each of these valleys; however, in each valley the largest lows occur well north of the plain. The low in Big Lost River Valley extends with diminished amplitude to the edge of the plain where it terminates. Just to the south, a small negative gravity feature continues the trend onto the plain and is bounded on the east by a gradient that suggests that the fault zone on the eastern side of Big Lost River Valley may extend into the plain. A low at the mouth of Little Lost River Valley arcs around the southern side of the hills east of Arco and becomes parallel to the edge of the plain. Where Birch Creek Valley broadens as it joins the plain, the gravity low in the valley follows the edge of the range to the west over outcropping Tertiary silicic volcanic rock. This low also terminates at the edge of the plain.

MAGNETIC ANOMALIES

The general magnetic high over the eastern Snake River Plain consists of a complex of local highs and lows (fig. 3). Extending west from Burley is the eastern end of the high that approximately coincides with the southern edge of the western Snake River Plain. This anomaly has been interpreted as indicating the southern edge of a thick, nearly flat layer of basalt, possibly of Miocene age (Mabey, 1976).

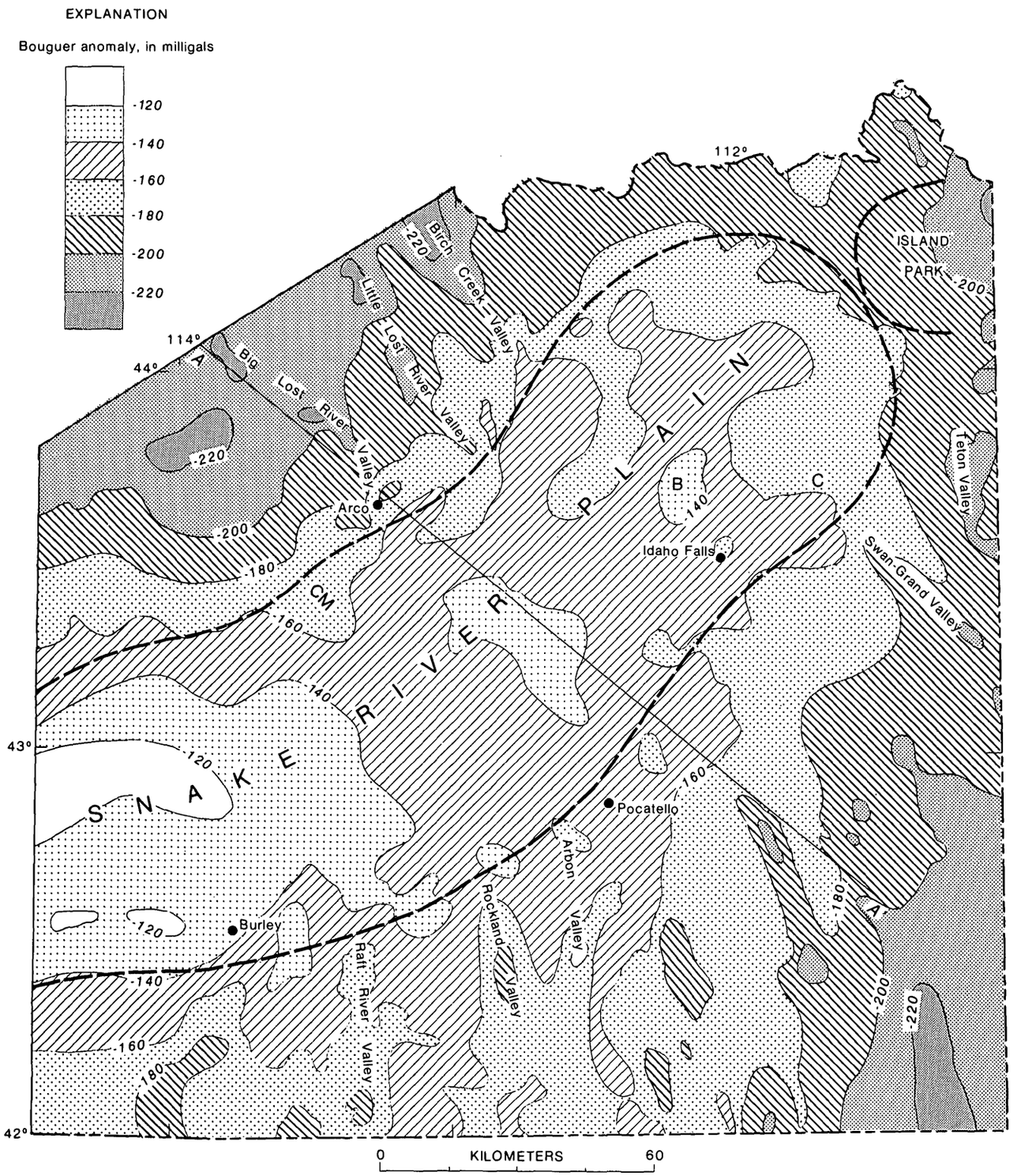

FIGURE 2.—Bouguer gravity anomaly map of southeastern Idaho generalized from Mabey and others (1974). Contour interval, 10 milligals. *A-A'* is the location of profile in figure 4. Dashed lines bound Snake River Plain and Island Park areas. CM, the Craters of the Moon; B and C, gravity highs.

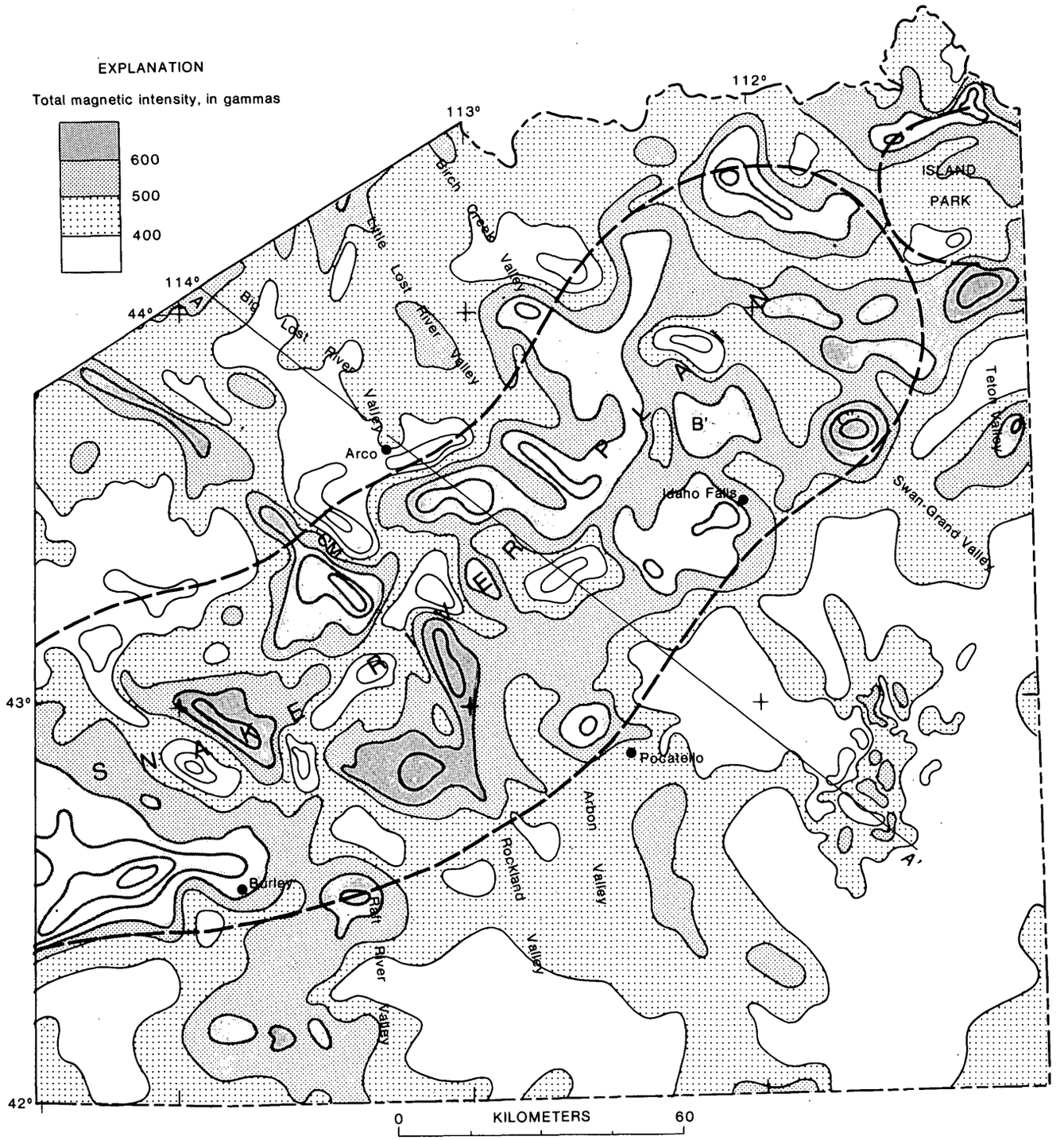

FIGURE 3.—Total intensity aeromagnetic map of southeastern Idaho modified from Mabey and others (1978). Flight elevations were 2750 to 3700 meters above sea level. Contour interval is 100 gammas relative to an arbitrary datum. *A-A'* is profile in figure 4. Dashed lines bound Snake River Plain and Island Park areas. CM, the Craters of the Moon; B' and C', magnetic highs.

Outside the plain, the magnetic intensity is, in general, low. Magnetic highs south of Burley and south of Pocatello are over outcrops of Precambrian rocks; however, the relation between outcropping Precambrian rocks and local magnetic anomalies is not clear. North of the plain, the anomaly that trends northwest about 40 km west of Arco apparently reflects an alinement of Tertiary intrusive rocks. The apparent continuation of this feature on the plain coincides in part with the Craters of the Moon (CM in fig. 3) but does not follow the Great Rift (Prinz, 1970) across the plain. The occurrence of three high-amplitude, approximately equidimensional magnetic highs along the southeastern margin of the plain suggests that these features may be related to the plain margin. All three occur where major valleys intersect the margin of the plain.

INTERPRETATION OF GRAVITY AND MAGNETIC ANOMALIES

The gravity anomaly over the eastern Snake River Plain can be separated into two components. The broad gravity high over the entire plain and extending well beyond the edge of the plain can be considered as a regional anomaly. About 40 km beyond the edge of the plain, the Bouger gravity values are increasing toward the plain by over 0.7 milligals per kilometer. This gradient is more than twice what could be produced by a near-surface dense mass confined to the area of the plain. The source of the regional gravity high either must be areally more extensive than the plain itself or must be deep under the plain; LaFehr and Pakiser (1962) also reached this conclusion. Within the plain and superimposed on the regional high are local gravity features that reflect mass anomalies underlying the plain at relatively shallow depths.

Over most of the eastern Snake River Plain, the Bouguer anomaly is only a few milligals higher than at the margins of the plain, and, in some areas of the plain, the anomaly is lower than at the margins. The residual gravity anomaly within the plain apparently is a complex low on the crest of the regional high. Such a low would be expected if the sedimentary and volcanic rocks of Cenozoic age within the Snake River depression had a density lower than that of average normal upper crustal rocks, and the local gravity relief would reflect the thickness and the lateral changes in density of the sedimentary and volcanic rocks. Because the gravity low over the plain produced by low-density Cenozoic rocks has an extent approximately coincident with the crest of the regional gravity high produced by the deeper structure under the plain, separation of the two features is difficult. Surface fitting to determine the regional high is not satisfactory because the calculated surface of the regional high would be significantly influenced by the superimposed broad low.

Figure 4 illustrates the gravity and magnetic anomaly across the plain where the best gravity control is available. The interpreted model, which will produce the total measured anomaly, assumes a simple deep structure producing the regional gravity high and a gravity low that reflects shallow Cenozoic rocks on the plain. The model attributes the regional anomaly to a thinning of the crust under the plain. The two major crustal layers on the southeastern side of the plain are assumed to be approximately the same thickness as those calculated by Willden (1965) from seismic refraction data obtained along a profile shot southeastward to Bear Lake from the American Falls reservoir, which is near the edge of the plain about 40 km southwest of the profile. An approximate match to the regional anomaly, as measured along the margin of the plain, can be obtained by thinning the total crust 7 km at the northwestern edge of the plain and 4.5 km at the southeastern edge. These values agree with LaFehr and Pakiser's (1962) interpretation of about 6 km of thinning. An additional thinning in the base of the crust is suggested near the southeastern end of the profile. Neither the gravity nor the magnetic data suggest that the pre-Cenozoic rocks underlying the plain are different from those to the north and south of the plain. Thus, rifting of the crust similar to that inferred for the western plain is not suggested for the eastern plain.

A major problem in interpreting the gravity anomalies within the plain is the estimation of the densities of the Cenozoic rocks that underlie the plain. The best information on physical properties of rocks in the area of the eastern Snake River Plain comes from studies done in the vicinity of the Idaho National Engineering Laboratory southeast of Arco. There the plain is underlain by the Pleistocene and Holocene Snake River Group, which consists of basalt flows interbedded with lake and stream deposits derived from the mountains to the north (Walker, 1964). Near the axis of the plain, the basalt is the dominant rock and the average bulk density is estimated to be about 2.65 grams per cubic centimeter. Near the margins of the plain, sediments predominate and their average density is probably about 2.2 g/cm^3. Thus, a large and systematic density increase in the section of interbedded basalts and

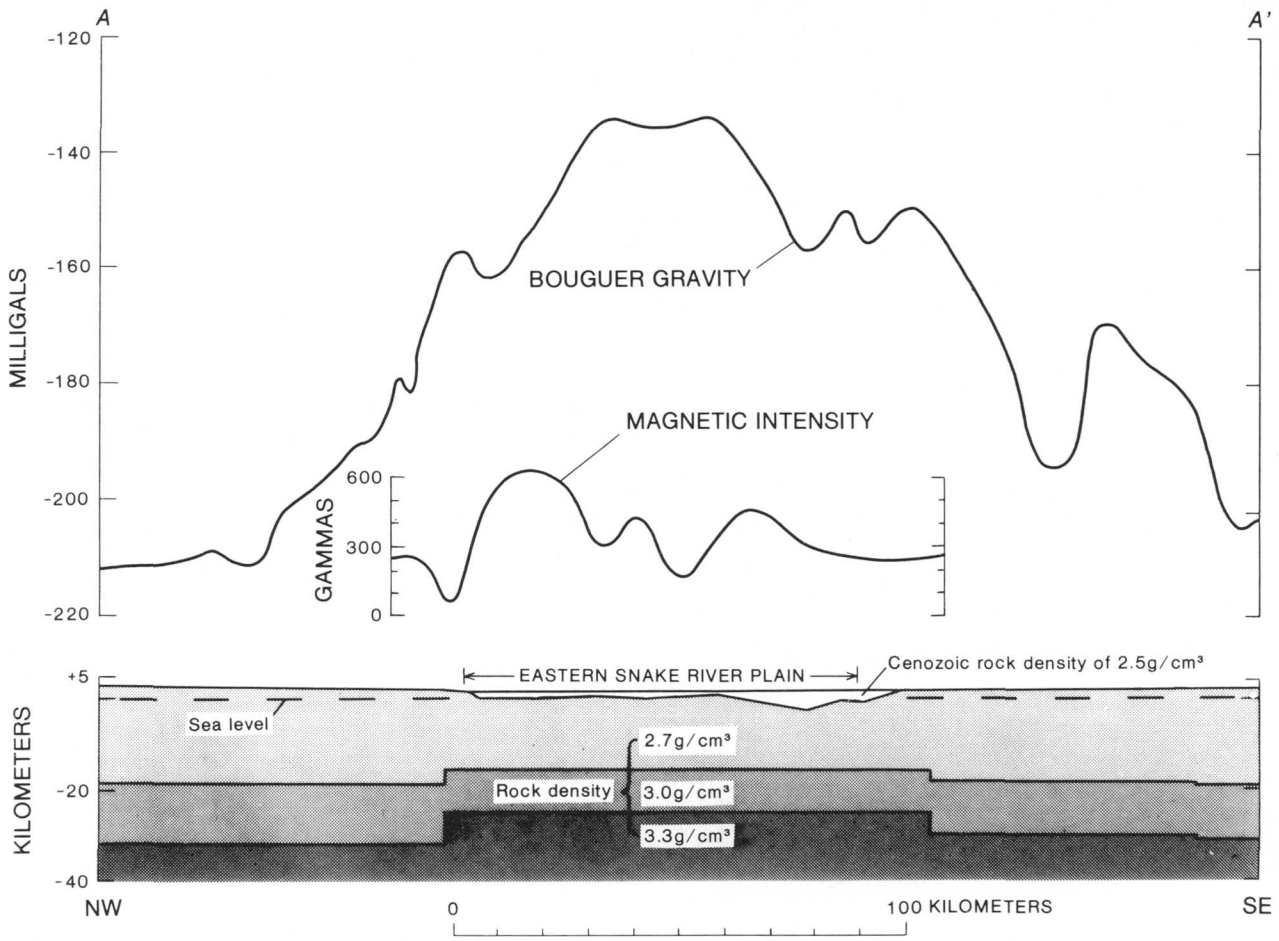

FIGURE 4.—Gravity and magnetic intensity profiles across the eastern Snake River Plain and a two-dimensional model that could produce the observed gravity anomaly. Location of profile is shown in figures 2 and 3.

sediments occurs laterally from the margin toward the axis of the plain. Underlying the basalt-sediment sequence and cropping out on both sides of the plain are Tertiary silicic volcanic rocks of unknown, but possibly great, thickness. These rocks have an average density of about 2.45 g/cm³ and thus are less dense than the basalt but more dense than the sediments of the overlying Snake River Group. The average density of the Cenozoic volcanic and sedimentary rocks is less than that of the pre-Tertiary rocks on both sides of the plain. The broad gravity low over the plain superimposed on the regional high undoubtedly, in large part, reflects the presence of these rocks.

The cause of the more local variations within this low over the plain is not always clear. The low gravity values near the edge of the plain east of Arco and southwest of Idaho Falls probably reflect depressions along the edge of the plain that contain thick Cenozoic sediments. LaFehr and Pakiser (1962) believed that the local gravity highs could be produced by variations in thickness of the basalt resulting from relief on the surface of underlying silicic volcanic rocks. If relief on the top of the silicic volcanic rocks reflects structure that also affects the underlying pre-Cenozoic rocks, the gravity anomaly produced by the density interface between the basalt and the silicic volcanic rocks would be opposite to the effect of the interface between the silicic volcanic rocks and the more dense pre-Cenozoic rocks. The local gravity highs in the eastern Snake River Plain more likely should be regarded as reflecting areas where Cenozoic rocks are thinned. As an approximation, a density contrast of -0.2 g/cm³ between the Cenozoic rocks and the older rocks was assumed in computing the model in figure 4. This contrast is a minimum value and is probably lower than the true average. Thus, the actual thickness of Cenozoic rocks is probably somewhat greater than that indicated on the profile and is perhaps substantially greater in some areas.

A gravity anomaly of about 10 mGal coincides with the rift at the Craters of the Moon. This low is alined with the low that trends across the plain from near

the northern end of Arbon Valley. Karlo and Kosiur (1975) suggest that gravity lows may be characteristic of areas of recent volcanism in the eastern Snake River Plain and may reflect a thermal effect. If a general pattern exists between the gravity anomalies and centers of basalt eruption, it is a complex one and not readily apparent.

Throughout southeastern Idaho, free-air anomalies average about +30 mGal; isostatic anomalies are also positive (Woollard, 1966; Mabey, 1966; and Mabey and Oriel, 1970). This area of positive anomalies is part of a large region of average positive anomalies that covers much of Idaho, Wyoming, and Montana and is in sharp contrast to the Great Basin to the southwest where free-air and isostatic anomalies average near zero. Because free-air anomalies strongly reflect local surface relief, they must be used with great care. The problem is particularly serious in areas of basin-and-range topography because of the high local relief and because of the large majority of the gravity observations that are made in the valleys at elevations well below the average. Local gravity lows in the valleys further bias the average. Thus, in an area of high local relief, the averaging of values of free-air anomalies for all available gravity stations will not usually produce a correct value for the average free-air anomaly. An approximation of the average free-air anomaly can be computed by subtracting the difference between the average elevation and the elevation at the station multiplied by the Bouguer correction from the free-air anomaly value for a representative station (Mabey, 1966). Although the computed average free-air value will depend on the method of determining "average" elevation and on the density assumed in the Bouguer correction, the values are reasonable approximations. Free-air anomalies thus computed will reflect local mass anomalies in about the same way as do the Bouguer anomalies. However, free-air anomalies reflect to a much lower degree regional mass anomalies that are in isostatic equilibrium.

If the depression of the Snake River Plain represents a local isostatic response to a block of thinner crust, free-air anomaly values (assuming no local relief except that of the step at the plain boundary) would rise above zero as the plain was approached, would become negative on the plain, and would rise toward but not reach zero toward the center of the plain. Even if the plain were in perfect isostatic balance, the gravity effect of the thicker crust in the adjoining areas would keep the values on the plain negative. Unadjusted free-air and average free-air anomalies for the profile across the eastern Snake River Plain are shown in figure 5. The central part of the profile is along the axis of one of the largest local gravity highs on the eastern Snake River Plain, and profiles across the plain 20 km to the southwest or northwest would show free-air anomaly values 15–20 mGal lower at the same distance from the edge of the plain. Thus, values about 10 mGal lower are probably more representative for the area of the axial part of the regional gravity high and are indicated by the dashed line.

To compute the average free-air anomaly, the average elevation within 32 km of the gravity station was determined. In the areas of basin-and-range topography, this technique of averaging the elevations filters the local relief between the valleys and ranges. The size of the area for which the average is made usually is not critical. However, on the plain and near the margins of the plain, the averaging over circular areas smooths the linear topographic margin of the plain and thus alters its form as a topographic step. Because relief on the plain is low, the unadjusted free-air anomalies on the plain are not strongly influenced

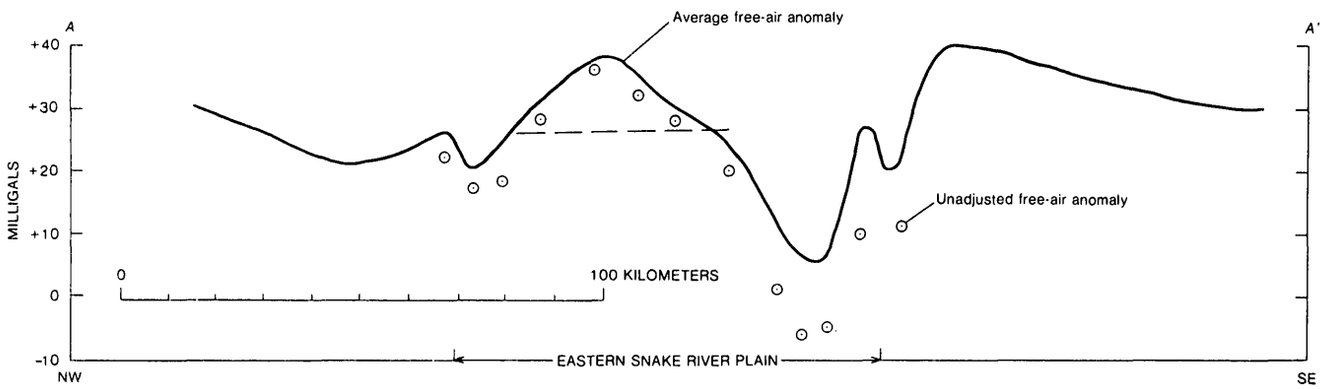

FIGURE 5.—Free-air gravity anomaly across the eastern Snake River Plain. Solid line values are adjusted to average elevation within 32 km of the observation. Dashed line is representative average free-air anomaly within 20 km of this part of the profile.

by local topography, and, near the margins of the plain, the unadjusted free-air values are more meaningful than the average values that are influenced by topography off the plain. A free-air anomaly comparable to the unadjusted values on the plain could be obtained for stations within 32 km of the plain by averaging elevations along a line through the station and parallel to the margin of the plain and adjusting the free-air anomaly values to this elevation. The adjusted values thus computed immediately northwest of the plain would be about 10 mGal higher than the average values based on elevations averaged over circular areas.

Regardless of how the average free-air anomalies across the eastern Snake River Plain are computed, the values determined over the plain are less positive than those in the adjoining areas. This observation is consistent with approximate isostatic balance of the plain relative to these areas. If a much more detailed definition of the free-air anomaly was obtained in the areas adjoining the plain, the data could be used to quantitatively study the isostatic compensation of the plain.

Thus, the free-air anomalies over the entire region are positive, and the Snake River Plain is in approximate isostatic balance with adjoining regions. This combination suggests that compensation of the plain is relatively shallow, whereas the entire region is held above the level of isostatic balance, perhaps by deeper dynamic forces.

If the gravity anomalies, in combination with surface topography, are accepted as indicators of the size and distribution of basin-and-range structures, several conclusions can be reached regarding the relation of these structures to the Snake River Plain. First, the relief of the basin-and-range structures decreases toward the plain and some features terminate before reaching it. Those that reach the plain apparently interact with the plain in a complex way; some extend a few kilometers onto the plain, whereas others terminate at the edge. In some areas, such as along the northwestern side of the plain east of Arco, the edge of the plain seems to coincide with a major bounding fault. In other areas, such as east of Burley, the rocks and structures from outside the plain dip under the volcanic and sedimentary rocks of the plain, but in those areas the gravity data suggest a fault paralleling the edge a few kilometers onto the plain.

The gravity anomalies within the eastern Snake River Plain do not have the same character as the anomalies in the regions of basin-and-range structure. The large gravity highs and lows within the plain are approximately twice as broad as those associated with the basin-and-range structures. Interpreted gravity lows adjoining the plain are apparently largely due to low-density Tertiary rocks underlying the Quaternary fill that covers the valley floors. In the valleys south and southeast of the plain, these low-density Tertiary rocks consist, in large part, of the Miocene and Pliocene Salt Lake Formation. The nature of these basins in which the Salt Lake Formation was deposited is not well understood. That the basins were much broader than the current basins is indicated by the presence of extensive Miocene and Pliocene deposits in the high parts of several of the ranges. Perhaps the gravity anomalies within the eastern Snake River Plain are reflecting the distribution of Tertiary rocks deposited or preserved in basins that were approximately twice the width of the current topographic basins in the basin-and-range areas. These younger basin-and-range structures do not seem to extend across the plain.

Although major volcanic features must exist under the cover of the youngest sedimentary and volcanic rocks that cover the eastern Snake River Plain, their expression is not readily apparent in the gravity anomalies. Large calderas, such as Long Valley, Calif., that contain thick piles of low-density sedimentary and volcanic rocks produce large negative gravity anomalies (Kane and others, 1976). The residual low in Long Valley is about 40 mGal, about half the amplitude of the total anomaly across the eastern Snake River Plain; and, if a negative anomaly of the size and extent of the Long Valley anomaly existed in the area of the eastern Snake River Plain, it would be apparent on the gravity map. However, not all large calderas produce large negative gravity anomalies. The Island Park caldera at the northeastern end of the Snake River Plain has no pronounced gravity expression. Some of the local gravity anomalies within the plain may relate to volcanic features underlying the plain; however, without supplemental information, the anomalies cannot, with confidence, be identified. Detailed geologic mapping combined with more detailed gravity surveys may reveal the relationship between the gravity anomalies and the volcanic features.

Although both the eastern Snake River Plain and the adjoining basin-and-range areas may reflect tension related to regional crustal spreading, the gravity data suggest that they represent different responses to what appear to be different strains. The individual basins and ranges are not in isostatic balance, and the differential load between them is supported by the strength of the lithosphere. In effect, they are superficial features, with the faults probably flattening with

depth and, in general, not displacing any major deep density horizons. The structure of the eastern Snake River Plain, on the other hand, involves the total thickness of the crust and perhaps the upper mantle. The plain is in approximate isostatic balance with the adjoining regions, and the gravity data suggest that a major part of the compensating mass is at the base of the crust.

Very few earthquakes are occurring in the area of the eastern Snake River Plain, and few fault scarps are apparent except near the margins of the plain. Apparently any deformation that may now be occurring in the plain is not accompanied by major faulting. In contrast, recent fault scarps and numerous earthquakes occur both north and south of the plain. This absence of evidence of active faulting and the indication of isostatic balance for the plain relative to the adjoining regions indicate that the crust in the area of the plain is a zone of very low stress. Such a condition is consistent with the eastern Snake River Plain being an area of high thermal gradients.

The complex magnetic anomalies over the eastern Snake River Plain have sources within a few kilometers of the surface and, at least in large part, relate to the volcanic rock underlying the plain. Some of the magnetic anomalies correlate with surface features. For example, the high 30 km east of Burley is centered over a dome of basalt and the elongate high 25 km southwest of Arco is over the Craters of the Moon. Probably most, if not all, of the large magnetic anomalies are produced by variations in the thickness, relative abundance, and magnetism of the Cenozoic volcanic rocks, primarily the basalt and related intrusive complexes. The apparent absence of deep magnetic anomalies may be partly due to a relatively near surface Curie temperature under the plain.

The relationship between the local gravity and magnetic anomalies on the eastern Snake River Plain is complex, but a pattern seems to exist. All the closed magnetic lows on the plain are in the area of relative gravity highs. Also, areas of high magnetic intensity are more abundant in the area of relative gravity lows; this relationship holds best for the more extensive magnetic highs. This general relationship of magnetic lows with gravity highs and magnetic highs with gravity lows is consistent with the sources of the gravity highs being structural highs where the Cenozoic rocks are relatively thin and the magnetic highs reflecting areas where the Cenozoic rocks are thickest.

A notable exception to the above correlation occurs about 10 km northwest of Idaho Falls. Here coincident gravity B and magnetic B′ highs occur, thus suggesting a dense and magnetic rock mass in the subsurface. Similar paired anomalies C and C′ occur about 30 km northeast of Idaho Falls.

Profile *A*-*A*′ illustrates the problem of correlating the gravity and magnetic anomalies. The magnetic high along the profile covers the northwestern three-fourths of the plain but does not extend to its southeastern edge. Probably basalt is not abundant in the Cenozoic rocks that produce the gravity low along this part of the southeastern margin of the plain. In the area of the gravity high near the center of the plain, the magnetic intensity is relatively low suggesting that the volcanic rocks are relatively thin.

Considerable evidence suggests that volcanic activity from Miocene to Quaternary time has migrated northeast along the present location of the Snake River Plain to the Yellowstone area (Eaton and others, 1975). Thus, the Yellowstone Plateau might be expected to evolve into an extension of the Snake River Plain. The low gravity and magnetic anomalies and the high elevation of the Yellowstone Plateau are exactly opposite to those of the high gravity and magnetic anomalies and low elevation of the eastern Snake River Plain. In Eaton and others (1975), it was suggested that the gravity low in the Yellowstone Plateau could reflect a large active magma chamber underlying the region. The shallow depth of the Curie isotherm and extensive hydrothermal alteration could account for the low magnetic intensity. If this magma chamber was to solidify without any major accompanying mass transfer, the resulting thermal contraction would produce a relative gravity high and topographic low similar to that of the Snake River Plain and basaltic volcanism would produce areas of high magnetic intensity. The northeastern part of the Snake River Plain may have developed over a complex of calderas, and the Island Park area may be a transitional phase between the Yellowstone Plateau and the Snake River Plain.

A topographic high is coincident with the axis of the eastern Snake River Plain. The gravity high down the axis of the plain and an approximately coincident subtle magnetic low trend suggest that Cenozoic rocks may be thinner along the axis of the plain than nearer the margins. If the topographic high along the axis was constructional, reflecting a thick pile of basalt, a magnetic high would be expected. The topography, gravity, and magnetic data suggest, but do not prove, that the margins of the plain have subsided more than the central part of the plain.

Any model of the eastern Snake River Plain based on an interpretation of the gravity and magnetic data alone should be considered as tentative. However, these data do provide significant constraints that will

be useful in constructing more precise models as information from other geophysical surveys and deep drilling becomes available.

REFERENCES CITED

Eaton, G. P., Christiansen, R. L., Iyer, H. M., Pitt, A. M., Mabey, D. R., Blank, H. R., Jr., Zietz, Isidore, and Gettings, M. E., 1975, Magma beneath Yellowstone National Park: Science, v. 188, p. 787–796.

Kane, M. F., Mabey, D. R., and Brace, Rosa-Lee, 1976, A gravity and magnetic investigation of the Long Valley caldera, Mono County, California: Am. Geophys. Union Jour. Geophys. Research, v. 81, no. 5, p. 754–762.

Karlo, J. F., and Kosiur, D. R., 1975, Thermal overprint as a possible effect on the gravity relations of the eastern Snake River Plain, Idaho: Geol. Soc. America Abs. with Programs, v. 7, no. 5, p. 615–616.

LaFehr, T. R., and Pakiser, L. C., 1962, Gravity, volcanism, and crustal deformation in the eastern Snake River Plain, Idaho, *in* Short papers on geology, hydrology, and topography: U.S. Geol. Survey Prof. Paper 450–D, p. D76–D78.

Mabey, D. R., 1966, Relation between bouguer gravity anomalies and regional topography in Nevada and the eastern Snake River Plain, Idaho, *in* Geological Survey research 1966: U.S. Geol. Survey Prof. Paper 550–B, p. B108–B110.

———1976, Interpretation of a gravity profile across the western Snake River Plain, Idaho: Geology, v. 4, no. 1, p. 53–55.

Mabey, D. R., and Oriel, S. S., 1970, Gravity and magnetic anomalies in the Soda Springs region, southeastern Idaho: U.S. Geol. Survey Prof. Paper 646–E, 15 p.

Mabey, D. R., Peterson, D. L., and Wilson, C. W., 1974, Preliminary gravity map of southern Idaho: U.S. Geol. Survey Open-File Rept. 74–78.

Mabey, D. R., Zietz, Isidore, Eaton, G. P., and Kleinkopf, M. D., 1978, Regional magnetic patterns in part of the Cordillera in the western United States: Geol. Soc. America Mem. (In press.)

Prinz, Martin, 1970, Idaho rift system, Snake River Plain, Idaho: Geol. Soc. America Bull., v. 81, no. 3, p. 941–948.

Walker, E. H., 1964, Subsurface geology of the National Reactor Testing Station, Idaho: U.S. Geol. Survey Bull. 1133–E, 22 p.

Willden, Ronald, 1965, Seismic-refraction measurements of crustal structure between American Falls Reservoir, Idaho, and Flaming Gorge Reservoir, Utah, *in* Geological Survey research 1965: U.S. Geol. Survey Prof. Paper 525–C, p. C44–C50.

Woollard, G. P., 1966, Regional isostatic relations in the United States, *in* The earth beneath the continents: Am. Geophys. Union Geophys. Mon. 10, v. 5, p. 557–594.

Jour. Research U.S. Geol. Survey
Vol. 6, No. 5, Sept.-Oct. 1978, p. 563-570

HELIUM IN SOIL GASES OF THE ROOSEVELT HOT SPRINGS KNOWN GEOTHERMAL RESOURCE AREA, BEAVER COUNTY, UTAH

By M. E. HINKLE, E. H. DENTON, R. C. BIGELOW, and
R. L. TURNER; Denver, Colo.

Abstract.—Soil samples were collected in two parallel traverses across the Dome fault zone of the Roosevelt Hot Springs Known Geothermal Resource Area. The samples were sealed in air-tight aluminum cans, and the soil gas was allowed to equilibrate with the atmospheric air in the cans. Gas from the cans was analyzed by mass spectrometry. Samples collected over faults contained anomalously high concentrations of helium. Samples collected close to a geothermal well 884 m deep contained more helium than samples collected near another geothermal well 1370 m deep.

Several workers have found anomalous concentrations of helium associated with hot springs and geothermal areas (Mazor and Wasserburg, 1965, Mazor and Fournier, 1973; Roberts and others, 1975). A helium sniffer test run near the area discussed in this report by the U.S. Geological Survey showed an apparent correlation between helium contents of subsurface air samples and a known fault (Denton, 1977).

The Roosevelt Hot Springs KGRA (Known Geothermal Resource Area) is being prepared for commercial development. The University of Utah and the Phillips Petroleum Co. have been studying the KGRA prior to its development. The objective of our study was to measure concentrations of helium over and near the area to see if helium anomalies could be related to faults or reservoir depths.

The area studied is located about 20 km northeast of the town of Milford, Utah, in the northwestern corner of the Minersville 2 NE 7½-minute quadrangle in Beaver County (fig. 1). The area is in the Basin and Range province. The KGRA is associated with Quaternary silicic volcanics which occur as domes, flows, and tuffs (Nash, 1976).

Roosevelt Hot Springs itself is located at the northern end of a wide north-south trending fault zone (Dome fault) on the western side of the Mineral Mountains; the hot water probably originates as meteoric water from the Mineral Mountains, which is heated by volcanic rocks. In the early 1900's, the spring issued boiling water, but, since then, it has dried up (Mundorff, 1970), and, at present, the only activity is emission of a little steam. Discontinuous elongate mounds of opaline sinter and other hot-spring deposits occur along the fault zone south of Roosevelt Hot Springs (Nash, 1976). The terrain slopes gently toward the valley from an elevation of 1908 m on the east to 1768 m on the west.

SAMPLING PROCEDURE

A total of 180 soil samples were collected in air-tight cans in two parallel east-west traverses across the KGRA, with the Dome fault cutting the approximate center of each traverse (fig. 1). Thirty of these samples were duplicates, collected at about every fourth site.

Traverses passing close to two Phillips Petroleum Co. drill sites were selected because the wells intersect hot water at different depths; well 3–1 is approximately 884 m deep, and well 13–10 is approximately 1370 m deep (Ron Forrest, Phillips Petroleum Co., oral commun., April 19, 1977).

The northern traverse started out along the line called "4000 N," which was established by the University of Utah, passed just south of the Phillips Petroleum Co. drill site 3–1 and continued east, where the traverse jogged north 30 m to the "4030 N" University of Utah line. The traverse contained 72 stations; the first 12 sites at the west end were spaced 100 m apart, and the rest were spaced 30 m apart. The southern traverse started in Little Cedar Cove and followed a line which passed just south of the Phillips drill site 13–10; soil samples were collected at 30-m intervals for 78 stations.

At each site, a hole 10 cm in diameter was drilled to a depth of about 0.5 m with a gasoline-powered auger. Along the northern traverse, the soil appeared to be cemented in the area of the Dome fault, and drilling was difficult even with the power auger. Loose soil at the bottom of each hole was dug out by hand and placed in an aluminum can coated with plastic on the inside. The soil was a mixture of sand, clay, and caliche. A dead-air space about 2–3 cm deep was left at the

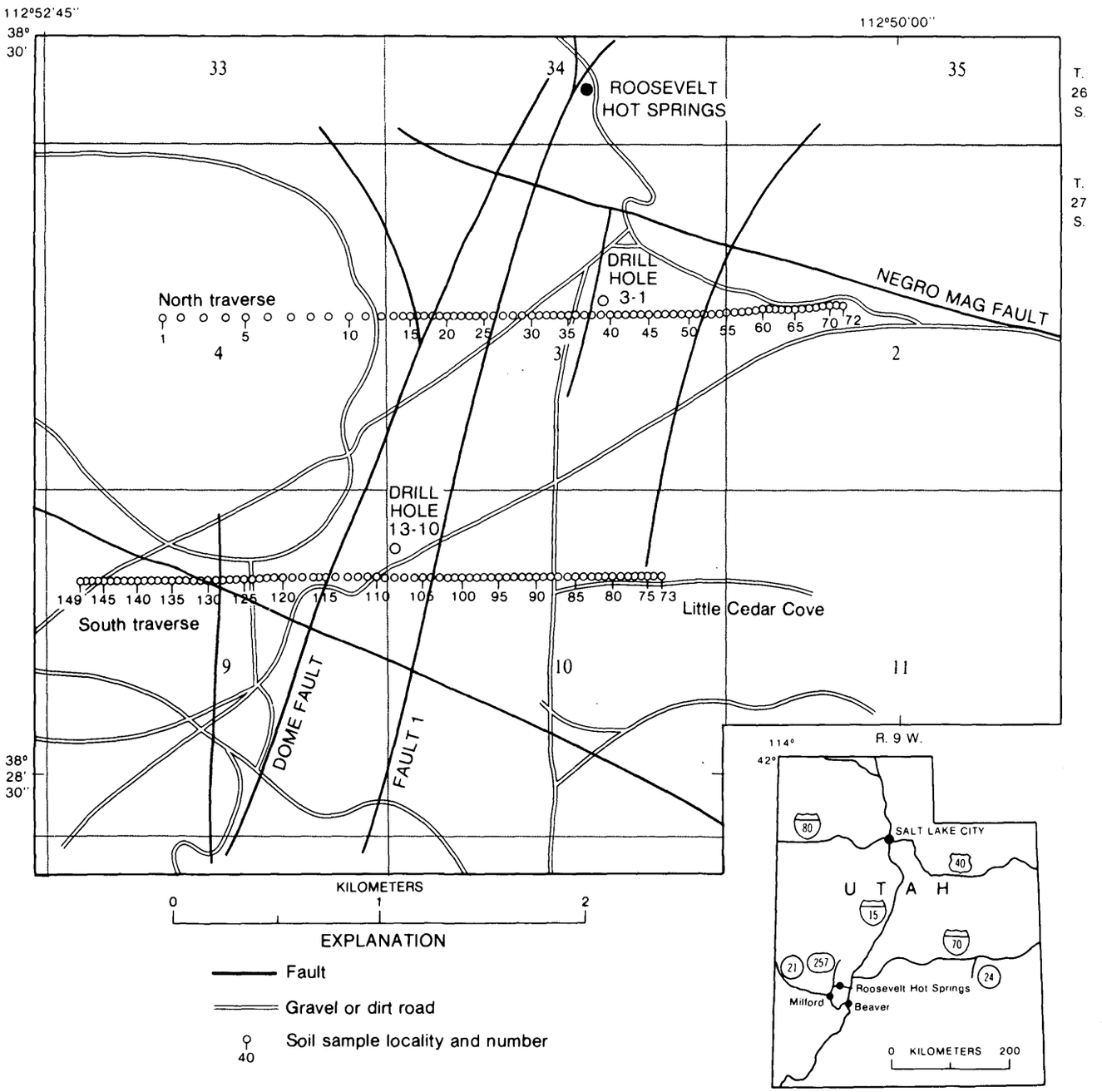

FIGURE 1.—Sample locality map, Roosevelt Hot Springs, Utah.

top of the can. The can was sealed with a plastic-coated aluminum plug by means of a hand canning device. At each site, the soil temperature and barometric pressure were recorded. Samples of ambient air were collected in stainless steel air sampling containers at 18 randomly selected stations along the traverses.

SAMPLE PREPARATION AND ANALYSIS

The field ambient air samples were analyzed for helium in the laboratory by means of a modified DuPont leak detector (Friedman and Denton, 1975). The precision of the instrument was ± 25 ppb (parts per billion). The detector was calibrated two times each day against a standard air mixture containing 7.59 ppm (parts per million) by volume helium as certified by the U.S. Bureau of Mines. Ambient laboratory air samples were run between each canned air sample. Analytical results were obtained as parts per billion of

helium in excess of helium in laboratory air. All of the field air samples contained 5.2 ± 0.16 ppm helium, the same concentration as the laboratory air samples.

The cans of soil samples were placed in an ultrasonic cleaning bath for 20 minutes to disaggregate clumps of clayey soil. The cans were left sitting at ambient laboratory temperature for 2 weeks to allow the helium from the disaggregated soil to equilibrate with the helium in the dead-air space in the can. Silicone rubber septa were glued on to the bottoms of the cans with silicone glue.

At the time of analysis, the laboratory temperature and barometric pressure were noted. Each can was punctured by pushing a thin ice pick through both the rubber septum and metal. A side-hole needle attached to a hypodermic syringe was inserted through the hole made by the ice pick. Then the can was placed in a hydraulic press and squeezed until about 10 cm^3 of air was expelled from the can into the syringe. The needle of the syringe was capped by slipping a small piece of silicone rubber tubing over the end of the needle. The air in the syringe was analyzed for helium in the same way as the ambient samples. A few of the canned samples gave less than ambient air or negative values on the leak detector scale; negative values are believed to be due to hydrogen or methane interference, so these samples were not used in the summation of results.

After the canned air samples were analyzed, the dented cans were split open, and the soil was poured into an intact can of the same type and tamped down lightly; the height of the air space above the soil was measured with a ruler, and the dead-space volume was calculated.

The concentration of helium in the dead-air space is only a partial measurement of the helium concentration of the total sample in the can. Additional helium is contained in the soil moisture of the sample. Helium degassed from soil moisture may also have contributed to the excess helium in the dead-air space. Therefore, the soils were weighed, dried at 35°C, and weighed again to determine the amount of soil moisture originally present.

CALCULATIONS AND RESULTS

Total helium in the sealed can had to be the same in the laboratory and in the field. Because the atmospheric concentration of helium was equal for the lab and the field, any excess helium determined in the air displaced from the can must have come from the sample, whether degassed from the soil moisture, or from the soil itself, or from both. The total helium in the canned samples was calculated as follows:

In the laboratory, total helium = (5.24 ppm + excess ppm) × volume dead space + ppm He dissolved in soil moisture × volume soil moisture + other (unmeasurable) helium;

and in the field, total helium = 5.24 ppm × volume dead space + ppm He dissolved in soil moisture × volume soil moisture + other helium.

Helium contents of the samples were calculated as either parts per billion helium in soil moisture (cm^3 He × $10^{-9}/cm^3$ H_2O) or parts per billion helium in original undried soil (cm^3 He × 10^{-9}/g soil). Parameters necessary for the calculations were volume of dead space in cans, weight of original undried soil sample, volume of soil moisture in sample, atmospheric pressure in both the field and the laboratory, and temperature in both the field and the laboratory.

Concentrations of helium in the soil moisture were calculated by use of Henry's law, which relates the concentration of a gas in a solution to the pressure of the gas over the solution. The Henry's law equation is:

$$C = KP,$$

where C is the concentration of the gas in solution; P is the pressure of the gas above the solution at equilibrium; and K is an experimentally determined proportionality constant which depends on the nature of the gas, the solvent, and the temperature (Maron and Prutton, 1958, p. 143–144).

The solubility of helium in water, at various temperatures and a pressure of 1 atmosphere of helium

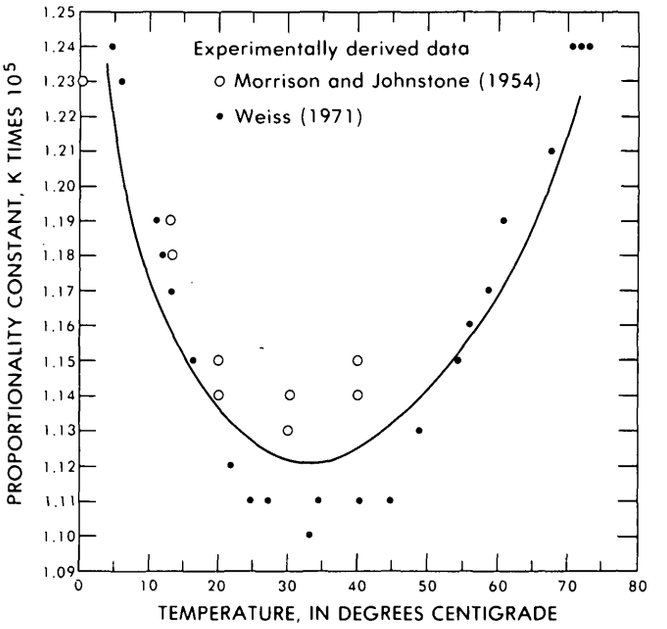

FIGURE 2.—Proportionality constant, K, versus temperature. Graph used to calculate theoretical concentrations of helium in soil moisture.

has been determined experimentally by Morrison and Johnstone (1954) and by Weiss (1971). The constant K was derived from their data in the following equation:

$$K = \frac{\text{cm}^3\ \text{He}}{\text{cm}^3\ \text{H}_2\text{O}} \times \frac{1}{760\ \text{mm}}.$$

The derived constants were plotted versus temperature (fig. 2). This plot was then used to recalculate the theoretical concentrations of helium in soil moisture at the laboratory and at the various field sample sites under the recorded conditions of temperature and pressure.

Absolute, rather than adjusted pressures, were used for the calculations. To convert adjusted pressures, as obtained from the U.S. Weather Service, to absolute pressures, the empirically determined equation below was used (Charles Knight, Nat. Center for Atmospheric Research, Boulder, Colo., oral commun., August 1976).

$$\frac{P\ \text{absolute, local}}{P\ \text{adjusted, local}} = [1 - (\text{elevation in meters} \times 2.25 \times 10^{-5})]^{5.256}.$$

The absolute local pressures thus calculated were then multiplied by 5.24×10^{-6}, the concentration of helium

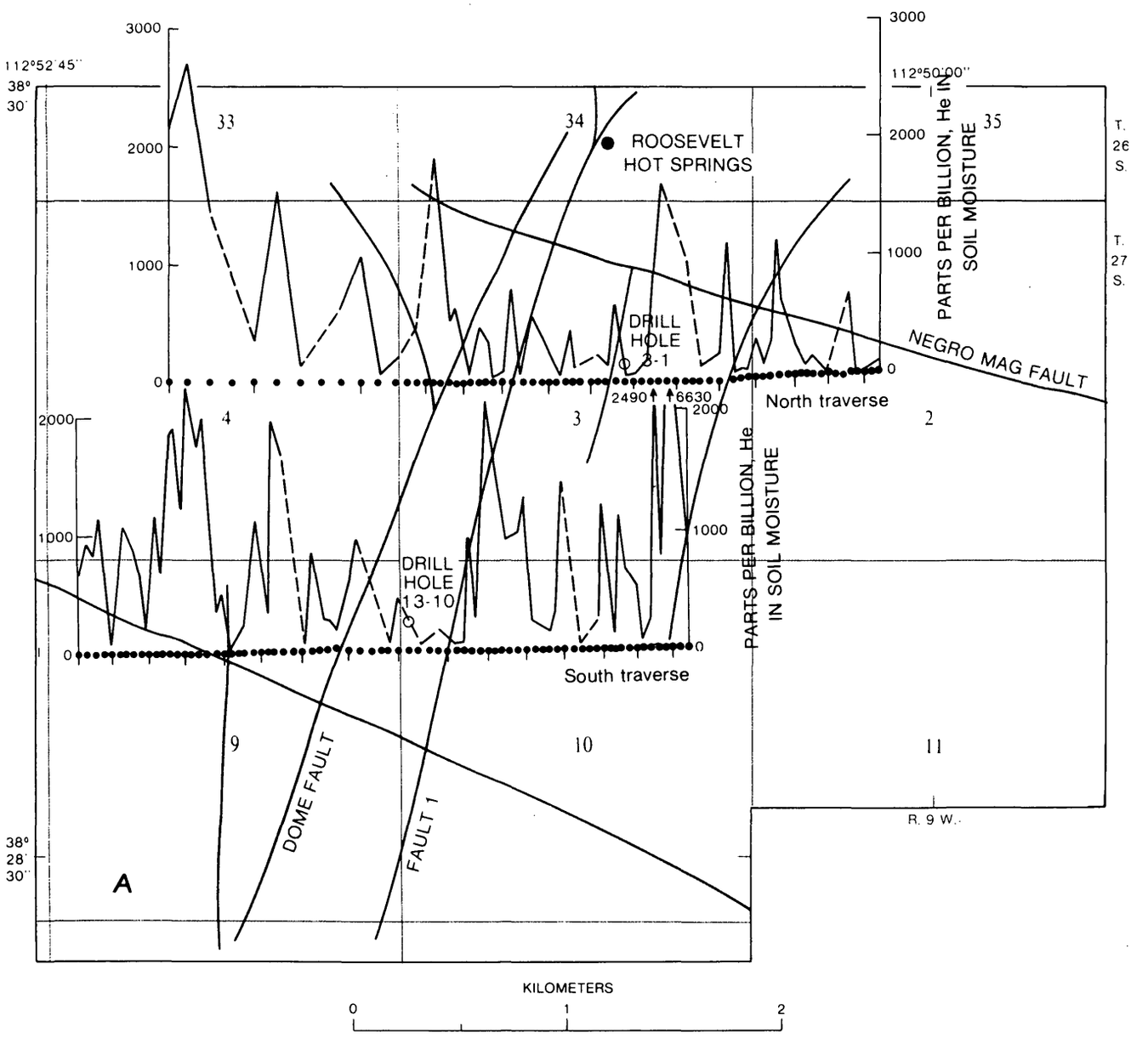

FIGURE 3.—Helium concentration in soil moisture (*A*) and undried soil samples (*B*), Roosevelt Hot Springs KGRA, Utah.

in air, to obtain the partial pressure of helium in the atmosphere at each sample site and also in the laboratory. This partial pressure was used in the Henry's law equation to calculate the concentrations of helium dissolved in the sample soil moistures in both the laboratory and the field.

Assuming that all the excess helium in the cans was derived from the soil moisture, the concentrations of helium which must have been present originally were calculated from the following equation:

$$\text{ppb helium originally present in soil moisture in field} = \frac{[\text{Excess helium (ppb)} \times \text{volume dead space} + \text{ppb He in soil moisture in lab} \times \text{volume soil moisture}]}{\text{volume soil moisture}}$$

These concentrations ranged from 37 ppb (the average theoretical concentration calculated from Henry's law) to over 6000 ppb (fig. 3*A*). The average concentration

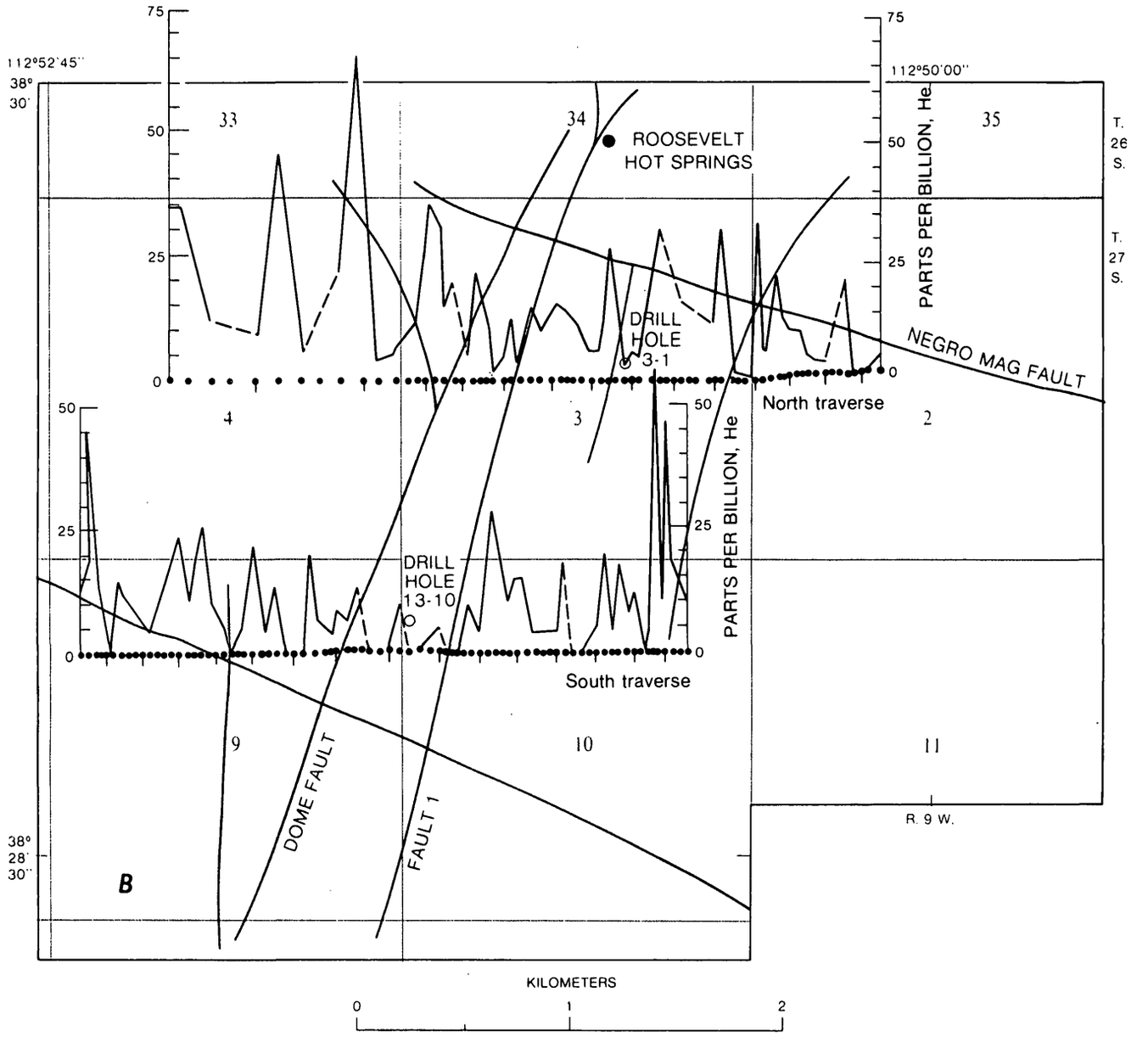

FIGURE 3—Continued.

of 140 samples was 660 ppb, or about 18 times the concentration theoretically present under equilibrium conditions. This high helium concentration may indicate that (1) equilibrium conditions do not exist in the area; that is, the soil moisture was supersaturated with helium, (2) the excess helium was derived from helium trapped in crystal lattices in the soil, (3) the helium was degassed from pore spaces in the soil, or (4) the helium came from a combination of these sources.

Because the excess helium could have originated in more than one part of the sample, the concentration of helium was recalculated on the basis of the weight of the entire sample as follows:

$$\text{ppb excess helium in original soil} = \frac{[\text{Excess helium (ppb)} \times \text{volume dead space} + \text{ppb He in soil moisture in lab} \times \text{volume soil moisture}]}{\text{weight of soil before drying}}.$$

These concentrations ranged from 1 to 67 ppb; the average of 140 samples was 12 ppb helium in soil (fig. 4).

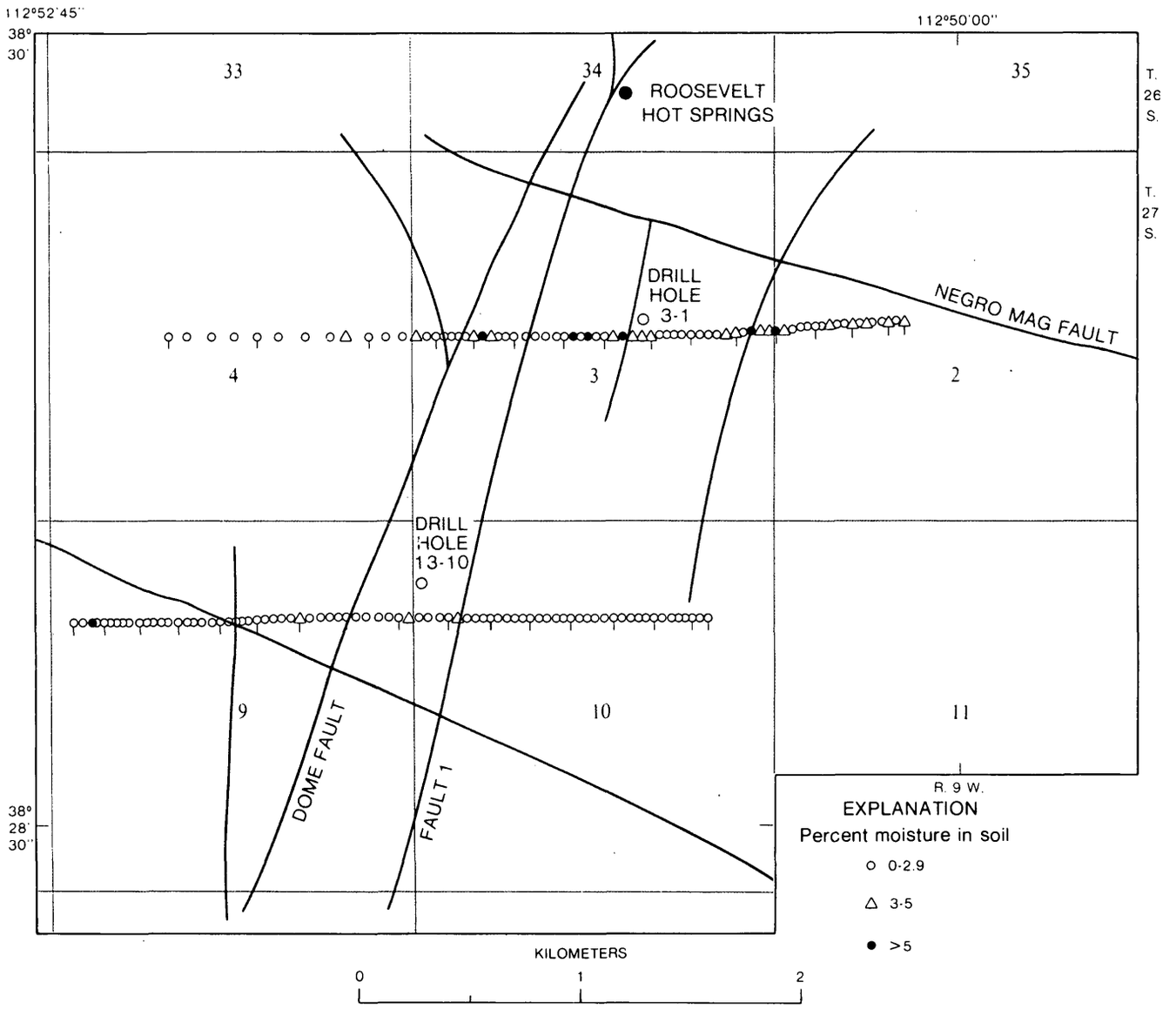

FIGURE 4.—Percent moisture in soil samples from Roosevelt Hot Springs KGRA, Utah.

DISCUSSION

Helium escapes from the geothermal system by migrating upward through faults and fractures either in the gaseous state or dissolved in steam which degasses the dissolved helium on cooling. Plan views of helium concentrations obtained along the two traverses show anomalous values clustered around known faults or the extensions of faults (fig. 3) regardless of whether the helium is assumed to be derived from the soil moisture alone or from the total undried sample.

Drill hole 3–1 is located adjacent to a fault, and hole 13–10 is in a zone of continuous fracturing between the Dome fault and Fault 1 (Ward and Sill, 1976). The helium concentrations along the traverses for an arbitrarily selected 100 m on each side of the drill holes average higher near hole 3–1 (884 m deep) than near hole 13–10 (1370 m deep) (fig. 3), indicating that higher helium concentrations can be expected over a shallower source. Helium concentrations near hole 3–1 average 260 ppb in soil moisture and 9 ppb in the undried soil, while concentrations of helium near 13–10 average 200 ppb in soil moisture and 4 ppb in undried soil. The helium rising from the deeper source may be more dispersed than helium from the shallower source. A better picture of the relationship of helium concentration to depth would be obtained by a study of the area between the two drill holes.

When the helium is assumed to be derived from the total undried soil sample, the average concentration of helium is 12 ppb for both north and south traverses (fig. 3*B*). However, when the helium is assumed to have come from the soil moisture alone, the average helium concentration along the southern traverse is 820 ppb, compared to 470 ppb along the northern traverse (fig. 3*A*). The moisture content of soils along the northern traverse is about 50 percent higher than that along the southern traverse (fig. 4). If soil moisture is assumed to collect helium, more helium would be expected where the moisture is higher. However, the opposite situation was observed when the samples of the north and south traverses were compared. This apparently contradictory observation, coupled with the calculation of extreme disequilibrium concentrations of helium in soil moisture, indicates that the helium contents of soil samples are best expressed in relation to the total original soil sample rather than in relation to soil moisture.

The results show that measurement of helium in soil gas is a good tool for exploration in a geothermal resource area. Fault zones can be distinguished from nonfaulted areas by higher helium concentrations in the soil gas over the fault zones. In addition, detailed study of helium concentrations over known geothermal reservoirs might be used with other methods in determining the depth to the hydrothermal system.

REFERENCES CITED

Denton, E. H., 1977, Helium sniffer field test, Roosevelt Hot Springs, Utah, October 1975 and March 1976: U.S. Geol. Survey Open-File Rept. 77–606, 6 p.

Friedman, Irving, and Denton, E. H., 1975, A portable helium sniffer: U.S. Geol. Survey Open-File Rept. 75–532, 6 p.

Maron, S. H., and Prutton, C. F., 1958, Principles of physical chemistry (3d ed.): New York, The MacMillan Co., 789 p.

Mazor, E., and Fournier, R. O., 1973, More on noble gases in Yellowstone National Park hot waters: Geochim. et Cosmochim. Acta, v. 37, p. 515–537.

Mazor, E., and Wasserburg, G. J., 1965, Helium, neon, argon, krypton, and xenon in gas emanations from Yellowstone and Lassen Volcanic National Parks: Geochim. et Cosmochim. Acta, v. 29, 443–454.

Morrison, T. J., and Johnstone, N. B., 1954, Solubilities of inert gases in water: Jour. Chem. Soc. (London), 1954, pt. 4, p. 3441–3446.

Mundorff, J. C., 1970, Major thermal springs of Utah: Utah Geol. and Mineralog. Survey Water-Resources Bull. 13, p. 42–43.

Nash, W. P., 1976, Petrology of the Quaternary volcanics of the Roosevelt KGRA, and adjoining area, Utah: Natl. Sci. Found. Final Rept., (Grant GI–43741), v. 1, 100 p.

Roberts, A. A., Friedman, Irving, Donovan, T. J., and Denton, E. H., 1975, Helium survey, a possible technique for locating geothermal reservoirs: Geophys. Research Letters, v. 2, no. 6, p. 209–210.

Ward, S. H., and Sill, W. R., 1976, Dipole-dipole resistivity surveys, Roosevelt Hot Springs KGRA: Natl. Sci. Found. Final Rept., (Grant GI–43741), v. 2, 43 p.

Weiss, R. F., 1971, Solubility of helium and neon in water and seawater: Jour. Chem. and Eng. Data, v. 16, no. 2, p. 235–241.

Jour. Research U.S. Geol. Survey
Vol. 6, No. 5, Sept–Oct. 1978, p. 571–578

CS_2 AND COS IN SOIL GASES OF THE ROOSEVELT HOT SPRINGS KNOWN GEOTHERMAL RESOURCE AREA, BEAVER COUNTY, UTAH

By MARGARET E. HINKLE and THELMA F. HARMS, Denver, Colo.

Abstract.—Soil-gas samples were collected in two parallel traverses across the Dome fault zone of the Roosevelt Hot Springs Known Geothermal Resource Area. Gas chromatographic analyses of the samples showed anomalous concentrations of CS_2 and COS east of the Dome fault; higher concentrations of CS_2 and COS also occurred over an area in which the hydrothermal system is close to the surface. Measurement of these gases may be useful in exploration for new geothermal sources.

Sulfur compounds in gaseous, dissolved, and precipitated forms are found in volcanic and hot spring areas all over the world. The Roosevelt Hot Springs KGRA (Known Geothermal Resource Area) near Milford, Utah, was chosen for a study of whether sulfur compounds migrating upward through alluvium from a KGRA could be collected and identified; this area was selected because the geophysics and geochemistry of the area are being intensely studied with regards to potential commercial development. The study area is located in the Basin and Range province, in the northwest corner of the Minersville 2 NE quadrangle in Beaver County, Utah, about 20 km northwest of the town of Milford (fig. 1, index map). The KGRA is associated with Quaternary silicic volcanic rocks that occur as domes, flows, and tuffs (Nash, 1976). Roosevelt Hot Springs itself is located at the north end of a wide north-south-trending fault zone (Dome fault) on the west side of the Mineral Mountains. The hot water is probably meteoric water that comes from the Mineral Mountains and is heated by the volcanic rocks. In the early 1900's, the spring issued boiling water, but it has since dried up (Mundorff, 1970); at present, the only activity is emission of a little steam. Discontinuous elongate mounds of opaline sinter and other hot spring deposits occur along the fault zone south of Roosevelt Hot Springs (Nash, 1976).

SAMPLE COLLECTION

The sulfur gas experiment reported here was run in conjunction with a soil-gas survey for helium, wherein anomalous concentrations of helium were found associated with the KGRA (Hinkle and others, 1978); the same sample sites were used for both studies. One hundred forty-four samples of soil gas were collected in two parallel east-west traverses of the KGRA; the Dome fault approximately bisects each traverse (fig. 1). The northern traverse started out along the line called "4000 N," which was established by the University of Utah for their studies, passed just south of Phillips Petroleum Co. drill site 3–1, and continued east, where the traverse jogged 30 m north to the "4030 N" University of Utah line. The traverse contained 72 stations; samples from the first 12 sites at the west end were collected at 100-m spacings, and samples from the rest were collected at 30-m spacings. The southern traverse started in Little Cedar Cove and followed a line that passed just south of the Phillips drill site 13–10; 72 soil-gas samples were collected at 30-m spacings. Traverses passing close to the two Phillips drill sites were selected because the wells intersect hot-water fracture zones at different depths; well 3–1 is approximately 884 m deep, and well 13–10 is approximately 1370 m deep (Ron Forrest, Phillips Petroleum Co. oral commun., April 19, 1977).

The gas collection method was the same as that used by Hinkle and Kantor (1978) to collect soil gases over buried sulfide mineralization at Johnson Camp, Ariz.; however, at Roosevelt Hot Springs, a mixture of 3A, 5A, and 13X types of mol sieve (molecular sieve) was used instead of only the 13X type used at Johnson Camp. Mol sieves are artificial zeolites with known-diameter cavities between the crystal lattices, in which the gases are trapped; type 3A has 0.3-nm (nanometer) cavities, type 5A has 0.5-nm cavities, and type 13X has 1-nm cavities. Mol sieves are used commercially for gas drying and for removal of sulfur compounds from natural gas. A 1–1–1 mixture of powdered molecular sieves was placed in screw-top glass jars and covered by a plug of cotton and crumpled nylon net. The open jars were inverted, placed in 0.5-m-deep holes that had been augered to collect soils for helium analysis, and covered with soil. The collectors were left buried in the ground for 8 weeks

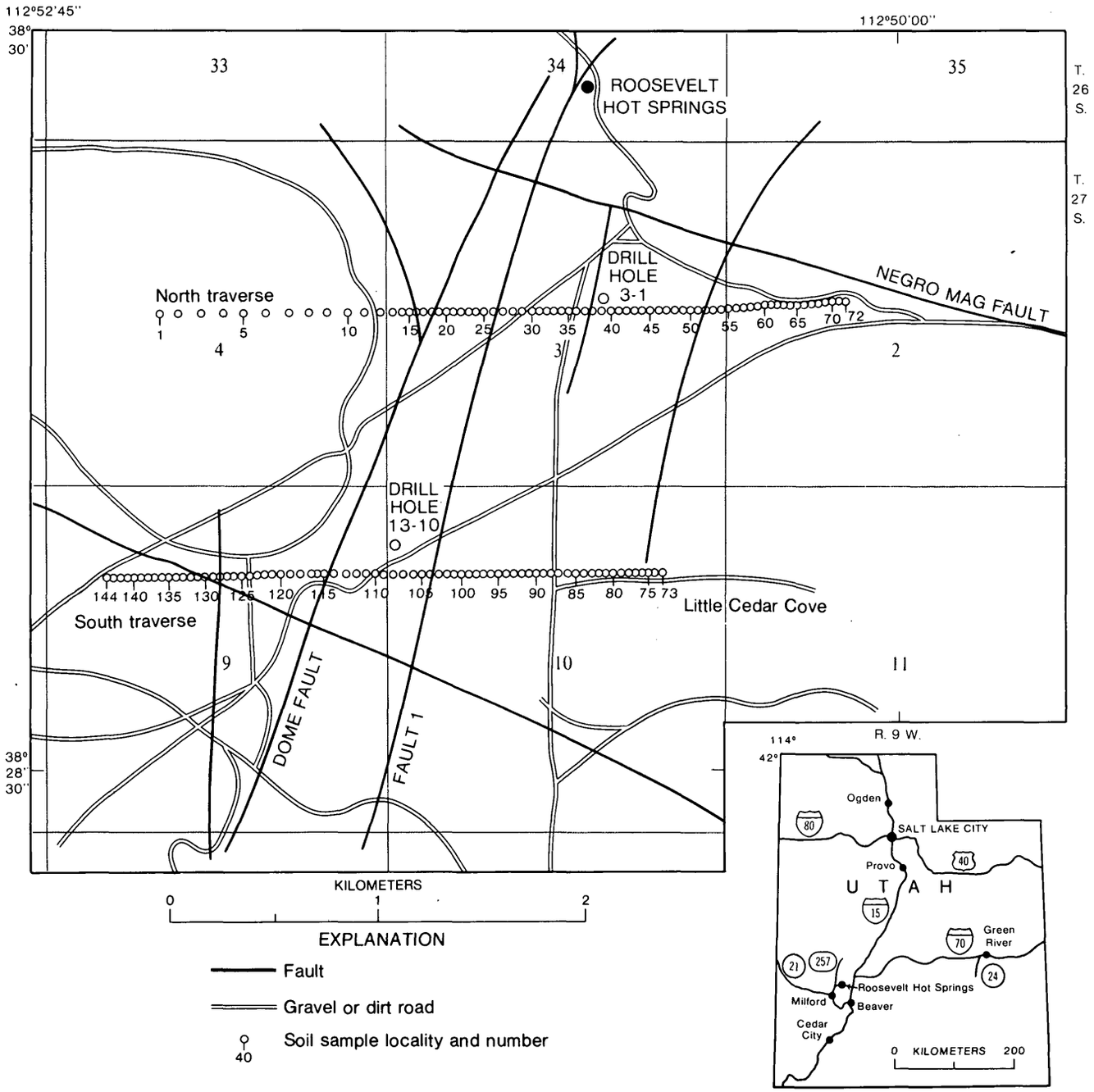

FIGURE 1.—Soil-gas sample stations, Roosevelt Hot Springs. Fault locations from Ward and Sill (1976, fig. 47).

from July 1, 1976, to September 1, 1976. The jars were then dug up, capped with an airtight screw cap, and returned to the laboratory for analysis.

ANALYSIS

Absorbed soil gases were analyzed by gas chromatography (GC). Sulfur compound analyses were completed within 4 weeks of collection. A Tracor 270 HM sulfur analyzer was used for the sulfur compounds (COS, H_2S, CS_2, and SO_2). The operating conditions were as follows:

column: 1.8 m×3 mm Teflon, packed with Chromosil 310,
carrier gas: nitrogen at 30 milliliters per minute,
detector: flame photometric,
temperature: column—ambient (25°C); detector —125°C.

One-gram portions of the mol sieves were placed in Vycor tubes. The Vycor tubes were connected to a gas delivery system that included the gas sampling loop

of the gas chromatograph. The entire gas delivery system was evacuated by means of a hand-operated vacuum pump, and the tubes containing the mol sieves were heated for 2 minutes in an electric tube furnace at 800°C. The gases absorbed on the mol sieve evolved into the gas sample loop, and activation of a gas sample injection valve transferred them from the loop into the gas chromatograph.

Known concentrations of COS, H_2S, CS_2, and SO_2 were prepared by dilution of emissions of permeation tubes with air, and standard curves were made. Lower limits of detection were COS, 40 ppb (parts per billion); H_2S, 70 ppb; CS_2, 50 ppb; SO_2, 100 ppb. Reproducibility of standards was ± 10 percent of concentration. Reproducibility of samples was ± 30 percent of concentration.

RESULTS

No H_2S or SO_2 was detected in any of the samples. COS concentrations ranged from less than 40 to 220 ppb. Along the north traverse, 28 of 72 samples contained detectable COS; these 28 samples averaged 55 ppb. Along the south traverse 23 of 72 samples contained detectable COS; these 23 samples also averaged 55 ppb. CS_2 concentrations ranged from less than 50 to 300 ppb. Along the north traverse, nine samples contained detectable CS_2, averaging 135 ppb. Along the south traverse, 14 samples contained an average of 65 ppb CS_2.

DISCUSSION

Both CS_2 and COS have been reported in magmatic gases (Finlayson and others, 1968; Nordlie, 1971). These compounds may migrate upward through faults and fractures either as gases or dissolved in steam.

A plan view of the traverses shows that CS_2 and COS are concentrated over known faults or their extensions (fig. 2).

Samples from the north traverse contain higher concentrations of both CS_2 and COS than do samples from the south traverse. In addition, both traverses contain more anomalous samples east of the Dome fault (fig. 3). The larger anomalies of sulfur compounds along the north traverse and east of the Dome fault may indicate greater proximity to the hydrothermal system in that area.

The small quantities of sulfur compounds collected by the mol sieves may indicate the great depths to the source of the compounds in the area sampled.

CONCLUSIONS

Sulfur compounds can be collected on mol sieves buried in the ground over a Known Geothermal Resource Area. Long-term burial of the mol sieve absorbers has two advantages over the grab-sample type gas collection: (1) the absorbers concentrate the minute quantities of desired gases present in the soil and (2) short-term fluctuations in barometric pressure or temperature that affect gas collection are eliminated. This study indicates that collection of sulfur compounds on mol sieve absorbers may be useful in exploration for geothermal sources.

Figures 2 and 3 follow "References Cited."

REFERENCES CITED

Finlayson, J. B., Barnes, I. L., and Naughton, J. J., 1968, Developments in volcanic gas research in Hawaii: Am. Geophys. Union Mon. 12, p. 428–438.

Hinkle, M. E., Denton, E. H., Bigelow, R. C., and Turner, R. L., 1978, Helium in soil gases in the Roosevelt Hot Springs Known Geothermal Resource Area, Utah: U.S. Geol. Survey Jour. of Research, v. 6, no. 5, p. 571–578.

Hinkle, M. E., and Kantor, J. A., 1978, Collection and analysis of soil gases emanating from buried sulfide mineralization in southeastern Arizona: Jour. of Geochem. Explor. (In press.)

Mundorff, J. C., 1970, Major thermal springs of Utah: Utah Geol. and Mineralog. Survey Water Resources Bull. 13, p. 42–43.

Nash, W. P. 1976, Petrology of the Quaternary volcanics of the Roosevelt KGRA, and adjoining area, Utah: Natl. Sci. Found. Final Rept. (Grant GI–43741), v. 1, 100 p.

Nordlie, B. E., 1971, The composition of the magmatic gas of Kilauea and its behavior in the near surface environment: Am. Jour. of Sci. v. 271, no. 5, p. 417–463.

Ward, S. H., and Sill, W. R., 1976, Dipole-dipole resistivity surveys, Roosevelt Hot Springs KGRA: Natl. Sci. Found. Final Rept. (Grant GI–43741), v. 2, 43 p.

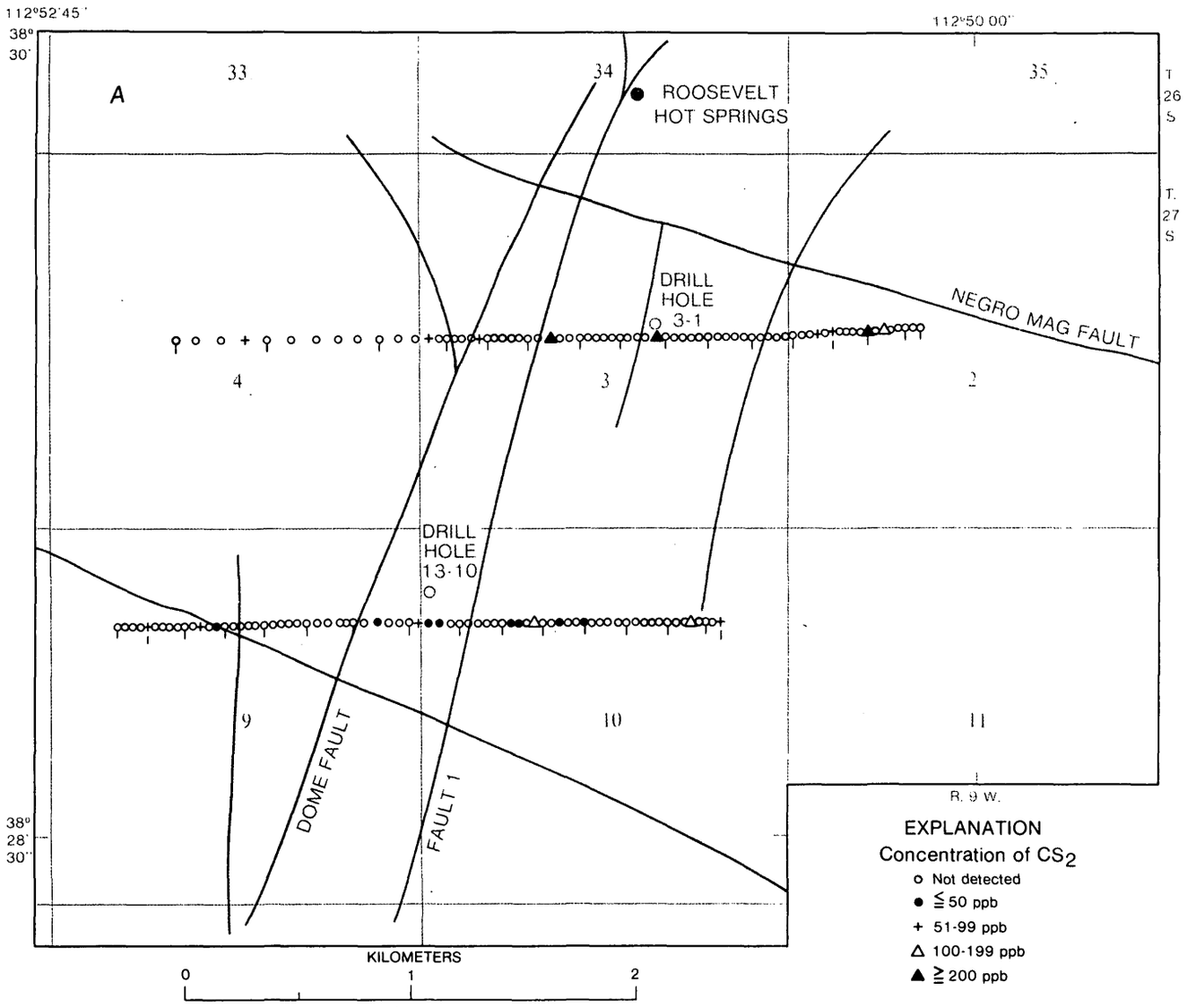

FIGURE 2.—CS_2 and COS collected on molecular sieve mixture (3A–5A–13X), buried two months. *A*, CS_2. *B*, COS. Heavy lines, faults (Ward and Sill, 1976, fig. 47).

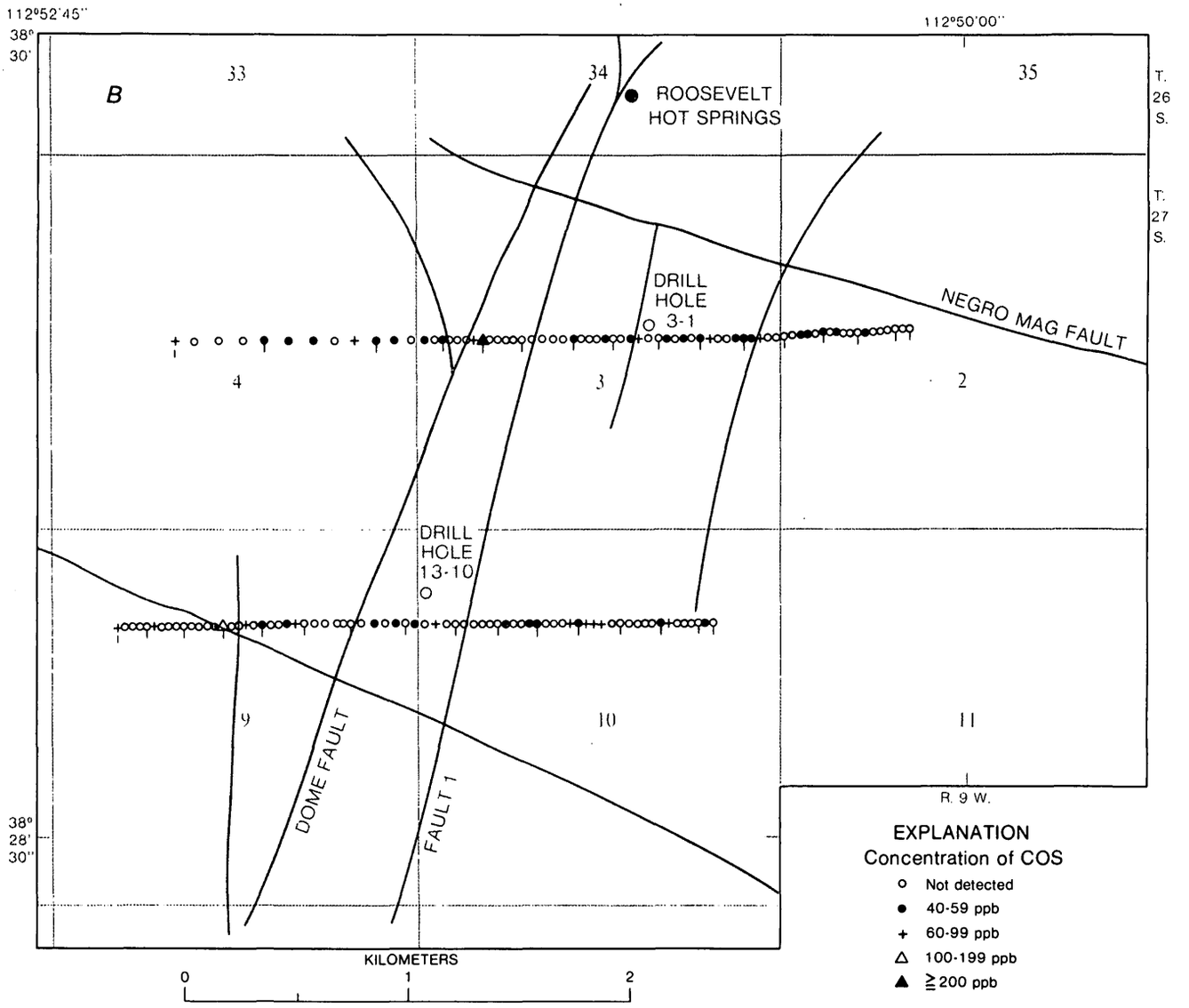

FIGURE 2.—Continued.

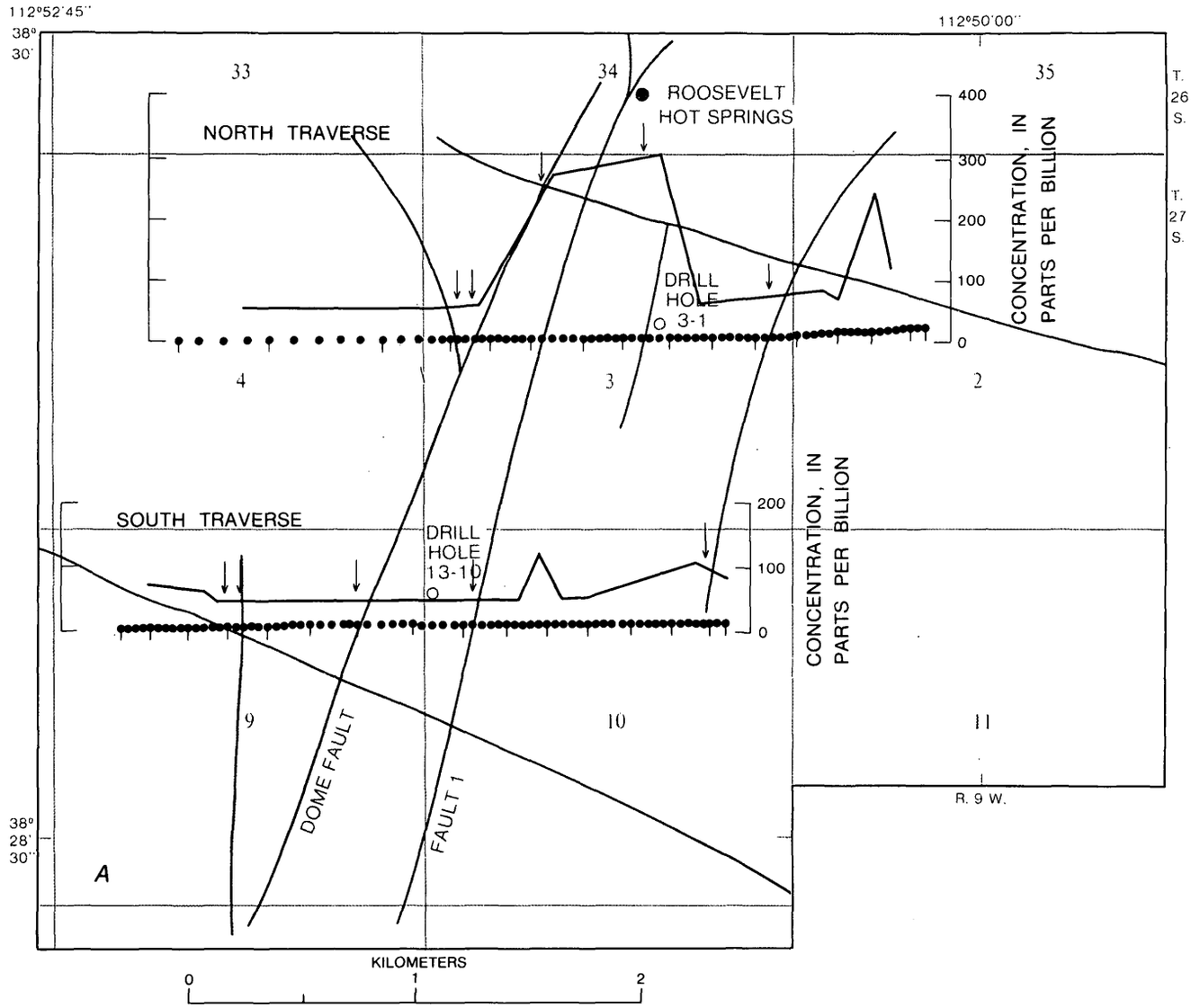

FIGURE 3.—Concentration of CS_2 and COS collected on molecular sieve mixture, Roosevelt Hot Springs KGRA. *A*, CS_2. *B*, COS. Arrows indicate position of faults (heavy lines) crossing the traverse.

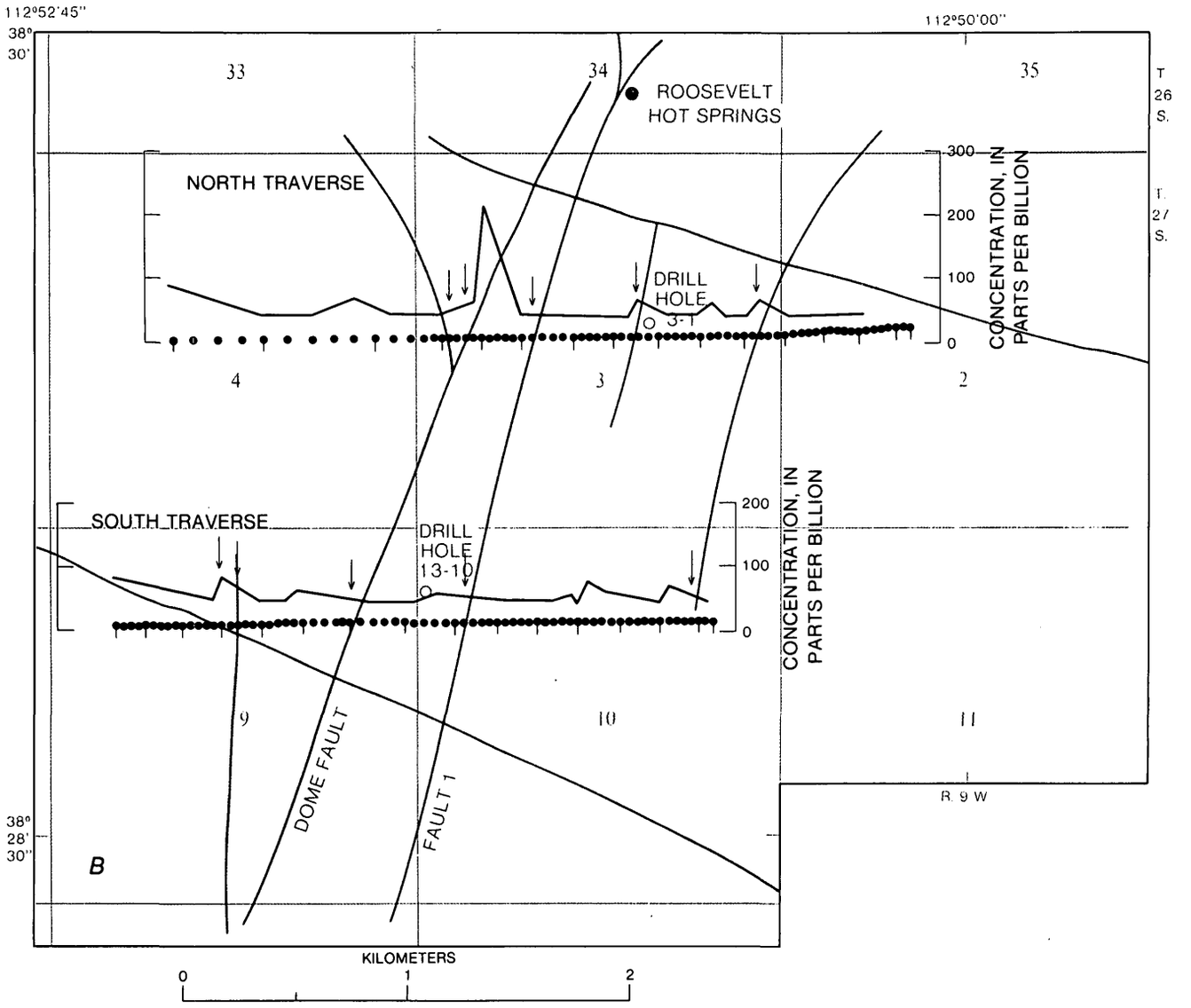

FIGURE 3.—Continued.

Jour. Research U.S. Geol. Survey
Vol. 6, No. 5, Sept.–Oct. 1978, p. 579–592

WOOD RIVER MINING DISTRICT, IDAHO—INTRUSION-RELATED LEAD-SILVER DEPOSITS DERIVED FROM COUNTRY ROCK SOURCE

By WAYNE E. HALL; ROBERT O. RYE, and BRUCE R. DOE,
Menlo Park, Calif.; Denver, Colo.

Abstract.—Lead-silver deposits in the Wood River mining district occur in shear zones in hornfelsed argillite of the Devonian Milligen Formation near granitic plutons and under the Wood River thrust fault. The principal ore minerals are argentiferous galena and sphalerite; siderite is the principal gangue. The $\delta^{34}S$ values of the sulfide minerals range from +2.2 to +15.0 permil, indicating that the sulfur had a shallow crustal source. $\Delta^{34}S$ values between sphalerite and galena range from +2.3 to +3.4 permil, corresponding to sulfur isotope temperatures between 280° and 182°C. Hydrothermal barite has a $\delta^{34}S$ of +13.2 permil. Lead isotope ratios are radiogenic, also pointing to a shallow crustal source. Quartz gangue has $\delta^{18}O$ of +16.4 permil and a calculated $\delta^{18}O_{H2O}$ at 270°C of +8.4 permil. This value is reasonable for a hydrothermal fluid that had reached equilibrium with the argillite country rock. The siderite gangue has $\delta^{18}O$ and $\delta^{13}C$ values of +14.0 and −5.5 permil, respectively. Fluid inclusions have homogenization temperatures of 244°–307°C and average 270°C. Freezing-stage measurements ranged from −1.85 to −2.8°C, suggesting salinities of 3.2 to 4.8 weight percent. The δD values of inclusion fluid in ore and gangue minerals are −110 to −120 permil. The geology, isotope, and fluid-inclusion data are consistent with a model of hydrothermal systems of meteoric water in faulted and shattered Paleozoic rocks near plutonic masses. This environment permitted deep circulation of the hydrothermal fluids, which dissolved the metals and sulfur from the Paleozoic host rocks and deposited ore in favorable beds or structures under the regional Wood River thrust fault.

The Wood River mining district is in Blaine County, south-central Idaho (fig. 1). The name is used informally here to include deposits clustered in three areas about 24 km (kilometers) apart on the east side of the Idaho batholith between Bellevue and Ketchum. Two areas are west of Hailey and Bellevue; the third is on the north side of the East Fork of the Big Wood River about 8 km east of Ketchum (fig. 1). The deposits west of Bellevue are also known as the Mineral Hill district (Anderson and others, 1950). We have not considered here the deposits a few kilometers west of Ketchum near Warm Springs Creek. These deposits would normally be included in the Wood River district, but we have not sampled them. However, they have generally similar geologic settings and probably similar origins to those reported here. The production from the Wood River district from 1880 to 1948 was about $38 million (Umpleby and others, 1930; C. W. Merriam and C. N. Bozion, unpub. data, 1942; Anderson and others, 1950). The Silver Star Queen and Triumph mines have produced substantial amounts of ore since 1948, but we do not have the records of production.

The lead-silver deposits were first described by Lindgren (1900). The Hailey 30-minute quadrangle, which includes all the Wood River mining district, was mapped by Umpleby, Westgate, and Ross (1930) during 1912–14 and 1923–29. Later the Idaho Bureau of Mines and Geology, under the supervision of A. L. Anderson (Anderson and others, 1950), studied the ore deposits and evaluated their potential. Hall and Czamanske (1972) studied the mineralogy and trace-element content of the lead-silver deposits that were being mined in 1969 near Bellevue and Hailey. The district was inactive at the time of this isotope study (1974–76); thus sampling was limited to dumps and samples collected for the earlier mineralogical study.

In this paper we apply the isotopes of carbon, hydrogen, lead, oxygen, and sulfur to interpret the origin of the hydrothermal fluids and the source of the metals and sulfur. Mapping by Hall of the Wood River (this study) and Darwin, Calif. (Hall and MacKevett, 1958, 1962), lead-silver districts indicated that both areas have very similar geologic settings—suggesting similar origins. The ore fluid components at Darwin were largely from a deep-seated magmatic source (Rye, Hall, and Ohmoto, 1974). This isotope study, however, gives an entirely different picture for the components of the hydrothermal ore fluids of the Wood River district and adds evidence to the point made by White (1974) that the origins of hydrothermal ore fluids are diverse.

Acknowledgments.—John Batchelder worked with Hall in the field and made many of the δD analyses and fluid inclusion extractions. Maryse Delevaux made

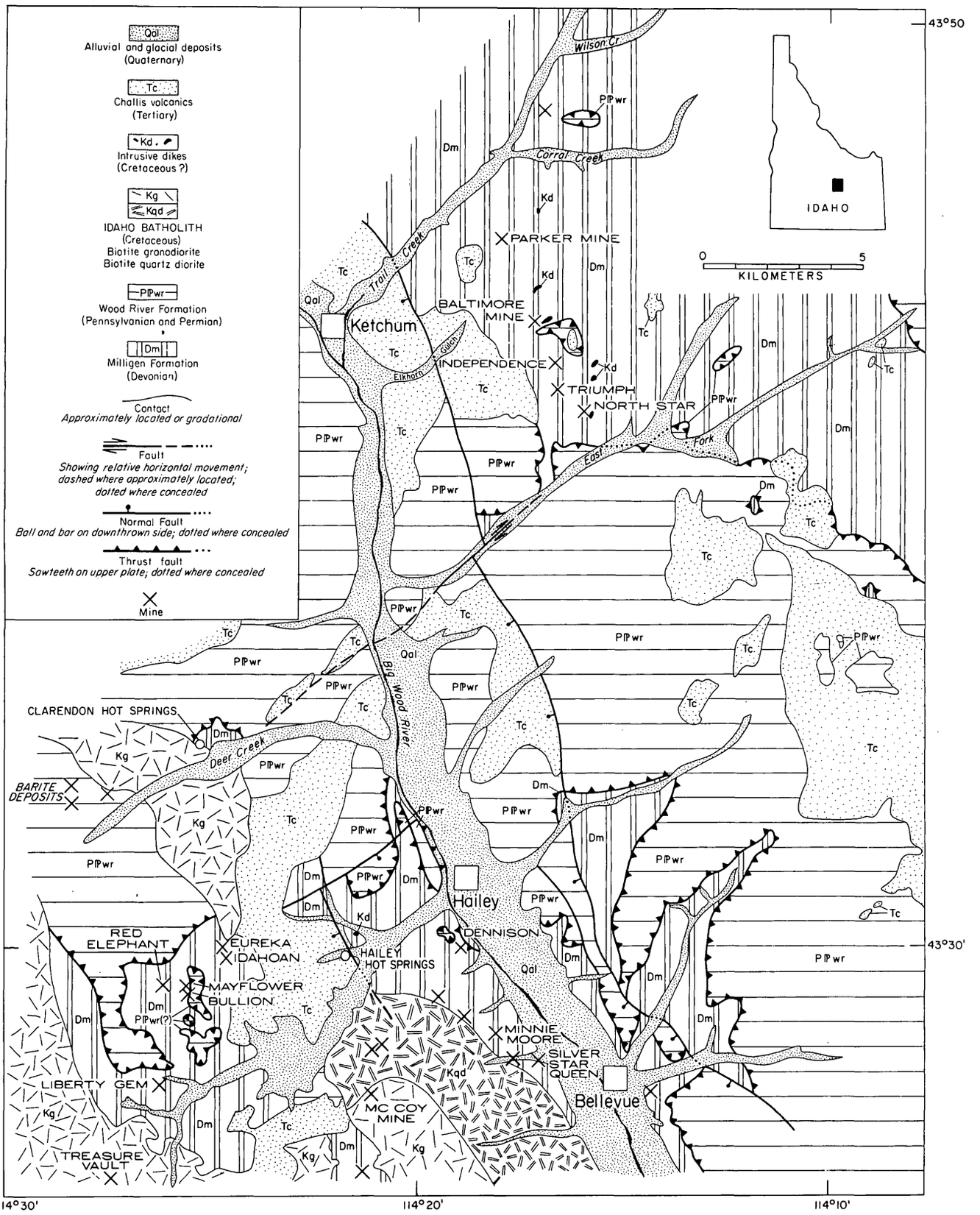

FIGURE 1.—Location and geologic map of the Wood River mining district, Blaine County, Idaho. Geology by W. E. Hall and J. N. Batchelder 1969–76.

the lead isotope analyses. L. A. Adami made the $\delta^{18}O$ analyses of biotite, quartz, and siderite in the laboratory of J. R. O'Neil. Rupert House, who has a lease on the North Star mine, provided us with deposit samples for which we are grateful. Guy Jones and J. J. Jones of the National Forest Service at Ketchum, Idaho, read the manuscript and made many helpful criticisms.

GEOLOGY AND ORE DEPOSITS

The Wood River area is underlain by a sequence of Paleozoic sedimentary rocks, more than 3650 m thick, that are intruded on the west by the Idaho batholith of Late Cretaceous age and by lamprophyre dikes and that are unconformably overlain by the Challis Volcanics of Eocene age. A buried intrusive body of probable Eocene age is inferred in the Triumph mine area in the northeast part of the mapped area (fig. 1).

Sedimentary rocks

The Milligen Formation is the oldest formation exposed in the Wood River area, and it is the host rock for most of the lead-silver deposits (fig. 1). The Milligen Formation consists of more than 1000 m of interbedded siliceous carbon-rich argillite, fine-grained quartzite, and some siltite, silty limestone, dolomite, and chert. The argillite has a moderately well developed fracture cleavage, which is absent in the other Paleozoic rocks; this cleavage is at a steep angle to the original bedding. The Milligen Formation is entirely Devonian on the basis of conodont collections studied by Sandberg, Hall, Batchelder, and Axelson (1975).

The Milligen Formation is overlain by the Wood River Formation of Middle Pennsylvanian to Permian age. The Wood River, which is more than 2990 m thick, consists of a basal conglomerate, 120 m thick, and a thick overlying sequence of calcareous sandstone, limestone, and quartzite; the formation was divided into seven units by Hall, Batchelder, and Douglass (1974). Since then Hall and Batchelder have mapped a younger sequence of Wood River Formation overlying unit 7 on the ridge between Wilson and Trail Creeks. This unit, here designated unit 8, consists of about 1770 m of interbedded gray and brown siltstone, siltite, quartzite, dark-gray siliceous argillite locally containing abundant worm trails that resemble Scalarituba, and minor silty and sandy limestone beds that contain a poorly preserved microfauna. The measured section of unit 8 contains at least one isoclinal fold and is cut by a fault, and part of the section is so very poorly exposed that the thickness is suspect. Thin sections of limestone from unit 8 were examined by G. P. Sossipatrova of the Institute of Arctic Geology, Leningrad, U.S.S.R., who identified lagenid forms (oral commun. to Betty Skipp, Sept. 1975), and by Bernard Mamet of the University of Montreal, who identified nodosariids; Mamet (oral commun. to Betty Skipp, Dec. 1975) said the assemblage looks post-Carboniferous, possible Late Permian or Early Triassic. J. C. Dover (unpub. data, 1976) collected a limited fauna of scaphopods and gastropods with fragments of pelecypods, bryozoans, and corals from apparently about the same or a slightly lower part of the Wood River Formation on the West Fork of Trail Creek, 13.6 km northwest of our measured section on Wilson Creek ridge. This fauna is tentatively assigned to the Permian (Leonardian or Guadalupian) by E. L. Yochelson.

Intrusive rocks

The Paleozoic rocks are intruded by two plutons of the Idaho batholith west of Bellevue, and a granitic intrusion of probable Eocene age is inferred at depth in the Triumph mine area southeast of Ketchum (fig. 1). The pluton in the mine area, 1.6 km west of Bellevue, is composed of equigranular medium-grained dark-gray biotite quartz diorite. The pluton is about 8 km long in a northwest-southeast direction and 3 km wide (fig. 1). It is a laccolithic body dipping about 30° west. The quartz diorite contains quartz, plagioclase (An_{40-45}), biotite, clinopyroxene, and minor potassium feldspar, hornblende, orthopyroxene, apatite, and opaque minerals. The potassium feldspar has a grid twinning. The mafic minerals are in a large part altered to chlorite, and the plagioclase has a saussuritic alteration. The ore deposits near Bellevue are peripheral to this intrusion. A pluton of similar lithology intrudes the Milligen and Wood River Formations in the Eureka mine area about 8 km west of Hailey (fig. 1).

A pluton of biotite granodiorite intrudes the quartz diorite pluton about 6 km west of Bellevue (fig 1). The biotite granodiorite is a coarse-grained porphyritic granitoid rock with phenocrysts of potassium feldspar as much as 1 cm long in a coarse-grained matrix. The rock contains quartz, potassium feldspar, and plagioclase (An_{30-35}) as major components and 5 to 10 percent biotite and euhedral 0.5- to 1-mm-long sphene as accessory minerals. The biotite is largely altered to chlorite, and the feldspar has a saussuritic alteration. A potassium-argon age of biotite from this pluton is 81.7 ± 2.5 million years (Berry and others, 1976, p. 10). The granitic rocks are cut by numerous

small mafic dikes. The Challis Volcanics, of Eocene age, locally nonconformably overlie the older igneous and sedimentary rocks.

Structure

The structural history of the Wood River area has been described by Dover (1969) and Skipp and Hall (1975). The Paleozoic rocks have been folded, thrust faulted, and subsequently intruded by the Idaho batholith, which deformed the thrust faults and contact metamorphosed the Paleozoic sedimentary rocks to hornfels and calc-hornfels. The Milligen and Wood River Formations are each allochthonous (Dover, 1969; Skipp and Hall, 1975). The Milligen allochthon moved eastward possibly as much as 48 km during the Antler and Sevier orogenies (Skipp and Hall, 1975). It is composed entirely of the Milligen Formation and is estimated to be 1220 m thick. The allochthon is highly deformed, containing tight drag folds with axial planes overturned toward the east. The base of the formation is not exposed in the mining district but is inferred to be a thrust fault (Dover, 1969; Skipp and Hall, 1975). The Wood River allochthon is composed entirely of the Wood River Formation; it is estimated to be 1520 m thick, which is much thinner than the formation. In most places the allochthon has broad open folds that are truncated by the Wood River thrust fault, but tight folds occur on the northeast side of the allochthon. It moved eastward on the Wood River thrust fault an estimated 16–24 km during the Sevier orogeny (Skipp and Hall, 1975).

The Paleozoic sedimentary rocks and the intrusive and volcanic rocks are cut by many steep faults that displace the thrust sheets. Faulting must have continued intermittently at least since the intrusion of the Idaho batholith to the Holocene. Many of the ore deposits are localized in faults that strike either about N. 20° W. or about N. 70° W. and dip 35° to 45° SW. The movement on the mineralized fissures is predominantly pre-intrusive and pre-thrusting in age. The fissures are strongly sheared zones that structurally controlled both ore and in some places dikes or sills, which are locally mineralized. Much of the ore is strongly sheared, and the veins show abundant evidence of shearing and rehealing.

Some large steep normal faults strike north to northwest and have moved during the Cenozoic. They displace the Challis Volcanics and some ore bodies. The hot springs west of the Wood River valley and the flowing wells at Indian Springs east of the Wood River valley are on or near these faults.

Ore deposits

Ore in the Wood River area occurs as veins in highly sheared zones in Paleozoic sedimentary rocks near granitic intrusions, as replacement bodies at the intersections of sheared zones and limestone beds, and as veins in granitic rocks. Most of the production has been from high-grade lead-silver ore bodies that contain some gold. Where the veins are in granitic rocks, the lead and silver values generally decrease and gold values increase.

The lead-silver deposits are in or near strongly sheared zones, predominantly in contact metamorphosed siliceous argillite and micritic limestone of the Milligen Formation near intrusive contacts and under the regional Wood River thrust fault. The deposits near Bellevue are in at least eight parallel sheared zones that strike N. 70° W. in contact metamorphosed Milligen Formation between the Wood River thrust fault on the east and the Idaho batholith on the west, and in a few places shear zones extend into the laccolith. The sheared zones dip at moderate angles to the southwest. Ore occurs in veins and lenses within the sheared zones and has sharp contacts with them. The veins may be as much as 750 m long, but high-grade ore is localized within shoots in the veins. The largest ore shoots that have been mined were in the Bullion and Minnie Moore mines (fig. 1). Umpleby, Westgate, and Ross (1930) reported that one of the ore shoots at the Bullion mine had a pitch length of 366 m, a maximum thickness of more than 4.5 m, and a breadth of about 20 m.

In the Triumph mine area north of the East Fork of the Wood River, the lead-silver ore occurs in veins striking about N. 70° W. and in replacement deposits at the intersections of sheared zones and limestone beds in metamorphosed Milligen Formation, similar to ore controls in the Bellevue area (Anderson and others, 1950, p. 44). The Milligen argillites and limestones are in part metamorphosed to hornfels and calc-hornfels. Intrusive rocks are limited to small dikes and sills of andesite and lamprophyre, but a buried granitic intrusion is inferred because of the widespread low-grade metamorphism; Umpleby, Westgate, and Ross (1930, p. 89) also inferred a buried intrusion in this area.

Mineralogy

The lead-silver deposits consist of massive sulfide ore or banded ore with alternate layers of sulfide minerals, siderite, and minor quartz. Originally the sulfide ore was coarse grained, but much of the ore subsequently was sheared to a foliated fine-grained mass.

The mineralogy and minor-element content of the lead-silver ores have been described by Hall and Czamanske (1972). Galena and sphalerite are the principal ore minerals in a gangue of siderite and sheared host rock. Arsenopyrite, bournonite, chalcopyrite, freibergite, gudmundite, marcasite, pyrite, and pyrrhotite occur in lesser amounts. The iron sulfide minerals were observed in moderate amounts only at the Liberty Gem mine and in veins in granitic rocks. The galena is argentiferous. Czamanske found, by electron microprobe analyses, that slightly less than half of the silver is coupled with antimony in solid solution in the galena; the rest is present in micrometer-size silver-antimony inclusions of five compositions, though principally as diaphorite (Hall and Czamanske, 1972). Where the veins extend into quartz monzonite or quartz diorite, the arsenopyrite, chalcopyrite, pyrite, and gold increase, and galena and silver decrease.

The paragenetic sequence of ore and gangue minerals has been described by Hall and Czamanske (1972). The paragenetic sequence given in table 1 is speculative because the veins have been repeatedly sheared and annealed, because the paragenetic sequence has been patched together from observations from widely spaced localities that could not be unequivocally related to each other, and because few mines were accessible for collection and observation.

TABLE 1.—*Mineral sequence, Wood River mining district*
[Each downrule indicates shattering]

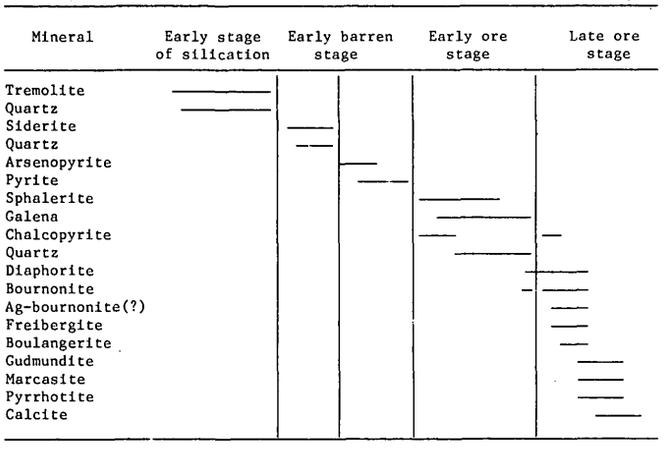

ISOTOPE AND FLUID INCLUSION DATA

$\delta^{34}S$ data

The $\delta^{34}S$ values of the sulfide minerals range from +2.2 to +15.0 permil (table 2). There is no systematic variation of $\delta^{34}S$ values of the sulfide minerals within a deposit or with distance from an intrusive contact or within a cluster of deposits. Most data are from the Silver Star Queen mine (table 2; fig. 1). The sulfur isotopic composition of individual minerals is similar from the surface to the 900-foot level. The Silver Star Queen ore consists of massive argentiferous galena, sphalerite, and bournonite. The order of enrichment of ^{34}S in these minerals is sphalerite > bournonite > galena. Where pyrite and (or) chalcopyrite are present, the order is pyrite ≈ chalcopyrite > sphalerite > galena. The systematic fractionation of ^{34}S between mineral pairs indicates ore deposition under approximate equilibrium conditions.

Sulfide minerals from the Treasure Vault and Liberty Gem mines have lower ^{34}S values than those from the other mines. The Treasure Vault is a gold-quartz vein with some disseminated pyrite and galena in a shear zone in biotite granodiorite. The Liberty Gem ore contains argentiferous galena and sphalerite and, in addition, considerable pyrite and chalcopyrite.

TABLE 2.—*Sulfur isotopes*

[gn, galena; sl, sphalerite; bour, bournonite; arg, argentiferous; sid, siderite; qtz, quartz; ct, calcite; py, pyrite. Temperatures from Czamanske and Rye (1974).]

Sample No.	Mine	Level	Mineral	$\delta^{34}S$	$\Delta^{34}S$	Temp., °C	Type of ore
WH70-6	Silver Star Queen	900	Bournonite Galena	12.56 10.83	1.73	----	Massive sheared fine-grained arg gn, and bour.
WH70-7	Silver Star Queen	900	Bournonite Galena	12.65 11.23	1.42	----	Massive sheared fine-grained arg gn, and bour.
WH70-11	Silver Star Queen	900	Sphalerite Galena	14.61 11.95	2.66	240	Massive sheared fine-grained gn-sl.
WH70-12	Dennison	Adit	Galena	10.91	----	----	Coarse-grained gn ore.
WH70-13B	Eureka	250	Galena	6.30	----	----	Sheared coarse-grained sl-gn ore in sid gangue.
WH70-16	Silver Star Queen	900	Sphalerite Galena	14.02 10.66	3.36	182	Coarse-grained massive gn-sl ore.
WH70-17	Silver Star Queen	450	Sphalerite Galena	14.10 10.99	3.11	201	Sheared gn-sl-py ore with qtz and sid gangue.
WH74-1B	Independence	Dump	Galena	11.41	----	----	Coarse-grained massive gn ore.
WH74-2B	North Star	Dump	Sphalerite Galena	9.47 7.18	2.29	280	Coarse-grained massive gn-sl ore.
A-176	Liberty Gem	Dump	Pyrite Chalcopyrite Galena	4.29 4.36 2.19	2.17, 2.10	270	Low grade chalcopyrite-gn-py ore with qtz-ct gangue.
A-43	Minnie Moore	Dump	Galena	6.10	----	----	Coarse-grained gn in qtz-sid gangue.
A-227	Treasure Vault	Dump	Pyrite Galena	7.16 3.96	3.20	----	Low-grade qtz-py-gn ore.
A-36	Silver Star Queen	Open cut	Galena	10.85	----	----	Specimen rod-shaped qtz, sid and disseminated gn.
D-247	Trail Creek Prospect	Open cut	Galena	6.73	----	----	Fine-grained high-grade gn ore.
D-831A	Sun Valley Barite	Open cut	Barite	13.20	----	----	Massive fine-grained hydrothermal barite.

Sulfur isotope geothermometry

The $\Delta^{34}S$ values between sphalerite and galena in the massive argentiferous galena ores at the Silver Star Queen, Eureka, Independence, North Star, and Dennison mines range from +2.3 to +3.4 permil, and the sulfur isotope temperatures range between 182° and 280° C. (Note: The fractionation factors used in this paper are those of Czamanske and Rye (1974) for sphalerite and galena determined over the temperature range 600° to 275°C.) The data are sparse but suggest that the temperature of ore deposition in the Bellevue area at the Silver Star Queen mine was lower than at the North Star–Independence area north of the East Fork of the Wood River (fig. 1). The ore at the Silver Star Queen mine is strongly sheared, and much of it recrystallized during shearing to a steel-textured galena. The lower temperatures recorded for this deposit may be real, or they may reflect a re-equilibrium during shearing. The two $\Delta_{bour-gn}$ values of 1.4 and 1.6 permil suggest that bournonite-galena could be developed into a useful sulfur isotope thermometer once fractionation factors are known.

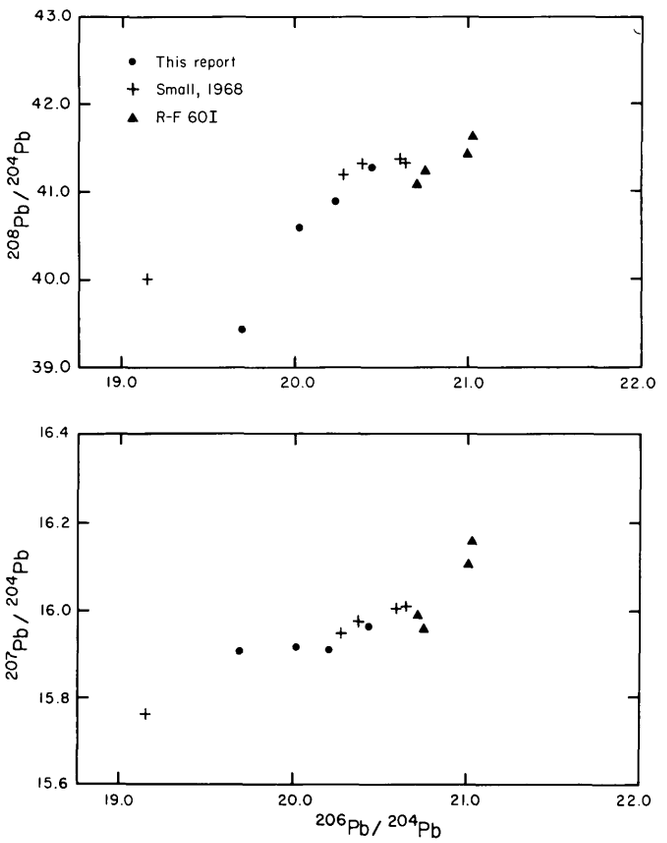

FIGURE 2.—Plot of lead isotope ratios, Wood River mining district.

Lead isotope data

The isotope composition of lead in the ores of the Wood River district is highly radiogenic (table 3; fig. 2). The plots of $^{208}Pb/^{204}Pb$ against $^{206}Pb/^{204}Pb$ and $^{207}Pb/^{204}Pb$ against $^{206}Pb/^{204}Pb$ fall within the data fields for sediments and mineral deposits formed in enclosed basins, that is, present-day sediments in Hudson Bay and ore deposits of the Mississippi Valley-type, and lie outside the field for deposits associated with magmatic waters or otherwise related to igneous activity (fig. 3). The most significant difference between the isotopic compositions of the Wood River ores and those of the Mississippi Valley is the relatively greater value of $^{207}Pb/^{204}Pb$ for the deposits of the Wood River district.

TABLE 3.—*Isotopic composition of lead in the Wood River mining district*

[Analyses on galena in this report are by the triple filament thermal emission method and on the rocks by the silica gel emittor technique. M.H. Delevaux, analyst. Analyses should be within 0.1 percent of absolute. Data of Small are by the thermal emission method and are of similar quality. Data of Bate and others are of reduced quality with uncertainties of about 1 percent for each ratio.]

Sample No.	Mine	Level (feet)	$\frac{206Pb}{204Pb}$	$\frac{207Pb}{204Pb}$	$\frac{208Pb}{204Pb}$	Reference
			Galena			
WH74-2B	North Star	Dump	19.688	15.906	39.438	This report
A-176	Liberty Gem	Dump	20.013	15.917	40.619	Do.
WH70-13B	Eureka	250	20.220	15.910	40.904	Do.
WH70-16	Silver Star Queen	250	20.421	15.962	41.301	Do.
UBC-577	Silver Star Queen	---	19.158	15.763	39.982	Small, 1968
UBC-581	do	---	20.279	15.947	41.214	Do.
UBC-579	do	---	20.378	15.978	41.275	Do.
UBC-578	do	---	20.597	16.018	41.387	Do.
UBC-580	do	---	20.623	16.021	41.320	Do.
	Minnie Moore	Stope 952 level 900	20.72	15.99	41.08	Bate and others[1]
	Minnie Moore	---	20.74	15.96	41.22	Do.
	Minnie Moore	---	21.00	16.11	41.45	Do.
	Minnie Moore	Stope 952 level 900	21.02	16.16	41.68	Do.

Sample No.	Location	Rock type	$\frac{206Pb}{204Pb}$	$\frac{207Pb}{204Pb}$	$\frac{208Pb}{204Pb}$	Concentration (ppm) U	Th	Pb
			Host rock					
A230	McCoy	Biotite grano-diorite	19.572	15.762	39.309	---	---	---
WH2112	Sawmill Gulch	Black siliceous argillite	19.308	15.673	39.526	1.05	4.41	4.12

[1]Data are from an unpublished manuscript and are published in Russell and Farquhar (1960). Data as published were not in absolute ratios and have been converted to absolute through comparison of analyses on deposits we have analyzed in common. Data of Bate and others have been divided by 1.0106 for $^{206}Pb/^{204}Pb$, 1.0155 for $^{207}Pb/^{204}Pb$, and 1.0228 for $^{208}Pb/^{204}Pb$.

To check the possible source of the lead in the deposits, we analyzed one sample of Milligan argillite (the host rock of the deposits) and one sample of potassium feldspar from the adjacent biotite granodiorite pluton. The argillite contains less lead (about 4 parts per million) than most granitic rocks (about 15–20 ppm), and its composition does not match the ores. However, semiquantitative emission spectrographic analyses of 34 samples of argillite and limestone of the Milligen Formation range from 7 to 70 ppm lead and average 25 ppm (Frank Simons, J. C. Dover, S. W. Hobbs, E. T. Tucket, and J. Ridenour, unpub. data, 1976). Perhaps our sample was not representative of the Milligen Formation. The potassium feldspar of the biotite granodiorite from the McCoy mine (A–230) likewise does not match the lead isotope composition of the ores (table 3). Three of the four ore samples have values of $^{208}Pb/^{204}Pb$ greater than any known Mesozoic or Cenozoic igneous rock in the Rocky Mountain region (fig. 3). Thus, the lead isotopes suggest a shallow crustal source for the lead, but the sparse data cannot pinpoint the source rock.

Oxygen and carbon isotope data in vein quartz and siderite and argillite host rock

The ^{18}O and ^{13}C data for vein quartz and siderite are given in table 4. The $\delta^{18}O$ values were determined on vein quartz from the Silver Star Queen mine, and the $\delta^{18}O$ and $\delta^{13}C$ values on two siderite gangue samples from the Eureka mine. Most of the quartz is fine grained and milky in color. It was introduced with galena and cuts sheared siderite. The quartz from the Silver Star Queen mine had a $\delta^{18}O$ of +16.4 permil. Calculated $\delta^{18}O_{H2O}$ in equilibrium with the quartz at 270°C is +8.4 permil. This value is heavier than a water that would be in equilibrium with a granitic rock and is one that would be expected of a water that had partially exchanged ^{18}O with the Paleozoic country rock with high ^{18}O values. Two samples of argillite were run. An unaltered argillite from Sawmill Gulch had a $\delta^{18}O$ value of +20.7 permil and a hornfelsed argillite from the Minnie Moore mine had a $\delta^{18}O$ of +18.8 permil, confirming that the country rock has high $\delta^{18}O$.

The $\delta^{18}O$ and $\delta^{13}C$ values were determined for two siderite samples from the Eureka mine. The $\delta^{18}O$ values were +14.8 and +13.3 permil; the $\delta^{13}C$ were −5.23 and −5.58 permil, respectively. The $\delta^{18}O_{H2O}$ of the water in equilibrium with the siderite at 270°C is +8.8 and 7.3 permil. The biotite granodiorite (A–230) has a $\delta^{18}O$ of 10.9 permil (table 4). The calculated $\delta^{18}O_{H2O}$ values of the fluids that deposited quartz (+8.4 permil) and siderite (about +8 permil) were either in approximate equilibrium with the argillite host rocks at the temperatures of ore deposition or with the plutonic rocks at very high temperatures.

Fluid inclusions

Abundant fluid inclusions were observed in quartz, siderite, and sphalerite in the veins and in quartz in the hornfelsed Milligen argillite. Most of the fluid inclusions are less than 5 μm in diameter and can be studied only optically using an oil-immersion lens. Less than 1 percent are in the range 5 to 15 μm in diameter, and some of these were studied with the freezing and heating stages.

Sphalerite has abundant small and a few large, primary, two-phase inclusions that are oriented on growth plates. The two-phase inclusions contain liquid H_2O and a vapor bubble that occupies about 25 percent of the inclusion. In some, the vapor bubble has an outer ring of liquid CO_2. In addition, many small secondary or pseudosecondary inclusions in sphalerite occur along cleavage planes and fractures. None of the fluid inclusions had daughter minerals. Siderite has abundant minute two-phase secondary and pseudosecondary inclusions along cleavage planes and fractures. Quartz also has abundant pseudosecondary and secondary inclusions, mostly along closely spaced fractures.

Quartz in hornfelsed argillite adjacent to the biotite granodiorite and quartz diorite near Bellevue contains minute, high-temperature inclusions with liquid H_2O, a vapor, and commonly several daughter minerals (Hall and Czamanske, 1972). Samples from areas peripheral to the biotite granodiorite pluton contain as many as four daughter minerals. The daughter minerals always include halite and some hematite; anhydrite(?), and sylvite(?) are less abundant. These high-salinity inclusions were not found in the ore or gangue minerals in the vein deposits. They were formed earlier than the ore during contact metamorphism of the Milligen Formation.

Heating- and freezing-stage measurements were possible only on the rare, large primary fluid inclusions in sphalerite in sample WH70–8A from the 250-foot level of the Eureka mine. The measured homogenization temperatures ranged from 244° to 307°C and average about 270°C (table 4). The stratigraphic cover at the time of mineralization was probably about 1500 m. This figure is the estimated thickness of the Wood River allochthon that overlies the ore deposits. The temperature correction for hydrostatic pressure would be about +20°C (Lemmlein and Klevtson, 1961). We consider 270°±20°C as the tem-

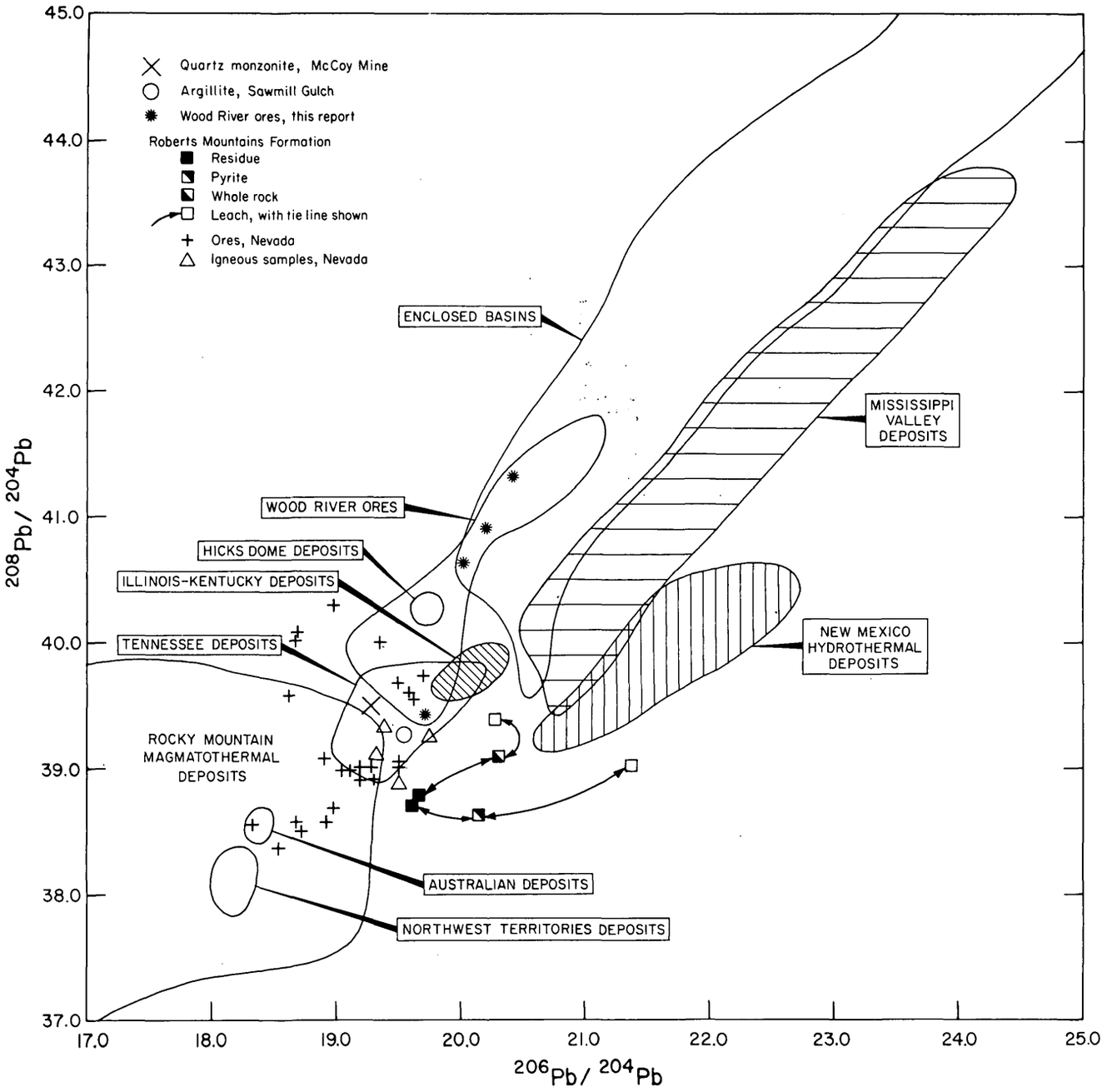

FIGURE 3.—Plots (above and on facing page) of lead isotope ratios, showing relation of Wood River mining district to other districts

perature of deposition for much of the sulfide ore in the area, on the basis of these homogenization temperatures and the data on fractionation of sulfur isotopes between coexisting sulfide minerals (table 2). This temperature is lower than the estimated temperature of 350°C or higher based on annealing experiments on galena by Czamanske (Hall and Czamanske, 1972), but we have no explanation for the difference.

The salinities of the ore fluid appear to be low. No fluid inclusions were observed with daughter minerals. Freezing stage measurements ranged from −1.85° to −2.8°C for primary fluid inclusions in sphalerite in specimen WH70-8A (table 4). These measurements suggest salinities in the range 3.2 to 4.8 weight percent NaCl equivalent for the sulfide stage ore fluid at the Eureka deposit.

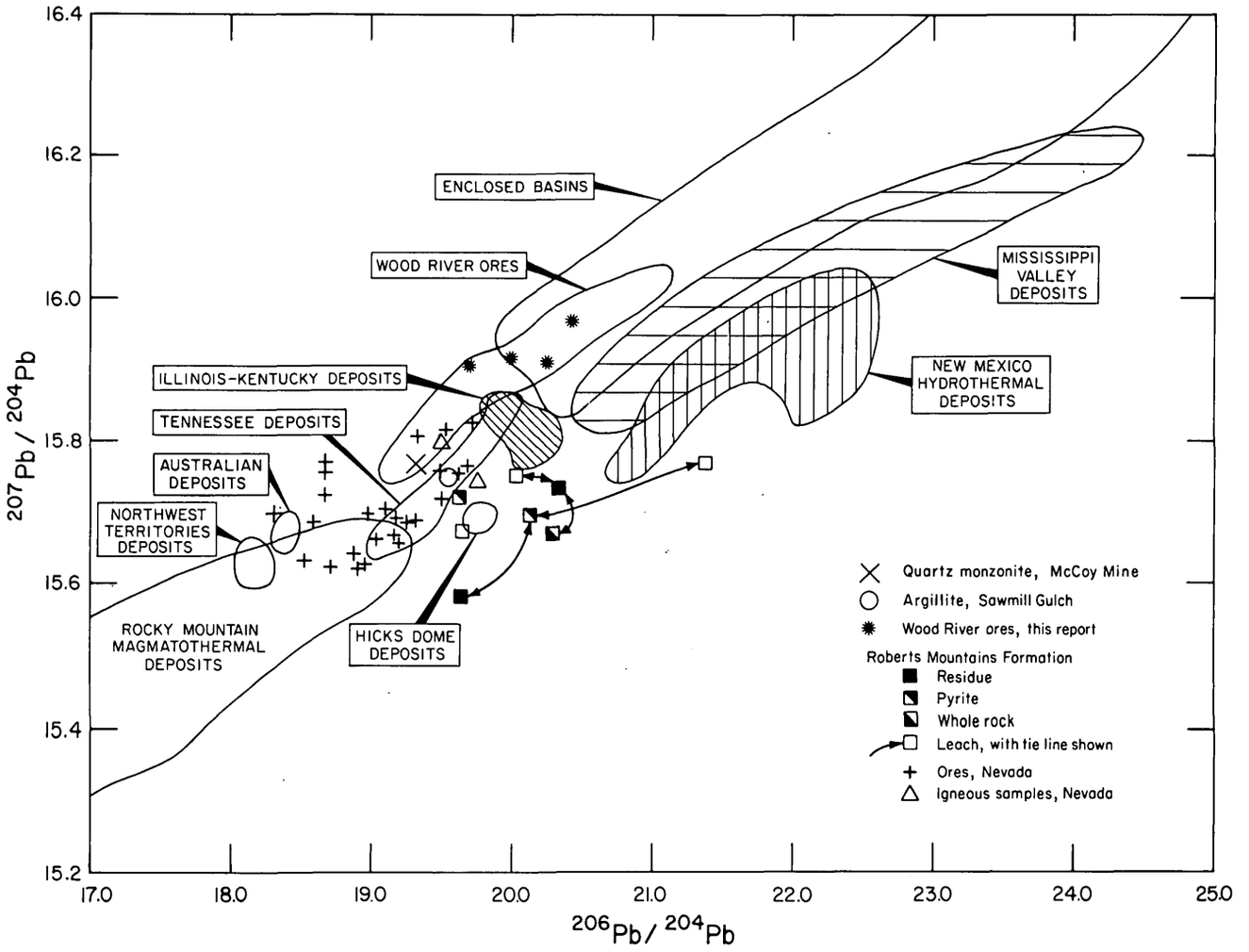

FIGURE 3.—Continued

Five samples of ore and gangue minerals were crushed in evacuated stainless-steel tubes to liberate inclusion fluid. The δD values of inclusion fluid in the quartz and siderite gangue minerals and in sphalerite and galena were all in the range −110 to −120 permil (table 4). CO_2 was detected in all the samples that were crushed, and optical observations suggest that liquid CO_2 was present sporadically in the fluid inclusions and that CO_2/H_2O was variable.

Inclusion fluids from hornfels from the Minnie Moore mine area and from a contact metamorphosed quartzite area 5.6 km southwest of Bellevue near Sky Ranch flat had δD values of −102 and −92 permil, respectively. These values are −8 to −28 permil larger than the range of δD values from the ore and gangue minerals. This difference could result from a heavier, possibly a magmatic water, mixing with meteoric water during metamorphism, but there is no evidence for the heavier water during formation of the ore deposits. A CH_4/H_2O fractionation during metamorphism of the graphite-rich Milligen Formation could also have resulted in larger δD values in the water.

Hydrogen, oxygen, and lead isotopic data of the biotite granodiorite

A sample of biotite granodiorite from the McCoy mine was crushed and sized, and mineral separates were made of the biotite, potassium feldspar, and quartz (table 4, sample A-230). The biotite was analyzed for its δD and $\delta^{18}O$ values. The $\delta^{18}O$ values of the quartz and potassium feldspar and the lead isotopic composition of the potassium feldspar were determined. The biotite is altered to chlorite over a large

TABLE 4.—*Hydrogen, oxygen, and carbon isotope and fluid inclusion data of vein quartz and siderite and host country rocks*

[Oxygen isotope analyses of quartz were made by the technique of Clayton and Mayeda (1963). The results are expressed in permil differences between the sample and SMOW standard water. Siderite was ground finely and then reacted with H_3PO_4 for 6 days at 50°C to evolve CO_2 (McCrea, 1950), and the gas was analyzed for $\delta^{13}C$ and $\delta^{18}O$. The $\delta^{13}C$ values are expressed in permil deviation from PDB standard (Craig, 1957). Results of both are reproducible to ±0.1 permil. Levels are given in feet]

Sample No.	Mine	Level	Mineral or rock	Fluid inclusions				Rock or mineral			
				δD	Filling temp., °C	Freezing temp., °C	Equiv. wt. % NaCl	CO_2 present	δD_{bio}	$\delta D^{bio}_{H_2O}$	$\delta^{18}O$	$\delta^{13}C$
WH70-8A	Eureka	250	Galena + sphalerite	-110	270±20	-1.85 to -2.8	3.2 to 4.8	Yes				
WH70-13B	Eureka	250	Siderite	----	---------	--------	----------	-------	------	------	+14.8	-5.23
WH70-15	Eureka	250	Siderite	-120	---------	--------	----------	Yes	------	------	+13.3	-5.58
WH70-16	Silver Star Queen	900	Galena + sphalerite	-120	---------	--------	----------	Yes	------	------		
A-36	Silver Star Queen	Surface	Quartz	-115	---------	--------	----------	Yes	------	------	+16.4	
A-227	Treasure Vault	Surface	Quartz	-116	--------	--------	----------	Yes	------	------		
A-230	McCoy	Surface	Potassium feldspar	----	--------	--------	----------	-------	------	------	+ 6.0	
			Quartz	----	--------	--------	----------	-------	------	------	+11.4	
			Biotite	----	--------	--------	----------	-------	-166	≈-130	+ 3.5	
			Whole rock	----	--------	--------	----------	-------	------	------	+10.9	
A-13	Minnie Moore	Surface	Hornfels (Milligen Formation)	-102	--------	--------	----------	-------	------	------	+18.8	
A-471	Sky Ranch Flat	Surface	Quartzite (Milligen Formation)	- 92								
2112	Sawmill Gulch	Surface	Argillite (Milligen Formation)	-----	--------	--------	----------	-------	------	------	+20.7	

part of the intrusion. As much of the chlorite as possible was eliminated from the biotite in the mineral separation. The δD value of the biotite was determined by the method described by Godfrey (1962).

The δD of biotite of sample A–230 is −166 permil, and this biotite is depleted in δD relative to the biotite in a normal granitic rock; biotites from most igneous rocks fall in the range −50 to −90 permil (Taylor, 1974, fig. 10). The fractionation of δD between biotite and water is a function of the chemical composition of the biotite and temperature (Suzuoki and Epstein, 1976). The biotite has not been analyzed chemically, but the $\delta D_{H2O\text{-}bio}$ is probably about 35 permil at magmatic temperature. Hence, the biotite is considered to have been in equilibrium with a water of about −130 permil. Considering the uncertainties, this value is probably about the same as that of the inclusion fluids in the ore and gangue minerals and about the same as that of the local present-day meteoric water.

The $\delta^{18}O$ value of the biotite in sample A–230 is +3.5 permil and that of quartz is +11.4 permil (table 4). The $\Delta_{q\text{-}bio}$ of 7.9 and $\Delta_{q\text{-}Kspar}$ of 5.4 permil are too large for unaltered igneous rocks and indicate post crystallization exchange. Different oxygen-bearing minerals undergo ^{18}O exchange at much different rates. Quartz, for example, exchanges ^{18}O at a much slower rate than potassium feldspar or biotite and is likely to retain its original value (Taylor, 1974, p. 856). The $\delta^{18}O$ of quartz is about typical of quartz in S-type granites. (See Chappell and White, 1974, for descriptions of S, sedimentary, and I, igneous, type granites and O'Neil, Shaw, and Flood, 1977, and O'Neil and Chappell, 1977, for their respective $\delta^{18}O$ values). The large $\Delta^{18}O_{q\text{-}bio}$ and $\Delta^{18}O_{q\text{-}Kspar}$ suggest partial re-equilibration of biotite and potassium feldspar of an S-type granite with a light meteoric water while the pluton was cooling, presumably prior to the time of ore formation.

The potassium feldspar of the biotite granodiorite of sample A–230 (table 3) has values of $^{207}Pb/^{204}Pb$

that are higher than those of igneous rocks in the oceanic regime (See Doe and Delevaux, 1973); this relationship must imply incorporation of continental crustal material in the magma, which also suggests an S-type granite.

S-type granites, which are derived from partial melting of a sedimentary source, have been described by Chappell and White (1974) from the Tasman orogenic zone of eastern Australia. They point out that tin deposits appear to be confined to the highly silicic S-type granites. The petrography and stable isotope data suggest that the biotite granodiorite in the Bellevue area is also an S-type, and we speculate that such granites also exist north of this study area in the Boulder Mountains, about 40 km to the north, where Tschanz and others (1974) have identified a substantial tin anomaly in lead-silver-antimony deposits.

INTERPRETATION

Few mines are accessible at present in the Wood River district; thus it was impossible to obtain abundant geologically controlled samples representing complete time-space relationships. Therefore, the isotope and fluid-inclusion data we obtained are sparse, and the interpretations we present here are somewhat speculative. However, our confidence in the interpretations is increased because all the isotope and fluid inclusion data are consistent with a single model for the origin of the deposits. The geology, isotope, and fluid inclusion data suggest that the Wood River ores were formed by hydrothermal systems of meteoric water that were activated along southwest-dipping faults in response to intrusion of several relatively small granitic plutons into allochthonous Paleozoic sedimentary rocks. The fluids dissolved at least lead and sulfur from adjacent or underlying host rocks and deposited most ore bodies in structures and favorable beds below the regional Wood River thrust fault in response to physical and chemical conditions induced by the thrust fault. Some ore also occurs above the thrust fault in the Wood River Formation (fig. 1).

Nature of the hydrothermal systems

The geology and the distribution of the ore deposits suggest that mineralization in the study area was related to three separate hydrothermal systems, each related to a small plutonic body. The southernmost system was in the Silver Star Queen–Minnie Moore mine area about 2 km west of Bellevue, the second in the Mayflower–Red Elephant mine area about 5.5 km west of Hailey, and the third in the Parker North Star area about 4.5 km east of Ketchum (fig. 1). The mineralized areas are in domed or arched structures over plutons or on the flanks of plutons (fig. 1). All lie close to but under the regional Wood River thrust fault. This shattered thrust zone may have been a principal recharge zone for the hydrothermal systems. The Milligen allochthon near the intrusive bodies is broken by many steep faults, which permitted deep circulation of meteoric water. Underground drill holes commonly tap extensive meteoric water under pressure, and the Hailey and Clarendon hot springs (fig. 1) corroborate deep circulation of the ground water.

Assuming that the fluid inclusion data are representative of the ore fluids, the ore fluids were highly exchanged meteoric water with a δD of -110 to -120 permil, a salinity of 3.2 to 4.8 percent, a temperature of about 270°C, and variable CO_2/H_2O. The large $\delta^{18}O$ values for the hydrothermal fluids indicate limited water-rock ratios and extensive exchange between the meteoric water and the argillite and granitoid country rocks.

The δD value of meteoric water in the area during ore deposition was only slightly larger than it is today (-135 permil in present-day meteoric water at Bullion gulch near the Eureka mine as compared to -110 to -120 permil for the ore fluid). There is a good correspondence between δD values of modern meteoric waters and the Tertiary meteoric waters associated with gold deposition in Nevada (O'Neil and Silberman, 1974). Our data suggest that this correspondence can be extended back to the Late Cretaceous or early Tertiary mineralization in southern Idaho.

Source of the materials

The highly radiogenic composition of the lead in ores of the Wood River district points to a shallow crustal source and an origin by lateral secretion. Three of the four ore samples analyzed here have values of $^{208}Pb/^{204}Pb$ greater than any known Mesozoic or Cenozoic igneous rocks in the Western United States. The association of the deposits, however, with plutonic rocks in the Wood River district, their high temperature formation, and their high silver content suggest a magmatothermal origin such as that postulated for the Cortez deposit in Nevada (Rye, Doe, and Wells, 1974). The term "magmatothermal" has been used by Doe and Zartman (1978) for aqueous fluids associated with and apparently heated by igneous activity. The term is distinguished from "hydrothermal," which refers to hot aqueous solutions with or without demonstrable association with igneous processes, and from "magmatic" as magmatothermal does not imply necessary derivation of the fluid or the metals from a magma. The highly radiogenic compo-

sition of the lead in the Wood River area requires that the source of the bulk of the lead be in the sedimentary rocks rather than in the plutonic rocks, as at Cortez. The relatively large $^{207}Pb/^{204}Pb$ value for the Wood River deposits can be explained by leaching of the lead from a Precambrian basement in Idaho, or from detritus derived therefrom in Phanerozoic rocks that were never subjected to metamorphism above amphibolite facies.

Minor-element content of the Milligen Formation

The Milligen argillites easily have the potential to be the source of all metals present in the Wood River ore deposits. Semiquantitative spectrographic analyses of 34 samples of Milligen argillite were made for a mineral resource evaluation of the proposed Pioneer Mountains National Recreation Area, which includes the area north and east of the Triumph mine (Frank Simons, J. C. Dover, S. W. Hobbs, E. T. Tucket, and J. Ridenour, unpub. data, 1976). These samples ranged from 10–1000 ppm of manganese, 70–1500 ppm of barium, 5–150 ppm of nickel, 10–300 ppm of copper, 10–70 ppm of lead, 5–1000 ppm of zinc, and 0.3–0.7 ppm of silver. Calculations can be made to show that leaching of a very small percentage of these metals over a rather small area could account for the metals in the deposits. The lead isotope data, howver, are not compatible with the concept of the Milligen argillite as the sole source rocks, and probably lead from underlying strata was also leached.

Sulfur

The deposits in the Wood River district occur in reduced argillite and in granitic rocks. Even though the deposits were formed from meteoric waters at shallow depths, they contain no mineralogic evidence of high f_{O_2} values in their ore fluids. The large $\delta^{18}O_{H_2O}$ values of the fluids further indicate that extensive equilibration occurred between the ore fluids and the argillites. If the f_{O_2} of the ore fluids was controlled by equilibration with the carbon-rich argillites, the $\delta^{34}S$ values of the hydrothermal sulfur must have been close to the values of pyrite and sphalerite or between 4 and 15 permil (Ohmoto, 1972).

The large positive $\delta^{34}S$ values for the ore fluids indicate that a substantial part of the sulfur must have been derived from a shallow sedimentary source, probably the same stratigraphic section that supplied the lead. The sedimentary source of sulfur could be diagenetic pyrite in the host rock or in the underlying Paleozoic rocks. The host rock, the Devonian Milligen Formation, has about 1 percent hematite, which apparently is an alteration product of disseminated sedimentary pyrite. Very little pyrite remains, so that it could not be analyzed for $\delta^{34}S$. The $\delta^{34}S$ values of sedimentary pyrites in the lower Paleozoic section in Nevada, however, typically have large $\delta^{34}S$ values (up to 12 permil) (Rye, Doe, and Wells, 1974; R. O. Rye, unpub. data, 1977) that reflect the large $\delta^{34}S$ values of early Paleozoic seawater sulfate from which pyrite was derived. This pyrite is probably the source of hydrothermal sulfur associated with disseminated gold deposits in central Nevada (A. S. Radtke, R. O. Rye, and F. W. Dickson, unpub. data, 1977) and is a likely source for much but possibly not all of the sulfur in the Wood River ores. Considerable hydrothermal barite occurs as conspicuous lenses in the Paleozoic rocks near the fringes of lead-silver mineralization near the North Fork of Deer Creek, about 6.4 km north of the Red Elephant–Mayflower area, and also in the Muldoon area about 25.6 km east of Hailey. The $\delta^{34}S$ value of 13.2 permil for this barite suggests a source of sulfur similar to that for the sulfide minerals (table 2).

It should be mentioned that $\delta^{34}S$ values of 10–15 permil are typical of late Paleozoic seawater sulfate. Since the Wood River Formation is Middle Pennsylvanian to Early Permian in age, an evaporite source of sulfur would be compatible with the data. We have found no evidence of evaporites in the area, but evaporite and carbonate deposition took place on the cratonic shelf to the east (Sando, 1976).

The range of $\delta^{34}S$ values of the sulfur could indicate that the sulfur source was isotopically inhomogeneous or that some mixing with deep sulfur (from a magma or leached from igneous rocks) may have occurred. At the Liberty Gem mine, for example, the sulfur could be predominantly deep seated. This deposit also has the least radiogenic lead in the district.

Carbon

The $\delta^{13}C$ values of the hydrothermal fluids at the Eureka deposit during deposition of siderite averaged about 5.2 permil. Such values are typical of carbon from deep-seated sources. The carbon isotope data, however, do not indicate a unique source for the hydrothermal carbon because similar $\delta^{13}C$ values can be obtained for CO_2 from ground water and from shallow sources that undergo exchange with graphite-bearing host rocks (Ohmoto and Rye, 1970). The presence of high ΣC contents in the ore fluids, as indicated by liquid CO_2 in the fluid inclusions, rules out the possibility that the carbon was derived from ground water.

Mechanisms of ore deposition

All the deposits occur at about the same elevation and approximately the same distance below the thrust

fault. Although the thrust zone contains no ore, it probably provided the physical and chemical environment for the precipitation of ore. Possible causes of ore deposition include:

1. Drop in temperature. Today the thrust zone is a regional water course. Hydrothermal fluids rising along vertical fractures in the footwall would undergo a rapid drop in temperature in the vicinity of the thrust fault.
2. Mixing of fluids. The meteoric water hydrothermal fluids rising through the fissures must have eventually mixed with cold meteoric water descending from the thrust zone. If such mixing occurred beneath the thrust in the ore zones, it would lead to the break up of chloride complexes in the hydrothermal solutions and the precipitation of ore.
3. Boiling of fluids. The deposits occur at approximately the same elevation, and when hydrothermal fluids entered the highly permeable thrust fault zone, it is likely that they boiled. Evidence for boiling has been found only in samples from the Liberty Gem deposit, where both vapor-rich and liquid-rich inclusions occur.

Any or all of these mechanisms may have operated during ore deposition. All are compatible with the rapid bottoming of ore in the various deposits. Unfortunately, we do not have enough data to evaluate which of these three mechanisms was most prominent.

Applications of lead isotopes to prospect evaluation

Doe and Stacey (1974) point out that most major base-metal deposits of the world have characteristic lead isotope ratios; many appear to have lead isotope compositions that evolved under conditions approximately single stage, whereas many minor deposits appear to have lead isotope compositions that were not evolved under these conditions. Using this difference in lead isotopes between major and minor districts, the Wood River district would be categorized as a minor district. Doe and Zartman (1978) have pointed out that size and production decrease with increasing radiogenic lead isotope composition in Mesozoic and Cenozoic magmatothermal base-metal deposits in the Western United States.

All the multibillion-dollar magmatothermal base-metal deposits have $^{206}Pb/^{204}Pb$ values less than 18.3. The lead in these deposits is approximately the same as that in the associated plutonic mass and was presumably derived from the parent magma or leached from the pluton. Available data indicate that the sulfur is apparently also from a magmatic source. Deposits with a production of roughly $100 million all have ratios less than 19.1. A possible explanation of why individual deposits in the Wood River district are relatively small compared to other magmatothermal deposits is that the physical condition did not permit formation of large hydrothermal systems. This restriction is suggested by the large rock-water ratios indicated by the high ^{18}O values of the gangue quartz. Thus the system did not circulate through large volumes of the country rock as would be necessary to leach the metals for large ore bodies.

REFERENCES CITED

Anderson, A. L., Kiilsgaard, T. H., and Fryklund, V. C., Jr., 1950, Detailed geology of certain areas in the Mineral Hill and Warm Springs mining districts, Blaine County, Idaho: Idaho Bur. Mines and Geology Pamph. 90, 73 p.

Berry, A. L., and others, 1976, Summary of miscellaneous potassium-argon age measurements, U.S. Geological Survey, Menlo Park, California, for the years 1972–74: U.S. Geol. Survey Circ. 727, 13 p.

Chappell, B. W., and White, A. J. R., 1974, Two contrasting granite types: Pacific Geology, v. 8, p. 173–174.

Clayton, R. N., and Mayeda, T. K., 1963, The use of bromine pentafluoride in the extraction of oxygen from oxides and silicates for isotopic analysis: Geochem. et Cosmochim. Acta, v. 27, p. 43–53.

Craig, Harmon, 1957, Isotopic standards for carbon and oxygen and correction factors for mass-spectrographic analysis of carbon dioxide: Geochim. et Cosmochim. Acta, v. 12, p. 133–149.

Czamanske, G. K., and Rye, R. O., 1974, Experimentally determined sulfur isotope fractionations between sphalerite and galena in the temperature range 600° to 275°C: Econ. Geol., v. 69, no. 1 p. 17–25.

Doe, B. R. and Delevaux, M. H., 1973, Variations in lead-isotopic compositions in Mesozoic granitic rocks of California: A preliminary investigation: Geol. Soc. America Bull., v. 84, no. 11, p. 3513–3526.

Doe, B. R., and Stacey, J. S., 1974, An application of lead isotopes to the problems of ore genesis and ore prospect evaluation: A review: Econ. Geol., v. 69, no. 6, p. 757–776.

Doe, B. R., and Zartman, R. E., 1978, Plumbotectonics I, The Phanerozoic, *in* Barnes, H. L., ed., The Geochemistry of hydrothermal ore deposits: [2d ed.]: New York, Wiley and Sons. (In press.)

Dover, J. H., 1969, Bedrock geology of the Pioneer Mountains, Blaine and Custer Counties, central Idaho: Idaho Bur. Mines and Geology Pamph. 142, 61 p.

Godfrey, J. D., 1962, The deuterium content of hydrous minerals from the east-central Sierra Nevada and Yosemite National Park: Geochim. et Cosmochim. Acta, v. 26, p. 1215–1245.

Hall, W. E., Batchelder, John, and Douglass, R. C., 1974, Stratigraphic section of the Wood River Formation, Blaine County, Idaho: U.S. Geol. Survey Jour. Research, v. 2, no. 1, p. 89–95.

Hall, W. E., and Czamanske, G. K., 1972, Mineralogy and trace element content of the Wood River lead-silver district, Blaine County, Idaho: Econ. Geology, v. 67, no. 3, p. 350–361.

Hall, W. E., and MacKevett, E. M., Jr., 1958, Economic geology of the Darwin quadrangle, Inyo County, California: California Div. Mines Spec. Rept. 51, 73 p.

———1962, Geology and ore deposits of the Darwin quadrangle, Inyo County, California: U.S. Geol. Survey Prof. Paper 368, 87 p.

Lemmlein, G. G., and Klevtson, P. V., 1961, Relations among the principal thermodynamic parameters in a part of the system H_2O-NaCl: Geochemistry, no. 2, p. 148–158.

Lindgren, Waldemar, 1900, The gold and silver veins of Silver City, De Lamar, and other mining districts in Idaho: U.S. Geol. Survey 20th Ann. Rept., pt. 3, p. 65–256.

McCrea, J. M., 1950, On the isotope chemistry of carbonates and a paleotemperature scale: Jour. Chem. Physics, v. 18, p. 849–857.

Ohmoto, Hiroshi, 1972, Systematics of sulfur and carbon isotopes in hydrothermal ore deposits: Econ. Geol., v. 67, no. 5, p. 551–578.

Ohmoto, Hiroshi, and Rye, R. O., 1970, The Bluebell mine, British Columbia I. Mineralogy, paragenesis, fluid inclusions, and the isotopes of hydrogen, oxygen, and carbon: Econ. Geol., v. 65, no. 4, p. 417–437.

O'Neil, J. R., and Chappell, B. W., 1977, Oxygen and hydrogen isotope relations in the Berridale batholith: Geol. Soc. London Jour., v. 133, p. 559–571.

O'Neil, J. R., Shaw, S. E., and Flood, R. H., 1977, Oxygen and hydrogen isotope compositions as indicators of granite genesis in the New England Batholith, Australia: Contr. Mineralogy and Petrology, v. 62, p. 313–328.

O'Neil, J. R., and Silberman, M. L., 1974, Stable isotope relations in epithermal Au-Ag deposits: Econ. Geol., v. 69, no. 6, p. 902–909.

Russell, R. D., and Farquhar, R. M., 1960, Lead isotopes in geology: New York, Interscience, 243 p.

Rye, R. O., Doe, B. R., and Wells, J. D., 1974, Stable isotope and lead isotope study of the Cortez, Nevada, gold deposit and surrounding area: U.S. Geol. Survey Jour. Research, v. 2, no. 1, p. 13–23.

Rye, R. O., Hall, W. E., and Ohmoto, Hiroshi, 1974, Carbon, hydrogen, oxygen, and sulfur isotope study of the Darwin lead-silver-zinc deposit southern California: Econ. Geology, v. 69, no. 4, p. 468–481.

Sandberg, C. A., Hall, W. E., Batchelder, J. N., and Axelsen, Claus, 1975, Stratigraphy, conodont dating, and paleotectonic interpretation of the type Milligen Formation (Devonian), Wood River area, Idaho: U.S. Geol. Survey Jour. Research, v. 3, no. 6, p. 707–720.

Sando, W. J., 1976, Mississippian history of the northern Rocky Mountain region: U.S. Geol. Survey Jour. Research, v. 4, no. 3, p. 317–338.

Skipp, Betty, and Hall, W. E., 1975, Structure and Paleozoic stratigraphy of a complex of thrust plates in the Fish Creek Reservoir area, south-central Idaho: U.S. Geol. Survey Jour. Research, v. 3, no. 6, p. 671–689.

Small, W. D., 1968, Cordilleran geochronology deduced from hydrothermal leads: Vancouver, B.C., Univ. British Columbia, Ph. D. thesis.

Suzuoki, T., and Epstein, Samuel, 1976, Hydrogen isotope fractionation between OH-bearing minerals and water: Geochim. et Cosmochim. Acta, v. 40, p. 1229–1240.

Taylor, H. P., Jr., 1974, The application of oxygen and hydrogen isotope studies to problems of hydrothermal alteration and ore deposition: Econ. Geol., v. 69, no. 6, p. 843–883.

Tschanz, C. M., and others, 1974, Mineral Resources of the Eastern part of the Sawtooth National Recreation Area, Custer and Blaine Counties, Idaho: U.S. Geol. Survey open-file rept., 314 p.

Umpleby, J. B., Westgate, L. G., and Ross, C. P., 1930, Geology and ore deposits of the Wood River region, Idaho: U.S. Geol. Survey Bull. 814, 250 p.

White, D. E., 1974, Diverse origins of hydrothermal ore fluids: Econ. Geology, v. 69, no. 6, p. 954–973.

Jour. Research U.S. Geol. Survey
Vol. 6, No. 5, Sept.–Oct. 1978, p. 593–602

PETROGRAPHIC DIFFERENTIATION OF DEPOSITIONAL ENVIRONMENTS OF SANDSTONES OF THE PENNSYLVANIAN BREATHITT FORMATION, NORTHEASTERN KENTUCKY AND SOUTHWESTERN WEST VIRGINIA

By ROMEO M. FLORES, Denver, Colo.

Abstract.—Petrographic properties of sandstone samples from the lower and middle Pennsylvanian Breathitt Formation in northeastern Kentucky and southwestern West Virginia were utilized to classify their environments of deposition. Simultaneous consideration of mineral composition, grain size, and sorting of the sandstones by using stepwise multiple discriminant-function analysis has permitted differentiation between alluvial-plain and delta-plain sandstones. Stepwise multiple discriminant-function analysis of the sandstone samples was performed in two parts. The first analysis assigned the sandstones of all grain-size classes to one of three environments of deposition: (1) alluvial plain, (2) upper delta plain, and (3) lower delta plain. The second analysis classed the sandstones by grain size and subdivided each grain-size class into these environmental groups. Discriminant analyses of sandstones of all grain-size classes led to correct assignment of depositional environment to 76 percent of the samples. Analyses of the sandstones classed by grain size led to correct classification of 67 percent of the medium-grained sandstones, 83 percent of the fine-grained sandstones, and 91 percent of the very fine grained sandstones. The discriminant-function method was adopted to classify the depositional environment and stratigraphic position of test sandstone samples. Analyses of fine-grained and very fine grained sandstones resulted in correct classification of 84 percent of the test samples to their depositional setting and stratigraphic position. The best discrimination is offered by analyses of fine-grained sandstones, which resulted in correct classification of 88 percent of the samples. Thus, this statistical method can be adopted as a powerful tool for exploration programs that concern delineation of genetically similar sandstones.

Mineral composition and grain size of sandstones have long been used in the interpretation of depositional environments. Mason and Folk (1958) and Visher (1969) demonstrated the diagnostic relations of grain size to specific depositional environments, and Van Andel (1958), Potter (1967), and Picard (1971) related mineral composition to environment. Although mineral composition and grain size behaved independently of the depositional processes operative in various environments, they were found to be interdependent (Flores, 1967). That is, coarse-grained sandstones tend to be high in quartz compared to fine-grained sandstones. Thus, a meaningful analysis of sensitivity of mineral composition to specific depositional environments should include correction of the grain-size effect, or comparison should be made only between sandstones of similar grain size.

Detailed stratigraphic studies of Whaley (1969), Ferm and others (1971), Horne and Baganz (1974), and Ferm (1976) of the Lower and Middle Pennsylvanian Breathitt Formation in northeastern Kentucky and southwestern West Virginia have led to identification of depositional settings of its sandstones. Recent mapping by the U.S. Geological Survey in this area (Hayes, 1978; Connor and Flores, 1978; Sanchez and others, 1978; Ward, 1978; Pillmore and Connor, 1978) has resulted in a clearer understanding of the vertical and areal relations of the sandstones to one another. The knowledge gained from these works guided the collection of many standstone samples from road cuts, strip mines, and borehole cores for detailed petrographic analysis. Previous studies that successfully used multivariate analysis to differentiate environments of deposition by mineralogical and textural properties of sandstones (Davies and Ethridge, 1975; Ethridge and others, 1975; Flores, 1977) provided a statistical model for this study. The purpose of this study was to test the utility of compositional and textural measurements in differentiating various depositional environments of sandstones of the Breathitt, and to test the feasibility of using multivariate analysis to identify depositional settings and stratigraphic positions of test sandstone samples. Simultaneous analyses of sandstones representing all grain-size classes resulted in correct classification of 76 percent of the sandstones, whereas 67, 83, and 91 percent of the sandstones were correctly classified when they were grouped as medium grained, fine grained, and very fine grained, respectively. By use of this multivariate method, 84 percent of the test sandstone samples were classified to their correct environmental group and stratigraphic position.

Acknowledgments.—Appreciation is extended to J. J. Connor for assistance in the statistical and com-

puter analyses. Stratigraphic cross sections along U.S. Highway 23, utilized as sampling guide, were provided by J. C. Horne of the University of South Carolina.

METHODS

Field and laboratory analysis

Sandstones were selected for analysis because they make up a major part of the Breathitt Formation. Samples of fluvial-channel, distributary-channel, distributary-mouth-bar, and crevasse-splay sandstones were collected from exposures in road cuts and strip mines and from borehole cores. The sampling localities (see fig. 1) were systematically selected to provide stratigraphic control of the sandstones. The lower- and upper-delta-plain sandstones were collected mainly from the southwestern part of the study area, where such sandstones are best exposed. The alluvial-plain sandstones and some upper-delta-plain sandstones were collected from excellent exposures in the northeastern part of the area. In addition, sandstones from all three environments were collected from boreholes where thick sequences were recovered by complete 51-mm (2-in)-diameter continuous cores. One coarse-grained sample and one fine-grained sample were collected from each unit. The replicate samples were collected to determine the differences in mineralogic characteristics of sandstones of different grain sizes.

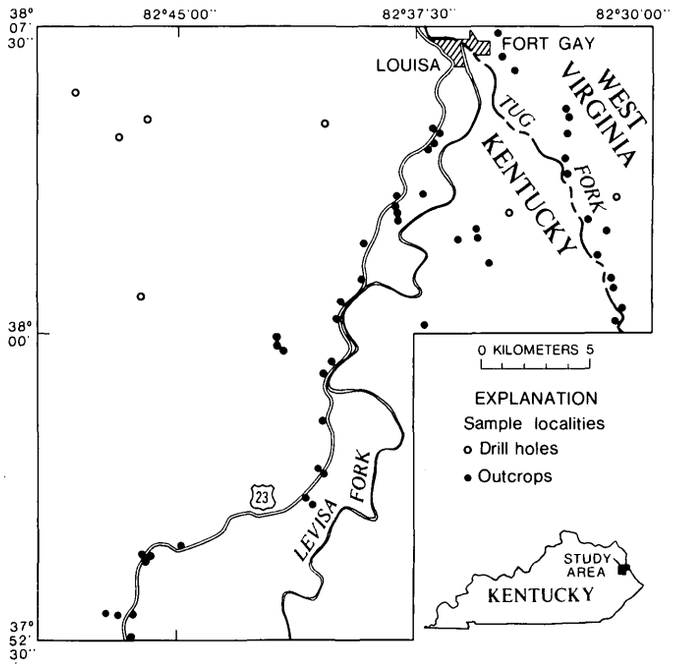

FIGURE 1.—Map of localities of 212 sandstone samples of the Breathitt Formation, northeastern Kentucky and southwestern West Virginia.

The petrographic properties of 212 sandstone samples were analyzed by thin-section study. Of these, 168 thin sections were of sandstones from three identified environments, and 44 thin sections were of sandstones of undetermined environment. The 44 sandstones were used as test samples and their stratigraphic positions were inferred from mapped coal beds or zones 0.5–2.5 km away. Two hundred points were counted in each thin section to determine percentages of framework grains (monocrystalline quartz, feldspar, coarse micas, and rock fragments that include polycrystalline quartz), matrix, and cement. Matrix consists of micaceous clay, and cement occurs as quartz overgrowths, calcite, and hematite. The mean grain size and sorting of quartz grain-size distribution were determined by measurement of 50 apparent long axes of monocrystalline quartz.

Statistical analysis

In order to analyze the simultaneous changes of measured variables of the sandstones, discriminant-function analysis utilizing the University of California biomedical package computer program (BMDO7M) by Dixon (1967) was selected among several multivariate methods. As used, the analysis would discriminate the established environmental groups by measurement of the petrographic characteristics of a unit or units in each group. On the basis of petrographic properties the discriminant-function analysis established, by mathematical manipulation, the best way to differentiate sandstones from each of the three depositional environments (alluvial plain, upper delta plain, and lower delta plain). In the process, the analysis determined not only the petrographic attributes that were most important in making the discrimination between environmental groups but also the best possible way to separate the groups. Thus, the analysis generated linear combinations of the petrographic data to produce separation between environmental groups. Moreover, this analysis can be adopted to classify depositional environments of test sandstone samples.

The stepwise multiple discriminant-function analysis was specifically utilized for the analysis because it is ideally suited to determine the relative significance of each petrographic variable in discriminating between environmental groups. The test of significance of each variable as a discriminator was performed in a stepwise procedure. At each step, one

variable was entered into or deleted from the set of discriminators on the basis of its value. Thus, a point was eventually reached where only the most important variables remained in the discriminator and addition of other variables could not significantly increase the separation. For discussions of discriminant-function analysis and its applications to geological problems, the reader is referred to Klovan and Billings (1967), Connor and Gerrild (1971), Davies and Ethridge (1975), and Ethridge, Gopinath, and Davies (1975). Mathematical treatment of the analysis can be found in Cooley and Lohnes (1962) and Davis (1973).

The interdependent relationship of mineral composition and grain size has necessitated regression analysis of the data. A linear regression was performed in order to determine a precise description of the concomitant variation of these properties. A stepforward regression STATPAC computer program prepared by G. I. Selner was used in calculating the regression analysis; this program is available at the U.S. Geological Survey computer center, Reston, Va., Denver, Colo., or Menlo Park, Calif.

GEOLOGIC SETTING

The Lower and Middle Pennsylvanian Breathitt Formation in northeastern Kentucky and southwestern West Virginia, which ranges from 290 to 330 m thick in the study area, consists of (in the order of abundance) sandstone, siltstone, shale, coal, limestone, flint clay, and siderite beds. Table 1 shows the stratigraphy and subdivision of environments of deposition of the Breathitt Formation. The upper part of the formation contains more abundant sandstone and thicker coal beds than the lower part. The fossiliferous zones of the formation are mainly concentrated in the lower part and are represented (in descending order) by the Vanport Limestone and Magoffin Members, and by the Kendrick Shale of Jillson (1919). These units in the Breathitt contain marine and brack-

TABLE 1.—*Generalized stratigraphic section and interpretation of depositional environments of the Pennsylvanian Breathitt Formation in northeastern Kentucky and southwestern West Virginia*

[Environmental stratigraphic classification is modified from Ferm and others (1971). SS, sandstone; SLTST, siltstone; SH, shale; LS, limestone]

SYSTEM	SERIES	ROCK UNITS			ENVIRONMENTS OF DEPOSITION	DIAGNOSTIC CHARACTERISTICS
		FM	MEMBER	COAL BED/ZONE		
PENNSYLVANIAN	LOWER AND MIDDLE PENNSYLVANIAN	BREATHITT		PRINCESS NO.9 PRINCESS NO.8 PRINCESS NO.7 PRINCESS NO.6	**ALLUVIAL PLAIN** FLUVIAL CHANNEL, POINT BAR, LEVEE, CREVASSE SPLAY, LAKE, & BACKSWAMP.	COAL: THICK & LATERALLY DISCONTINUOUS. SS: MULTIPLE CHANNEL FILLS SHOWING LARGE-SCALE ACCRETION BEDS; MASSIVE & TROUGH-CROSSBEDDED LOWER PART; & PLANAR CROSS-BEDDED, RIPPLED, & CONVOLUTED UPPER PART. SLTST & SH: RIPPLED, PARALLEL-LAMINATED, ROOT-PENETRATED, & CARBONACEOUS.
			VANPORT LS 🐟	RICHARDSON BROAS PEACH ORCHARD HAZARD HADDIX	**UPPER DELTA PLAIN** DISTRIBUTARY CHANNEL, POINT BAR, LEVEE, CREVASSE SPLAY, MARSH, & INTERDISTRIBUTARY BAY.	COAL: THIN TO THICK & LATERALLY VERY EXTENSIVE. SS: CHANNEL FILL SHOWING SMALL-SCALE ACCRETION BEDS; TROUGH & PLANAR CROSSBEDDED LOWER PART; & RIPPLED & PARALLEL-LAMINATED UPPER PART. SLTST & SH: BURROWED, ROOT-PENETRATED, FLASER-BEDDED, RIPPLED, & PARALLEL-LAMINATED. LS: SIDERITIC & CONTAINS CALC. BRACHIOPODS (VANPORT).
			MAGOFFIN 🐟	TAYLOR HAMLIN FIRE CLAY RIDER FIRE CLAY LITTLE FIRE CLAY WHITESBURG	**LOWER DELTA PLAIN** DISTRIBUTARY CHANNEL, MOUTH BAR, DISTAL BAR, LEVEE, CREVASSE SPLAY, MARSH, INTERDISTRIBUTARY BAY, & PRODELTA.	COAL: THIN & LATERALLY MODERATELY EXTENSIVE. SS: CHANNEL FILL SHOWING SMALL-SCALE TROUGH & PLANAR CROSSBEDDING, CLIMBING & ASSYMETRIC RIPPLES, CONVOLUTION, & BURROWS. SLTST & SH: CONTAIN ROOT MARKS, BURROWS, FLASER BEDDING, RIPPLE & PARALLEL LAMINATIONS, & GAS HEAVE STRUCTURES. LS, SH, SLTST & SS: CONTAIN PHOSPHATIC & CALC. BRACHIOPODS, MOLLUSCS, & CRINOIDS (MAGOFFIN & KENDRICK).
			KENDRICK SH (1) 🐟			
				WILLIAMSON VAN LEAR WHEELERSBURG		

🐟 FOSSILIFEROUS
(1) OF JILLSON (1919)

ish-water brachiopod, mollusk, and crinoid faunas that are embedded in shale, siltstone, sandstone, limestone, and siderite beds. Thus, based on the distribution of coal beds, sandstones, and marine and brackish-water fauna, and on stratigraphic environmental relations of the rock types previously established by Ferm and others (1971), Horne and Baganz (1974), and Ferm (1976), the lower and upper parts of the Breathitt Formation respectively are made up of delta-plain and alluvial-plain deposits.

The delta-plain deposits consist mainly of thin to thick, relatively persistent coal beds separated by distributary-channel, mouth-bar, and crevasse-splay sandstones. These rock types are interbedded with bay-fill siltstone and shale that contain brackish-water or marine fossils. The delta-plain deposits are subdivided into lower- and upper-delta-plain deposits. The lower-delta-plain deposits are characterized by the abundance of distributary-channel–mouth-bar sandstones that are surrounded by thick, marine-fossil-bearing bay siltstone, shale, and limestone beds, and thin and not too persistent coal beds. This depositional setting is represented by the interval between the Wheelersburg coal bed and the Magoffin Member. The overlying interval from the Magoffin Member to the Vanport Limestone Member represents the upper-delta-plain deposit, which contains relatively thicker and more persistent coal beds than the lower-delta-plain deposit. These coal beds are mainly separated by distributary-channel and crevasse-splay sandstones, which are intercalated with shallow bay-fill sediments that contain brackish-water and marine fossils.

The upper part of the Breathitt Formation, represented by the interval between the Vanport Limestone Member and the Princess No. 9 coal beds, contains relatively thick, laterally discontinuous coal beds and lacks brackish-water or marine fossils. In this interval are the alluvial-plain deposits, which contain coal beds that are commonly eroded by multiple-channel, accretion-bedded (point-bar) sandstones and that are interbedded with backswamp, crevasse-splay, and lacustrine detritus.

PETROGRAPHIC DIFFERENTIATION OF ENVIRONMENTS

Sandstones of the Breathitt Formation range from very fine grained to coarse grained and are generally dirty, immature, and moderately sorted. The sand-

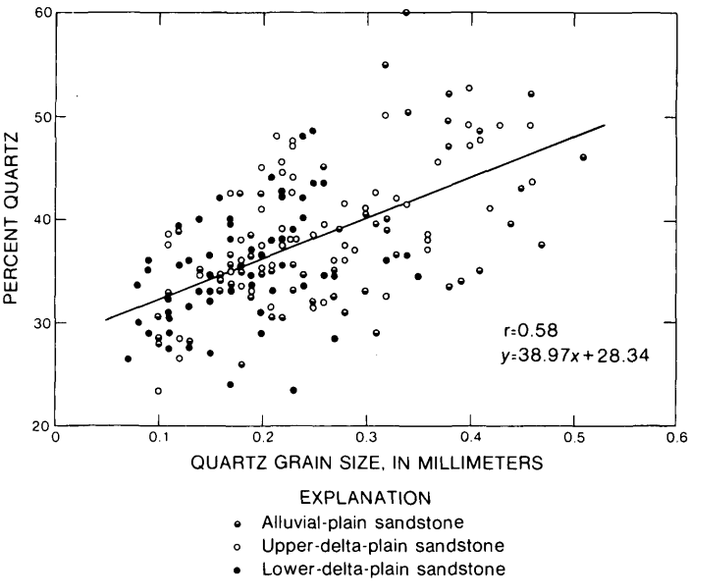

FIGURE 2.—Bivariate plot of quartz grain size and quartz content of 168 alluvial-plain and delta-plain sandstones of the Breathitt Formation.

TABLE 2.—*Mineral composition and texture of sandstone types in the Breathitt Formation*

Depositional environment	Mineral composition (percent)						Grain size (mm)	Standard deviation (Phi)
	Quartz	Feldspar	Coarse micas	Rock fragments	Matrix	Cement		
Alluvial plain	37.6	9.4	6.6	19.7	14.2	12.5	0.26	0.89
Delta plain	37.7	7.5	7.0	15.7	12.0	20.1*	0.22	0.87
Upper delta plain	39.7	7.4	5.1	16.3	12.6	18.9*	0.25	0.89
Lower delta plain	35.2	7.7	8.9	15.3	11.5	21.4*	0.18	0.82

*Many of these samples contained 1 to 17 percent calcite cement.

stones contain 26 to 60 percent quartz, 2 to 19 percent feldspar, 0 to 16 percent coarse micas, 9 to 28 percent rock fragments, 4 to 26 percent micaceous clay matrix, and 4 to 31 percent cement. Table 2 summarizes the mineral composition and texture of 168 alluvial-plain, upper-delta-plain, and lower-delta-plain sandstones examined in this study. A bivariate scatter plot (fig. 2) illustrates that coarse-grained sandstones tend to have higher quartz content than fine-grained sandstones. The correlation coefficient (r) suggests that 34 percent of the variation in quartz content can be accounted for by grain size. Thus, in order to minimize the effect of grain size on mineral composition variation, the discriminant analysis must include classification of sandstones of the same grain-size class. In addition, the distribution of the sandstone types in the scatter plot suggests to some degree that grain size is sensitive to environments of deposition. That is, the lower-delta-plain sandstones tend to be finer grained than the upper-delta-plain and alluvial-plain sandstones.

Discriminant analysis of sandstones in all grain-size classes

For sandstone samples not classed by grain size, discriminant-function analysis on the basis of six compositional variables, grain size, and sorting yielded a satisfactory differentiation between the alluvial-plain, upper-delta-plain, and lower-delta-plain environments. The 168 sandstone samples, arranged into 3 environmental groups, were subjected to stepwise multiple discriminant-function analysis. The analysis was based on the F statistic (a measure of the statistical significance of the amount of group separation attributable to that variable) of 2.5, or about a 90-percent confidence level. Three petrographic variables—coarse micas, matrix, and cement—were determined to be the most important discriminators.

The results of the discriminant analysis are best visualized by plotting discriminant function 1 on the x-axis and discriminant function 2 on the y-axis of a two-dimensional graph. Figure 3 is the scatter plot of discriminant function 1 against discriminant function 2; the reference axes are linear combinations of the three discriminator variables. The alluvial-plain sandstones appear to be distinctly different from the delta-plain sandstones, but there is considerable overlapping of the upper- and lower-delta-plain sandstones. As table 3 shows, 127 of the 168 sandstones (about 76 percent) may be assigned correctly to their depositional environment by means of coarse micas, matrix, and cement content. That is, random assignment of sandstones to their correct depositional settings can be expected for 7.5 in 10 samples by discriminant analysis.

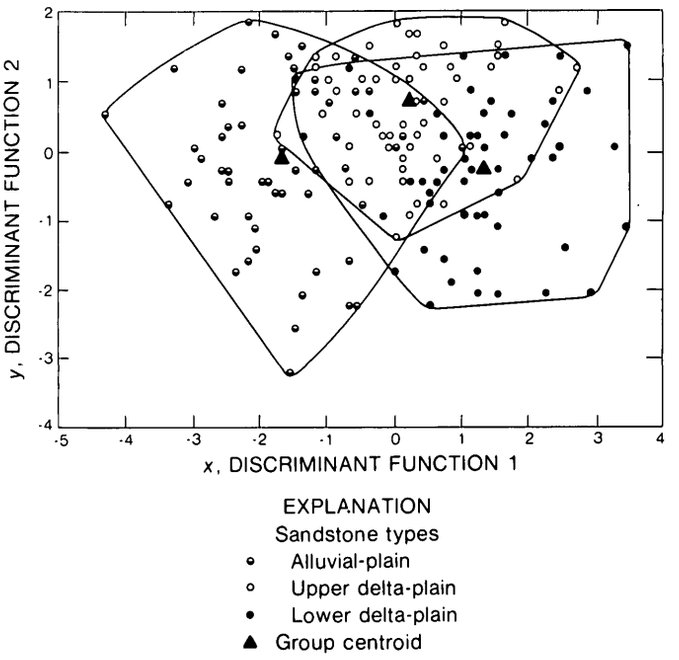

FIGURE 3.—Stepwise multiple discriminant-function analysis of alluvial-plain and delta-plain sandstones of the Breathitt Formation, not classed by grain size. Discriminant function 1 is described by: $x = 0.076$(percent coarse mica-6.884) -0.097(percent matrix-12.741)$+0.281$(percent cement-17.711). Discriminant function 2 is described by: $y = -0.277$(percent coarse mica-6.884)$+0.057$(percent matrix -12.741)$+0.073$(percent cement-17.711).

TABLE 3.—*Depositional environments of known and test samples of sandstone of the Breathitt Formation, as determined by multiple discriminant-function analysis*

Known environment of deposition	Analytically determined environment: Alluvial plain	Upper delta plain	Lower delta plain	Percentage classified correctly
Sandstones not classed by grain size				
Alluvial plain	45	8	1	76
Upper delta plain	4	37	15	
Lower delta plain	4	9	45	
Medium- and coarse-grained sandstones				
Alluvial plain	20	3	4	67
Upper delta plain	4	16	6	
Lower delta plain	2	1	5	
Fine-grained sandstones				
Alluvial plain	20	2	0	83
Upper delta plain	0	21	4	
Lower delta plain	0	8	29	
Test	3	8	6	[1]88
Very fine grained sandstones				
Alluvial plain	5	0	0	91
Upper delta plain	0	4	1	
Lower delta plain	0	1	12	
Test	1	2	11	[1]79

[1]Determined later by comparison of stratigraphic data.

The analysis of sandstones of all grain-size classes indicates that coarse micas, matrix and cement content fluctuate significantly between the alluvial-plain, upper-delta-plain, and lower-delta-plain environments and that the most pronounced differences are between the alluvial-plain and delta-plain environments. The indistinct separation between the deltaic subenvironments suggests less sensitivity of the mineral composition to the differences between environments modified by closely related sedimentary processes. As shown in table 2, the delta-plain sandstones, particularly the lower-delta-plain sandstones, contain more coarse micas than the alluvial-plain sandstones. In contrast, the matrix content of the delta-plain sandstones is not as abundant as that of the alluvial-plain sandstones. The cement content is relatively high in the delta-plain sandstones and particularly high in the lower delta-plain sandstones, compared to that of the alluvial-plain sandstone. The variations of mineral composition probably reflect the local processes operative and the process intensity in the various environments. The high concentration of coarse micas and concomitant low matrix content of the delta-plain sandstones may suggest that reworking and winnowing processes in the delta environment are more efficient than those in the alluvial environment. The high cement content and common occurrence of calcite cement (see table 2) in the delta-plain sandstones are diagenetic changes that resulted directly from their proximity to open marine conditions.

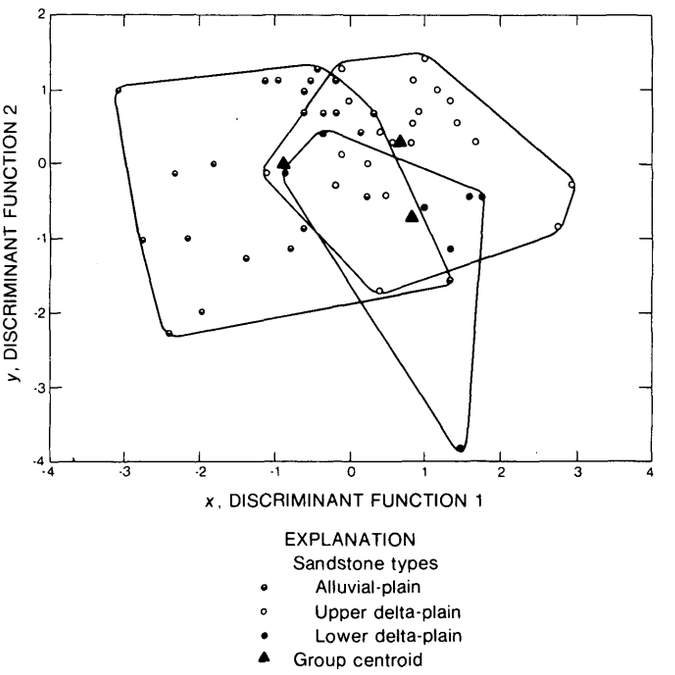

FIGURE 4.—Stepwise multiple discriminant-function analysis of medium-grained alluvial-plain and delta-plain sandstones of the Breathitt Formation. Discriminant function 1 is described by: $x = -0.038(\text{percent matrix} - 3.910) + 0.272(\text{percent cement} - 16.066)$. Discriminant function 2 is described by: $y = -0.362(\text{percent matrix} - 3.910) - 0.008(\text{percent cement} - 16.066)$.

Discriminant analysis of sandstones classed by grain size

In an effort to improve differentiation of the sandstones of the three environmental groups, analyses were performed separately on three grain-size classes: medium and coarse grained (>0.26 mm), fine grained (0.25 to 0.125 mm), and very fine grained (0.124 to 0.08 mm). Only 6 of the 61 sandstone samples in the medium- and coarse-grained class are actually coarse (>0.45 mm). The sandstones of each size class were subjected to stepwise multiple discriminant-function analysis based on an F-value for variable inclusion into the discriminator of 2.5, about a 90-percent confidence level.

A total of 61 medium- and coarse-grained sandstones arranged in three environmental groups were subjected to the stepwise procedure. Two out of eight variables, matrix and cement content, were selected as significant discriminators. The success in differentiating the environmental groups is illustrated in figure 4 on a two-dimensional graph. The scatter plot indicates that the three environmental groups are not well differentiated, and that differentiation of the depositional environments was least successful using medium-grained sandstones. Despite the poor visual separations of the groups, table 3 shows that of 61 samples used in the analysis, 41 can be correctly assigned to their proper environmental classification if each sample is assigned to the nearest centroid. Thus, approximately 67 percent of the sandstones, or more than 6 of 10 samples, are successfully classified in this manner.

The discrimination of 84 samples of fine-grained sandstone among the three environments was more successful. Four of eight mineral variables were determined to be significant discriminators by the stepwise procedure; these are feldspar, coarse micas, matrix, and cement. The two-dimensional graphic plot of the environmental groups is shown in figure 5. The scatter plot shows a very distinct separation of the alluvial-plain group centroid from the delta-plain group centroid. In addition, the separation of the upper-delta-plain and lower-delta-plain centroids is greater than the separation between the same groups in the

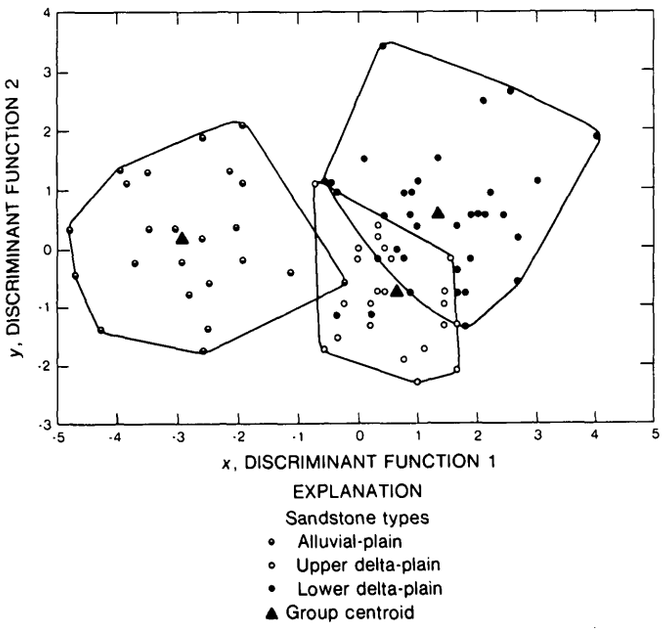

FIGURE 5.—Stepwise multiple discriminant-function analysis of fine-grained alluvial-plain and delta-plain sandstones of the Breathitt Formation. Discriminant function 1 is described by: $x = -0.028$(percent feldspar-8.520)-0.090(percent coarse mica-7.830)-0.267(percent matrix$-12.500+0.286$(percent cement-18.380). Discriminant function 2 is described by: $y = 0.288$(percent feldspar-8.520)$+0.329$(percent coarse mica-7.830)$+0.054$(percent matrix-12.500)$+0.137$(percent cement-18.380).

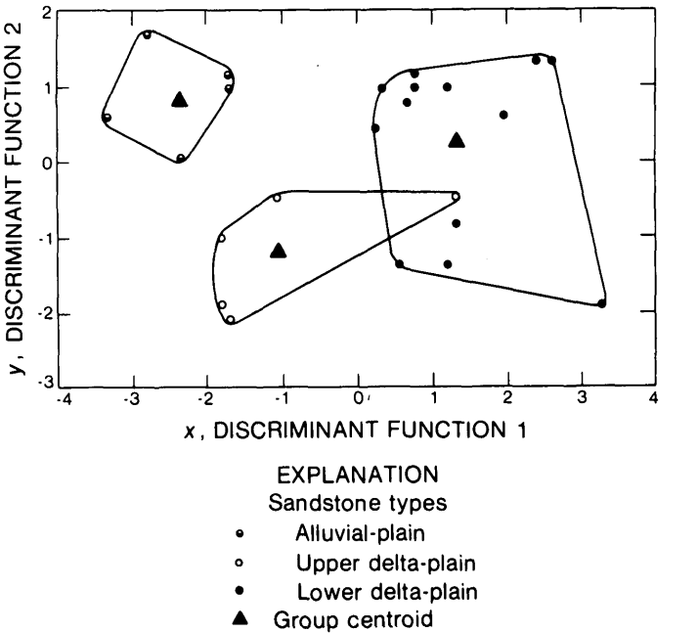

FIGURE 6.—Stepwise multiple discriminant-function analysis of very fine grained alluvial-plain and delta-plain sandstones of the Breathitt Formation. Discriminant function 1 is described by: $x = -0.185$(percent matrix-15.826)$+0.304$(percent cement-19.630)-47.193(grain size-0.103). Discriminant function 2 is described by: $y = -0.206$(percent matrix-15.826)-0.150(percent cement-19.630)-34.043(grain size-0.103).

medium-grained sandstones. Of 84 samples analyzed, 70 can be successfully allocated to their proper environments (table 3). Thus, 83 percent, or more than 8 out of 10 samples, have been correctly assigned. In addition, the discriminators for the fine-grained sandstones included the greatest number of mineral variables—four.

The discriminant analysis of 23 samples of very fine-grained sandstone best differentiated the three environments. The discriminator is based on three variables: matrix, cement, and grain size. The scatter plot displays equally distinct separations between the environmental groups (fig. 6). More importantly, separation of the upper delta plain from the lower delta plain is more distinct in this analysis than in the previous ones. Table 3 indicates that 21 of 23 sandstones were correctly classified to their environmental groups. Thus, 91 percent, or about 9 out of 10 samples, have been successfully classified.

Differentiation of sandstones of the alluvial-plain and delta-plain environments is more successful when analyzing sandstones in the same grain-size class than when analyzing those in all grain-size classes and the best differentiation is yielded by the fine-grained and very fine grained sandstones. However, because fine-grained sandstones make up half of the sandstone samples and yield a moderately high percentage (83 percent) of correct classification, they are probably most practical to use for environmental differentiation.

The sensitivity of the mineral composition to processes operative in the alluvial-plain and delta-plain environments is apparent in the fine-grained sandstones. Fine-grained sandstones of the alluvial plain are high in feldspar, coarse micas, and matrix content (10.7, 8.7, and 16 percent, respectively) compared to the delta-plain sandstones (7.8, 5.9, and 11.2 percent, respectively). In contrast, the delta-plain sandstones have more cement (20.7 percent) than the alluvial-plain sandstones (11.7 percent). The high feldspar and coarse micas content of alluvial-plain sandstones probably indicate deposition in relatively quiet water with little or no reworking. On the other hand, the delta-plain environment is in close proximity to open water, and a vigorous winnowing process probably reworked

fine feldspars and coarse mica particles and transported them farther offshore. Winnowing by marine-related processes (wind, wave, and tide) is also indicated by the matrix content, which is lower in the delta-plain sandstones than in the alluvial-plain sandstones. Partial removal of the matrix by winnowing probably created pore spaces in which interstitial cement precipitated during diagenesis of the sediments.

PRACTICAL ENVIRONMENTAL STRATIGRAPHIC APPLICATIONS

The most obvious practical application of the discriminant-function analysis is the identification of depositional environments by classification of test sandstone samples. Furthermore, assignment of a sandstone to a depositional setting would allow a much closer assignment of its stratigraphic position. In the Breathitt Formation in northeastern Kentucky and southwestern West Virginia, the alluvial-plain and delta-plain sandstones occupy the upper and lower parts of the stratigraphic section, respectively. In order to test the feasibility of this classification, 44 sandstone samples were collected from random localities where their stratigraphic positions were doubtful because of the absence of recognized marker beds of marine and flint clay. The mineral composition and textural data of these sandstones were subjected to stepwise multiple discriminant-function analysis with emphasis on the fine-grained and very fine grained sizes.

Of 17 test fine-grained samples, 3 were classified as alluvial-plain sandstones, 8 as upper-delta-plain sandstones, and 6 as lower-delta-plain sandstones (table 3). Figure 7 shows a plot of the environmental groups of known sandstones and distribution of test sandstones among these groups. In order to determine the reliability of this environmental classification, each test sandstone was checked against its stratigraphic position as determined from mapped coal beds or zones. Out of the 17 samples, two samples were misclassified: an alluvial-plain sandstone was classified as upper delta plain, and an upper-delta-plain sample was assigned to the lower delta plain. (See fig. 7.)

Similar discriminant analyses were performed on the known and test very fine grained sandstones. Table 3 shows that out of 14 test samples, one is classified as alluvial-plain sandstone, 2 as upper-delta-plain sandstones, and 11 as lower-delta-plain sandstones. The two-dimensional scatter plot of the environmental groups of known sandstones and distribution of test sandstones among these groups are shown in figure 8. A stratigraphic check of the positions of the test sandstones with respect to mapped coal beds or zones indi-

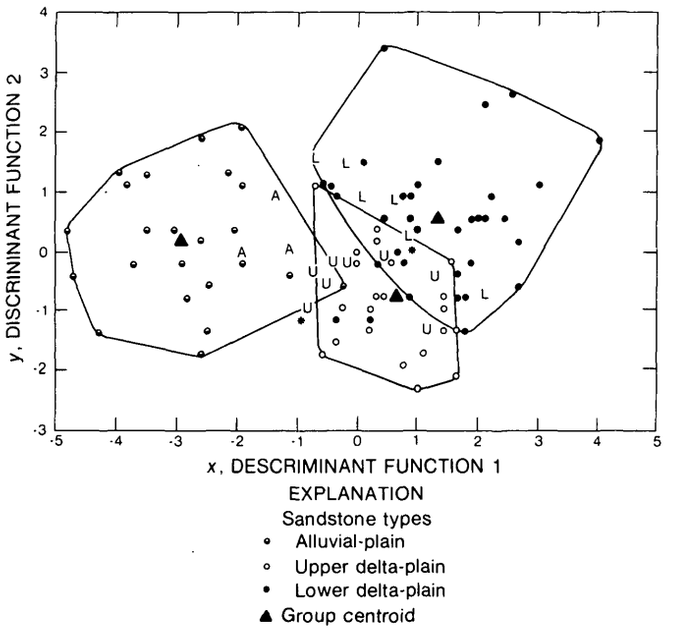

FIGURE 7.—Simultaneous multiple discriminant-function analysis of identified and test fine-grained alluvial-plain (A), upper-delta-plain (U), and lower-delta-plain (L) sandstones of the Breathitt Formation. The equations for discriminant functions 1 and 2 are the same as equations on figure 5. Misclassified test sandstones are noted by asterisks.

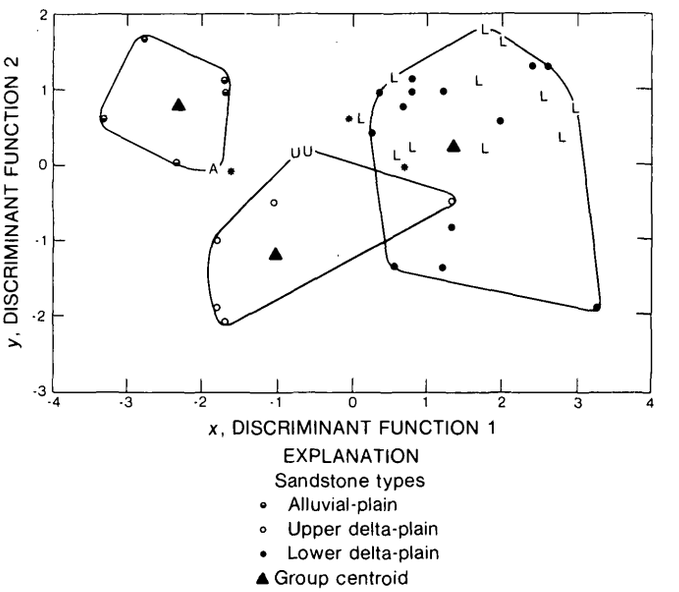

FIGURE 8.—Simultaneous multiple discriminant-function analysis of identified and test very fine grained alluvial-plain (A), upper-delta-plain (U), and lower-delta-plain (L) sandstones of the Breathitt Formation. The equations for discriminant functions 1 and 2 are the same as equations on figure 6. Misclassified test sandstones are noted by asterisks.

cates that three sandstones were misclassified by the analysis. The "alluvial-plain" sandstone and two "lower-delta-plain" sandstones were all identified as upper-delta-plain sandstones. (See fig. 8.)

Although the number of test sandstone samples that were used in the discriminant analysis is limited, the differences among sandstones of the Breathitt Formation are apparently distinct enough to permit their environmental and stratigraphic classification. On a provisional basis, the success of the discriminant analysis in classifying test sandstones to their depositional environment and general stratigraphic position is indicated by the correct assignment of 26 of 31 sandstones (84 percent). That the fine-grained sandstones yield the best analysis is indicated by correct assignment of 15 of 17 samples (88 percent), compared to the very fine grained sandstones, in which 11 of 14 samples (79 percent) were correctly classified.

SUMMARY

Differentiation of depositional environments of sandstones of the Pennsylvanian Breathitt Formation can be accomplished by performing stepwise multiple discriminant-function analysis of their petrographic properties. Analysis of the content of coarse micas, matrix, and cement in sandstones of all grain-size classes indicates that 76 percent of the samples can be assigned to their proper environment of deposition. Environmental assignment of sandstone samples of the same grain-size class was most successful when analyzing the finer grained samples. Discriminant analysis of medium- and coarse-grained sandstones based on matrix and cement content indicates that 67 percent of the samples can be correctly classified to their environmental groups. However, analysis of the fine-grained sandstones based on feldspar, coarse micas, matrix, and cement content resulted in correct assignment of 83 percent of the samples to their environmental groups. In contrast, 91 percent of the very fine grained sandstones were correctly assigned to their environmental groups on the basis of their matrix and cement content and grain size. In all test cases, discrimination was most successful between sandstones of the alluvial-plain and delta-plain environments.

The discriminant-function method was adopted to classify sandstone samples of uncertain depositional environments and stratigraphic positions. Eighty-four percent of the test fine-grained and very fine grained sandstone samples were correctly classified to their environmental groups and corresponding stratigraphic positions. The analysis of the fine-grained sandstones yielded the best discrimination, with 88 percent of the samples correctly assigned, in contrast to 79 percent success in classification of very fine grained sandstones.

In conclusion, the most obvious practical application of discriminant-function analysis is the classification of depositional environments of sandstones. This method, furthermore, can provide more precise correlation of genetically similar stratigraphic units. The adaptability of this method is measured by its versatility. That is, simultaneous consideration of petrographic or other properties of genetically similar sandstones or other rock types may yield usable differences to permit their delineation. Thus, the discriminant-analysis method can be a powerful tool for exploration programs that concern targeting genetically similar sandstones or other rock types.

REFERENCES CITED

Connor, C. W., and Flores, R. M., 1978, Geologic map of the Louisa quadrangle, Kentucky-West Virginia: U.S. Geol. Survey Geol. Quad. Map GQ–1462. (In press.)

Connor, J. J., and Gerrild, P. M., 1971, Geochemical differentiation of crude oils from six Pliocene sandstone units, Elk Hills U.S. Naval Petroleum Reserve No. 1, California: Am. Assoc. Petroleum Geologists Bull., v. 55, no. 10, p. 1802–1813.

Cooley, W. W., and Lohnes, P. R., 1962, Multivariate procedures for the behavioral sciences: New York, John Wiley and Sons, 211 p.

Davies, D. K., and Ethridge, F. G., 1975, Sandstone composition and depositional environment: Am. Assoc. Petroleum Geologists Bull., v. 59, no. 2, p. 239–264.

Davis, J. C., 1973, Statistics and data analysis in geology, *with* FORTRAN programs by R. J. Sampson: New York, John Wiley and Sons, 550 p.

Dixon, W. J., ed., 1967, BMD biomedical computer programs [2d ed., revised by Laszlo Engelman]: California Univ. Pubs. Automatic Computation, no. 2, 600 p.

Ethridge, F. G., Gopinath, T. R., and Davies, D. K., 1975, Recognition of deltaic environments from small samples, *in* Broussard, M. L., ed., Deltas, models for exploration [2d ed.]: Houston Geol. Soc., p. 151–164.

Ferm, J. C., 1976, Depositional models in coal exploration and development, *in* Saxena, R. S., ed., Sedimentary environments and hydrocarbons: Short course sponsored by Am. Assoc. Petroleum Geologists and New Orleans Geol. Soc., New Orleans, La., May 23, 1976, p. 60–78.

Ferm, J. C., Horne, J. C., Swinchatt, J. P., and Whaley, P. W., 1971, Carboniferous depositional environments in northeastern Kentucky, *in* Geol. Soc. Kentucky Ann. Spring Field Conf., April 23–24, 1971: Kentucky Geol. Survey, 30 p.

Flores, R. M., 1967, Variations in mineral composition during transport: Jour. Sed. Petrology, v. 37, no. 1, p. 235–239.

———1977, Differentiation of sandstone depositional environments in Pennsylvanian Breathitt Formation of northeastern Kentucky and southwestern West Virginia [abs.]: Am. Assoc. Petroleum Geologists Bull., v. 61, no. 5, p. 785.

Hayes, P. T., 1978, Geologic map of the Sitka quadrangle, Johnson and Lawrence Counties, Kentucky: U.S. Geol. Survey Geol. Quad. Map GQ–1398. (In press.)

Horne, J. C., and Baganz, B. P., 1974, Correlations of coal bearing strata in eastern Kentucky: Geol. Soc. America Abs. with Programs, v. 6, no. 7, p. 800.

Jillson, W. R., 1919, The Kendrick Shale—a new calcareous fossil horizon in the coal measures of eastern Kentucky: Kentucky Dept. Geology and Forestry, Mineral and Forest Resources of Kentucky, ser. 5, v. 1, no. 2, p. 95–104.

Klovan, J. E., and Billings, G. K., 1967, Classification of geological samples by discriminant-function analysis: Canadian Petroleum Geology Bull., v. 15, no. 3, p. 313–330.

Mason, C. C., and Folk, R. L., 1958, Differentiation of beach, dune, and aeolian flat environments by size analysis, Mustang Island, Texas: Jour. Sed. Petrology, v. 28, no. 2, p. 211–226.

Picard, M. D., 1971, Petrographic criteria for recognition of lacustrine and fluvial sandstone: Geol. Soc. America Abs. with Programs, v. 3, no. 7, p. 672.

Pillmore, C. L., and Connor, C. W., 1978, Geologic map of the Blaine quadrangle, Lawrence County, Kentucky: U.S. Geol. Survey Geol. Quad. Map GQ–1507. (In press.)

Potter, P. E., 1967, Sand bodies and sedimentary environments —A review: Am. Assoc. Petroleum Geologists Bull., v. 51, no. 3, pt. 1, p. 337–365.

Sanchez, J. D., Alvord, D. C., and Hayes, P. T., 1978, Geologic map of the Richardson quadrangle, Lawrence and Johnson Counties, Kentucky: U.S. Geol. Survey Geol. Quad. Map GQ–1460. (In press.)

Van Andel, T. H., 1958, Origin and classification of Cretaceous, Paleocene, and Eocene sandstones of western Venezuela: Am. Assoc. Petroleum Geologists Bull., v. 42, no. 4, p. 734–763.

Visher, G. S., 1969, Grain-size distributions and depositional processes: Jour. Sed. Petrology, v. 39, no. 3, p. 1074–1106.

Ward, D. E., 1978, Geologic map of the Adams quadrangle, Lawrence County, Kentucky: U.S. Geol. Survey Geol. Quad. Map GQ–1489. (In press.)

Whaley, P. W., 1969, A litho-genetic model for rocks of a lower deltaic plain sequence: Louisiana State Univ. and Agr. and Mech. Coll., Baton Rouge, Ph. D. thesis, 135 p.

Jour. Research U.S. Geol. Survey
Vol. 6, No. 5, Sept.-Oct. 1978, p. 603-610

FERROAXINITES FROM THE FEATHER RIVER AREA, NORTHERN CALIFORNIA, AND FROM THE McGRATH AND RUSSIAN MISSION QUADRANGLES, ALASKA

By ANNA HIETANEN and RICHARD C. ERD, Menlo Park, Calif.

Abstract.—In the Feather River area, California, and in the McGrath quadrangle, Alaska, axinite-bearing veins occur as fracture fillings along or near the fault zones, suggesting that boron was introduced along the fractures. An unusual occurrence of axinite as a possible primary constituent of a plutonic rock is in the Russian Mission quadrangle, Alaska. The four analyzed axinites from these widely different localities and from different host rocks are surprisingly similar in chemistry and optics. All are ferroaxinites, having high iron and low manganese and magnesium contents. The number of calcium ions is very close to two, which is in agreement with the idealized formula $Ca_2(Fe,Mn,Mg)Al_2BSi_4O_{15}(OH)$. The indices of refraction increase slightly with increasing FeO : MgO ratio over the small range studied.

Boron, when present in metamorphic terranes, commonly forms tourmaline; a rarer boron-bearing mineral, axinite, crystallizes in a calcium-rich and mafic environment. Because tourmaline, as well as axinite, crystallizes within a wide temperature-pressure range, its presence is an indication of a high boron content rather than of certain geologic conditions. It is hoped that the new material presented in this paper will contribute to the knowledge of the dependence of the composition of axinite upon its environment.

FERROAXINITE IN THE FEATHER RIVER AREA

In the Bucks Lake quadrangle, northern California, brown axinite occurs with white quartz in veins that cut a fine-grained metadacite and meta-andesite just west of the serpentine belt that is bounded by the Melones fault in the northeast and by the Rich Bar fault in the southwest. The host rock of the axinite-bearing veins is next to the Rich Bar fault for a distance of 2 km. The specimens of axinite were collected in sec. 16, T. 25 N., R. 8 E., along a small dirt road leading to Silver Creek (fig. 1, loc. 933).

The wallrock of the quartz-axinite veins is a fine-grained metavolcanic rock shown as metadacite on the geologic map of the Bucks Lake quadrangle (Hietanen, 1973). In section 16, it consists of clinopyroxene, amphibole, chlorite, plagioclase, quartz, hematite, and leucoxene. Small laths of plagioclase, many showing Carlsbad twinning, and interstitial grains of plagioclase and quartz are in the rusty-colored mesh of pyroxene and chlorite. All these dark constitutents are so heavily clouded by hematite and leucoxene that the identification could be made only by X-ray diffraction or, along the less clouded edges, by optical methods. Amygdules of quartz are transected by slender needles of amphibole. Some aggregates of quartz include one or two prisms of pyroxene rimmed by amphibole.

The southward extension of this metavolcanic unit contains less hematite, thereby allowing the identification of the minerals under the microscope. In this rock, small prisms of pyroxene partly altered to hornblende occur in radiating bundles resembling spherulites.

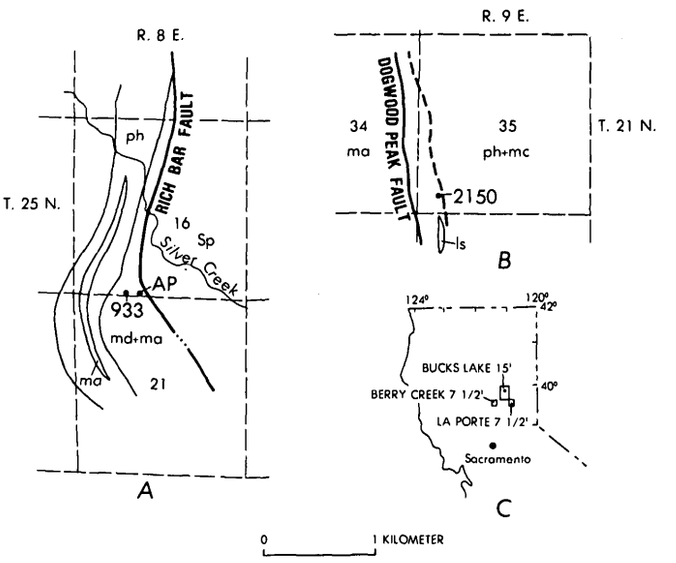

FIGURE 1.—Sketch maps showing location and geologic environment of analyzed axinite specimens. *A*, Specimens 933 and AP in Bucks Lake quadrangle. *B*, Specimen 2150 in La Porte quadrangle; Sp = serpentine, md = metadacite, ma = meta-andesite; ph = phyllite, mc = metachert, and ls = limestone of Calaveras Formation; geology from Hietanen (1973). *C*, Sketch map of northern California showing locations of Bucks Lake, La Porte, and Berry Creek quadrangles.

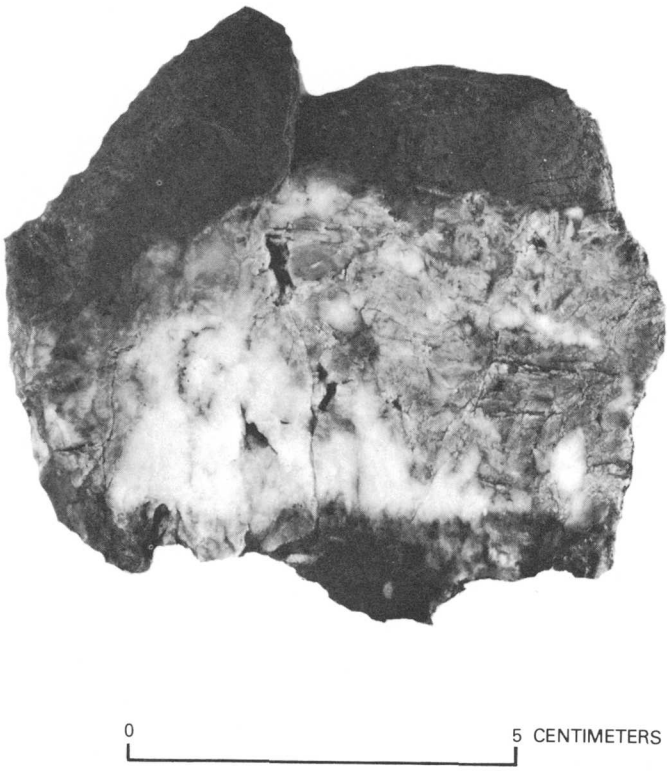

FIGURE 2.—Specimen 933 from axinite-quartz vein in metaandesite (dark gray). White mineral is quartz; light gray is mainly axinite with some quartz and minor amphibole and hematite.

Albite occurs as small scattered laths and also as an interstitial mineral with quartz and chlorite. Most of the quartz is in pods and veinlets and includes hairlike needles of amphibole. Amygdules are filled with chlorite and quartz. In places, the quartz content is high enough to make the total composition dacitic. The pyroxene in this rock is probably a primary mineral, and hornblende, chlorite, and albite crystallized during the metamorphism at the temperatures of the epidote-amphibolite facies.

The axinite-bearing veins in the locality of specimen 933 are 3 to 15 cm thick (fig. 2) and include small angular to elongate fragments of host rock, suggesting that the vein material occurs as a fracture filling. Thin veins of gray quartz are common parallel to the axinite-bearing veins. Thin sections show small fragments of host rock at every stage of replacement by the vein material. The large inclusions have irregular hazy outlines, giving an impression that their size has been reduced by marginal replacement. Small clusters of tiny grains of hematite represent the last remnants of many replaced inclusions. Some large inclusions consist of sodarhyolitic rock with irregular radiating laths of albite and small grains of hematite. The proportion of axinite relative to quartz in the veins is highly variable; some parts of veins are about 70 volume percent axinite, whereas others are mainly quartz with only a few small crystals of axinite. Quartz next to the walls of the veins and next to the fragments of the host rock in the veins is transected by hairlike amphibole needles that extend from the walls at an angle of 20°–70°. In places, amphibole needles rim the axinite crystals near the walls and next to the inclusions.

The axinite is either in large subhedral crystals or in well-developed platy crystals, 0.5 to 2 cm long, that show euhedral crystal faces toward large interstitial grains of quartz. In places, however, small euhedral quartz crystals are included in large grains of axinite. These mutual relations suggest contemporaneous crystallization of quartz and axinite. In the center of the vein, well-developed euhedral crystals of axinite and quartz are attached to the walls of small vugs. The indices of refraction of axinite in specimen 933 are $\alpha=1.671(1)$, $\beta=1.677(1)$, $\gamma=1.682(1)$. Chemical analysis (table 1, analysis 1) shows that it contains 5.96 percent B_2O_3 and 1.62 percent H_2O^+. The FeO content is high and the MnO and MgO contents are low, indicating that it is a ferroaxinite. In the calculated formula $Ca_2(Fe,Mn,Mg)Al_2BSi_4O_{15}(OH)$, the Fe:Mn:Mg ratio is 67:7:26. In a ternary Fe-Mn-Mg diagram (fig. 3), this composition plots near the Fe-corner.

Analysis 2 (table 1) and the remaining part of the analyzed specimen were kindly provided by Adolf Pabst, University of California, Berkeley, who collected this specimen from a crest of a small hill on the east side of the Silver Creek road (fig. 1, loc. AP). The analysis made by W. H. Herdsman, Glasgow, Scotland, shows no water but has a higher boron content than specimen 933. The MgO content is higher, and the FeO content lower. The indices of refraction ($\alpha=1.671(1)$, $\beta=1.676(1)$, $\gamma=1.682(1)$, and $-2V \approx 82°$) and the unit-cell data (table 2), however, are nearly identical.

The occurrence of axinite with quartz as a fracture filling in a metavolcanic rock near a major fault zone suggests that boron along with quartz was introduced along the fracture zones. The replacement character

TABLE 1.—Composition and optical properties of axinites from the Bucks Lake quadrangle, California (analyses 1, 2), and from the McGrath and Russian Mission quadrangles, Alaska (analyses 3, 4)

[Chemical analyses 1, 3, 4, by Marcelyn Cremer, USGS; SiO_2, Al_2O_3, and total Fe as Fe_2O_3 were determined spectrophotometrically; MgO, CaO, H_2O+, and H_2O-, gravimetrically; MnO and MgO by atomic absorption spectroscopy; K_2O and Na_2O by flame photometry; and B_2O_3 by potentiometric titration; analysis 2 by W. H. Herdsman, Glasgow, Scotland. Spectrographic analysis 1 by Chris Heropoulos, analyses 3 and 4 by R. E. Mays]

Specimen no.-933	AP	68AHr57	370
Analysis----- 1	2	3	4
Chemical analyses (in weight percent)			
SiO_2----- 42.5	43.63	43.0	41.9
TiO_2----- .04	.12	----	----
B_2O_3----- 5.96	7.04	5.6	6.0
Al_2O_3---- 17.8	18.02	17.2	18.4
Fe_2O_3---- -----	.06	----	----
FeO------ 8.91	7.76	9.4	9.9
MnO------ .93	.59	1.7	1.4
MgO------ 1.94	3.03	2.1	1.3
CaO------ 19.91	19.76	19.8	19.5
Na_2O----- .01	.06	----	----
K_2O------ .01	.08	----	----
H_2O+----- 1.62	Nil	1.4	1.5
H_2O^------ .06	Nil	.0	.0
Cl------- -----	.02	----	----
Total-- 99.69	100.17	100.2	99.9
Spectrographic analyses (in parts per million)			
Ag ----- -----		5	<2
Ba------ 110		<2	10
Be------ -----		<2	23
Co------ 13		----	----
Cr------ <2		34	8
Cu------ 7		34	<2
Ni------ 10		7	<2
Sc------ -----		13	<4
Sr------ 180		36	55
V------- 130		260	60
Zn------ 470		----	----
Y------- -----		30	40
Zr------ -----		<20	80
Ga------ 23		19	20
Yb------ -----		5	6
Number of ions on the basis of 32 (O, Oh, Cl)			
B-------- 1.94	2.282	1.83	1.96
Si------- 8.01	8.192	8.13	7.93
Al^{+3}----- 3.96	3.988	3.83	4.10
Fe^{+3} ----- } 3.97	.009 } 4.014	-----	-----
Ti------- .01	.017	-----	-----
Mg^{+2}----- .54	.849	.59	.37
Fe^{+2} ----- 1.40 } 2.09	1.219 } 2.162	1.49 } 2.35	1.57 } 2.16
Mn------- .15	.094	.27	.22
Ca------- 4.02	3.975	4.01	3.95
Na------- .00	.023 4.018	-----	-----
K-------- .00	.020	-----	-----
OH------- 2.04	------	1.77	1.89
Cl------- -----	.007	-----	-----
Optical properties			
α-------- 1.671±0.001	1.671±0.001	1.672±0.001	1.676±0.001
β-------- 1.677±0.001	1.676±0.001	1.678±0.001	1.681±0.001
γ-------- 1.682±0.001	1.682±0.001	1.684±0.001	1.686±0.001
-2V------	82°±		

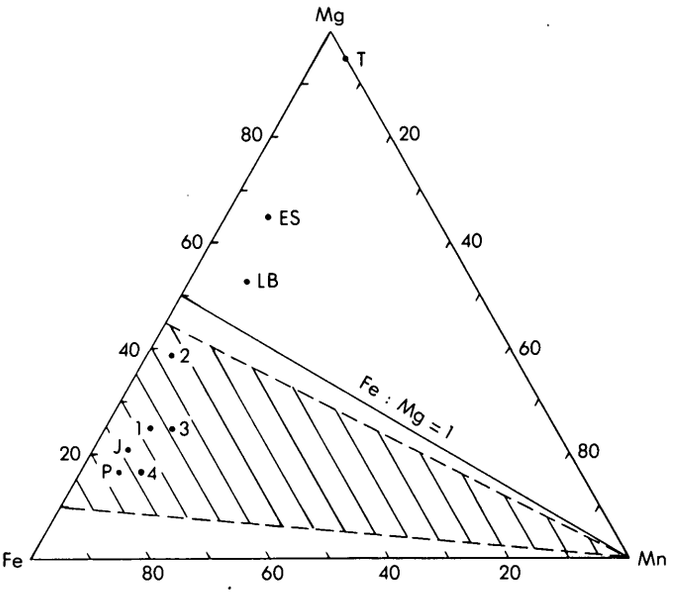

FIGURE 3.—Ternary diagram showing the variation of Fe, Mn, and Mg in analyzed axinites. Most axinites described in literature plot within shaded area of this diagram. Numbers 1 to 4 refer to analyses in table 1; P and J, ferroaxinites from Petsamo and Jokioinen (Simonen and Wiik, 1952); LB, magnesioaxinite from London Bridge, New South Wales, Australia (Vallance, 1966); ES, magnesioaxinite from eastern Siberia (Nekrasov, 1971); and T, magnesioaxinite from Tanzania (Jobbins and others, 1975).

of the vein material indicates that the other elements needed to form axinite may have been derived from the host meta-andesite in which these other elements occur in ratios comparable to those in the axinite except for much less Fe_2O_3 (compare analysis 463 of Hietanen, 1973) in the axinite. Presumably, the excess Fe_2O_3 migrated to the walls and inclusions, enriching them in hematite.

About 34 km south-southeast of the Silver Creek locality in the south-central part of the La Porte quadrangle (fig. 1), axinite, with albite and some quartz, fills fractures in a brecciated hornblende-albite-epidote-sphene rock that lines up parallel to the trends with a discontinuous layer of marble exposed in a roadcut 0.3 km to the south. The marble is interbedded with metachert and phyllite of the Calaveras Formation. Brecciated meta-andesite is exposed in a roadcut 0.5 km to the north. The occurrence of axinite is on the north slope of Canyon Creek about 0.25 km east of the Dogwood Peak fault in sec. 35, T. 21 N., R. 9 E. A thin layer of talc schist is exposed next to the brecciated hornblende-albite rock.

TABLE 2.—Unit-cell data for axinites

[Data for specimens 933, AP, 68AHr57, and 370 obtained from refinement of X-ray powder data using the least-squares program of Appleman and Evans (1973). X-ray diffractometer conditions are: Cu/Ni radiation λ CuKα_1 = 1.540598 Å; aluminum used as internal standard; scanned at ¼° per minute from 9–85° 2θ.]

Specimen-------	933	AP	68AHr57	370	Ferro-axinite[1]	Mangan-axinite[2]	Magnesio-axinite[3]	Tinzenite[4]
a (A)----------	8.959(])	8.952(1)	8.954(1)	8.963(2)	8.958(2)	8.978(3)	8.933	8.947(2)
b (A)----------	9.194(1)	9.192(1)	9.194(1)	9.203(1)	9.200(2)	9.190(3)	9.155	9.120(5)
c (A)----------	7.150(1)	7.147(1)	7.150(1)	7.156(1)	7.157(2)	7.161(3)	7.121	7.165(2)
α----------	102°40(1)'	102°37(1)'	102°39(1)'	102°37(1)'	102°42(1)'	102°44(1)'	102°35'	103°06(18)'
β----------	98°08(1)'	98°10(1)'	98°11(1)'	98°09(1)'	98°08(1)'	98°12(2)'	98°17'	98°48(18)'
γ----------	88°09(1)'	88°09(1)'	88°09(1)'	88°08(1)'	88°15(50)'	88°16(2)'	88°05'	88°06(6)'
Volume (A^3)—	568.8(1)	568.1(1)	568.5(1)	570.3(1)	569.6	570.3	562.4	562.8
a/b----------	.974	.974	.974	.974	.974	.977	.976	.981
c/b----------	.778	.778	.778	.778	.778	.779	.778	.786

[1]Ito and others (1969). Specimen from Woodlake, Tulare County, Calif. (Type collection no. 9620, Colorado School of Mines); Fe:Mn approximately 1:1. Material used for crystal structure study (Takéuchi and others, 1974). Data slightly modified for comparison; cell changed to standard setting, transformation matrix 001/0$\bar{1}$0/001.

[2]French and Fahey (1972). Specimen from the Peter Mitchell pit of the Reserve Mining Co. near Babbitt, St. Louis, County, Minn. (Specimen MF-62-85); MgO 0.25, Fe_2O_3 0.10, FeO 3.27, MnO 11.66 wt percent. Changed to standard setting, transformation matrix 001/0$\bar{1}$0/001.

[3]Jobbins, Tresham, and Young (1975). Specimen from Tanzania (registered number MI 34610 of the Institute of Geological Sciences, London); MgO 6.9, Fe_2O_3 not found, FeO not found, MnO 0.4 wt percent.

[4]Basso, Della Giusta, and Vlaic (1973). Specimen from Cassagna, Italy. Chemical analysis (Penco and Sanero, 1964) shows MgO 0.14, Fe_2O_3 1.21, FeO trace, MnO 20.65 wt percent. Changed to standard setting, transformation matrix 001/0$\bar{1}$0/100.

The host rock of the axinite veins consists of light-green hornblende and albite or of albite, quartz, epidote, hornblende, and sphene. The albite includes alteration products, sericite and epidate. Some of the fractures are filled mainly with axinite and less albite and quartz; others contain albite, quartz, and hornblende. A part of albite and quartz in the veins is transected by hairlike needles of amphibole. Tabular crystals of albite (An_5) line the walls of many narrow vugs. The axinite is very light brown to almost colorless. The indices of refraction measured in specimen 2150 are α=1.672(1), β=1.678(1), γ=1.683(1), and $-2V\approx80°$.

Axinite occurs in many other localities in the Feather River area and has been of interest to mineral collectors during recent years. The indices of refraction determined in a sample collected along the West Branch at the west border of the Berry Creek quadrangle (now covered by water of Lake Oroville) are α=1.671(1), β=1.677(1), γ=1.683(1), and $-2V\approx85°$, similar to indices of other axinites in the Feather River area. In this locality, axinite occurs with quartz and calcite.

In most occurrences described in the literature, calcite is considered an essential constituent of the axinite-bearing assemblages (Deer and others, 1962; Vallance, 1966; Simonen and Wiik, 1952). In the Bucks Lake quadrangle, no calcite was found in the quartz-axinite veins. In the wallrocks of these veins, calcium is in pyroxene and amphibole, whereas, in meta-andesite and metadacite elsewhere, it is in epidote and actinolitic hornblende. The combined percentage of calcium-rich minerals in most meta-andesites is 40 to 60 mole percent, providing a calcium-rich environment for the boron-bearing solutions moving along the fracture zones.

FERROAXINITES FROM ALASKA

In the McGrath A–5 quadrangle, Alaska (fig. 4), gray axinite occurs in narrow-veins in metamorphosed argillite that is interbedded with limestone within the Farewell fault zone. Specimen 68AHr57 was collected at lat 62°0′ N., long 155°8′ W. In the Russian Mission C–1 quadrangle, Alaska (fig. 4), crystals of violet-gray axinite occur as scattered clusters in the quartz monzonite of the Russian Mountain pluton. Specimen 370 was collected at lat 61°31′ N., long 159°10′ W. Samples of the axinite-bearing rocks were kindly provided by Joe Hoare, U.S. Geological Survey.

A thin section of specimen 68AHr57 shows axinite in veins that fill fractures in hornfelsed argillite along the Farewell fault zone. The argillite is interbedded with limestone and is recrystallized as a fine-grained mixture of quartz, feldspars, actinolitic hornblende, epidote, calcite, and magnetite. The veins consist of a medium-grained mixture of axinite, light-green amphibole, diopside, calcite, quartz, and some magnetite. Remnants of diopside are included in subhedral prisms of hornblende. Calcite, quartz, and magnetite are interstitial. Axinite is in large subhedral to anhedral crystals in the coarser center of the veins. Chemical

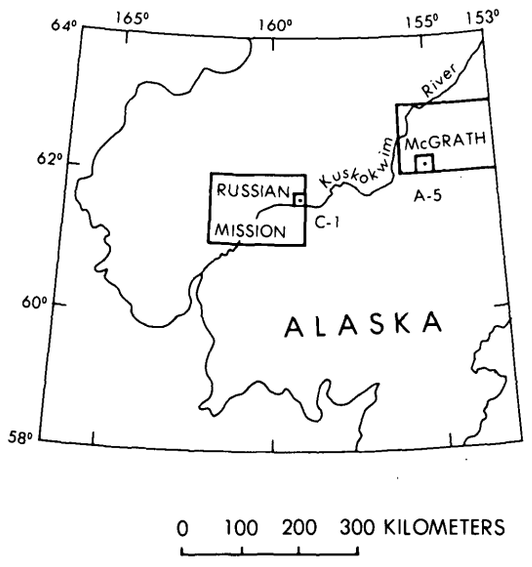

FIGURE 4.—Sketch map of southwestern Alaska showing locations of McGrath A–5 (Specimen 68AHr57) and Russian Mission C–1 (Specimen 370) quadrangles. Dot indicates specimen location.

analysis (table 1, analysis 3) shows that it is a ferroaxinite with only a little higher manganese and lower boron content than the axinite from the locality of 933 in the Bucks Lake quadrangle; the indices of refraction (table 1) are somewhat higher.

Thin sections of quartz monzonite (specimen 370) from the Russian Mission quadrangle show 1-cm-long clusters of subhedral to anhedral crystals of axinite (1–2 mm long), large (3–5 mm long) twinned and weakly zoned crystals of plagioclase (An_{30}), and large twinned crystals of orthoclase embedded in a medium-grained mixture of quartz, plagioclase, and potassium feldspar. The feldspars contain abundant alteration products, calcite, and muscovite. Chlorite is a scanty constituent and is probably an alteration product after hornblende; it occurs in large flakes, many of which have shapes of hornblende and centers consisting of calcite. Apatite, magnetite, sphene, epidote, and zircon occur as accessory minerals. The axinite crystals are clustered with subhedral crystals of quartz and include grains of calcite, some as intergrowths. In some spots, the fine-grained mixture of chlorite and calcite includes small grains of axinite.

The occurrence of axinite in the quartz monzonite may be unique for the axinite crystallized as a primary constituent from a boron-bearing magma. Normally, boron-bearing solutions escape from the crystallizing magma, and axinite is deposited with quartz in veins or pegmatites cutting the host rock or in skarns in intruded carbonate rocks. Here, however, boron was probably trapped locally in the crystallizing rock and formed axinite in the presence of abundant calcium and sufficient aluminum and iron. The last hydrothermal solutions were rich in CO_2, altering a part of the calcium-aluminosilicates to calcium carbonate. Occurrences of axinite in rhyolite, granodiorite, granite, and diabase as "host rock" were mentioned by Ozaki (1970b, p. 169), but he did not state whether any of these occurrences were primary. We could find no other description of axinite as a primary mineral in a search of the rather extensive literature on this mineral.

The chemical composition of the axinite in the quartz monzonite (table 1, analysis 4) is close to that of the ferroaxinite in the argillite except for a somewhat lower magnesium content and higher iron content. The ratio of Fe:Mn:Mg in the formula unit is 73:10:17, making it one of the most iron-rich axinites found. In the Fe-Mn-Mg diagram (fig. 3), only the axinite from Petsamo, Finland (Simonen and Wiik, 1952), plots closer to the Fe corner. High-iron ferroaxinites, with total iron as FeO ranging from more than 10.5 to 11.88 weight percent, have been reported by Azimov (1970), Kurshakova (1968), Kurshakova and Tikhomirova (1974), Otroshchenko (1971), and Serdyuchenko and Pavlov (1962). The ferrous-ferric oxide ratio varies widely for these and for other analyses of axinite. Kurshakova (1968, table 1, analysis 41, by Kikuchi in 1893), for example, reports an analysis showing 11.79 weight percent Fe_2O_3 and no FeO. A more modern analysis, reported by Kurshakova and Tikhomirova (1974, table 3, analysis 1), shows Fe_2O_3 6.27 and FeO 5.74 weight percent; Otroshchenko (1971, table 2. analysis 8) gives an analysis showing no Fe_2O_3 and FeO 11.0 weight percent. Ferric iron may substitute for aluminum in the axinite structure (described by Takéuchi and others, 1974), but most modern chemical analyses suggest that the substitution is limited and that ferric oxide in ferroaxinite generally amounts to less than about 2 weight percent. Possibly the analyses showing high percentages of ferric iron have resulted from the oxidation of ferrous iron during the analytical procedures; the wet-chemical analysis of axinite is difficult (Ito, 1962). Study of the Mössbauer spectra should resolve the question of the ferrous-ferric oxide ratio in ferroaxinite. The only such study known to us, that of Takashima and Ohashi (1968), shows good agreement between the ratio determined chemically and that obtained using the Mössbauer effect.

UNIT-CELL DATA

The unit-cell data for the ferroaxinites from California and Alaska are compared in table 2 with those given for the other members of the axinite group. The nomenclature for this group is that of Sanero and

Gottardi (1968) with the addition of magnesioaxinite in which magnesium predominates over iron. Magnesioaxinite was named and described by Jobbins, Tresham, and Young (1975) for an axinite recently found in Tanzania that approaches the Ca_2Mg end-member composition. Other magnesioaxinites have been described from London Bridge, New South Wales, Australia (Vallance, 1966), and from eastern Siberia (Nekrasov, 1971). All of the ferroaxinites of this study are dimensionally close to one another and to the ferroaxinite of Takéuchi and others (1974); the $a:b:c$ ratios are identical. Magnesioaxinite and tinzenite have somewhat smaller unit-cell volumes, and manganaxinite, a slightly larger unit-cell volume than that of ferroaxinite. Our data suggest that the unit-cell dimensions are not particularly useful as a criterion for cation substitution. There is, however, surprisingly little published information giving unit-cell data for axinites.

CONCLUSIONS

All four analyzed axinites are ferroaxinites as defined by Sanero and Gottardi (1968). They have a high iron content and low manganese and magnesium contents. The number of calcium ions in a formula unit is very close to 2, as is typical of most ferroaxinites described in the literature. The differences in composiunit can be shown in the ternary Fe-Mg-Mn diagram tion of axinites with two calcium ions in their formula (fig. 3). The new analyses plot close to the Fe-Mg edge; the ferroaxinite from the quartz monzonite is closest to the Fe corner. The magnesioaxinites from London Bridge and eastern Siberia plot on the Mg side of the Fe: Mg=1 division line, and the magnesioaxinite from Tanzania, near the Mg corner.

This study suggests that the high iron content of axinite is a reflection of a high iron content of the host rock in which the axinite-bearing veins occur. Other occurrences of ferroaxinite in veins cutting metavolcanic rocks have been described in Transvaal, South Africa (Barbour and others, 1957), and Norway (Carstens, 1965). In Japan, ferroaxinite occurs with quartz and calcite in veins that cut tuffaceous slate metamorphosed to albite-quartz-epidote-chlorite rock (Ozaki, 1970a) and with datolite, epidote, quartz, grunerite, and chlorite in calcareous xenoliths in metamorphosed rhyolite (Ozaki, 1972).

REFERENCES CITED

Appleman, D. E., and Evans, H. T., Jr., 1973, Job 9214; indexing and least-squares refinement of powder diffraction data: U.S. Dept. Commerce, Natl. Tech. Inf. Service, PB–216 188.

Azimov, P. T., 1970, Beryllium-containing axinite from pegmatized granite-aplites in Ziaetdin Mountains, western Uzbekistan: Uzbek. Geol. Zhur., v. 14, p. 21–23. [*Through* Chem. Abs., v. 74, 33425 *y*]

Barbour, E. A., Bird, H. H., and Gold, D. P. 1957, An occurrence of axinite in Vertersdorp lavas from Kinross, Transvaal, South Africa: Mineral Mag., v. 31, p. 495–496.

Basso, R., Della Giusta, A., and Vlaic, G., 1973, La struttura della tinzenite: Period. Mineralogia, v. 42, p. 369–379.

Carstens, Harold, 1965, Axinite in the Norwegian Caledonides, *in* Contributions to the mineralogy of Norway, No. 32: Norsk. Geol. Tidsskr., v. 45, p. 397–415.

Deer, W. A., Howie, R. A., and Zussman, J., 1962, Rock-forming minerals— v. 1, Ortho- and ring silicates: New York, John Wiley & Sons, 333 p.

French, B. M., and Fahey, J. J., 1972, Manganaxinite from the Mesabi Range, Minnesota: Am. Mineralogist, v. 57, nos. 5–6, p. 989–992.

Hietanen, Anna, 1973, Geology of the Pulga and Bucks Lake quadrangles, Butte and Plumas Counties, California: U.S. Geol. Survey Prof. Paper 731, 66 p.

Ito, Jun, 1962, A new method of decomposition for refractory minerals and its application to the determination of ferrous iron and alkalies: Chem. Soc. Japan Bull., v. 35, p. 225–228.

Ito, Tei-Ichi, Takéuchi, Yoshio, Ozawa, Toru, Araki, Takaharu Araki, Zoltai, Tibor, and Finney, J. J., 1969, The crystal structure of axinite revised: Japan Acad. Proc., v. 45, p. 490–494.

Jobbins, E. A., Tresham, A. E., and Young, B. R., 1975, Magnesioaxinite, a new mineral found as a blue gemstone from Tanzania: Jour. Gemmology, v. 14, p. 368–375.

Kurshakova, L. D., 1968, Composition and paragenesis of axinites, *in* Marakushev, A. A., ed., Metasomatizm i drugie voprosy fiziko-khimicheskoi petrologii: Akad. Nauk SSSR. Inst. Geol. Mestorozhdeniy, Petrog. Mineralog. i Geokhim. Moscow, Izdatelstvo "Nauka," p. 289–311.

Kurshakova, L. D., and Tikhomirova, V. I., 1974, Axinite and its paragenesis with hedenbergite: Internat. Geol. Rev., v. 16, p. 1360–1369. [Trans. *from* Akad. Nauk SSSR Izv. Ser. Geol. 1973, no. 11, p. 66–76.]

Nekrasov, I. Ya., 1971, Features of tin mineralization in carbonate deposits, as in eastern Siberia: Internat. Geol. Rev., v. 13, p. 1532–1542. [Trans. *from* Sovetskaya Geologiya 1970, no. 12, p. 41–54.]

Otroshchenko, V. D., 1971, Detection conditions and features of the chemical composition of central Asian axinities: Vses. Mineralog. Obshch. Zapiski, v. 100, p. 471–476.

Ozaki, Masaharu, 1970a, Manganese-poor axinite from Hata, Maji, Fukuoka Prefecture, Japan: Kyushu Univ., Fac. Sci. Mem., Ser. D, Geol., v. 20, no. 2, p. 191–194.

———1970b, The chemical variation of axinites in reference to their modes of occurrence: Japanese Assoc. Mineralogists, Petrologists, and Econ. Geologists Jour., v. 64, p. 157–172.

Ozaki, Masaharu, 1972, Chemical composition and occurrence of axinite: Kumamoto Jour. Sci., Geology, v. 9, no. 2, p. 1–34.

Penco, A. M., and Sanero, Edoardo, 1964, Nuove ricerche sulla tinzenite di Cassagna (Liguria) e sue analogie con l'axinite: Doriana, v. 5, no. 154, p. 1–14.

Sanero, E., and Gottardi, G., 1968, Nomenclature and crystal-chemistry of axinites: Am. Mineralogist, v. 53, nos. 7–8, p. 1407–1411.

Serdyuchenko, D. P., and Pavlov, V. A., 1962, Composition and classification of axinites: Vses. Mineralog. Obshch. Zapiski, v. 91, p. 81–84.

Simonen, Ahti, and Wiik, H. B., 1952, The axinites from Jokioinen and Petsamo: Finlande Comm. Géol. Bull. No. 157, p. 1–6.

Takashima, Yoshimasa, and Ohashi, Shigeru, 1968, The Mössbauer spectra of various natural minerals: Chem. Soc. Japan Bull., v. p. 88–93.

Takéuchi, Y., Ozawa, T., Ito, T., Araki, T., Zoltai, T., and Finney, J. J., 1974, The $B^2Si_8O_{30}$ groups of tetrahedra in axinite and comments on the deformation of Si tetrahedra in silicates: Zeitschr. Kristallographie, v. 140, p. 289–312.

Vallance, T. G., 1966, A contact metamorphic axinite paragenesis at London Bridge, near Queanbeyan, N. S. W.: Royal Soc. New South Wales Jour. and Proc., v. 99, p. 57–67.

Jour. Research U.S. Geol. Survey
Vol. 6, No. 5, Sept.-Oct. 1978, p. 611-624

HOLOCENE PYROCLASTIC-FLOW DEPOSITS FROM SHASTINA AND BLACK BUTTE, WEST OF MOUNT SHASTA, CALIFORNIA

By C. DAN MILLER, Denver, Colo.

Abstract.—A broad apron of pyroclastic-flow deposits derived from dacitic domes of Holocene age at Black Butte and Shastina covers an area of more than 110 km² on the west flank of Mt. Shasta volcano. The stratigraphy of the deposits is exposed in roadcuts along a northwest-southeast line between the cities of Weed and Mount Shasta and includes, from bottom to top, pre-Shastina diamictons, a Shastina pyroclastic-flow assemblage, and a Black Butte pyroclastic-flow assemblage. Pyroclastic flows from Shastina, a volcanic cone on the west flank of Mt. Shasta, form a fan of nonvesicular rock debris that overlies part of the Shastina cone and pre-Shastina deposits; the fan deposits thicken northward and underlie the town of Weed. Pyroclastic-flow deposits of both vesicular and nonvesicular rock debris caused by eruptions at the site of Black Butte, a large volcanic dome at the foot of Mt. Shasta, thicken southward and underlie part of the city of Mount Shasta. Soil-profile oxidation is 75–80 cm thick on deposits from both Shastina and Black Butte. As much as 10 m of vertical displacement occurred along east-trending faults 3.5 km northwest of Black Butte after deposition of the youngest two pyroclastic flows from that source. Evidence that faulting and volcanism were nearly simultaneous suggests that the area northwest of Black Butte subsided during a late eruptive phase of the plug dome. Future eruptions similar to those that produced the pyroclastic flows could endanger people and property in any direction downslope from vents, including the communities of Weed and Mount Shasta and possibly other communities in the Shasta Valley and upper Sacramento River area.

A broad apron of pyroclastic-flow deposits covers an area of more than 110 km² on the west flank of Mt. Shasta volcano. The apron is composed chiefly of material derived from vents of Holocene age at the sites of Black Butte and Shastina, west of Mt. Shasta (fig. 1). Shastina is a cone on the flank of Mt. Shasta about 2.5 km west-northwest of the main summit cone. The Shastina cone is composed chiefly of pyroxene-andesite lava flows and a series of hornblende-dacite summit domes (Williams, 1932, 1934; Christiansen and Miller, 1976; Christiansen and others, 1977, fig. 2, this report). Black Butte is a composite hornblende-dacite dome located about 10 km southwest of Shastina between the cities of Weed and Mount Shasta (Williams, 1932, 1934; Crandell, 1973; Miller and Crandell, 1975; figs. 3, 4, this report).

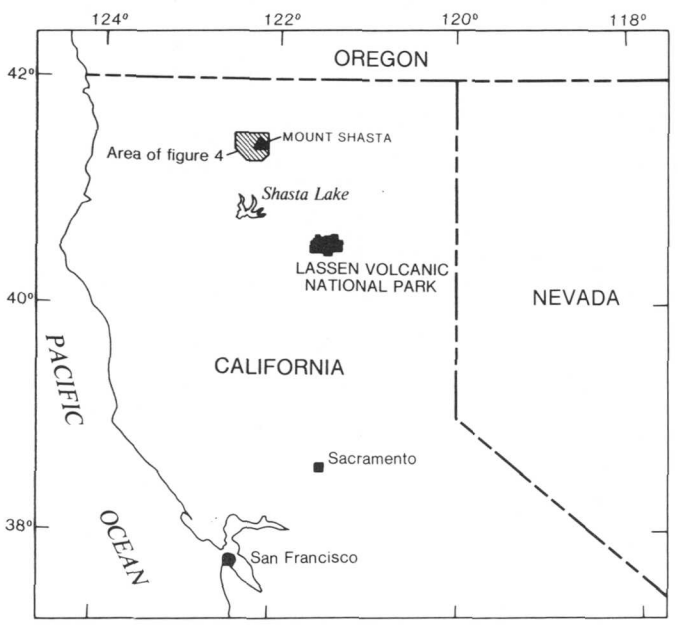

FIGURE 1.—Index map of northern California, showing Mt. Shasta region.

FIGURE 2.—View toward the northeast of multiple dacite domes at summit of Shastina. Diller Canyon in left foreground. Circular summit area is approximately 1 km across. This photograph and all other photographs, except where noted, taken by author. Photograph taken summer 1975.

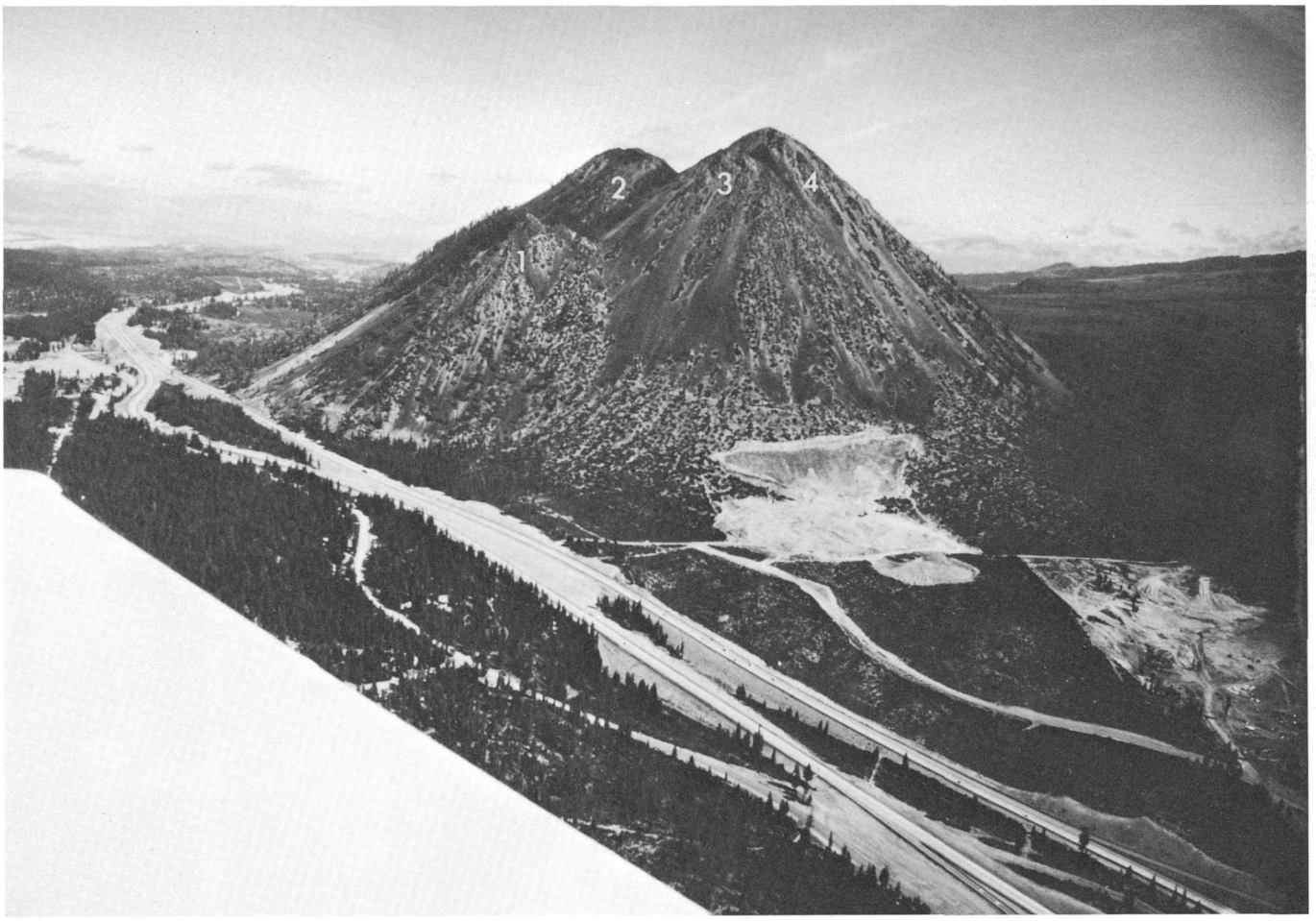

FIGURE 3.—View toward the north of the four dacite domes of Black Butte. Dome segments are numbered 1 through 4, oldest to youngest. Photograph taken summer 1976.

This report describes the lithology, origin, age, and stratigraphy of the apron of pyroclastic-flow material and discusses the kinds of eruptions at Black Butte and Shastina that formed the pyroclastic-flow assemblages. The report results from a detailed evaluation of the stratigraphy and Holocene eruptive history of the Mt. Shasta area undertaken by the U.S. Geological Survey to assess potential volcanic hazards from future eruptions.

The first detailed study of Shastina and Black Butte was by Williams (1932, 1934), who described the petrography of their lavas and recognized the genetic relationship between the summit domes of Shastina and the fan of pyroclastic-flow material below Diller Canyon (fig. 4), to the west. Williams also described some of the deposits from pyroclastic eruptions at Black Butte and recognized its plug-dome origin. The composite fan of pyroclastic-flow debris was briefly described by Crandell (1973) and Miller and Crandell (1975). Initial results of studies on the age, origin, and eruptive behavior of Shastina have been discussed by Christiansen and Miller (1976) and Christiansen and others (1977).

Acknowledgments.—Many of the interpretations and conclusions of this study are the result of discussions with R. L. Christiansen of the U.S. Geological Survey. Christiansen is studying the volcanological and petrological evolution of Mt. Shasta and also recently directed a resource evaluation of the Wilderness Study Area. His work at Shasta is being carried out simultaneously and in cooperation with studies by the author. Meyer Rubin and Elliot Spiker supervised the analysis of radiocarbon samples in the laboratories of the U.S. Geological Survey. Paleomagnetic studies were by R. P. Hoblitt and K. S. Kellogg of the U.S. Geological Survey.

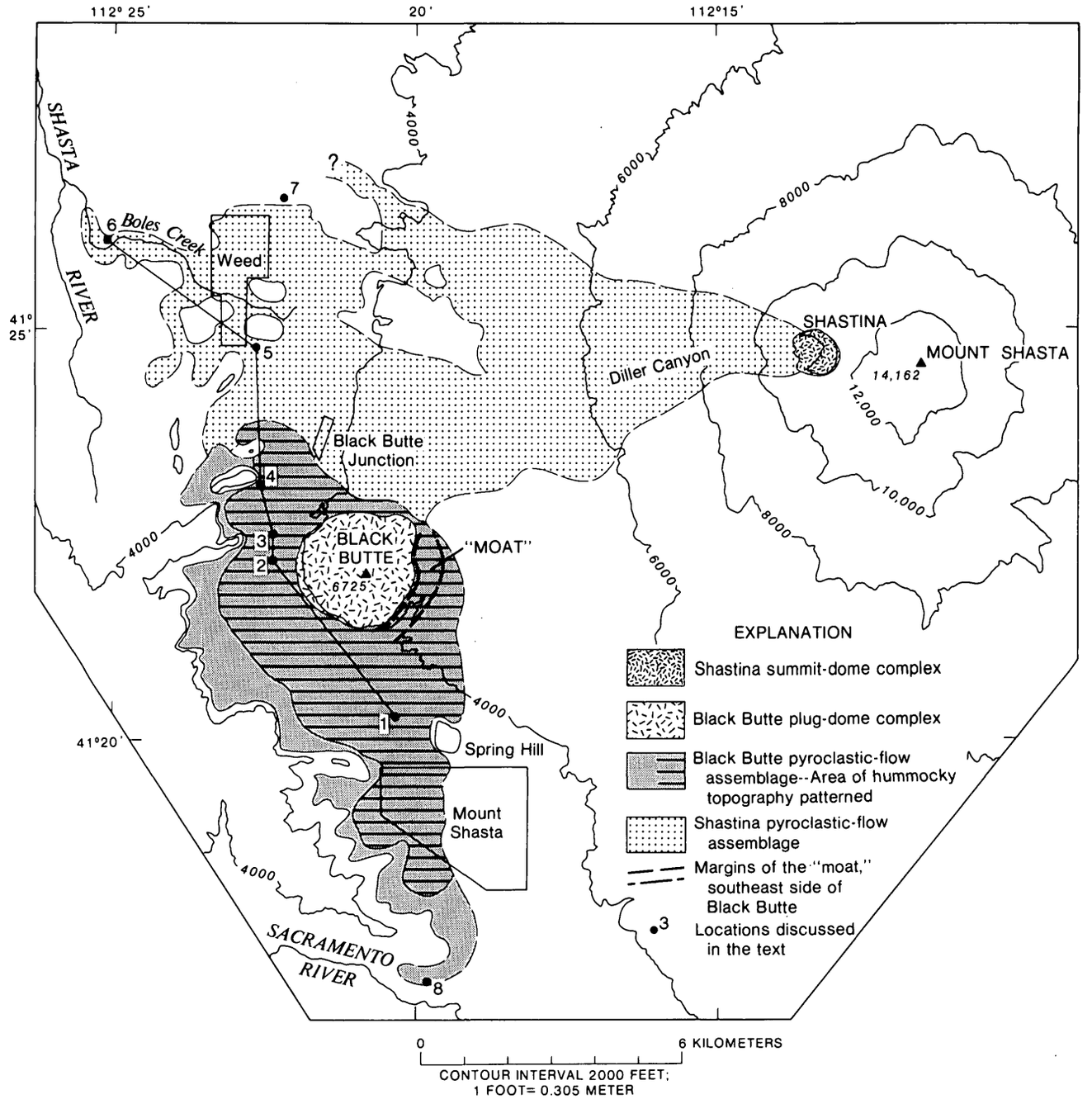

FIGURE 4.—Map of pyroclastic-flow assemblages from Black Butte and Shastina. Outlines dashed or queried where extent uncertain. Base modified from U.S. Geological Survey 1:62 500, Weed, Shasta, 1954.

CHARACTERISTICS OF PYROCLASTIC FLOWS

Pyroclastic flows are masses of hot, dry rock fragments mixed with hot gases, which travel rapidly as a fluidized mixture. The term "pyroclastic flow" as used in this paper includes a group of phenomena often called ash flows and otherwise called glowing avalanches, glowing clouds, nuées ardentes, block-and-ash flows, pumice flows, and hot avalanches. The main distinctions among these phenomena generally involve composition and texture of the constituent particles. The gases in a pyroclastic flow may have been erupted along with the rock debris or emitted by the rocks themselves (Perret, 1935). Air also may be incor-

porated and heated by the moving mass (Perret, 1935; McTaggart, 1960; Crandell and Mullineaux, 1973). As used here, block-and-ash flows consist mostly of nonvesicular rock debris of a wide range in size mixed with hot volcanic gases or hot air. Pumice flows consist of highly vesicular fragments of widely varying sizes in a matrix of ash.

Pyroclastic flows commonly consist of a basal flow of coarse fragments above which finer particles rise in a turbulent cloud. Deposits of ash-size material that settle out from such a cloud have been called ash-cloud deposits by Crandell and Mullineaux (1973). These deposits may be graded and have the characteristics of airfall ash beds and may also be confused with ash deposited by tonguelike pyroclastic flows consisting mostly of ash-size material. Deposits of two or more pyroclastic flows are referred to in this report as a pyroclastic-flow assemblage.

Pyroclastic flows generally follow valleys or other depressions but can have enough momentum to overtop some hills or ridges in their paths (Aramaki and Ui, 1966; Sparks, 1976; Miller and Smith, 1977). They travel at speeds of 50 to more than 150 kilometers per hour and contain debris with temperatures as high as many hundred degrees Celsius.

The pyroclastic-flow deposits discussed here are unstratified, poorly sorted, coarse diamictons composed of dacite fragments as large as 1 m in diameter in an ash matrix. Pyroclastic-flow deposits may closely resemble diamictons produced by lahars, avalanches, or glaciers but can often be distinguished on the basis of some characteristic features (Crandell and Mullineaux, 1975, table 2). The most essential characteristic of pyroclastic-flow deposits is evidence of deposition at high temperature, whereas glacial deposits, some lahars, and most avalanche deposits are deposited at much lower temperatures. Lahars that result directly from volcanic eruptions, however, may contain hot clasts.

The emplacement temperature of a diamicton can be estimated by studying the TRM (thermoremanent magnetization) of its clasts (Hoblitt and Kellogg, 1976, 1978). If the directions of TRM's of clasts in a diamicton are well grouped, it is inferred that the clasts were emplaced above their maximum blocking temperatures (roughly 400°C or higher), and the diamicton probably represents a pyroclastic flow. On the other hand, random directions of TRM's indicate that the clasts were rotated, presumably by transport, after they cooled through their maximum blocking temperatures and before they came to rest. Some hot flowage deposits may have come to rest at temperatures lower than maximum blocking temperatures but higher than ambient; their clasts may possess two or more TRM's superimposed on one another.

A pinkish-gray to hematite-red zone in the upper part of a flowage deposit suggests that the deposit was emplaced when hot and probably was formed by a pyroclastic flow (Williams, 1960; Crandell and Mullineaux, 1973). Although the presence of a pink top seems to be restricted to pyroclastic-flow deposits, the absence of a pink top is not diagnostic; it may be missing from some pyroclastic-flow deposits.

Another indication of high temperature at the time of emplacement is the presence of prismatically jointed blocks that resemble a three-dimensional jigsaw puzzle (Perret, 1935; Verhoogen, 1937; Francis and others, 1974; fig. 5, this report). Many such blocks have disintegrated in place during cooling after they came to rest. Such blocks generally are common in pyroclastic flows produced by collapse of lava domes, and their presence may be diagnostic of such an origin (R. S. J. Sparks, written commun., 1977).

The presence of charcoal is indicative of emplacement at a high temperature, when it can be shown that the charcoal formed in place. Evidence for wood burning in place includes the presence of openwork gravel "pipes" above the charcoal that were produced by escape of volatiles released during destructive distillation of the wood after the enclosing deposit came to rest. Small charcoal branches and twigs that are too fragile to have been transported unbroken as charcoal also provide evidence of having been formed in place after deposition. Some deposits discussed in this report have been identified as pyroclastic flows by one or more of these indications of high temperature.

PYROCLASTIC-FLOW DEPOSITS FROM SHASTINA AND BLACK BUTTE

Pyroclastic-flow deposits from Shastina and Black Butte cover an area of about 110 km^2 that extends about 20 km south from Weed and is as wide as 17 km from east to west (fig. 4).

The Shastina and Black Butte pyroclastic-flow assemblages can be differentiated by the Fe-Mg silicate mineral suites of their constituent clasts. Rocks in the Shastina assemblage contain various proportions of hypersthene, augite, and hornblende, but clasts in the Black Butte assemblage contain only hornblende as the Fe-Mg heavy-silicate mineral.

The stratigraphy of the composite apron formed by the Shastina and Black Butte assemblages is best illustrated by a northwest-southeast stratigraphic cross section from Boles Creek, west of Weed (figs. 4, 6; loc. 6), to the Shasta asphalt quarry, north of the city

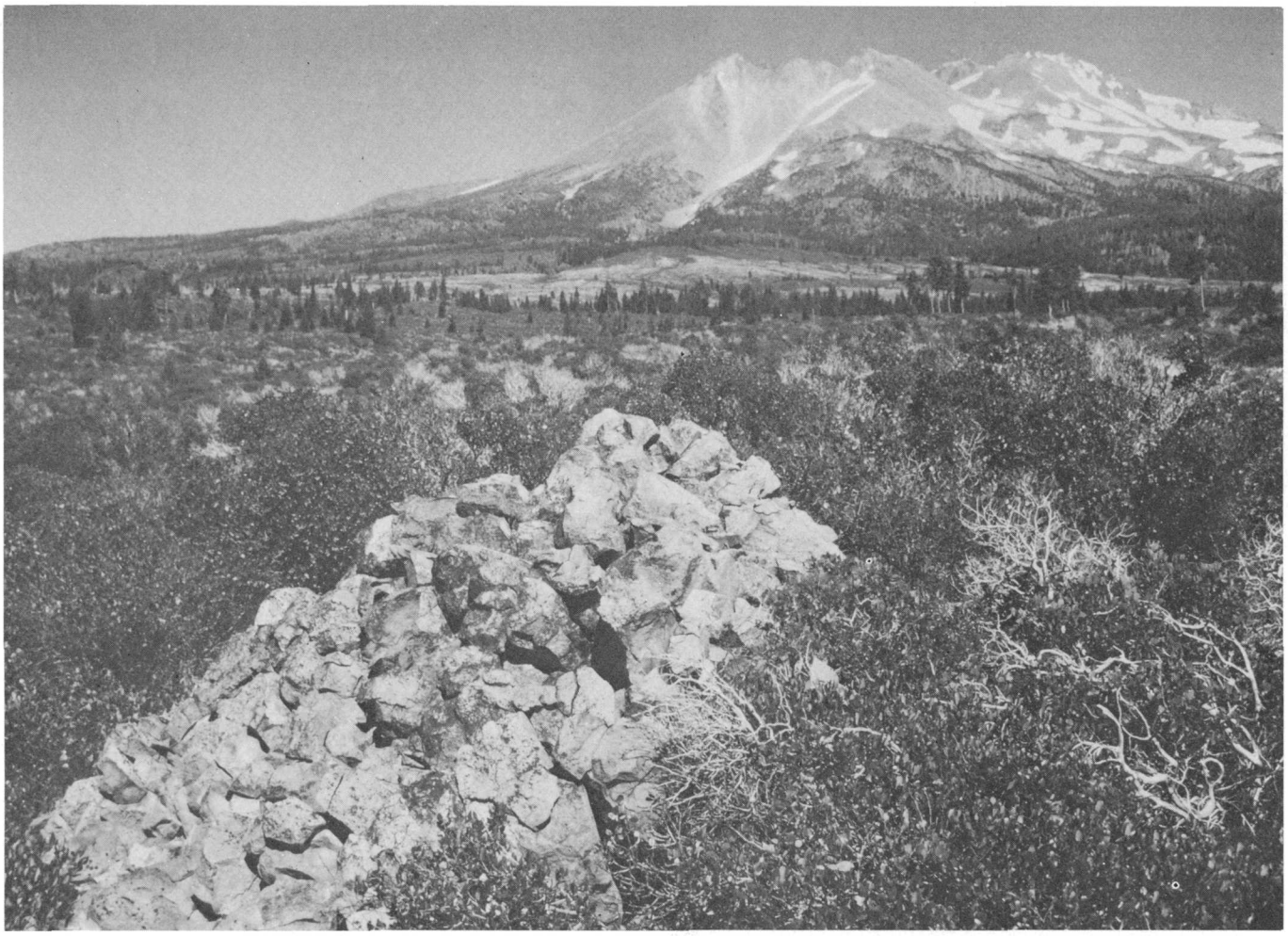

FIGURE 5.—Prismatically jointed boulder on Shastina fan; Diller Canyon, Shastina, and Mt. Shasta (far right) in background. Boulder is about 4 m in maximum dimension. Photograph taken summer 1974.

of Mount Shasta (figs. 4, 6; loc. 1) and west of Spring Hill. The cross section spans about 15 km, following Interstate 5, where roadcuts expose a complex series of diamictons.

The essential details of the cross section are shown diagrammatically in six stratigraphic sections numbered in figures 4 and 6. The stratigraphic units can be divided, from bottom to top, into (1) pre-Shastina diamictons, (2) Shastina pyroclastic-flow assemblage, and (3) Black Butte pyroclastic-flow assemblage. These stratigraphic units are all well exposed in a single roadcut about 1 km northwest of Black Butte (figs. 6, 7; loc. 2). At the base of the section are three pre-Shastina diamictons, the upper and lower of which have buried soils developed at their tops. The upper pre-Shastina diamicton contains striated and faceted boulders in a clayey matrix and evidently is a glacial till. Oxidation and a textural B horizon extend to a depth of several meters in the till at locality 2, and to a depth of more than 4 m at locality 3, farther north (fig. 4). Soil-profile development to such a depth suggests that the till is more than about 100 000 years old and is possibly equivalent to the drift of early Tahoe(?) or latest pre-Tahoe(?) age in Lassen Volcanic National Park (Crandell, 1972). The origin and age of the middle and lower diamictons are not known.

Above the till are unconsolidated pyroclastic-flow deposits of the Shastina and Black Butte assemblages that lap out or thin on pre-Shastina topographic highs and thin toward the south and north, respectively (fig. 6).

DESCRIPTION OF THE SHASTINA ASSEMBLAGE

A fan composed of Shastina pyroclastic-flow deposits extends from Diller Canyon (figs. 2, 5) on the

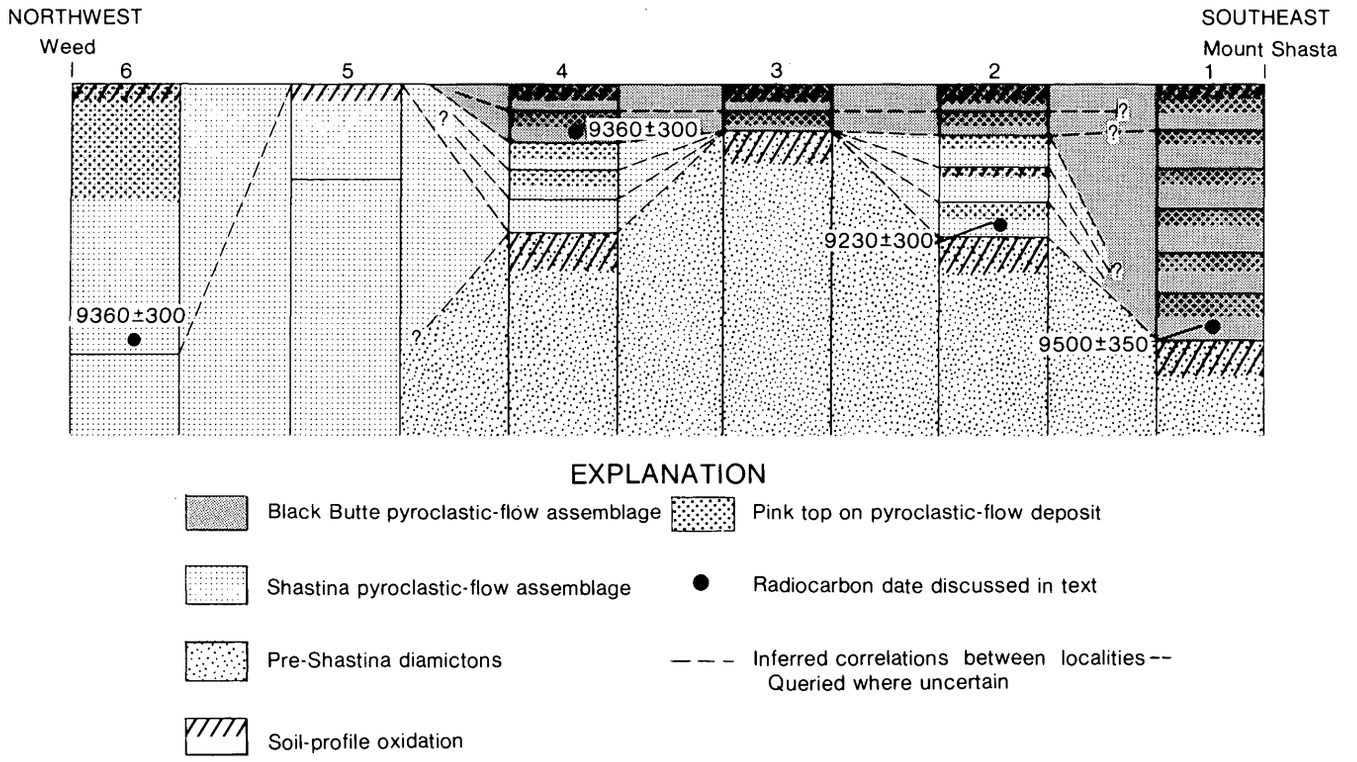

FIGURE 6.—Diagrammatic cross section along Interstate 5 between Weed and the city of Mount Shasta. Numbers 1–6 refer to localities (fig. 4). Cross section is about 15 km long and individual exposures are between 3 and 12 m high.

west side of Shastina westward about 17 km and merges with a fill terrace along Boles Creek that is underlain by two pyroclastic flows from Shastina (fig. 4). The fan is as wide as 6.5 km and underlies an area of about 65 km², including most of the town of Weed. The surface of the Shastina fan exhibits ridges and furrows that have relief of as much as 25 m and are alined in downslope directions. The fan slopes generally to the west from about 500 meters per kilometer near the top of Diller Canyon to 75 m/km near Black Butte Junction (fig. 4), about two-thirds of the way down the fan; the terrace along Boles Creek (fig. 4) slopes less than 25 m/km. Several isolated, topographically high "islands" are surrounded by the fan debris but are not covered by it.

Clasts in the Shastina assemblage are composed of hornblende-pyroxene dacite identical in lithology to dacite domes exposed at the summit of Shastina. Generally pyroclastic-flow deposits of the Shastina assemblage are poorly sorted and unstratified, in some outcrops, however, they are normally or reversely graded. Vesicular dacite blocks are rare in most deposits of the Shastina assemblage.

Three Shastina pyroclastic-flow deposits are exposed at locality 2, where they are draped over a pre-Shastina hill. The three deposits (fig. 7) vary in thickness, but together they are about 4.5 m thick. In most outcrops, they display pink tops over gray basal parts, and no textural break is apparent at the color change. These flowage deposits are unconsolidated and are poorly sorted and unstratified. At locality 2, they consist of angular to subangular dacite blocks and lapilli in an ash matrix. The largest blocks are about 10 cm in maximum dimension. The rocks are mostly nonvesicular hornblende-pyroxene dacite containing varying proportions of hypersthene, augite, hornblende, and plagioclase phenocrysts. Many dacite blocks in these three deposits are prismatically jointed, suggesting that they were hot when they came to rest. The lowest Shastina pyroclastic flow displays chaotic structure at locality 2; stringers or lenses of the underlying oxidized till extend at odd angles into the pyroclastic flow. The origin of this structure is unknown, but it may result from postdepositional faulting or some peculiarity of the emplacement mechanism of these pyroclastic flows.

Bits and pieces of charcoal have been found near the base of the lowest pyroclastic flow at locality 2, and a charcoal log from the same stratigraphic position in the Interstate 5 roadcut immediately opposite

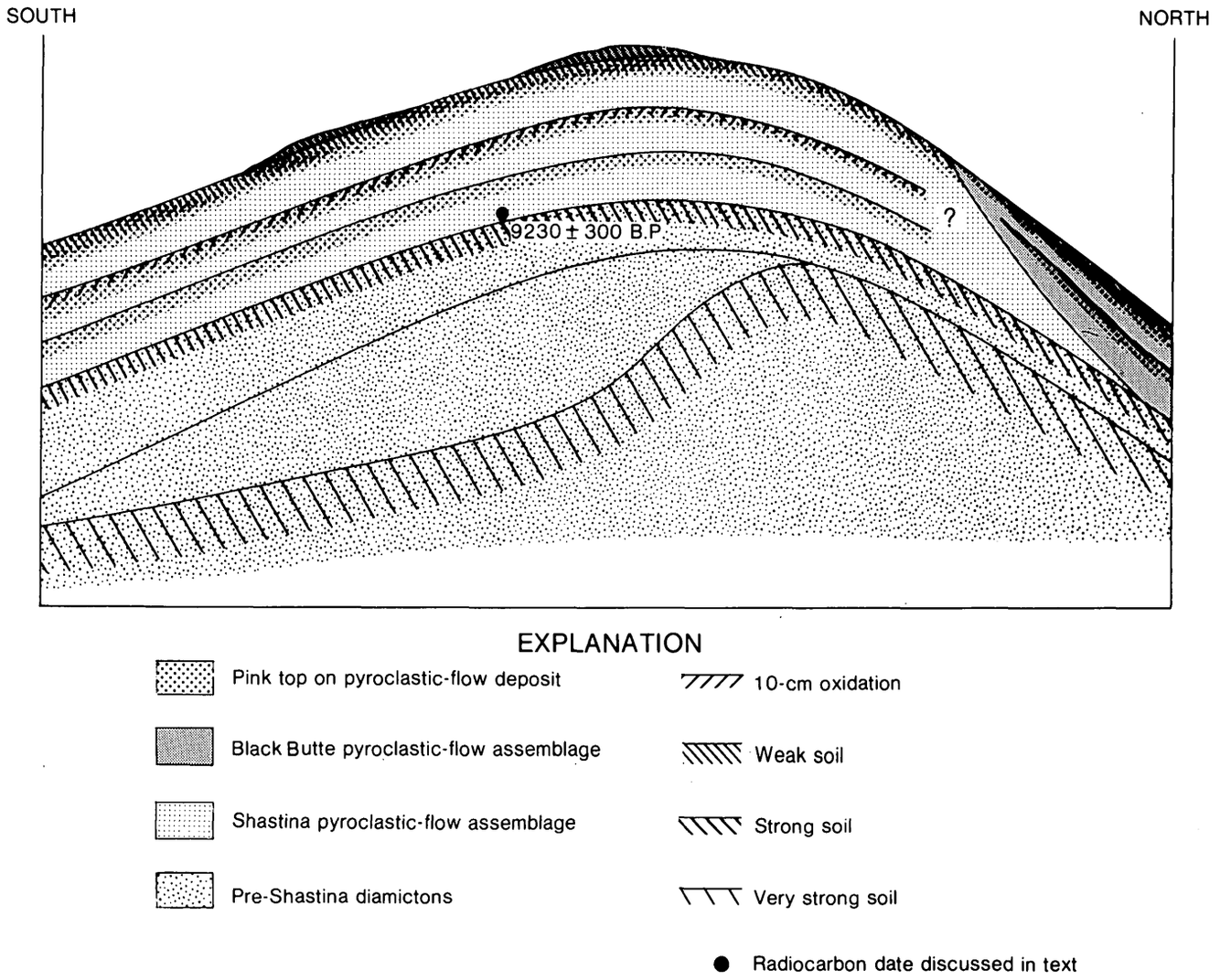

FIGURE 7.—Diagrammatic sketch of stratigraphic units exposed in roadcut at locality 2, 1 km northwest of Black Butte. The section as shown is vertically exaggerated and is about 12 m high and 85 m long. Stratigraphic relationship queried where uncertain.

yielded a radiocarbon date of 9230±300 years B.P. (before present) (W–2814). (See figs. 6, 7.)

Ten centimeters of yellowish-brown oxidation at the top of the middle pyroclastic flow may represent a thin soil profile. Radiocarbon dates from deposits above and below the oxidation of 9360±300 and 9230±300 years B.P., respectively, indicate that the color more likely resulted from high-temperature oxidation at the time of deposition of the pyroclastic flow or that it is a baked zone produced by the overlying pyroclastic flow.

At locality 3, which is the crest of a hill, the Shastina assemblage is missing and the Black Butte assemblage directly overlies oxidized till like that at locality 2. Pyroclastic flows from Shastina apparently did not extend over this hill, or, if they did, they were still mobile enough to flow off the hill into adjacent low areas.

North of locality 3 (fig. 6), the Shastina assemblage thickens and, in places, consists of as many as five pyroclastic flows. At locality 4, the Shastina and Black Butte assemblages are faulted but otherwise are similar to those exposed at locality 2 (figs. 6, 8). The stratigraphic position of the lowest pyroclastic flow of the Shastina assemblage is occupied by silt-sized ash as thick as 20 cm. This deposit has a heavy-mineral suite typical of the Shastina deposits. Its texture suggests that the silt-sized ash was deposited from an ash cloud beyond the margin of a pyroclastic flow.

At locality 5 (fig. 6), the upper of two Shastina

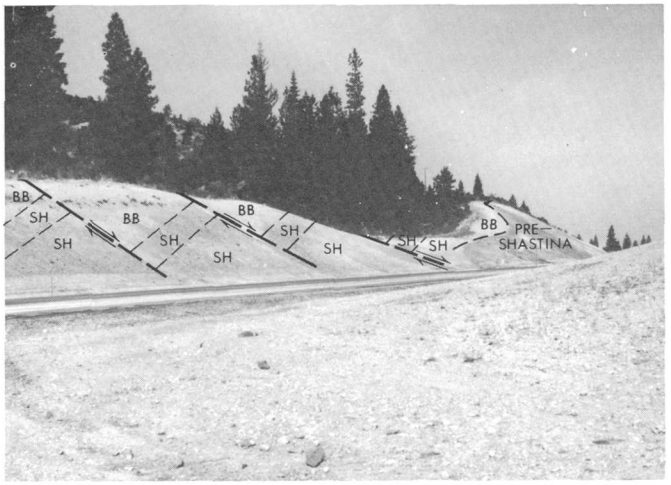

FIGURE 8.—Stratigraphy of Shastina (SH) and Black Butte (BB) pyroclastic-flow assemblages of locality 4. High-angle faults (long dashes) cut both assemblages; arrows show direction of movement. Exposure is about 10 m high. Photograph taken summer 1974.

flowage deposits contains blocks of vesicular hornblende-pyroxene dacite as large as 1 m in maximum dimension, which are prismatically jointed and are part of a diamicton composed of both vesicular and nonvesicular blocks and lapilli in an ash matrix. Farther north, the Shastina assemblage consists of two exposed pyroclastic-flow deposits, which, at locality 6, are more than 8 m thick and contain both vesicular and nonvesicular blocks of hornblende-pyroxene dacite (figs. 4, 6, 9). The upper 2.5 m of the deposit has a faint pink color and commonly contains prismatically jointed blocks. Blocks of both vesicular and nonvesicular dacite in this deposit have TRM's that are preferentially oriented (R. P. Hoblitt, oral commun., 1977); thus, the blocks were hot when they were emplaced. A charcoal log found near the base of this pyroclastic flow has a radiocarbon age of 9360±300 years B. P. (W–3535).

Just north of the Shastina fan, at locality 7 (fig. 4), lies a very well sorted, faintly stratified ash deposit more than 4 m thick. This deposit contains small pieces of charcoal, has a heavy-mineral suite characteristic of the dacites from Shastina, and is immediately adjacent to the Shastina pyroclastic-flow assemblage. These facts suggest that it is an ash-cloud deposit associated with one or more of the Shastina pyroclastic flows.

DESCRIPTION OF THE BLACK BUTTE ASSEMBLAGE

The Black Butte pyroclastic-flow assemblage covers an area of about 44 km^2, surrounding Black Butte and extending as far as 10 km south of the butte (fig. 4). Overall, this pyroclastic-flow assemblage forms a nearly flat surface, although about 23 km^2 (fig. 4) is covered by mounds and depressions with local relief of as much as 10 m. The westernmost and southernmost parts of the Black Butte pyroclastic-flow assemblage are flat topped and slope toward the south 25 m/km or less. All pyroclastic flows from Black Butte contain only hornblende dacite similar to the rock that makes up the Black Butte domes.

Stratigraphically above the Shastina assemblage, and exposed as a wedge on the north side of the outcrop at locality 2, are two pyroclastic flows from Black Butte (fig. 7). Although both units thin upslope along the flank of a hill composed of pre-Shastina diamictons and the Shastina assemblage, scattered thin patches of Black Butte rubble can be traced over the top of the hill. The pyroclastic flows evidently were mobile enough to rise more than 15 m and surmount the hill. The spectacular mobility of some ash flows has recently been discussed by Sparks (1976) and by Miller and Smith (1977). The pyroclastic-flow deposits are thickest in low areas adjacent to such topographic highs.

Both pyroclastic flows from Black Butte at locality 2 are unconsolidated, poorly sorted, and unstratified and have well-developed pink tops. They contain angular to subangular, prismatically jointed, red and gray blocks of hornblende dacite. The combined thickness of the two pyroclastic flows here is as much as 4 m. The lower unit is composed primarily of blocks and lapilli with a sparse ash matrix. Dacite blocks as large as 30 cm are occasionally found, about half of which are vesicular. The upper pyroclastic flow is composed of about 80 percent nonvesicular and 20 percent vesicular clasts but is otherwise lithologically similar to the lower one, except that its matrix contains more ash.

Results of paleomagnetic studies of samples from the Black Butte assemblage indicate that the deposits were emplaced at temperatures above the maximum blocking temperatures of their constituent magnetic minerals, probably above 400°C (R. P. Hoblitt, oral commun., 1977).

North of locality 2, both Black Butte pyroclastic flows are present above the till at locality 3, where they thin and pinch out toward the top of the hill; they thin abruptly to the north and terminate about 1 km north of locality 4 (fig. 4). A radiocarbon date of 9360±300 years B.P. (W–3543), shown in the lower Black Butte pyroclastic flow at locality 4 (fig. 6), was obtained from charcoal twigs collected in the lower pyroclastic flow about 1 km west of locality 4.

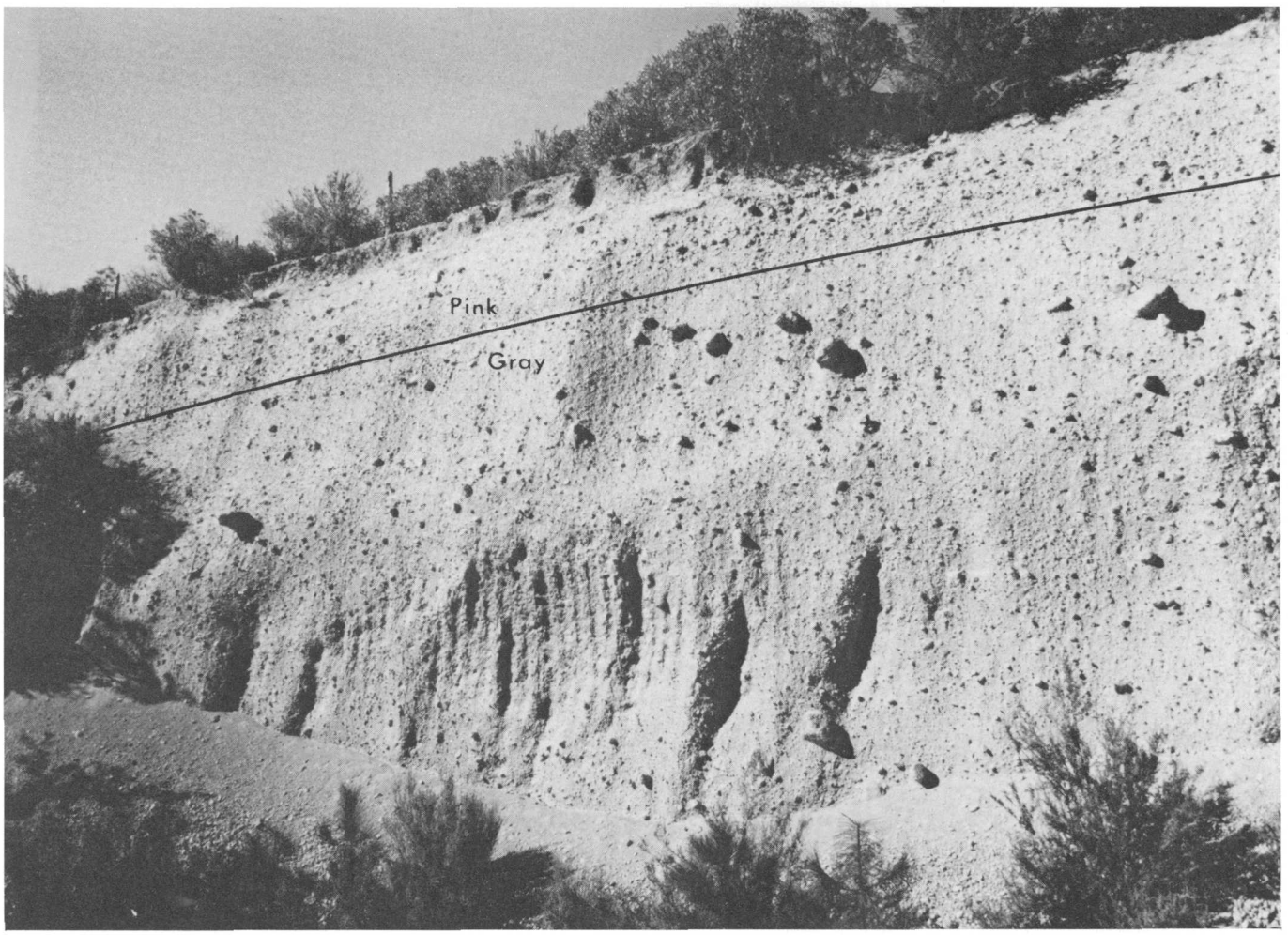

FIGURE 9.—Upper pyroclastic-flow deposit of the Shastina assemblage exposed at locality 6 north of Boles Creek, west of Weed (figs. 4, 6). Upper 2.5 m above line is faint pink in color. The uppermost 70–80 cm is oxidized light yellowish brown (table 1). Lower pyroclastic-flow deposit, not visible in this picture, is exposed along the south bank of Boles Creek. Photograph taken summer 1975.

The Black Butte assemblage thickens southward toward the city of Mount Shasta (figs. 4, 6). As many as 11 pyroclastic flows can be seen in exposures in gravel pits at locality 1, northwest of the city of Mount Shasta. These deposits contain vesicular as well as nonvesicular rock debris, and individual flow units can be distinguished by color, texture, and the presence of pink tops.

As many as six pumiceous pyroclastic flows are exposed at locality 1 (figs. 4, 6, 10), some of which contain vesicular blocks as large as 1 m in maximum dimension; all these flowage deposits are older than the pyroclastic flows from Black Butte exposed at locality 2 (fig. 6). These vesicular block-and-ash flows represent explosive eruptions that are thought to predate the present Black Butte edifice and that represent the earliest recognized eruptions at the site of Black Butte. Charcoal twigs and branches collected from the lowest of the exposed pumice flows yielded a radiocarbon age of 9500±350 years B.P. (W–3537).

Most of the block-and-ash flows at locality 1 contain vesicular blocks and have pink tops, and many are reversely graded, the largest vesicular blocks being concentrated near the top of the flow and maximum clast size decreasing downward. Nonvesicular fragments, however, are concentrated near the bottom of some of these flowage units. Such reverse grading of vesicular clasts, often accompanied by normal grading of nonvesicular clasts, is characteristic of many ignimbrite flow units (Sparks, 1976). The pyroclastic flows ex-

FIGURE 10.—Vesicular block-and-ash flows exposed at locality 1 northwest of the city of Mount Shasta (figs. 4, 6). Photograph taken by D. R. Crandell, U.S. Geological Survey, summer 1972.

posed at locality 1 contain more ash matrix than do the blocky pyroclastic flows from Black Butte described at locality 2 and those exposures farther north.

A Black Butte block-and-ash flow similar in texture to the two Black Butte pyroclastic flows at locality 2 is exposed at locality 8, at the south end of the Black Butte assemblage (fig. 4). This deposit was above 400°C when emplaced (R. P. Hoblitt, oral commun., 1977).

The mounds exposed in the area of hummocky topography (fig. 4) are constructional in form rather than erosional, have no recognizable pattern, and appear to be of two types. One type of mound consists of monolithologic, prismatically jointed blocks derived from the disintegration in place of a single large block, which evidently was transported to its present location in a pyroclastic flow. Some of these blocks are as large as 20 m in maximum dimension (figs. 11, 12). Some masses of unconsolidated pre-Black Butte diamictons were carried at least several kilometers by a pyroclastic flow without being disrupted. A second type of mound, exposed west of Black Butte, is a composite mound composed partly of pre-Black Butte material. Many such mounds consist of material derived from the Shastina assemblage, mantled by one or more layers of pyroclastic-flow debris from Black Butte. Such a pre-Black Butte mound may be the result of erosion or may itself be a rafted block in a pyroclastic-flow deposit.

A series of east-trending, high-angle faults cuts the Black Butte assemblage and older deposits at locality 4 (figs. 4, 8). As much as 10 m of total vertical displacement occurred either concurrently with, or immediately after, deposition of pyroclastic deposits from Black Butte; downthrown sides are consistently to the north (fig. 8). A typical post-Black Butte soil

FIGURE 11.—Mound about 6 m high composed of monolithologic rubble of dacite from Black Butte. Most if not all of the rubble in the mound is thought to have been derived from a single large block of hot rock that disintegrated during and after cooling. Mound is 3 km south of Black Butte. Photograph taken summer 1974.

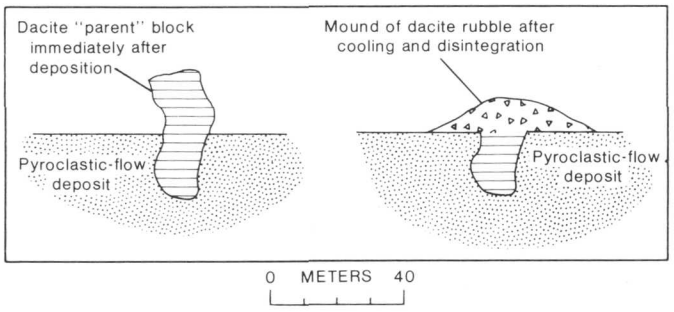

FIGURE 12.—Inferred origin of some of the mounds on the Black Butte assemblage. Scale approximate.

mantles the fault scarps and the Black Butte pyroclastic-flow assemblage, suggesting that faulting and volcanism were nearly simultaneous and that the area northwest of Black Butte subsided during a late eruptive phase of the Black Butte plug-dome complex.

AGE OF THE SHASTINA AND BLACK BUTTE ASSEMBLAGES

Weak soil-profile development at the surface of the Shastina and Black Butte assemblages and radiocarbon dates from charcoal collected from the pyroclastic-flow deposits indicate that both assemblages are Holocene in age. Two radiocarbon dates from the Black Butte assemblage and two radiocarbon dates from the Shastina assemblage all range in age from 9230±300 to 9500±350 years B.P. (fig. 6). Thus, the eruptions at Shastina and Black Butte that produced the assemblages could have been nearly simultaneous but also may have been as much as several hundred years apart. Stratigraphic relationships indicate that the Shastina assemblage is older than the Black Butte assemblage (fig. 6).

Soils on both assemblages are comparable in development. They consist of A/C profiles showing no textural change with depth and have depths of oxidation of 70–100 cm (table 1). Oxidation colors in these profiles vary according to the color of the parent material. Where soil-profile oxidation is superimposed on the pink top of a pyroclastic flow, colors are redder than the colors resulting from oxidation of gray parent material.

TABLE 1.—*Representative soil profiles developed on the Shastina and Black Butte assemblages. Parent materials are unconsolidated dacitic pyroclastic-flow debris*

[No textural change or clay present in any horizon. Depth in centimeters. Colors taken dry following the Munsell system (Munsell Color Co., 1954)]

Post-Shastina soil			Post-Black Butte soil		
Horizon	Depth	Color	Horizon	Depth	Color
A	0 - 5	10YR 5/3	A	0- 6	10YR 5/3
Cox	5 - 75	[1]10YR 7/3	Cox	6-80	[3]10YR 6/4
	to 100 (variable)	[2]10YR 7/6			[4]2.5Y 7/4
Cn	75+-100+	[3]2.5YR 7/2 [4]N 7/0	Cn	80+	5Y 7/1

[1]Matrix. [3]Pink parent material.
[2]Pebbles. [4]Gray parent material.

CHARACTER OF ERUPTIONS AT SHASTINA AND BLACK BUTTE

The character and composition of volcanic deposits in the Shastina assemblage indicate that early Holocene eruptions at Shastina consisted of a series of extrusions of viscous dacitic magma near the present summit. Eruptions of volatile-poor magma formed a succession of at least four domes and(or) spines, primarily of nonvesicular dacite (fig. 2). Repeated disintegration and collapse of the domes caused a series of hot pyroclastic flows to move down the west side of Shastina. Diller Canyon, a deep V-shaped gash on the west side of Shastina (figs. 2, 5) may have originated from lateral or downward blasts, as Williams (1932) first suggested, by collapse, or from erosion by pyroclastic flows. Once formed, Diller Canyon provided a channel for later pyroclastic flows descending to the west from the summit area of Shastina.

Pyroclastic flows spread out below Diller Canyon, forming a fan of deposits that were emplaced at temperatures below their welding temperature and above a temperature of at least, but probably higher than, 400°C. The pyroclastic flows followed topographic depressions but locally had enough mobility and momentum to travel over low hills in their path.

Eruptions at the site of Black Butte resulted from intrusion of a viscous magma body at shallow depth. Eruptions began with ejection of volatile-rich dacitic magma, producing pyroclastic flows of vesicular debris. Later eruptions of viscous volatile-poor dacite produced domes and (or) spines. At least two pyroclastic flows caused by dome collapse spread out to the west and south, mantling preexisting topography. These pyroclastic flows carried nonvesicular dacite blocks as large as 20 m in maximum dimension as far as several kilometers from Black Butte.

On the south and southeast sides of Black Butte is a topographically low, semicircular feature, here termed the "moat." The moat apparently predates the present Black Butte edifice and probably is part of a crater produced either by explosion (Williams, 1932; R. L. Christiansen, oral commun., 1976) or by collapse associated with emptying of a shallow magma chamber. The present Black Butte edifice, a succession of four plug domes (fig. 3), occupies part of the inferred crater but has not filled in or modified the moat, which may have channeled pyroclastic flows to the south and west from Black Butte. Explosion or collapse of the Black Butte plug domes produced the block-and-ash flows, which comprise the upper part of the Black Butte assemblage (figs. 4, 6).

Closely spaced eruptions of dacite magma from Black Butte and the Shastina summit, two vents about 10 km apart, suggest the possibility that both eruptive bodies originated from the same parent magma at some shallow depth under the Mt. Shasta area.

POTENTIAL VOLCANIC HAZARDS FROM FUTURE ERUPTIONS

Pyroclastic flows such as those described here are hazardous to people and to works of man because they generally travel at very high velocities, contain gases and rock debris that have very high temperatures, and can spread over large areas, sometimes as far as tens of kilometers from their source. Eruptions could occur again at Shastina or Black Butte or at some other locality in the vicinity of Mt. Shasta volcano. Such eruptions may include preliminary airfall tephra and pumice flows, followed by emplacement of viscous domes and (or) spines that could disintegrate to produce voluminous pyroclastic flows of nonvesicular rock debris. If such eruptions occurred within about 10 km of Black Butte, they could endanger people and property downslope from the vent in any direction, including the cities of Weed and Mount Shasta and perhaps other communities in the Shasta Valley and upper Sacramento River area. Eruptions of volcanoes elsewhere in the world usually are preceded by noticeable warnings, such as small earthquakes, ground tilt, or the formation of hot areas or fumaroles. Such indications of an impending eruption, if adequately monitored and observed, probably will give adequate warning time for officials to implement plans for protecting or evacuating people living within a potentially dangerous area.

REFERENCES CITED

Aramaki, S., and Ui, T., 1966, The Aira and Ata pyroclastic flows and related caldera and depressions in southern Kyushu, Japan: Bull. Volcanol., v. 29, p. 29–47.

Christiansen, R. L., Kleinhampl, F. J., Blakely, R. J., Tuchek, E. T., Johnson, F. L., and Conyac, M. D., 1977, Resource appraisal of the Mt. Shasta Wilderness study area, Siskiyou County, California: U.S. Geol. Survey Open-File Rept. 77–250, 53 p.

Christiansen, R. L., and Miller, C. D., 1976, Volcanic evolution of Mt. Shasta, California: Geol. Soc. America Abs. with Programs, v. 8, no. 3, p. 360–361.

Crandell, D. R., 1972, Glaciation near Lassen Peak, northern California, *in* Geological Survey research 1972: U.S. Geol. Survey Prof. Paper 800–C, p. C179–C188.

——— 1973, Hot pyroclastic-flow deposits of probable Holocene age west of Mount Shasta volcano, California: Geol. Soc. America Abs. with Programs, v. 5, no. 1, p. 28.

Crandell, D. R., and Mullineaux, D. R., 1973, Pine Creek volcanic assemblage at Mount St. Helens, Washington: U.S. Geol. Survey Bull. 1383–A, 23 p.

——— 1975, Technique and rationale of volcanic-hazards appraisals in the Cascade Range, northwestern United States: Environmental Geology, v. 1, no. 1, p. 23–32.

Francis, P. W., Roobol, M. J., Walker, G. P. L., Cobbold, P. R., and Coward, M., 1974, The San Pedro and San Pablo volcanoes of northern Chile and their hot avalanche deposits: Geol. Rundschau, v. 63, no. 1, p. 357–388.

Hoblitt, R. P., and Kellogg, K. S., 1976, Emplacement temperatures of unsorted and unstratified deposits of volcanic rock debris as determined by paleomagnetic techniques: Geol. Soc. America Abs. with Programs, v. 8, no. 6, p. 919–920.

——— 1978, Emplacement temperatures of unsorted and unstratified deposits of volcanic rock debris as determined by paleomagnetic techniques: Geol. Soc. America Bull. (In press.)

McTaggart, K. C., 1960, The mobility of Nuées Ardentes: Am. Jour. Sci., v. 258, p. 369–382.

Miller, C. D., and Crandell, D. R., 1975, Postglacial pyroclastic-flow deposits and lahars from Black Butte and Shastina, west of Mt. Shasta, California: Geol. Soc. America Abs. with Programs, v. 7, no. 3, p. 347–348.

Miller, T. P., and Smith, R. L., 1977, Spectacular mobility of ash flows around Aniakchak and Fisher calderas, Alaska: Geology, v. 5, no. 3, p. 173–176.

Munsell Color Co., Inc., 1954, Munsell soil color charts: Baltimore, Md., Munsell Color Co., Inc.

Perret, F. A., 1935, The eruption of Mt. Pelée, 1929–1932: Carnegie Inst. Washington Pub. 458, 126 p.

Sparks, R. S. J., 1976, Grain size variations in ignimbrites and implications for the transport of pyroclastic flows: Sedimentology, v. 23, no. 2, p. 147–188.

Verhoogen, Jean, 1937, Mount St. Helens, a recent Cascade volcano: Berkeley, California Univ. Dept. Geol. Sci. Bull., v. 24, no. 9, p. 263-302.

Williams, Howel, 1932, Mount Shasta, a Cascade volcano: Jour. Geology, v. 40, no. 5, p. 417–429.

——— 1934, Mount Shasta, California: Zeitschr. Vulkanologie, v. 15, no. 4, p. 225–253.

——— 1960, Volcanic history of the Guatemalan Highlands: Berkeley, California Univ. Pubs. Geol. Sci., v. 38, no. 1, p. 1–87.

Jour. Research U.S. Geol. Survey
Vol. 6, No. 5, Sept.-Oct. 1978, p. 625-636

REFRACTION STUDIES BETWEEN ICY BAY AND KAYAK ISLAND, EASTERN GULF OF ALASKA

By K. C. BAYER, R. E. MATTICK; GEORGE PLAFKER, AND T. R. BRUNS,
Reston, Va.; Menlo Park, Calif.

Abstract.—Results of five seismic refraction lines shot by the U.S. Geological Survey in the Gulf of Alaska between Icy Bay and Kayak Island indicate the following: (1) The Continental Shelf is underlain by as much as 11 km of sedimentary rock of probable Tertiary age where refraction velocities range from 1.2 to 5.5 kilometers per second; (2) a section approximately 5 km thick, which has velocities of 4.1–5.5 km/s and which could represent the Orca Group (lower Tertiary), is present in the western part of the study area but not in the eastern part; and (3) consistent basement velocities of approximately 7.0 km/s could indicate oceanic crust underlying the continental margin.

This report describes five seismic refraction lines acquired during the 1974 U.S. Geological Survey cruise aboard the University of Washington research vessel *Thomas G. Thompson* in the eastern Gulf of Alaska between Icy Bay and Kayak Island (fig. 1). The length of the refraction lines totals approximately 500 km. Refraction data were recorded in forward and reverse runs along each line; thus, the average length of each profile was 50 km (30 miles). The primary purpose of the cruise was to delineate the overall structural framework of the eastern Gulf of Alaska Continental Shelf by single-channel seismic reflection, seismic refraction, high-resolution sparker, gravity, and magnetic methods in anticipation of offshore oil and gas lease sales. Data and results of the cruise are available in various publications (Bruns and Plafker, 1975a, b, 1976; Plafker and others, 1975; Carlson and others, 1975; Carlson and Molnia, 1975; Molnia and Carlson, 1975a, b; Molnia and others, 1976; von Huene and others, 1975; Core and others, 1975).

Refraction lines A, C, and D are seaward of Icy Bay (fig. 1) in an area of relatively simple geologic structure and, when combined with the refraction lines of Shor (1966), they form a refraction transect across the Continental Shelf. Lines E and H were shot near Kayak Island in a zone characterized by a more complex geologic structure, a shelf edge arch, and a deep shelf basin behind the arch (Bruns and Plafker 1975b, 1976).

STRATIGRAPHIC SUMMARY

The eastern Gulf of Alaska forms a complex continental margin basin. Onshore, more than 10 km of marine and nonmarine terrigenous clastic rocks are intercalated with subordinate mafic volcanic and volcanistic rocks and with minor coal. These rocks are also presumed to underlie much of the contiguous Continental Shelf. Tertiary rocks are bordered on the north and, in part, are underlain by highly deformed, metamorphosed and intruded Cretaceous and older bedded sedimentary and volcanic rocks. Recent summaries of the onshore geology of the province have been made by Plafker (1967, 1971, 1974) and Plafker and others (1975).

Considering the degree of induration and, hence, perhaps velocity, we can broadly divide the Tertiary sequence into a lower unit of well-indurated intensely deformed rocks of early Tertiary (mainly Paleocene and Eocene age and a notably less deformed and indurated upper unit of mainly middle and late Tertiary (and locally Pleistocene) age.

On the basis of fossils and gross lithologic characteristics, three major subdivisions of Tertiary rocks are believed to correspond to major changes in the depositional environment of the basin. The subdivisions are (1) the Paleocene through lower Oligocene, (2) the middle Oligocene through lower Miocene, and (3) the middle Miocene through Pleistocene. The changes in depositional environment are characteristically gradational and appear to be time-transgressive in different parts of the basin.

Lower Tertiary Sequence

The oldest Tertiary rocks consist of complexly intertonguing, deepwater marine pillow lava, tuff, and tuffaceous sandstone and siltstone that constitute the Orca Group and its equivalent in the Katalla district and the "unnamed siltstone" unit of the Yakataga and Malaspina districts (place names are shown on fig. 1).

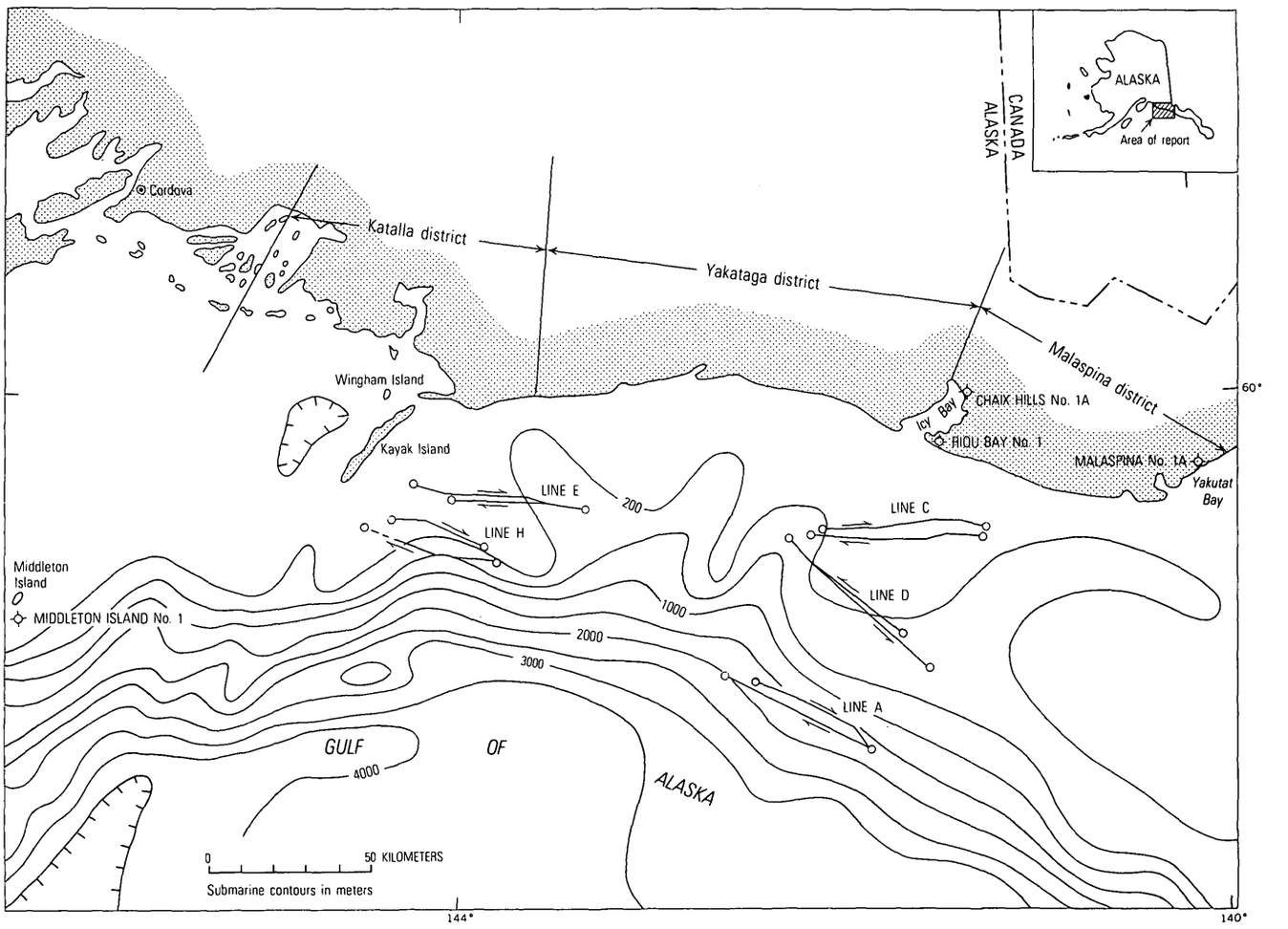

FIGURE 1.—Map of study area showing location of seismic refraction lines, selected wildcat wells, and geographic features referred to in the text. Arrows along lines indicate shooting direction. Refraction lines are dashed where data was not recorded.

These rocks are inferred to be of Paleocene and possibly earliest Eocene age on the basis of their stratigraphic position, the few diagnostic fossils collected from them, and their relationship to radiometrically dated plutonic rocks that intrude them.

The lower units appear to grade upward and laterally towards the northeast into rocks characterized by abundant intertonguing arkosic, pebbly, and coal-bearing standstone that is commonly calcareous; the sandstone also is zeolitized in many places. Their fauna and flora suggest that they were deposited during late Paleocene to late Eocene and possibly early Oligocene time in a subtropical to temperate environment. Rocks of this age include the Kushtaka Formation and perhaps the lower part of the Tokun Formation in the Katalla district and the Kultheith Formation in the Yakataga and Malspina districts.

All the lower Tertiary sedimentary rocks are characteristically hard, dense, and intensely deformed. Although many of the cleaner sandstones appear porous and friable in outcrop, surface samples that have been examined microscopically have negligible porosity.

In outcrop, the Orca Group is estimated to be at least 5000 m thick in the Katalla district and thins to the east.

Middle Tertiary Sequence

The lower Tertiary rocks are overlain unconformably by a marine sequence consisting predominantly of interbedded concretionary mudstone and siltstone and subordinate sandstone. This sequence is characterized locally by the presence of interbedded aquagene tuff,

agglomerate, glauconitic sandstone, and pillow lavas. The middle Tertiary sequence, which includes the Katalla, upper part of the Tokun(?), and Poul Creek Formations, was deposited during Oligocene and early Miocene time in temperate water. Intermittent submarine volcanic activity is recorded by mafic flow and pyroclastic rocks throughout much of these units. The mudstone and siltstone are richly organic in the Katalla, Yakataga, and Malaspina districts, and the sequence there contains many petroliferous beds and oil and gas seeps. The sandstone—"shale" (actually mainly siltstone and mudstone) ratio of these units is 30 percent or less; most of the thicker sandstone beds are concentrated near the base.

The middle Tertiary sequence extends offshore at least to the continental margin (200 m) where approximately 2000 m of middle Tertiary rocks were penetrated in a well drilled by the Tenneco Oil Co. near Middleton Island (fig. 1). The sequence probably crops out on the sea floor between Kayak and Middleton Islands but is not known to be exposed elsewhere in the offshore parts of the basin.

Upper Tertiary and Pleistocene Sequence

Marine clastic rocks of Miocene to Pleistocene age that locally are characterized by abundant glacial detritus lie on the temperate-water sequence with local unconformity. The sequence consists mainly of rocks of the Yakataga Formation—fossiliferous thick-bedded mudstone, muddy sandstone, conglomerate sandy mudstone (marine "tillite"), and minor conglomerate.

The megafauna indicate the base of the sequence is probably of early Miocene age in the Yakataga and Malaspina districts and possibly as old as late Oligocene in the Katalla district (Plafker and Addicott, 1976).

The composite onshore outcrop thickness of the Yakataga Formation is about 5000 m. The sandstone content of the formation ranges from as much as 55 percent in sections on the mainland near the northern margin of the basin to as little as 9 percent at Middleton Island near the edge of the Continental Shelf.

On the basis of its onshore distribution and the character of near-surface reflectors over adjacent offshore areas, the Yakataga Formation is inferred to underlie most of the Continental Shelf in the area of the refraction survey. Extrapolation of data from onshore sections and wells and offshore seismic reflection data suggests that the depositional axis of the Yakataga Formation in the east area of Kayak Island is probably offshore and within 15–30 km of the coast.

Much of the Continental Shelf is mantled with a veneer of unconsolidated Holocene, and possibly upper Pleistocene, deposits (Molnia and Carlson, 1975a). Bottom sediments on the shelf include submarine moraines of poorly sorted till and their closely associated fluvioglacial outwash fans of sand and gravel near the present major glaciers. In addition, mud and silt discharged into the sea by streams have been widely dispersed offshore by current and wave action.

VELOCITIES FROM WELL LOGS

Sonic velocity logs from the Middleton Island No. 1, the Malaspina No. 1A, the Chaix Hills No. 1A, and the Riou Bay No. 1 wells (locations shown on fig. 1) have been used to derive velocity/depth curves for the part of the sedimentary sequence penetrated by these wells (fig. 2).

The Middleton Island No. 1 well penetrated the Katalla and Tokun Formations (Oligocene to Eocene). The Malaspina No. 1A well penetrated the Yakataga

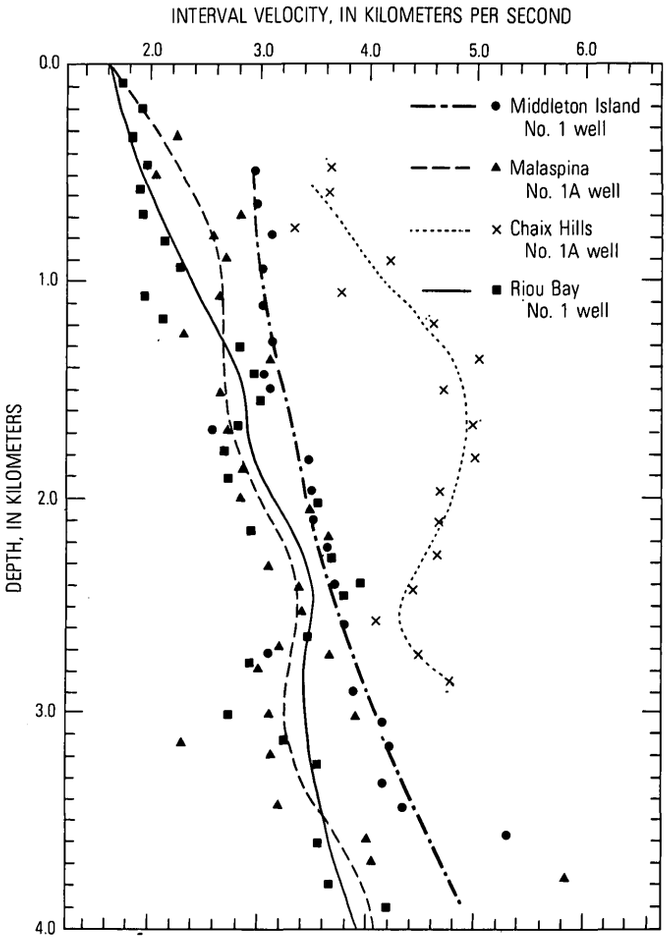

FIGURE 2.—Plot of interval velocity as a function of depth for selected wells in the Gulf of Alaska Tertiary Province. See figure 1 for locations of wells.

and Kulthieth Formations (Pleistocene to Paleocene). The Chaix Hills well penerated the Yakataga and Poul Creek Formations (Miocene to Oligocene). The Riou Bay No. 1 well spudded in Holocene deposits and bottomed in the lower part of the Yakataga Formation (Pleistocene to lower Miocene). The Riou Bay No. 1 and Malaspina No. 1A wells are in relatively simple structural settings; the Chaix Hills No. 1A and Middleton Island No. 1 wells are in structurally complex settings.

In general, the velocity data of figure 2 do not show any apparent relationship of interval velocity to rock age or lithology. Velocities in the Malaspina No. 1A and Riou Bay No. 1 wells appear to be somewhat similar. The plots from these two wells indicate a gradual increase of velocity as the depth increases, approaching a velocity of about 4 kilometers per second at a depth greater than 4 km. Velocities in the Middleton Island No. 1 well are slightly higher than those in the Malaspina No. 1A and Riou Bay No. 1 wells to a maximum depth of about 3 km. At depths greater than 3 km, the velocity increases rapidly. The interval velocity at about 3.7 km in the Middleon Island No. 1 well is more than 5 km/s. Interval velocities in the Chaix Hills No. 1A well are generally about 4–5 km/s at depths below about 1 km. These higher velocities suggest uplift and erosion of approximately 2 km of section at this locality and possible tectonic compaction of the sequence, as would be expected from the well location on the south limb of an overturned, faulted anticline. Interval velocities measurements from rocks of the Orca Group are not available. These velocities might be expected to be high (≈ 5 km/s), considering the intense deformation and mild metamorphism of these older Tertiary rocks.

In general, the wells suggest that middle Miocene and younger rocks have velocities of about 4 km/s or less, and lower Tertiary rocks can have velocities greater than 4 km/s.

FIELD PROCEDURES

Field procedures for the marine refraction survey involved deploying one or two sonobuoys at the start of each refraction line and "shooting away," at speeds of about 15 kilometers per hour with a 4917 cm^3 (300 in^3) air gun at intervals at 5–30 seconds. Energy from the air gun source was insufficient at a distance of 1–2 km, and shooting was continued using chemical explosives at intervals of 1–30 min. Upon loss of radio signal from the sonobuoy or loss of energy from the chemical explosives (usually at a distance of about 50 km), the refraction line would be terminated. The ship would then turn 180° and return along the same general course, at which time sonobuoys would again be deployed for the reverse line.

The sonobuoy (product of Select International, Inc.) detects the seismic arrivals with its hydrophone, amplifies this signal, modulates an FM transmitter, and telemeters the seismic signal to a recording system aboard ship via an FM radio link. The recording system includes a high sensitivity–low noise–solid-state receiver for each channel, antialiasing filters for digital recording, broad-band data for analog recording and monitoring, and a special water break filter amplifier for the accurate determination of the direct water arrival. Figure 3 is a generalized flow diagram from energy source to realtime paper record

Navigational control was provided by satellite and loran A. Owing to the Alaska current gyre (influencing the free-floating sonobuoys), and lack of more precise navigational aids, the attempt to spatially rerun a refraction trackline within accuracy of about 1 km proved unsuccessful. Table 1 lists the minimum and maximum deviations for each of the five "reversed" refraction lines and the locations of the sonobuoys deployed during the survey.

The general shooting configuration is shown in figure 4. A facsimile of a part of a seismic refraction record is shown in figure 5. The galvo-camera produces a 15.24-cm-wide continuous photographic record at a uniform rate of 15.24 centimeters per second. Timing lines are marked across the seismogram at intervals of 0.01 s. The apparent wave-dispersion effect noted on the refraction record is not real and denotes merely reflected and refracted wave arrivals subsequent to the initial refracted wave at 3.01 s (see fig. 5).

A preliminary interpretation was made aboard ship as the records were being recorded. This involved an immediate cursory examination of the records for signal-to-noise ratios to determine the charge size needed for the next shot and the plotting of the direct water wave as a function of the refracted arrival for on-the-spot checks.

Environmental considerations limited the charge size to about 110 kilograms of chemical explosive. In addition, possible fish kill was avoided by adjusting explosion depth of the charges to prevent detonation at the sea floor or within schools of fish detected in the water column, and shotpoints were delayed or canceled if any marine life could not be avoided.

Data on which this report is based were tabulated in digital format by Core and others (1975). This data was first analyzed by Bayer and others (1977). Microfilm copies of the refraction records may be obtained from the National Geophysical and Solar-

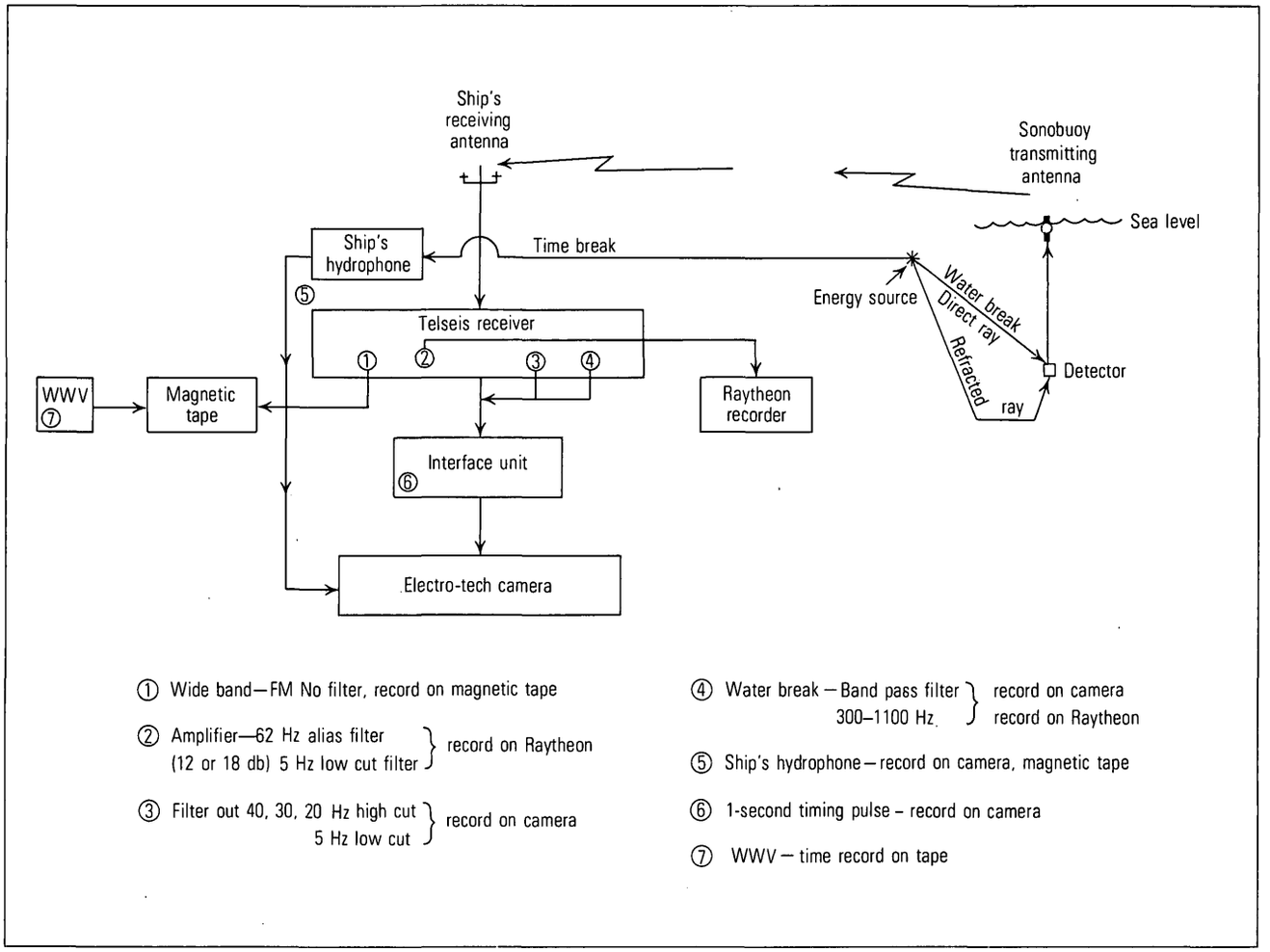

FIGURE 3.—Flow diagram showing configuration of seismic refraction transmission.

TABLE 1.—*Minimum and maximum refraction profile deviations*

Refraction profile	Minimum distance (km) between reversed lines	Maximum distance (km) between reversed lines	Sonobuoy locations			
			West		East	
			Lat (N)	Long (W)	Lat (N)	Long (W)
A	0	5.6	59° 18.2′	142° 25.7′	59° 06.5′	141° 48.5′
C	2.8	5.6	59° 41.3′	142° 01.8′	59° 42.1′	141° 14.0′
D	0	4.6	59° 40.0′	142° 16.0′	59° 21.1′	141° 32.2′
E	0	6.5	59° 47.0′	144° 16.5′	59° 44.3′	143° 14.0′
H	3.5	14.8	59° 43.1′	144° 24.5′	59° 37.0′	143° 39.5′

Terrestrial Data Center (NGSDC/EDS/NOAA, Code D 621, Boulder, Colo. 80302).

RESULTS

The approximate locations of the five seismic refraction lines are shown in figure 1. Disparities in locations between the forward and reversed sections of the lines are listed in table 1. Seismic events were picked to the nearest 5 milliseconds and plotted as a function of the direct water arrival. The observed points were then adjusted to form straight line segments. Depths to refracting horizons were calculated by a standard time-intercept method in areas of gentle or no dip. For areas where significant dip was indicated by the data, the graphical method of Slotnick (1950) was employed.

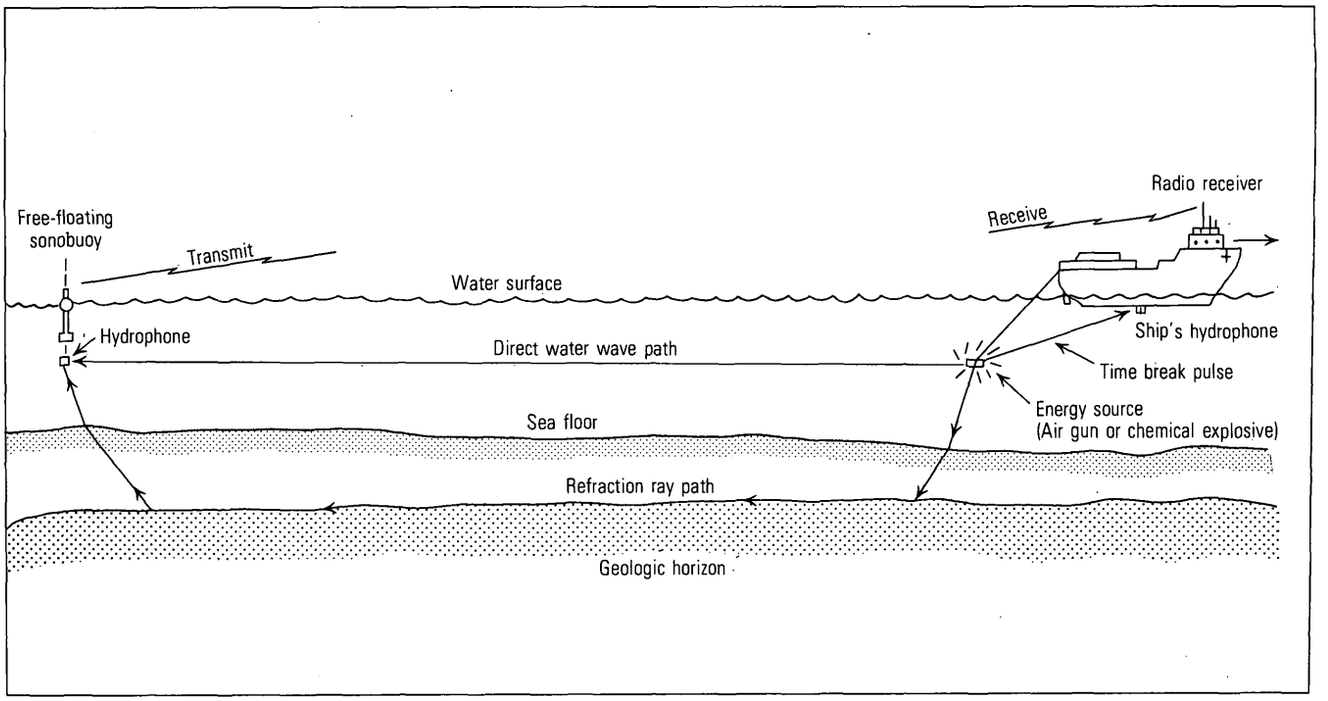

FIGURE 4.—Diagram showing the general shooting configuration used for the seismic refraction survey.

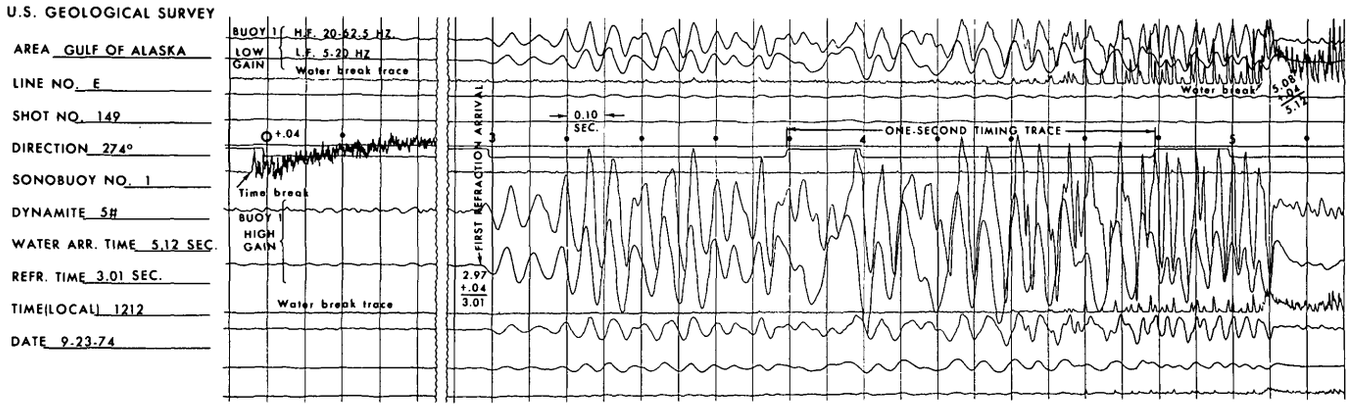

FIGURE 5.—Sample seismic record from the galvo-camera.

Refraction line A

Refraction line A is seaward of the Continental Shelf in water depths between 1500 and 2000 m (fig. 1). The results from this line are shown in figure 6 where refracted wave events are plotted as a function of the direct water wave travel time. Excluding the water column (velocity of 1.5 km/s), three layers having velocities of about 3.4, 4.2, and 7.0 km/sec were recorded. The uppermost layer (velocity 3.4 km/s) is represented by two distinct points near the west end of the line; near the east end of the line, the layer either was not recorded or may be represented as a first arrival only along a very short segment of the traveltime plot as indicated in figure 6. The intermediate layer (4.2 km/s) was clearly recorded from at least four shotpoints while shooting away from both the east and west sonobuoys. The equal apparent velocities recorded on both the forward and reversed segments of the profile indicate that this layer is flat lying. The deepest layer (velocity 7.0 km/s) is represented by an apparent velocity of 6.9 km/s in shooting from east to west and 7.1 km/s shooting in the reversed direction. This small difference in apparent velocity may be due

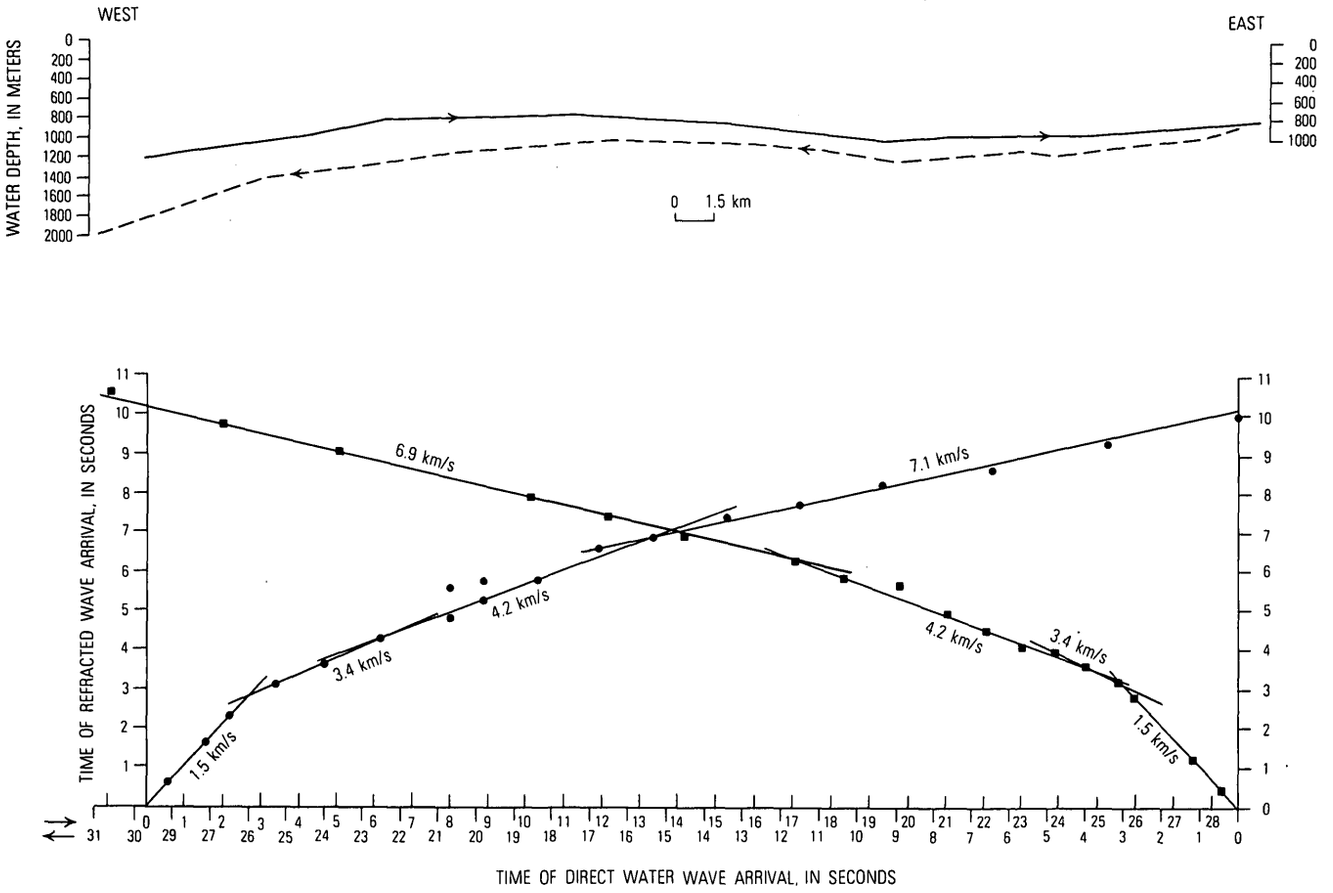

FIGURE 6.—Plot of time of refracted wave arrivals as a function of the times of direct water wave arrivals for refraction line A.

to random error or can be explained by a westward dip of about one-half degree. Assuming horizontal layers, the depths to the tops of the 3.4-, 4.2-, and 7.0-km/s layers at line A are calculated to be 1.35, 2.3, and 6.5 km, respectively (fig. 11).

Refraction line C

Refraction line C is on the Continental Shelf seaward of Icy Bay in water depths of about 100 m (fig. 1). A plot of refracted wave arrivals as a function of the direct water wave arrival is shown in figure 7. Excluding the water column (velocity, 1.5 km/s), three velocity layers were defined. The shallowest layer has an apparent velocity of 2.7 km/s on the west and 2.5 km/s on the east. Our interpretation is that this difference is not due to dip but is probably due to lateral velocity variations in a thin, flat layer that averages about 2.6 km/s. Again as on line A, a flat-lying intermediate layer has a velocity of 4.2 km/s that was clearly recorded on both the forward and reversed segments of the line. The results of lines A and D suggest that a layer characterized by a velocity of about 3.5 km/s might lie between the 2.6- and 4.2-km/s layers, but no arrivals were found to substantiate this. In shooting from the west, a deep layer with an apparent velocity of 7.0 km/s was recorded from six shotpoints. On the reversed segment of the line, these arrivals did not appear. The results of lines A and D suggest, however, that the apparent velocity of 7.0 km/s represents a flat-lying layer with a true velocity of 7.0 km/s. Assuming that the layers are horizontal, the depths to the tops of the 2.6-, 4.2-, and 7.0-km/s layers in line C are calculated to be 0.5, 1.6, and 9.8 km, respectively (fig. 11).

Refraction line D

Refraction line D is on the Continental Shelf, about 10 km seaward of line C at its northwest end, in water depths of about 200 m (fig. 1). A plot of refracted wave arrivals as a function of the direct water wave arrival is shown in figure 8. Excluding the water column (velocity, 1.5 km/s), the data suggest four horizontal layers

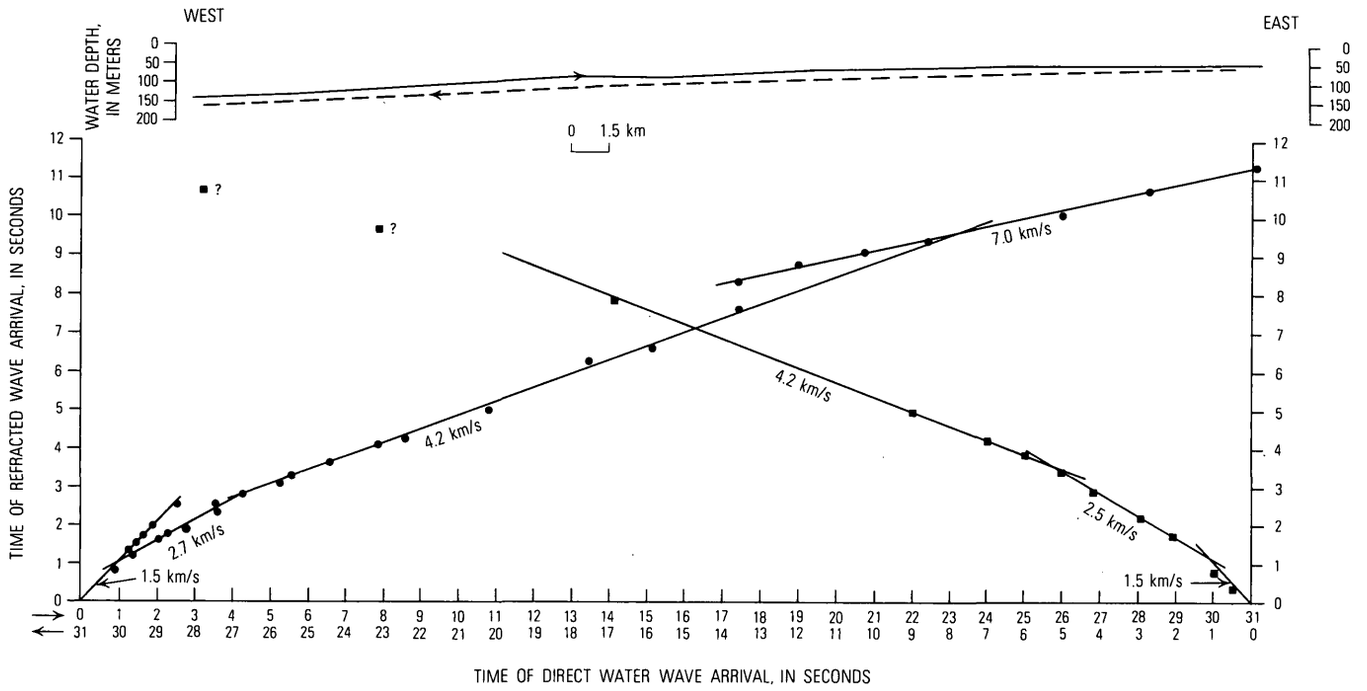

FIGURE 7.—Plot of time of refracted wave arrivals as a function of the time of direct water wave arrivals for refraction line C.

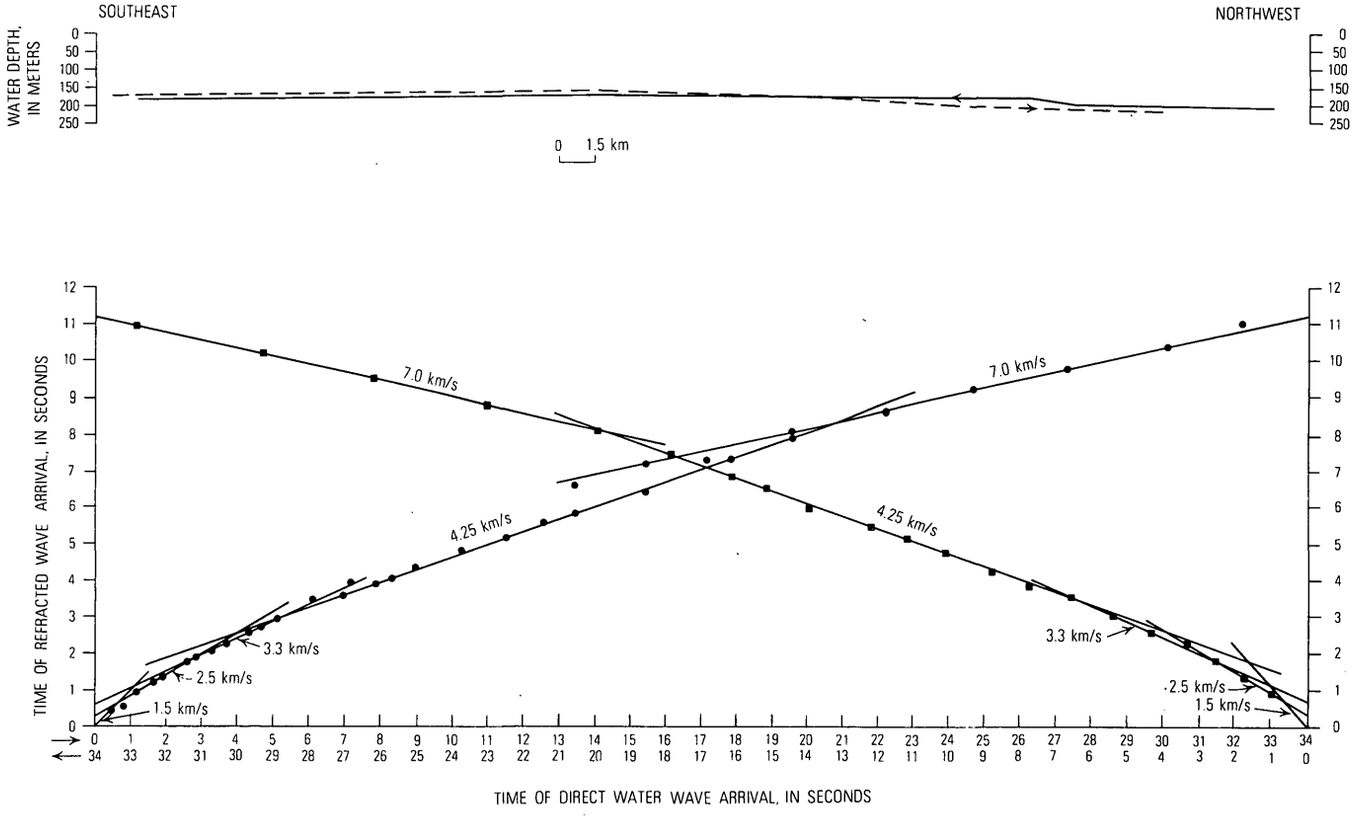

FIGURE 8.—Plot of time of refracted wave arrivals as a function of the time of direct water wave arrivals for refraction line D.

whose velocities are 2.5, 3.3, 4.25, and 7.0 km/s. This line differs from lines A and C in that the 4.2-km/s layer is overlain by two discrete lower velocity layers instead of only a single layer. This difference may be a result of the higher resolution obtained along line D because of the many closely spaced shotpoints at the southeast end of the line. On all three lines (A, C, and D), closer spaced shotpoints might show that, rather than comprising discrete layers, the sediments overlying the 4.2- or 4.25-km/s layer gradually increase in velocity as depth increases. This is suggested by the fact that the first arrivals at the southeast end of line D could be fitted to a curve as well as to straight line segments. This latter interpretation is attractive in that most of the well data (fig. 2) also show a continuous increase in velocity with depth.

If we assume a simple, horizontal four-layer solution on line D, depths to the tops of the 2.5-, 3.3-, 4.25-, and 7.0-km/s layers are calculated to be 0.25, 0.9, 2.0, and 8.5 km, respectively (fig. 11). Except for the 7.0-km/s layer, these depths agree quite well with depths obtained on line C for similar velocity layers. The depth to the 7.0-km/s layer indicates dip landward from line A to line C of this layer (fig. 11).

Refraction lines E and H

Refraction lines E and H are on the Continental Shelf about 15–20 km east-southeast of Kayak Island (fig. 1). Line E is about 10 km shoreward of line H. The profiles are discussed together not only because of their geographic proximity but also because of the similar results and the fact that only parts of various refractors were recorded on each line, and a consistent interpretation requires that they be interpreted in conjunction with one another. A plot of refracted wave arrivals as a function of the direct water wave arrival for line E is shown in figure 9 and for line H, in figure 10.

A thin upper layer that has an apparent velocity ranging from 2.3 to 2.6 km/s was recorded on both lines. The changes in apparent velocity were interpreted to be local velocity variations in the near-surface sediments rather than dip. The average velocity for this shallowest layer was assumed to be 2.4 km/s (fig. 11). On line E, a second layer with an average velocity of 3.6 km/s (apparent velocity 3.5 km/s at the west sonobuoy and 3.7 km/s at the east sonobuoy) was recorded. This layer is calculated to be about 2.5 km thick and to have an easterly dip of about 1°. On line H, this same depth interval appears to be represented by two layers that have average velocities of 3.2 km/s (apparent velocities, 3.1 and 3.3 km/s) and 4.1 km/s (apparent velocities, 4.0 and 4.2 km/s). The total thickness of the 3.2- and 4.1-km/s layers is about 3.5 km. The situation is similar for the deeper part of the section. On line H, a layer with an apparent

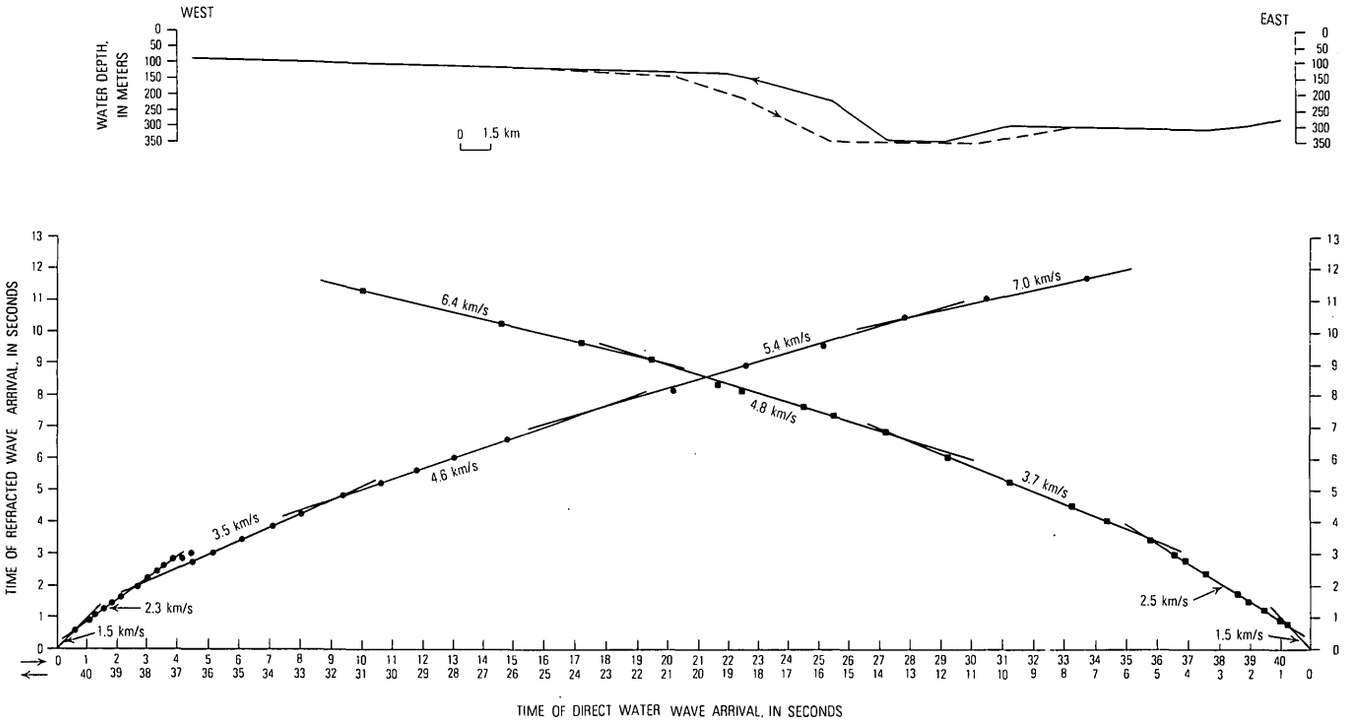

FIGURE 9.—Plot of time of refracted wave arrivals as a function of the time of direct water wave arrivals for refraction line E.

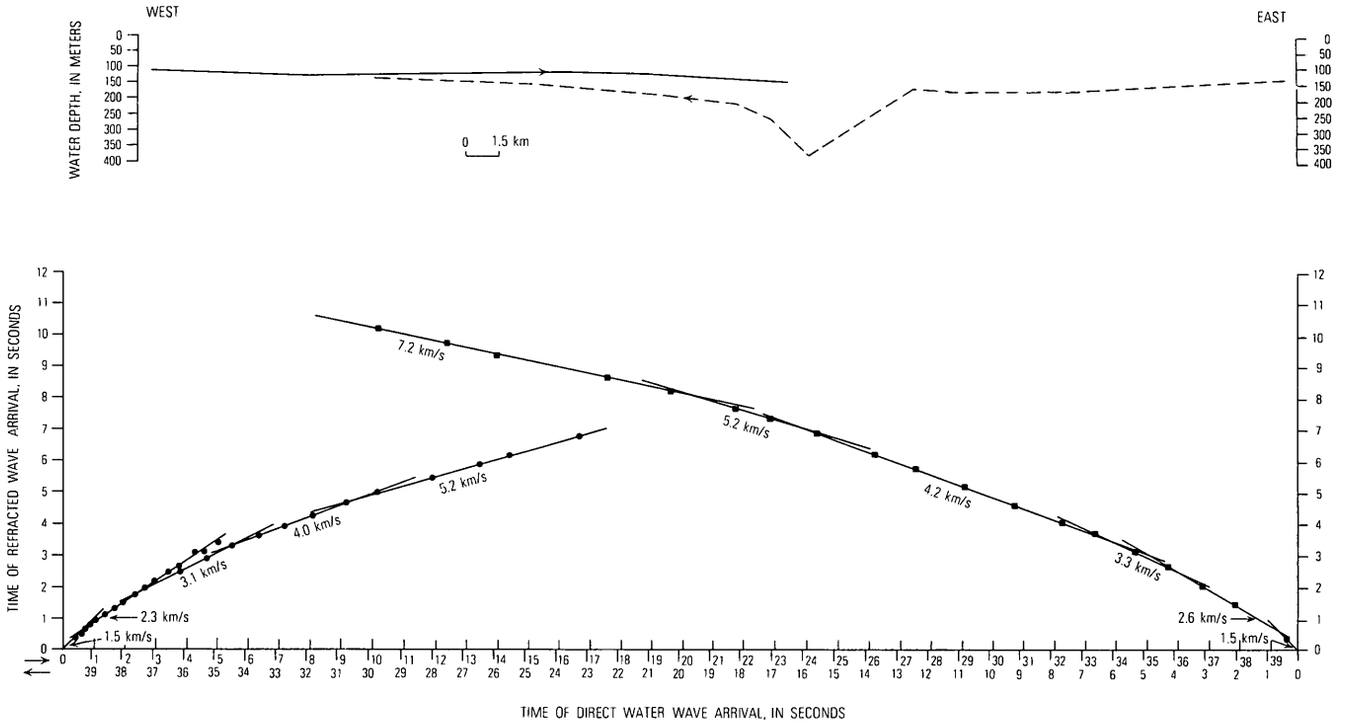

FIGURE 10.—Plot of time of refracted wave arrivals as a function of the time of direct water wave arrivals for refraction line H.

velocity of 5.2 km/s appears on both the forward and reversed segments of the line. On line E, the section of the time-distance plot that corresponds to approximately the same depth interval shows two layers. The upper layer is represented by apparent velocities of 4.6 km/s (west sonobuoy fig. 9) and 4.8 km/s (east sonobuoy). Its true velocity is calculated to be about 4.7 km/s. The other layer that has an apparent velocity of 5.4 km/s was recorded only at the west sonobuoy; its true velocity was assumed to be about 5.5 km/s.

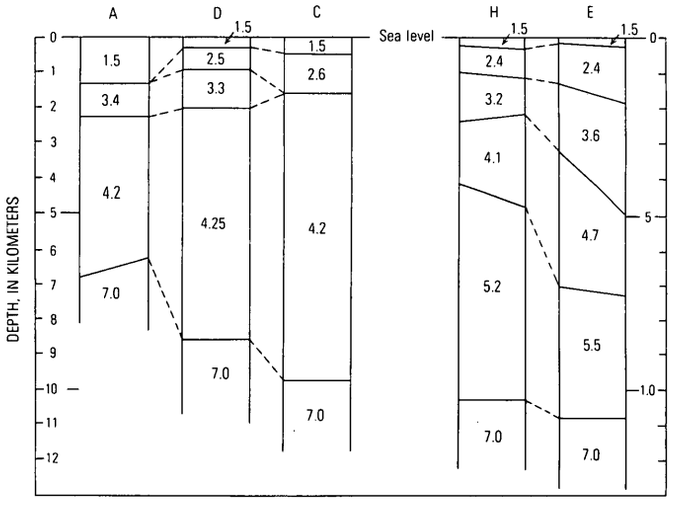

FIGURE 11.—Diagram correlating velocity layers determined for refraction lines A, D, C, H, and E (see fig. 1 for locations). Numerals in columns indicate velocity in kilometers per second; the eastern ends of the refraction lines are to the right. Horizontal dimension is not to scale.

Therefore, the velocity layering for lines E and H might be similar, and closer shotpoint spacing might show a continuous increase in velocity as depth increases, from about 2.0 km/s at the water bottom to perhaps 5.5 km/s at a depth of 10 km.

The deepest layer penetrated on line E is represented by an apparent velocity of 7.0 km/s, which was recorded only at the east sonobuoy. On line H this layer appears to be represented by an apparent velocity of 7.2 km/s. If we assume that these velocities represent a layer with a true velocity of 7.0 km/s, its depth would be about 10.8 km beneath line E and 10.3 km beneath line H. The slightly greater depth calculated beneath line E, compared to that calculated for line H, may be due to dip but could also reflect inaccuracies in velocities used in the calculation for line H.

Except for the 4.7-km/s layer on line E and the 5.2-km/s layer on line H, the layering appears to be nearly horizontal. However, the time-intercept of the 4.7-km/s layer on line E at the west sonobuoy is about 1.7 s, whereas at the east sonobuoy it is about 2.55 s. This large difference in intercept-times, together with

the nearly equal apparent velocities of 4.6 and 4.8 km/s on the forward and reversed segments of the lines, suggests that the horizon may be vertically offset by as much as 1 km. Similar reasoning suggests vertical offset of about 0.5 km on the 5.2-km/s layer of line H.

An anomalous apparent velocity of 6.4 km/s was recorded from the results of three shotpoints from the east sonobuoy on line E. Although the energy was strong, the authors were unable to relate this segment of the time-distance plot to any of the previously discussed refractors on either line E or line H. Multichannel seismic reflection data show that this area has a complex geologic structure, which may extend into the lower crust. Therefore, although this apparent velocity could be due to a change in lithology, it could also be due to a change in lip of the deep refractors beneath the west end of line E.

DISCUSSION

The marine refraction results are summarized in figure 11. The deepest layer penetrated on all five of the refraction lines has a seismic velocity of about 7.0 km/s. This velocity is comparable to lower crustal velocities measured in other refraction studies in the Gulf of Alaska near Kodiak Island (Shor and von Huene, 1972), near Dixon Entrance (Johnson and others, 1972), and between Icy Bay and Dry Bay to the east (Shor, 1966). The 7.0-km/s velocity appears to be typical of the transition zone between oceanic and continental crust in the Gulf of Alaska. It is also within the range of typical oceanic crustal velocities as discussed by Worzel (1974), and could represent generally oceanic crust underthrusting the coast at a relatively shallow angle as is suggested by the oceanic magnetic data in this region (Naugler and Wageman, 1973; Taylor and O'Neill, 1974). Lines A, C, and D show a thickening of the overlying sedimentary rocks from about 6 km at the shelf edge to at least 10 km near the coast, and Shor (1966), on a refraction line from Icy Bay to the shelf edge, indicated that there may be more than 12 km of sedimentary section overlying the lower crustal layer. Lines E and H indicate a somewhat thicker overlying sedimentary sequence than is present near Icy Bay.

Velocities on lines A, C, and D above the 7.0-km/s layer are about 4.2 km/s. Velocities on lines E and H are substantially higher, ranging from 5.2 to 5.5 km/s. Comparison of these velocities suggests that there is a distinct difference in the underlying geology of the two areas, and, by comparisons with velocities seen in wells, the 5.2- to 5.5-km/s velocities could indicate either truncation of the higher velocity section towards the east or an eastward decrease in structural deformation within the section. Plafker (1971) noted that in outcrop the deformed metamorphosed rocks of early Tertiary age thin from west to east, and the lack of higher velocity rocks in the eastern lines may indicate that the lower Tertiary rocks are not present in substantial thickness offshore. Alternatively, Plafker (1974) and Bruns and Plafker (1975 a, b) noted that Kayak and Wingham Islands as well as the contiguous Continental Shelf show greater structural complexity to the west of Icy Bay than to the east, which suggests that the higher velocities measured in lines E and H may be due to greater deformation of the rocks underlying this part of the Continental Shelf.

SUMMARY

The initial layer on all profiles indicates that water and thin unconsolidated sediments have a velocity of 1.5 km/s. In the offshore area of Icy Bay, maximum velocities of about 4.2 km/s for the sedimentary section suggest a thickness as great as 11 km of clastic sedimentary rocks where velocity increases primarily as a function of depth of burial. Velocity discontinuities within this clastic sequence may be due to the presence of regional unconformities rather than to major lithologic contrasts. These sediments probably correlate with a sequence of upper Tertiary rocks that are exposed onshore and have been penetrated in exploratory wells.

In the area southeast of Kayak Island, velocities of 4.7–5.5 km/s in the lower one-half of the sedimentary section indicate a distinctly different unit or, possibly, the same unit that has undergone a much greater amount of deformation and (or) compaction. These higher velocities probably reflect the presence of the Orca Group (lower Tertiary).

Beneath the sedimentary section, rock velocities were measured, or inferred to be, 7.0 km/s on all five profiles. These velocities are typical of lower crustal velocities across the continental margin in other areas of the Gulf of Alaska, and probably indicate oceanic crust beneath the continental margin. On a short segment of profile E, east of Kayak Island, an anomalous unreversed velocity of 6.4 km/s may indicate a sliver of buried continental crust or a granitic pluton, although it could also be caused by an abrupt change in dip of the deep reflectors.

REFERENCES CITED

Bayer, K. C., Mattick, R. E., Plafker, George, and Bruns, T. R., 1977, Refraction studies between Icy Bay and Kayak Island, eastern Gulf of Alaska: U.S. Geol. Survey Open-File Rept. 77–550, 45 p.

Bruns, Terry, and Plafker, George, 1975a, Preliminary results of a 1974 geophysical study of the offshore Gulf of Alaska Tertiary Province: Am. Assoc. Petroleum Geologists Pacific Sec. mtg., April 23–26, 1975, Program and abs., p. 32.

——— 1975b, Preliminary structural map of part of the offshore Gulf of Alaska Tertiary Province: U.S. Geol. Survey Open-File Rept. 75–508, 7 p., 1 map.

——— 1976, Structural style of part of the Outer Continental Shelf in the Gulf of Alaska Tertiary Province, *in* Cobb, E. H., ed., The United States Geological Survey in Alaska —Accomplishments during 1975: U.S. Geol. Survey Circ. 733, p. 13.

Carlson, P. R., Bruns, T. R., and Molnia, B. F., 1975, Submarine slides and nearsurface faults, northern Gulf of Alaska: U.S. Geol. Survey Open-File Rept. 75–504, 6 p.

Carlson, P. R. and Molnia, B. F., 1975, Preliminary isopach map of Holocene sediments, northern Gulf of Alaska: U.S. Geol. Survey Open-File Rept. 75–507, 8 p.

Core, Kenneth, Mattick, Robert, and Bayer, Kenneth, 1975, Seismic refraction records from a survey in the Gulf of Alaska: U.S. Geol. Survey Open-File Rept. 75–283, 21 p.

Johnson, S. H., Couch, R. W., Gemperle, M., and Banks, E. R., 1972, Seismic refraction measurements in southeast Alaska and western British Columbia: Canadian Jour. Earth Sci., v. 9, no. 12, p. 1756–1765.

Molnia, B. F., and Carlson, P. R., 1975a, Surface sediment distribution map, northern Gulf of Alaska: U.S. Geol. Survey Open-File Rept. 75–505, 5 p.

——— 1975b, Base may of the northern Gulf of Alaska: U.S. Geol. Survey Open-File Rept. 75–506, 1 p.

Molnia, B. F., Carlson, P. R., and Bruns, T. R., 1976, Report on the environmental geology, OCS Area, eastern Gulf of Alaska: U.S. Geol. Survey Open-File Rept. 76–206, 28 p., 18 figs.

Naugler, F. P., and Wageman, J. M., 1973, Gulf of Alaska magnetic anomalies, fracture zones, and plate interactions: Geol. Soc. America Bull., v. 84, no. 5, p. 1575–1584.

Plafker, George, 1967, Geologic map of the Gulf of Alaska Tertiary Province, Alaska: U.S. Geol. Survey Misc. Geol. Inv. Map I–484, scale: 1: 500 000.

——— 1971, Possible future petroleum resources of Pacific margin Tertiary basin Alaska, *in* Future petroleum provinces of the United States, their geology and potential, v. 1: Am. Assoc. Petroleum Geologists Mem. 15, p. 120–135.

——— 1974, Preliminary geologic map of Kayak and Wingham Islands, Alaska: U.S. Geol. Survey Open-File Rept. 74–82, 1 pl., scale 1: 31 680.

Plafker, George, and Addicott, W. O., 1976, Glaciomarine deposits of Miocene through Holocene age in the Yakatage Formation along the Gulf of Alaska margin, *in* Miller, T. R., ed., Recent and ancient sedimentary environments in Alaska: Anchorage, Alaska Geological Society, p. Q1–023.

Plafker, George, Bruns, T. R., and Page, R. A., 1975, Interim report on petroleum resource potential and geologic hazards in the outer shelf of the Gulf of Alaska Tertiary province: U.S. Geol. Survey Open-File Rept. 75–592, 74 p.

Shor, G. G., Jr., 1966, Continental margins and island arcs of western North America, *in* Continental margins and island arcs: Internat. Upper Mantle Comm., Symposium, Ottawa 1965, Canada Geol. Survey Paper 66–15, p. 216–221.

Shor, G. G., Jr., and von Huene, Roland, 1972, Marine seismic refraction studies near Kodiak, Alaska: Geophysics, v. 37, no. 4, p. 697–700.

Slotnick, M. M., 1950, A graphical method for the interpretation of refraction profile data: Geophysics, v. 15, no. 2, p. 163–180.

Taylor, P. T., and O'Neill, N. J., 1974, Results of an aeromagnetic survey in the Gulf of Alaska: Jour. Geophys. Research, v. 79, no. 5, p. 719–723.

von Huene, Roland, Molnia, B. F., Bruns, T. R., and Carlson, P. R., 1975, Seismic profiles of the offshore Gulf of Alaska Tertiary province, R/V Thompson, Sept.–Oct. 1974: U.S. Geol. Survey Open-File Rept. 75–664, 14 p.

Worzey, L. J., 1974, Standard oceanic and continental structure, *in* Burk, C. A., and Drake, C. L., eds. The geology of continental margins: New York, Springer-Verlag, Inc., p. 59–66.

Jour. Research U.S. Geol. Survey
Vol. 6, No. 5, Sept.-Oct. 1978, p. 637-650

GEOMETRY AND RATES OF CHANGE OF FAULT-GENERATED RANGE FRONTS, NORTH-CENTRAL NEVADA

By ROBERT E. WALLACE, Menlo Park, Calif.

Abstract.—Characteristic features of fault-generated range fronts, such as those on the Humboldt and Tobin Ranges, include sets of elongate basins extending normal to the range crest, interbasin spurs having crests sloping 10° to 20° toward the range front, spur facets having slopes of 25° to 35°, basin headwalls having slopes of 20° to 30°, and a basal fault scarp. The basal fault scarp is rejuvenated by vertical movements recurring at intervals on the order of 10 000 years. Fault scarps in colluvium that lie within a few tens of meters of the base of faceted spurs remain clearly recognizable for only a few tens of thousand years. Initial fault-scarp slopes of 50° to 90° are replaced by debris-controlled slopes of 30° to 37° within a few thousand years. In fractured bedrock, slope angles in the range of 25° to 35° remain relatively stable for hundreds of thousands of years and account for the relative stability of facets on spurs. Piedmont slopes are greatly affected by tectonic tilting or warping toward or away from the range front. The formation of pediments is believed to result from a low ratio of uplift relative to downcutting. A few million years is required for the development of a pediment a few kilometers wide.

Fault-generated mountain fronts have received much attention in the literature. Papers by Davis (1903), Louderback (1904), Blackwelder (1928), and Gilbert (1928) are among the classics. More recently the subject has not received much specific attention except for a study of the Wasatch front (Hamblin, 1976), but concepts of the erosional processes that modify slopes have evolved considerably. Books by Young (1972) and Carson and Kirkby (1972) provide excellent reviews, an entree into the rather voluminous literature on the subject, and definitions of terms in current use.

The overriding goal of this study is to learn how to use geomorphology to improve understanding of the tectonic history of the Basin and Range province. The study considers the rates at which geomorphic changes take place, discusses how faulting and the rates of tectonic change influence geomorphology, and speculates, from data gathered in north-central Nevada, about the origin of typical features. Geometric forms, many of which were recognized by earlier workers, are reexamined and some new elements are described.

The ranges studied are in north-central Nevada and lie between lat 40° and 41° N. and long 116° and 118.3° W. (fig. 1). Faults along 14 ranges have been studied, but the fault-generated fronts of the Humboldt, Tobin, and East Ranges, and the Cortez Mountains are particularly suitable as examples to which other ranges can be compared.

The region is considered arid, but annual precipitation varies widely as a function of local relief. Between 12 and 20 cm of precipitation falls on the basins at elevations of about 1200 m, but in the mountains at elevations of 1500–3000 m, the precipitation may be 35–45 cm. Freezing temperatures are common in November through March, and the average annual number of times of freeze and thaw is between 120 and 130 (Visher, 1954).

Channeling in the ranges and on the alluvial fans appears to be accomplished in large measure during flash floods in the summer and during periods of high runoff in the spring. Solifluction and mudflows stimulated by freezing and thawing are important in modifying slopes. Deflation is important, particularly from the barren playas during the summer months.

Differences in lithology have a major effect on landforms, but in this study the focus is on the effects of young faulting and the patterns of erosion that result from the tectonic disruption of the land surface. In order to deal with this selected part of the total problem of landform evolution, most examples described are in parts of the ranges where landforms are least affected by lithologic variations. But even where lithologic differences cause complex erosion patterns, the geomorphic forms that are a consequence of range-front faulting rarely are completely obscured.

Acknowledgments.—I wish to thank W. B. Bull, K. R. Lajoie, Malcolm Clark and Clyde Wahrhaftig, for very helpful discussion on the subject.

BASINS

Individual basins along fault-generated mountain fronts have the pattern variously termed "wineglass valley," "goblet valley," or "hourglass valley" (von

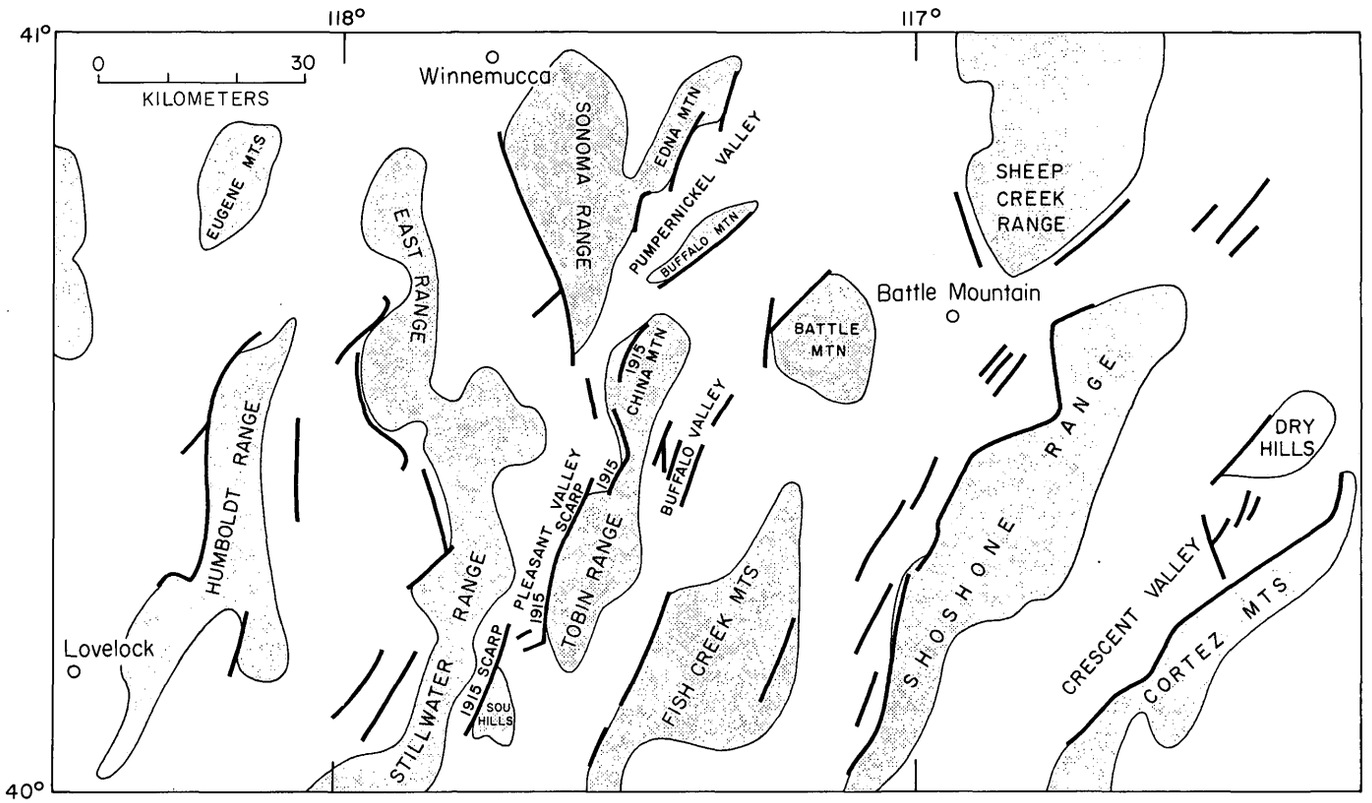

FIGURE 1.—Index map. Heavy lines are young faults.

Engeln, 1942, p. 377), indicating a basin that is constricted at its mouth and broad in its headwaters. The characteristic pattern of a fault-generated mountain front is one composed of a set of uncomplicated, elongate, roughly parallel wineglass valleys which extend from the front of the mountains to the crest. Both sides of the northern Tobin Range (fig. 2*A*) and the west side of the Humboldt Range (fig. 2*B*) display this basin pattern. The overall pattern of basins and divides is well illustrated in the side-looking radar image of the northern part of the Tobin Range (fig. 8). The pattern of a set of these basins may be termed a "dentate basin pattern," alluding to the appearance of teeth set in a jaw. This pattern may be recognized long after facets of spurs, indicative of faulting, have been so eroded as to lose their planarity.

Other basin patterns reflect other influences; the palmate basin pattern on the east side of the Humboldt Range (fig. 2*B*) is interpreted to have been caused by consequent streams developed on the tilted basalt surface or louderback which originally covered the range block. The patterns of basins in the central Tobin Range block (fig. 2*C*) may be termed "irregular" or "amoeboid" and reflect a complex history of faulting and differential erosion that has disrupted simple drainage patterns. The faceted spurs attest to the fault origin of the range front despite the more complicated basin form.

Basin patterns on the Granite Mountain block (fig. 2*D*) are complex because of erosion along two fault-generated fronts that are roughly at right angles. The basins become curved because drainage tends to be normal to the two boundaries, the ridge crest, and the mountain front.

A certain ratio of the spacing of basins to the length of basins appears to be characteristic of fault-generated mountain fronts. Spacings of basin mouths along several range fronts and the lengths of the basins were measured and averaged. The average basin length is also the average width of the range front from crest to base. Ratios of spacing to length are between 0.25 and 0.55. For example, on the west flank of the Humboldt Range the ratio is about 0.41, on the west flank of the Tobin Range it is 0.46, and on the east side of the Tobin Range it is 0.34.

In contrast to the low ratios exhibited by simple fault-generated range fronts, the ratios of basin spac-

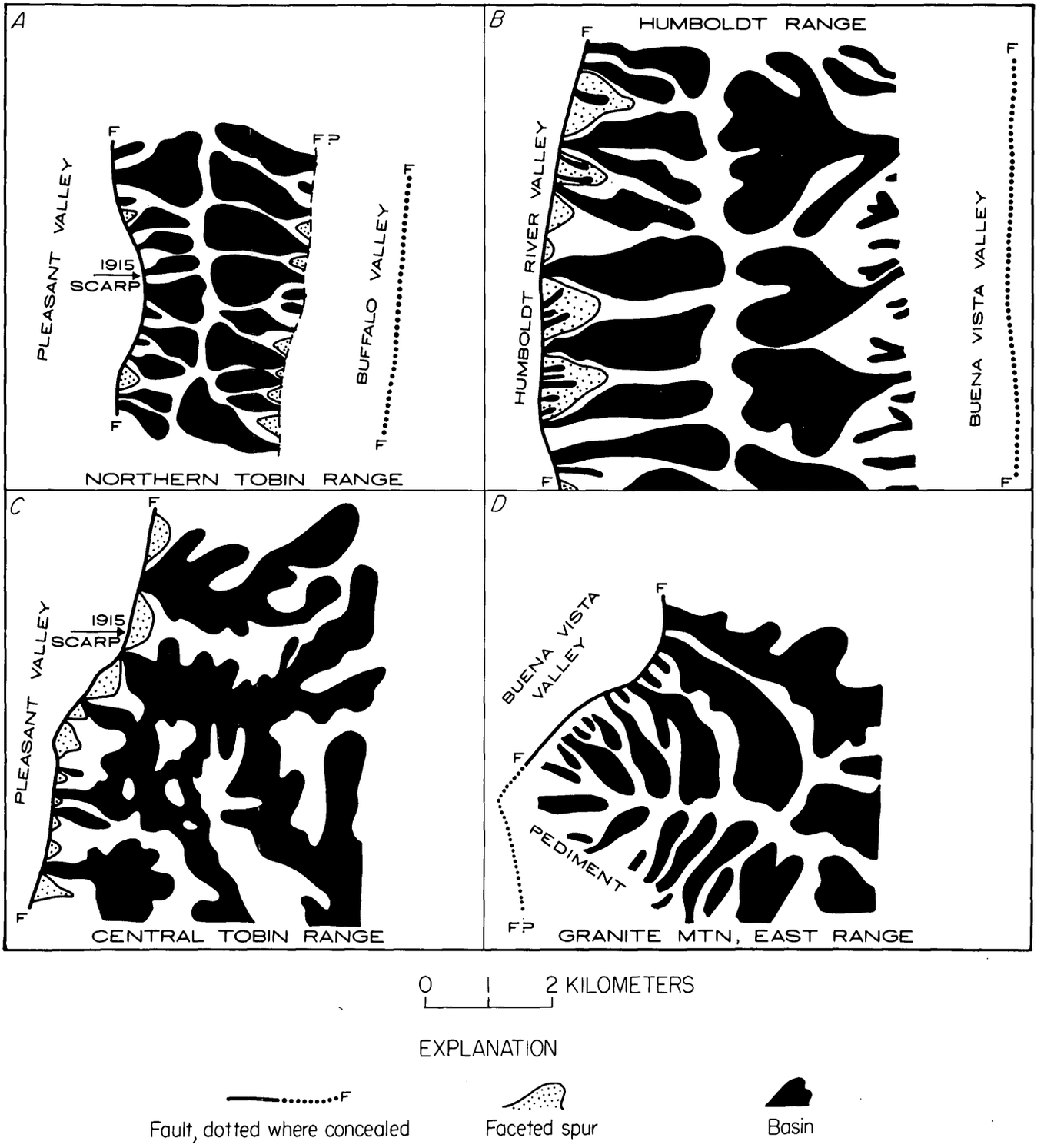

FIGURE 2.—Examples of patterns of basins along fault-generated mountain fronts.

ing to length of basins apparently are larger in more complex tectonic and geomorphic systems. For example, on the east flank of the Humboldt Range (fig. 2*B*), where palmate basin forms are exhibited, the ratio is 0.87.

I find it helpful in examining the patterns of basins

to generalize their shapes and to fill in this outline (fig. 2), taking care to represent the divides by broad enough belts so that the basins appear as separate, discrete shapes. Generalization may be aimed at smoothing or deemphasizing features of any desired size. The patterns shown in figure 2 tend to deemphasize divide features less than one-third of a kilometer long. Undoubtedly the process could be mathematically formulated, but a simple, rapid, subjective, smoothing process has served to outline and characterize basin shapes.

Individual basins have a V-shaped cross section in most of the examples studied. The valleys terminate uphill in a triangular headwall commonly sloping 20°–30° and are bounded downstream by the margins of triangular facets (see C and D in fig. 4). Hanging valleys may be present at the basin mouth, and terraces may flank incised gulches in the lower reaches of the basins.

At the rate of step uplifts of one 3-m event every 10 000 years (Wallace, 1976, 1977b), erosion seems to keep pace and to regrade the channels in a small fraction of 10 000 years. Indeed, along main channels cutting the 2–5 m scarp developed in 1915, conspicuous knickpoints have disappeared after only 60 years. For example, in Wood Canyon (sec. 12, T. 27 N., R. 38 E., Cain Mountain quadrangle), a knickpoint in alluvium was still easily identified in 1957, but not in 1975.

DIVIDES—CREST AND SPUR FORM

The pattern of divides along a fault-generated range front is distinctive. The most characteristic pat-

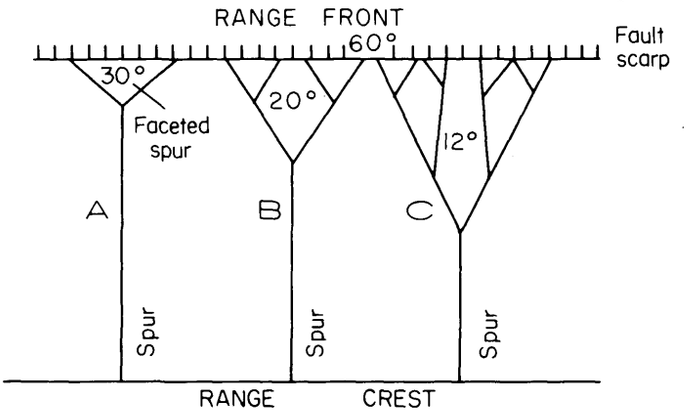

FIGURE 3.—Diagram of drainage divides along fault-generated mountain fronts. Shown are the orthogonal patterns of crest and spurs, the division of the faceted spur with age (A–C), and the change in slope of the facets with age.

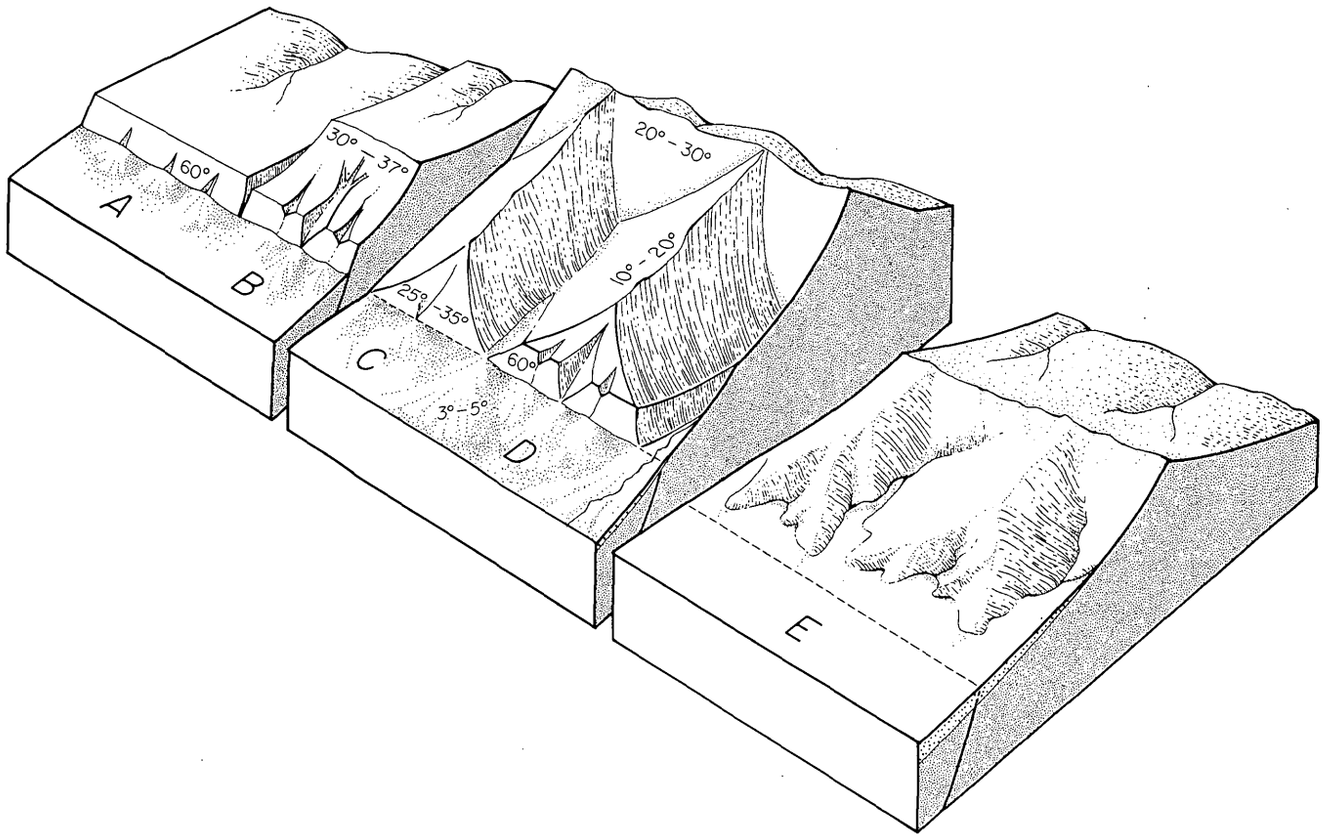

FIGURE 4.—Block diagrams showing sequence of scarp development (A–E). The scale of each new increment of fault displacement as shown is greatly exaggerated. See text for discussion.

tern is the crest and spur form, the crest subparallel to the range front and the spurs trending orthogonally to the crest (figs. 3 and 4).

I conceive that the crest and spur form originated in the following way. The initial faulting, or period of accelerated uplift, created a linear scarp crest (A in fig. 4), which, after becoming sufficiently high to divide drainage, began to migrate away from the fault trace. Rills on the young scarp faces a few meters high became gulches as the scarp height grew to tens of meters, and ultimately gulches enlarged to valleys and basins when the range crest became a thousand or more meters high (C and D in fig. 4). Dissection was continuously rejuvenated in this microprovince because of repeated uplift of a few meters at a time along the frontal fault. In the early stages when the range front was narrow, divides and basins oriented perpendicular to the range front may have been relatively close together, as the rills on scarps only a few meters high are spaced only a few meters or tens of meters apart. On older, wider fronts the spacing of divides and basins is wider because dominant channels apparently destroy smaller adjacent channels. Downcutting is greatest in the dominant channel, and smaller adjacent channels, unable to keep pace in downcutting with the larger channels, are destroyed as the larger channels widen (fig. 5).

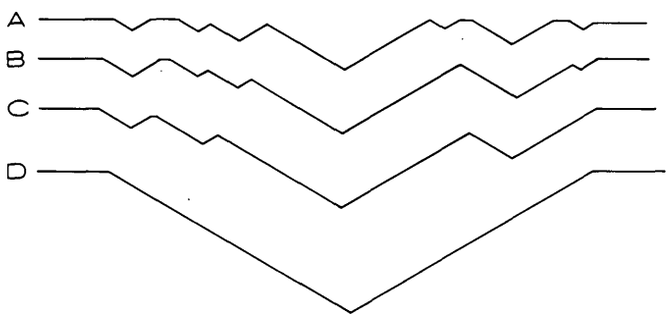

FIGURE 5.—Diagrammatic cross section of channels, showing how one channel tends to become dominant as downcutting progresses through stages A to D.

In both the Humboldt and Tobin Ranges, the range crest and orthogonal spurs are sharp, and the spurs slope 10°–20° away from the crest. Sharp crests probably have persisted for a long period of time because of repeated rejuvenation by faulting in increments of a few meters over periods of the order of 10 m.y. (million years).

Undoubtedly a time will finally be reached when active uplift slows or ceases and erosion can proceed to older, more subdued stages. Nevertheless, the spurs and crests arranged in an orthogonal pattern may persist to reflect the original generation by faulting.

A contrast in the sharpness of crests of spurs can be seen by comparing those on the west flanks of the Cortez Mountains and East Range (fig. 13). The topography near the range fronts is far more subdued in the East Range than in the Cortez Mountains. An interpretation of this relation is given in the section on pediments.

FAULT SCARPS

Fault scarps progress through a particular sequence of forms over various periods of time (Wallace, 1977a). The original scarp, which may be vertical and is usually less than 4 m high, spalls to produce a debris slope standing at between 30° and 37° at the base of the scarp and a free face sloping between 45° and 90° at the top of the scarp. The debris slope enlarges, and finally all the free face disappears and the crest of the scarp becomes rounded. Rill erosion, frost action, rain splash, and other processes cause the slope to decline in angle until it is indistinguishable from the slopes of alluvium or colluvium in which the scarp most commonly forms.

Renewed movement on faults commonly produces steep, new scarps along the line of the older, subdued scarps, and thus a record of multiple displacements is preserved. Many examples of later faulting occur almost precisely along the scarps created during earlier faulting, suggesting that parallel retreat of scarps is not an essential phase in the process of degradation in relatively homogeneous materials.

For those scarps and faults which lie directly at the base of the range front, each new increment of scarp becomes added to the base of the faceted spurs as described in the following section.

FACETED SPURS

"Faceted spur," "triangular facet," and "trapezoidal facet" are terms referring to relatively planar surfaces at the ends of mountain spurs at the range front. The planar form is inherited from the planar nature of the bounding fault, but only indirectly. Except for a time span of a very few hundred years following a fault offset, and at a scale of a fault scarp a few meters high, the facets represent eroded fault planes (Wallace, 1977a). The slopes of the facets may range from about 25° to 35°, whereas the fault plane generally dips at angles of 50° to 90°, less commonly as low as 45°. This relation was recognized by Blackwelder (1928) and has been discussed by Hamblin (1976).

The initial scarp, which is a fault-plane surface, is

replaced within a few hundred years by a debris slope (Wallace, 1977a), and it is the debris slope angle or angle of repose of coarse clasts that largely controls the facet slopes for hundreds of thousands of years or even a few million years.

Many examples of faceted spurs in various stages of erosion can be found in north-central Nevada. Some of the simplest planar facets are along the west side of the Pearce block (central Tobin Range) south of Miller Basin (fig. 6). Facets are also present on both flanks of the northern Tobin Range, but there the simple planar surface on many facets has been modified by one or more channels which have developed on the facet. The east flank of the Humboldt Range displays triangular forms on which pronounced channels are distributed very much as less conspicuous channels are on fresher facets. The channels differ only in the degree of dissection, and the triangular patterns of divides on the east flank of the Humboldt Range are thus interpreted to have originated as faceted spurs.

This sequence of degradation of faceted spurs is interpreted diagrammatically in figure 3. A triangular facet truncating a fully developed spur at the base of which is a young fault scarp is shown in A in figure 3. Repeated faulting in steps of a few meters every 10 000 years (Wallace, 1977a, b) continually extends the faceted spur at its base. The lower part of the facet thus tends at all times to be a younger surface than the upper part. Erosion on the flanks of the spur, which lowers the top of the spur, and erosion on the facet itself lessen the slope of the facet. When the facet is small, a central channel develops from the apex of the facet to the base and causes the divides to bifurcate (B in fig. 3). As the facet grows in area, additional channels flanking the main channel develop and bifurcation of the divides is repeated (C in fig. 3). With time, the planar nature of the facet becomes decreasingly obvious.

The triangular pattern of range-front divides within which is a pattern of bifurcated divides appears to be a characteristic recognizable as a criterion of range-front faulting long after the predecessor triangular facet has lost its identity.

Not all facets are triangular. The triangular facet would occur only where the spur is sharp crested. If the spur truncated were flat topped, perhaps a relict of an upland surface, the facet would be trapezoidal. Once an upland surface is destroyed, the sharp-crested spur remains dominant for a long period of time.

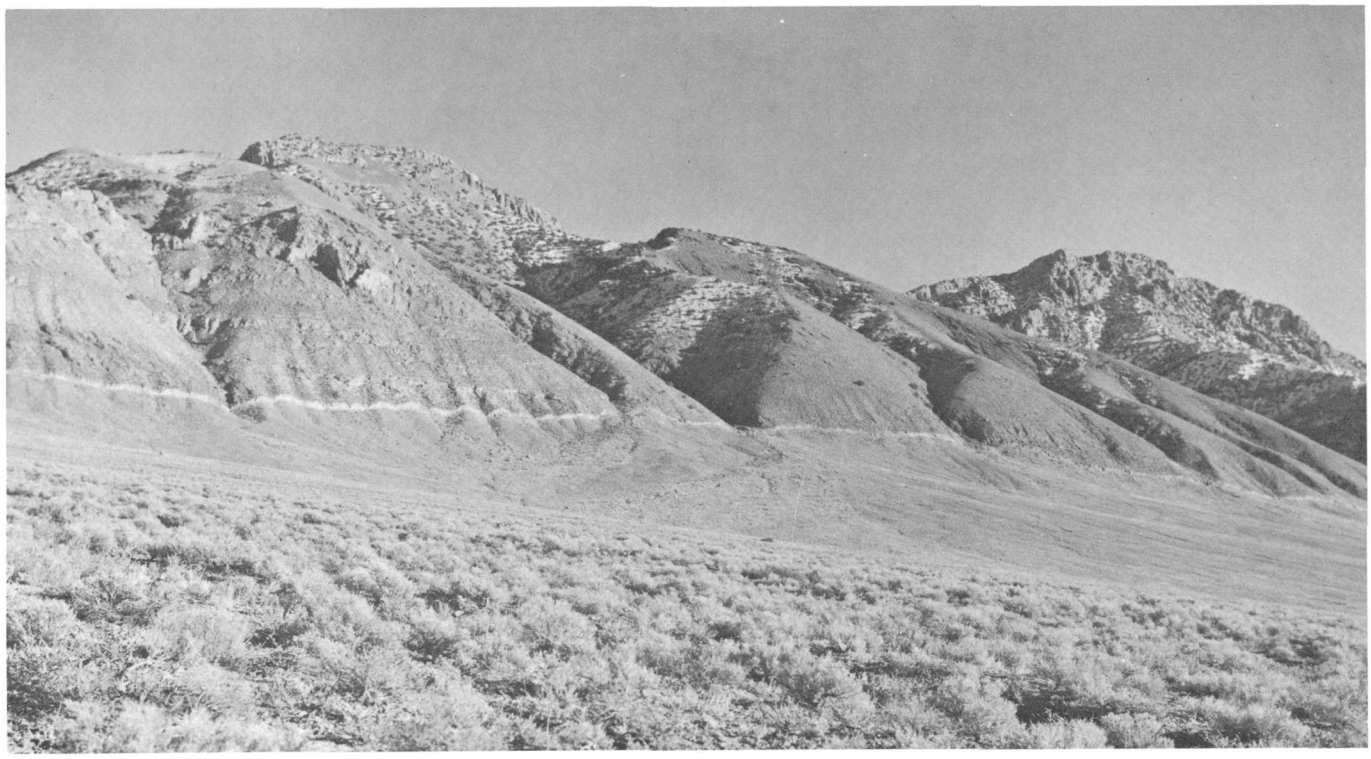

FIGURE 6.—West side of Pearce block of Tobin Range showing scarp developed during earthquake of 1915 and triangular facets on spurs.

Repeated uplift creates rejuvenation and perpetuates the sharp-crested form.

Facets having different degrees of dissection in A, B, and C of figure 3 have slopes of 30°, 20°, and 12°, respectively, and 60° is the assumed slope of the original fault scarp. These slopes are representative of slopes associated with different degrees of dissection in the study area. The decrease from slopes over 50° to those in the range of 30° to 37° apparently takes place relatively rapidly, as compared to the decrease from 30° to 20° (fig. 7). The facets thus are stable over a relatively long period of time.

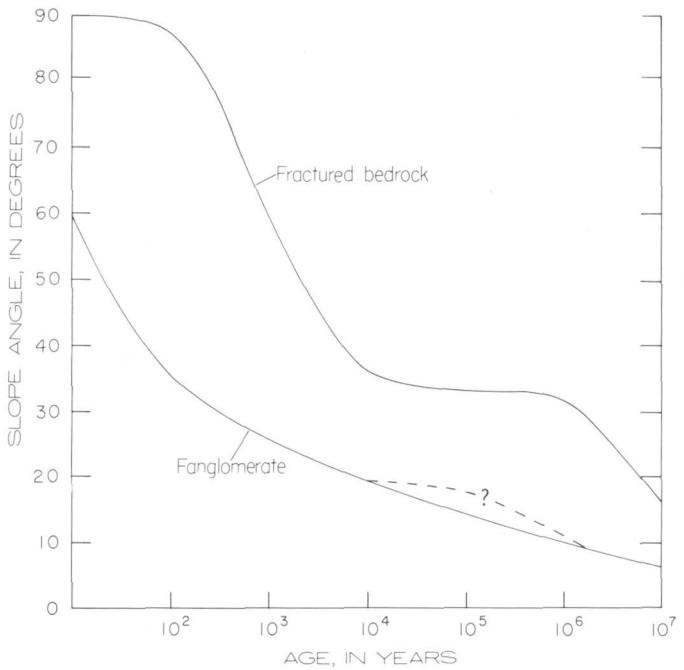

FIGURE 7.—Slope angle of fault scarps in relation to age. The angles of scarps supported by fractured bedrock and fanglomerate represent the most common extremes (from Wallace, 1977a). Dashed line represents a possible stable range of slope angles, but significance is not understood.

PIEDMONT SLOPES

Piedmont slopes adjacent to fault-generated mountain fronts are intimately related to the mountain fronts themselves. Contrasts in the geomorphic forms developed on piedmont slopes result from a combination of factors alluded to by many investigators, for example, Denny (1967), Bull (1964a, b, 1968, 1973), Cooke and Warren (1973). Among the most important factors are climate, sediment yield, areas of deposition and erosion, and tectonics.

Many forms of piedmont slopes border the ranges in north-central Nevada. For example, at least three different types of piedmont slopes, planar bajada, conical fans, and upraised pediment, border the Tobin Range (figs. 8 and 9). On the northwest flank of the

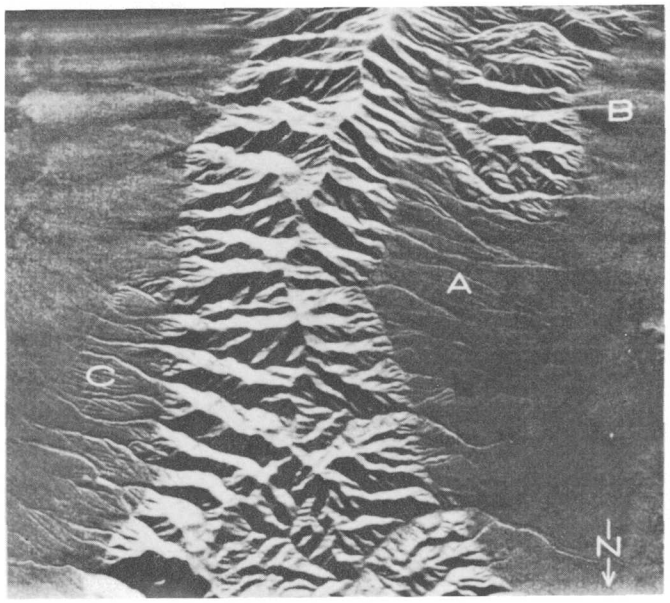

FIGURE 8.—Side-looking radar image of the northern part of the Tobin Range showing characteristic patterns of basins and divides along fault-generated mountain fronts. The 1915 fault scarp is at the base of the west flank of the range, and other young fault scarps are at and near the east flank. See text for discussion of piedmont slopes at A, B, and C. Image from AN/APQ–97, U.S. Army Electronics Command and National Aeronautics and Space Administration.

Tobin Range (area A, fig. 8; fig. 9*A*), contours are relatively linear and parallel and represent slopes of the piedmont surface which increase from less than 3° to the west near the basin center to as steep as 14° near the range-front fault. The range-front fault and fault-generated mountain front truncate the northeasterly trend of the linear segments of the contours. This configuration suggests a nearly planar bajada that originally was more extensive and developed adjacent to an ancestral Tobin Range front more nearly parallel to the contours on the bajada. Later faulting at the north end of the Pearce block and along the northwest-trending segment of the Tobin Range front may have dismembered the original bajada. The slopes near the southeast corner of the bajada are so steep as to suggest that the bajada may also have been steepened by warping.

Channels on this slope are deeply incised in the

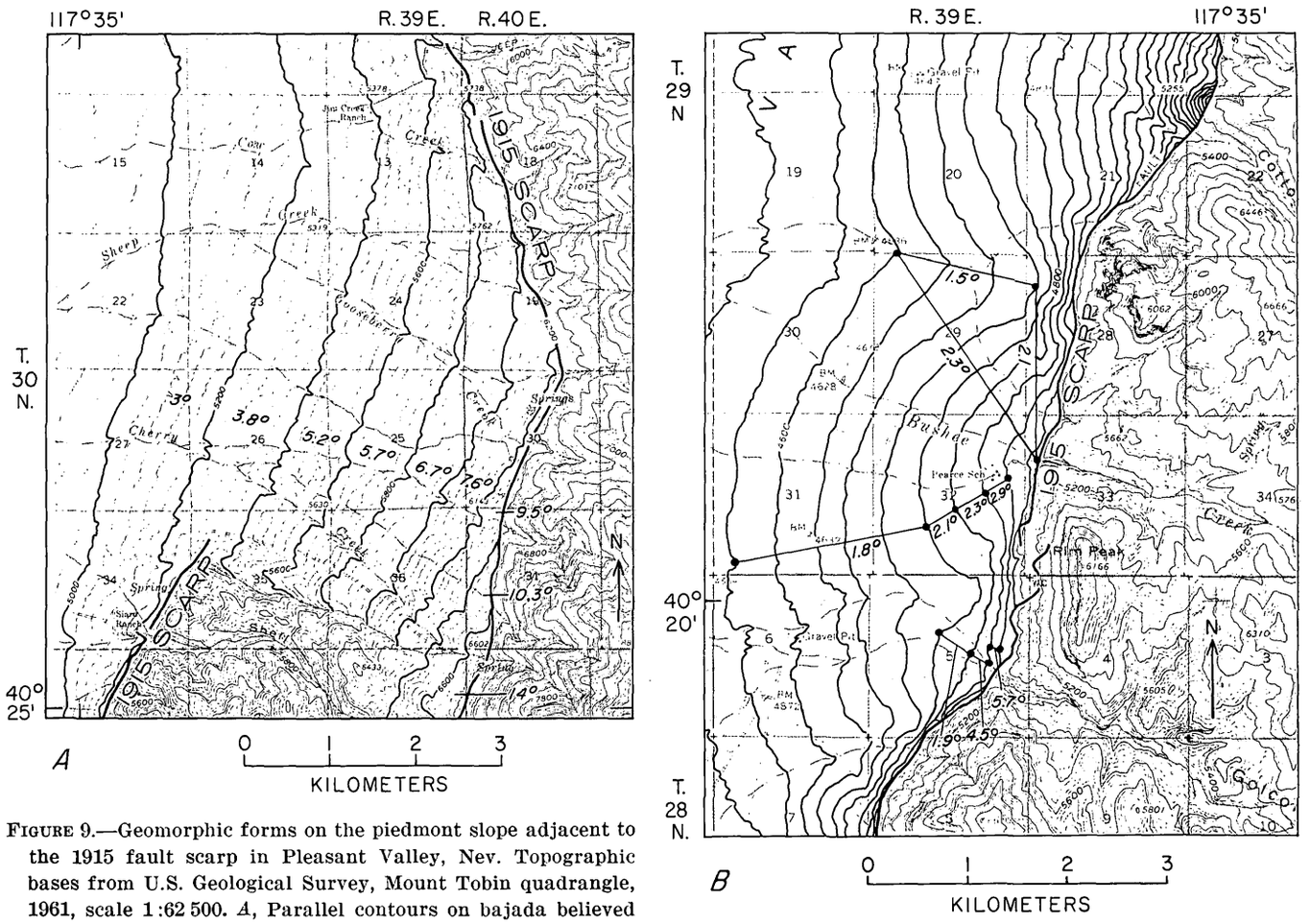

FIGURE 9.—Geomorphic forms on the piedmont slope adjacent to the 1915 fault scarp in Pleasant Valley, Nev. Topographic bases from U.S. Geological Survey, Mount Tobin quadrangle, 1961, scale 1:62 500. *A*, Parallel contours on bajada believed to be tilted as much as 14° to the west. *B*, Characteristic fans along piedmont slope south of *A*.

upper parts where slope exceeds approximately 7°, but aggradation dominates in the lower reaches where slopes are below approximately 5°. At slopes between 5° and 7°, given the climatic conditions here, aggradation and dissection alternate, dominance depending upon the energy of a given storm runoff. Hooke (1967, 1972) has described similar incision related to tilting of the basin of Death Valley, but Beaty (1961) suggests that the uplift of the Grapevine Mountains in the Death Valley area caused the incision of fans.

In contrast, conical fans dominate area B (fig. 8) south of the planar bajada. There arcuate, concentric contours (fig. 9*B*) are typical of alluvial fans. The fan at the mouth of Bushee Creek has slopes ranging from 1.8° to 3°, which are common values for slopes of fans in this region. Fan slopes of 5°, however, are not rare. Within 100 m of the apices of very recent cones of boulders and cobbles adjacent to the active scarp, a few slopes are as steep as 15°, but nowhere in this region are planar, bajadalike slopes as steep unless deformed.

The piedmont surface on the east flank of the Tobin Range (area C, fig. 8) is upraised with respect to the basin along faults that are parallel to but a few kilometers or more from the range front. The piedmont surface on the uplifted block is deeply incised as a result of the lowered base level.

Tectonics are believed to have been the most significant factor controlling these geomorphic forms. At area A (fig. 8) deformation tilted the surface away from the range and truncated the piedmont surface. At area B (fig. 8) the piedmont surface either was tilted toward the range or dropped relative to the range at a rate that exceeded the rate of accretion of material in the piedmont area. At area C (fig. 8) the piedmont surface was raised with little or no tilting and was incised.

Figure 10*A* diagrammatically postulates the effect of tectonic steepening of the piedmont slope adjacent

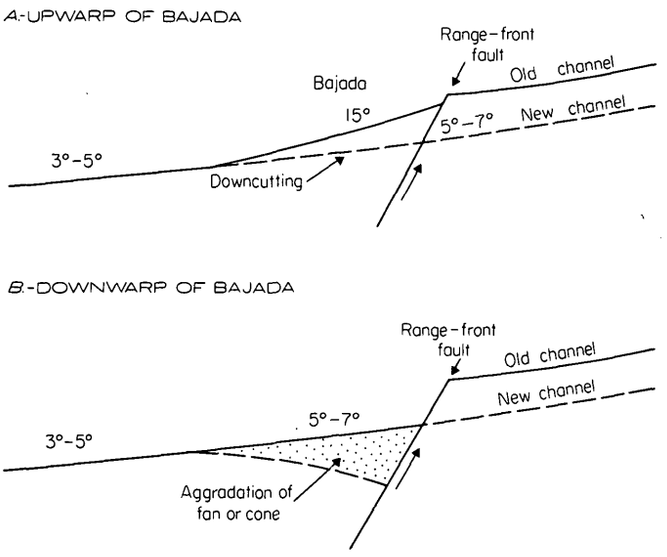

FIGURE 10.—Effects of tectonic warping or tilting of piedmont slope adjacent to a fault-generated mountain front. *A*, Tilting away from the range. *B*, Tilting toward the range.

to the mountain front either by tilting or warping. If a slope were tectonically steepened to more than 7°, no major fan would form at the mountain front under present climatic conditions. Instead, the bajada would be dissected and a cut surface would develop; possibly a pediment could be formed by lateral planation of dissecting streams. Broad fans would develop downslope from the hinge line or break in slope between those slopes less than 5° and those that are steeper.

In figure 10*B*, the effect is diagrammatically postulated of tectonic downwarping or tilting which decreases the slope of the piedmont surface along the mountain front. If a slope were decreased to less than 3°, conspicuous fan forms could develop. Original slopes of the piedmont surface below 1.5° should foster the development of well-formed fans. Although the slope of the original surface on which a fan is deposited could have a pronounced influence on the shape of the fan, probably as important are the rate of displacement along the frontal fault as compared to the rate of erosion of the mountain block, and the resulting rate of accumulation of sediments on the graben block as discussed by Bull (1973).

Near Unionville (Unionville 15-minute quadrangle topographic map), on the east flank of the Humboldt Range, the tectonic setting is similar to that on the east flank of the Tobin Range. Gradients of distributaries on the fan at the mouth of Buena Vista Creek are steepened by faults that cut the fan. The head of the fan has been stepped upward a few meters at the fault, and distributaries on the fan have become incised upstream of the fault. Downstream of the fault secondary fans have formed, but these secondary fans are not large enough to be conspicuous as discrete fans on a 15-minute quadrangle map. However, in aggregate the newly formed fans and other redistributed materials on the lower parts account for a modification of the contours of the lower part of the fan. The arcuate contours on the lower parts of the fan have a center of rotation upstream from the range front, whereas the arcuate contours of the upper part of the fan have their center of rotation at the mountain front (fig. 11).

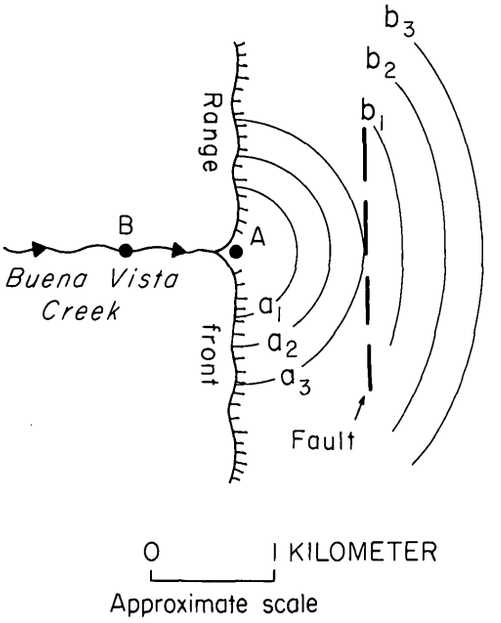

FIGURE 11.—Geometry of concentric contours of fans affected by faulting. Contours a_1, a_2, and a_3 have their center of rotation at A, and contours b_1, b_2, and b_3 have their center of rotation at B.

PEDIMENTS

Extensive pediments have formed adjacent to some of the mountain fronts. They are known primarily from gravity studies because they are covered by a veneer of gravel from a few meters to more than 100 m thick. A pediment on the east flank of the Humboldt Range is illustrated in cross section in figure 12. A pediment of similar dimensions also is present on the east side of the Tobin Range (R. B. Grannell, written commun., 1976) and on the west side of the East Range (R. G. Reeves, written commun., 1977). Limited parts of some of the pediments can be observed in a few places near the mountain fronts where erosion has

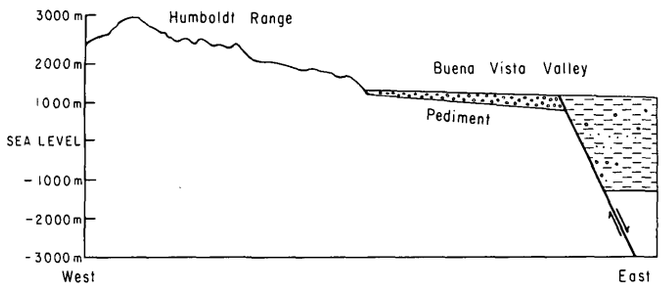

FIGURE 12.—Profile across the Humboldt Range and Buena Vista Valley showing the pediment on the east flank of the range. This profile is from an interpretation of gravity data by Donald Mabey (Wallace and others, 1969).

cut channels through the covering gravels. The main range-front faults, which produced thousands of meters of relief on the bedrock surface and now bound the pediments, in each area are a kilometer or more from the present range front. The process of pediment development thus seems to be linked to the process of parallel retreat of mountain fronts.

Why broad pediments have formed on the east sides of the Humboldt and Tobin Ranges but not on the west sides is obscure. The difference may be primarily the length of time available for pediment development since the last period of accelerated uplift along the range front. If the uplift ceases or the rate of uplift is extremely slow relative to erosion, a pediment tends to form (Bull, 1973). The range front degrades, slopes decline, and sheet wash becomes a more dominant process, resulting in pediment development (see the discussion of the role of sheet floods in Robinson and others, 1964, p. 135). In contrast, if the rate of uplift of the range greatly exceeds the average rate of downcutting, the range front might be expected to be at or near the bounding fault, and relief at the mountain front would be large.

Two range fronts, the west flank of the East Range and the northwest flank of the Cortez Mountains (fig. 13), illustrate the contrast postulated in the previous paragraph. The two ranges have very comparable geometry, and their crests stand about 700 to 900 m above the valley floors and are capped by basalt flows that have been tilted a few degrees to the east or southeast. Underlying the basalt in each range is an assortment of sedimentary rocks of Paleozoic or Mesozoic age. The widths of the fronts from base to range crest are a few kilometers in both ranges. The principal difference between the fronts of the two ranges is the sharpness of the breaks in slope at the range fronts. A fault lies immediately at the base of the front of the Cortez Mountains producing a linear front, adjacent to which is relief of hundreds of meters. In contrast, the margin of the East Range is very irregular; large reentrants of alluvium alternate with irregular spurs that become lower and more subdued near the range front. A pediment clearly has not begun to form on the range side of the bounding fault along the Cortez Mountains but is well advanced along the flank of the East Range.

The main range-bounding fault along the East Range, as indicated by gravity studies, is as much as 1 km west of the ends of the range spurs (R. G. Reeves, written commun., 1977). The fault scarp, along which Kyle Hot Springs occurs, probably is in part the surface expression of the range-bounding fault, but Reeves reports that at least two faults, which produce steps in the bedrock below the alluvial cover, are along the front.

If the difference between the fronts of the two ranges indeed relates primarily to the difference in the length of time since the last period of accelerated uplift along the fronts, then accelerated uplift along the west flank of the Cortez Mountains was relatively later than that along the west flank of the East Range. Both uplifts must have occurred since the basalt flows were implaced about 10–14 m.y. ago. If, as described in the section on scarps, no appreciable retreat can be shown for scarps several hundred thousand years old, it follows that the front of the East Range took many times that long, or probably millions of years, to form. Also, if the uplifts are in increments of 3 m every 10 000 years, 300–500 m of uplift represented along the Cortez Mountains front would require between 1 and 2 m.y. to form. Thus, pediment formation along the East Range and high relief along the Cortez Mountains each may require millions of years, and both must have occurred within the 10–14 m.y. since the basalts were emplaced. The argument thus might be made that the principal period of accelerated uplift of the East Range must have occurred within the earlier part of the 10- to 14-m.y. period, whereas that of the Cortez Mountains occurred during the last part of the period.

Periods of accelerated uplift or range tilting, however, may be of much shorter duration. Hooke (1972), for example, found that the present rate of range tilting in Death Valley, Calif., is 0.016° every 1000 years. That rate is an order of magnitude greater than the rate indicated in north-central Nevada by assuming a uniform rate of tilting of the ranges since the capping basalts were extruded. Furthermore, Hooke found that tilting rates were nonuniform, doubling every 23 000 years during late Wisconsin time.

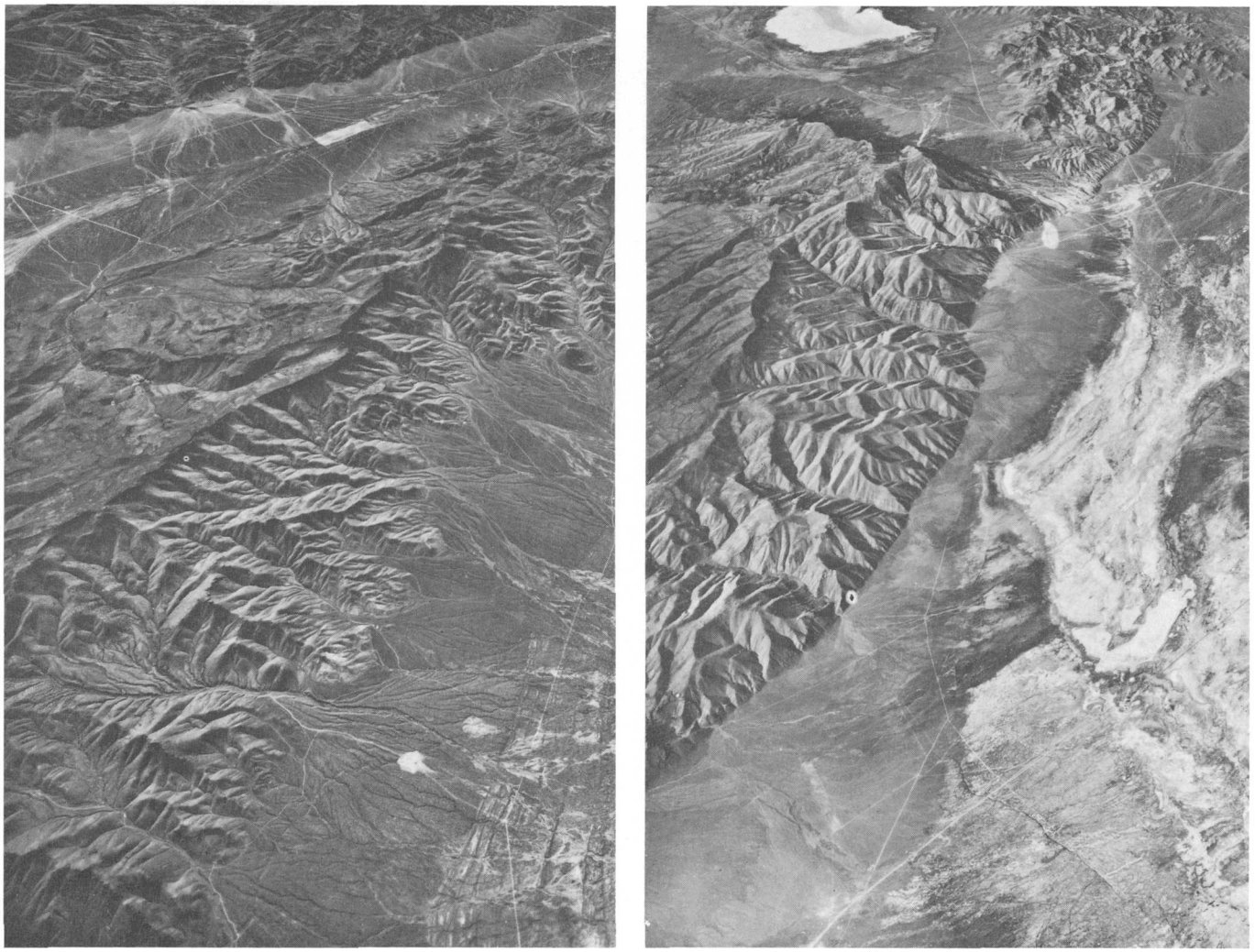

A B

FIGURE 13.—Range fronts showing differences that may be a function of the relative rates of uplift and downcutting. *A*, East Range. Oblique view toward south from altitude of about 20 000 m. *B*, Cortez Mountains. Oblique view toward southwest from altitude of about 20 000 m. U.S. Geological Survey photographs taken by U.S. Air Force.

Applying the concept to the Humboldt and Tobin Ranges, the asymmetry of the two flanks of the ranges suggests that the eastern flanks were more active at an earlier time than the western flanks. Inasmuch as both ranges have been tilting eastward most recently, they may have been tilting westward at an earlier time, and uplift may have been accomplished in a rocking style of motion.

Another process possibly affecting pediment development, one that perhaps contributes to the asymmetric development of pediments on several ranges, relates to the distribution of basalt flows. Remnants of basalt flows lie along the eastern flanks of many of the ranges and dip eastward at angles of between 5° and 10°. The basalt once covered far more extensive areas of the eastern flanks of the eastward-tilted range blocks. If the basalt cover tilted eastward, erosion on the eastern flanks would have proceeded by the development of consequent streams. As these streams cut through the basalt cover, the slopes on the flanks of the stream channels would have tended to retreat laterally, parallel to the streams, according to the sug-

gestion of Cunningham and Griba (1973) that parallel slope retreat requires a resistant capping unit. The valley floors thus would have widened and downcutting would have ceased at slope angles below 5.5°. The combination of the eastward tilt of the block, coupled with the presence of basalt having a relatively planar surface, might well have enhanced the planarity of the erosion surfaces or pediments produced on the eastern flanks of the ranges.

RATES OF PROCESSES AND THEIR INTERACTION

Key factors governing the geomorphic forms produced along a fault-generated mountain front include: (1) the rate of faulting, that is, the rate of relative movement between the horst and graben block, (2) the rate of downcutting of major channels on the horst block, (3) the rate of slope decline in bedrock and alluvial deposits, and (4) the rate of sediment accumulation in the graben.

None of the rates is linear. Faulting is believed to proceed in incremental steps of a few meters every 8000–10 000 years, and faulting events appear to cluster in time, but the process of faulting continues in this style for several million years (Wallace, 1977a). Downcutting of major channels is sensitive to the changes in base level created by the faulting events; cutting proceeds rapidly into the fault step created but then slows markedly at the step after grade is reestablished. Erosion in the upper reaches of the channel is probably relatively insensitive to the short-term changes caused by faulting at the range front.

On a time scale of tens to a few thousand years, most erosion is accomplished incrementally at the times of infrequent flash floods in the desert environment in Nevada. At one time the dominant factor controlling microrelief forms may be faulting, whereas at another time it may be a catastrophic erosion event.

The rate of sediment yield undoubtedly increases on a long-term basis as the fault-generated front grows in height and width, but the rate eventually must decrease as relief is decreased. Probably the rate of erosion increases as the height of the mountain front itself increases and causes increased local precipitation in the uplands. Several changes in climate, which undoubtedly created nonlinearity in all the erosional and sedimentation processes, probably occurred during the lifetime of the range fronts. Peltier (1975) has developed formulas to express the relations of some of these variables.

The change in rates of slope decline suggests that slopes in the 20° to 35° range are relatively stable; angles of slopes above 37° decrease rapidly (fig. 7).

RELATIVE LIFETIMES OF GEOMORPHIC FEATURES

Despite the complexities of the processes and rates, some generalizations about the lifetime of the geomorphic features in north-central Nevada can be made (fig. 14). This interpretation is highly speculative because

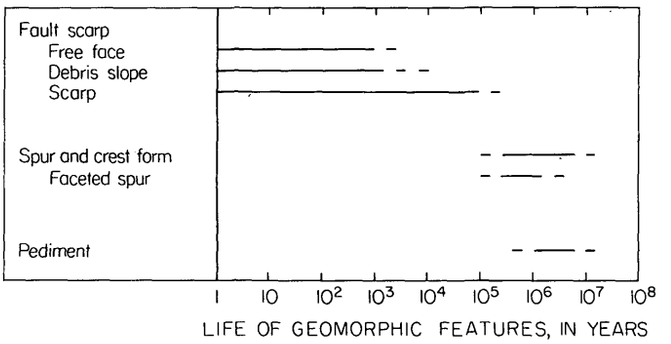

FIGURE 14.—Lifetime of geomorphic features characteristic of fault-generated mountain fronts, north-central Nevada.

it is based on relatively few known late Cenozoic ages of rock units and geologic events and great uncertainty about the nonlinearity of the rates of processes.

Among the important known ages in late Cenozoic time is the age of glacial Lake Lahontan, the high stand of which may have been approximately 12 000 years ago (see discussion in Morrison and Frye, 1965). Some fault scarps cut the high stand, and others are truncated by the high stand. Another known age is that of basalts capping many of the ranges. Dates ranging from 10.4 ± 0.5 to 12.9 ± 0.7 m.y. have been obtained by the potassium-argon method (M. L. Silberman, written commun., 1976). The basalts covered the landscape not only after the basic form of the ranges was first established, but also after erosion had greatly subdued the topography so that extensive flows were spread across several ranges.

Other evidence of the age of events was obtained from carbon-14 dating of wood in sediments along young faults and of lacustrine shells and tufa along beaches of Lake Lahontan; from an occurrence of Mazama ash ($6600 \pm$ years) in the free face of the 1915 fault scarp; and from tree-ring dating of trees adjacent to or on scarps. Interpretation of relative ages has been based on rates of slope decline and relative development of lichens, desert pavement, and vegetation.

From the relation of fault scarps to the high shoreline of Lake Lahontan, fault scarps in semiarid climates are believed to last as conspicuous features for a relatively few hundred thousand years. The lifetime

of free faces, debris slopes, and of the scarp itself is suggested by Wallace (1977b). A free face lasts no more than 2000 years, and the scarp possibly no more than a few hundred thousand years unless the fault is reactivated.

Uplift of the ranges at average rates of 3 m each 8000–10 000 years (Wallace, 1977b) would produce 100 m of relief in about 330 000 years. The crest and spur forms would probably not become pronounced before that much relief existed. Faceted spurs form concurrently with the spurs, and the facet is relatively stable because of the stability of slopes in the 28° to 37° range (fig. 7). But a clear facet generally is obliterated well before the orthogonal crest and spur form are destroyed. Crest and spur are perpetuated during several thousand meters of uplift, which suggests a duration of millions of years. The formation of pediments, whether special conditions are required or not, seems to require degradation of the spurs over at least some of their extent, so pediments are interpreted as being significant only after many hundreds of thousands, and probably millions of years. Most of the modern relief of the ranges appears to have been formed within the past 10–14 m.y., although the ranges were blocked out before then. As a late or end phase of erosion, the pediment would survive many times 10 m.y.

REFERENCES CITED

Beaty, C. B., 1961, Topographic effects of faulting, Death Valley, California: Assoc. Am. Geographers Annals, v. 51, no. 2, p. 234–240.

Blackwelder, Eliot, 1928, The recognition of fault scarps: Jour. Geology, v. 36, no. 4, p. 289–311.

Bull, W. B., 1964a, Alluvial fans and near-surface subsidence in western Fresno County, California: U.S. Geol. Survey Prof. Paper 437–A, 70 p.

———1964b, Geomorphology of segmented alluvial fans in western Fresno County, California: U.S. Geol. Survey Prof. Paper 532–F, p. F89–F128.

———1968, Alluvial fans: Jour. Geol. Education, v. 16, p. 101–106.

———1973, Local base-level processes in arid fluvial systems: Geol. Soc. America Abs. with Programs, v. 5, no. 7, p. 562.

Carson, M. A., and Kirkby, M. J., 1972, Hillslope form and process: London, Cambridge University Press, 475 p.

Cooke, R. V., and Warren, Andrew, 1973, Geomorphology in deserts: Berkeley, University of California Press, 374 p.

Cunningham, F. F., and Griba, Walter, 1973, A model of slope development and its application to the Grand Canyon, Arizona, U.S.A.: Zeitschift für Geomorphologie, Band 17, Heft 1, p. 43–77.

Davis, W. M., 1903, The mountain ranges of the Great Basin: Harvard Univ. Mus. Comp. Zoology Bull., v. 42, p. 129–177.

Denny, C. S., 1967, Fans and pediments: Am. Jour. Sci., v. 265, p. 81–105.

Gilbert, G. K., 1928, Studies of Basin-Range structure: U.S. Geol. Survey Prof. Paper 153, 92 p.

Hamblin, W. K., 1976, Patterns of displacement along the Wasatch fault: Geology, v. 4, no. 10, p. 619–622.

Hooke, R. LeB., 1967, Processes on arid-region alluvial fans: Jour. Geol., v. 75, p. 438–460.

———1972, Geomorphic evidence for late Wisconsin and Holocene tectonic deformation, Death Valley, California: Geol. Soc. America Bull., v. 83, no. 7, p. 2073–2097.

Louderback, G. D., 1904, Basin-range structure of the Humboldt region: Geol. Soc. America Bull., v. 15, p. 289–346.

Morrison, R. B., and Frye, J. C., 1965, Correlation of the Middle and Late Quaternary successions of the Lake Lahontan, Lake Bonneville, Rock Mountain (Wasatch Range), southern Great Plains, and eastern Midwest areas: Nevada Bur. Mines Rept. 9, 45 p.

Peltier, L. C., 1975, The concept of climatic geomorphology, *in* Melhorn, W. N., and Flemal, R. C., eds., Theories of landform development: State Univ. New York Pubs., Geomorphology, v. 6, p. 129–143.

Robinson, G. D., Wanek, A. A., Hays, W. H., and McCallum, M. E., 1964, Philmont country: U.S. Geol. Survey Prof. Paper 505, 152 p.

Visher, S. S., 1954, Climatic atlas of the United States: Cambridge, Harvard Univ. Press, 403 p.

von Engeln, O. D., 1942, Geomorphology: New York, The Macmillan Co., 655 p.

Wallace, R. E., Tatlock, D. B., and Silberling, N. J., 1969, Geologic map and cross sections of the Unionville quadrangle, Nevada: U.S. Geol. Survey Geol. Quad. Map GQ–820.

Wallace, R. E., 1976, Seismicity of north-central Nevada on the basis of young fault scarps: Seismol. Soc. America Abs. with Programs, Ann. Mtg., May 1976, p. 23.

———1977a, Profiles and ages of young fault scarps, north-central Nevada: Geol. Soc. America Bull., v. 88, p. 1267–1281.

———1977b, Time-history analysis of fault scarps and fault traces—A longer view of seismicity: World Conf. on Earthquake Engineering, 6th, New Delhi, India, Proc., v. 2, p. 409–412.

Young, Anthony, 1972, Slopes: Edinburgh, Oliver and Boyd, 288 p.

Jour. Research U.S. Geol. Survey
Vol. 6, No. 5, Sept.-Oct. 1978, p. 651-662

MORPHOLOGY OF CHASMA WALLS, MARS

By B. K. LUCCHITTA, Flagstaff, Ariz.

Abstract.—The landforms developed on the walls of the Valles Marineris system of chasmas are of three major types, which are locally transitional. The most common type is composed of steep spurs and gullies. The dominant process in the formation or modification of this type appears to be the downslope movement of material under the influence of gravity, resulting in the accumulation of extensive talus deposits. The type is morphologically similar to high, steep terrestrial scarps in desert or alpine environments. The second morphologic type consists of walls dissected by tributary canyons with characteristic V-shaped cross profiles and blunt canyon heads that locally contain lobate deposits. The tributary canyons may be relict features of the time when the existence of running water was possible on the surface of Mars. The third morphologic type consists of landslide scars forming broad curved or straight recessed sections of chasma wall. This type is accompanied by landslide deposits that form hummocky floors at the base of the recessed sections. The landslides developed at the expense of other wall morphologies. Chains of rimless depressions and craters that parallel the main structural trends of the chasmas are best interpreted as collapse holes. The origin of the chasmas on Mars is conjectural and may have been structural (grabens), but, on the basis of morphologic studies of their walls, it is suggested that most of the present wall configuration is the result of erosional scarp retreat, where erosion follows preestablished structural planes of weakness.

Pictures returned from the Viking mission to Mars will give us new insights into the processes that formed and modified the martian chasmas. It may be appropriate, therefore, to summarize briefly what the Mariner 9 pictures have shown us about the martian chasmas and their geomorphic development. The present study builds on and generally confirms what has been previously suggested by McCauley and others (1972) and Sharp (1973).

Valles Marineris, a system of troughs or chasmas, extends from the Noctis Labyrinthus system of closed depressions in the west (about lat 5° S. long 93° W.) to the chaotic terrain in the east (about lat 15° S, long 40° W) over a distance of 3200 km (fig. 1).) The chasmas are subparallel and interconnected except for Hebes Chasma, which is entirely enclosed. The straight segments of Ius and Tithonium Chasmas in the west are separated from the straight Coprates Chasma in the east by the wide areas of Ophir, Melas, and Candor Chasmas. The chasmas are typically 50 to 100 km wide and 2000 to 4000 m deep (Wu and others, 1973; Hord and others, 1974; U.S. Geological Survey, 1976), and the plateau surface and trough floors slope gently (about 8′) to the east (U.S. Geological Survey, 1976).

Acknowledgments.—The work was performed under NASA contract W13,576. The constructive criticism by J. F. McCauley and J. P. Schafer is greatly appreciated.

PLATEAU SURFACE

The plateau into which the Valles Marineris troughs are cut is relatively flat, sparsely to moderately cratered (Soderblom and others, 1974; McCauley, 1978), has ridges resembling lunar wrinkle ridges (fig. 2), and resembles some terrestrial lava plateaus seen on satellite images. Therefore, the material near the surface, which can be seen in the upper cliff faces of the chasma walls, is probably composed predominantly of volcanic material.

Near the chasma edges the plateau surface displays linear light and dark markings, which probably delineate grabens (fig. 3) and fractures as shown on high-resolution pictures. The grabens are numerous, mostly subparallel, and similar in trend to the main chasma in many places. Nearly rimless, flat-floored, apparently ancient craters are locally superposed on the grabens (fig. 3). The chasma walls locally are parallel to the older graben scarps but elsewhere truncate the older structures, and it appears that some time elapsed between the development of the grabens and the development of the chasma walls. This is similar to the development of the fracture system of the Tharsis dome, which antedates the formation of the shield volcanoes and served to control their distribution (Carr, 1974). Chains of craters also parallel the troughs.

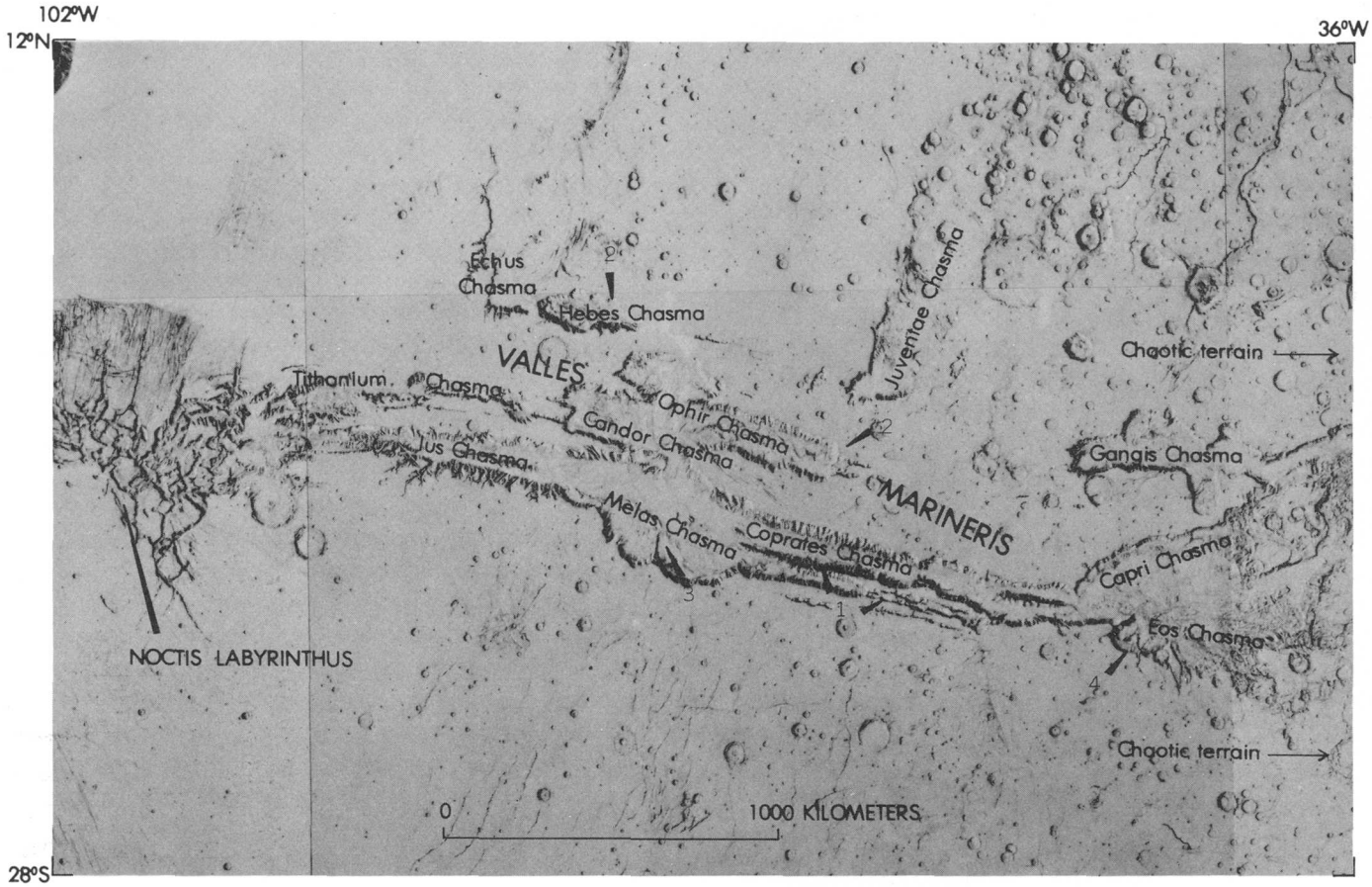

FIGURE 1.—Valles Marineris system of chasmas. Chasmas are interconnected, except for Hebes Chasma, which is entirely enclosed. Chasma floors slope gently to east and have outlet towards north through chaotic terrain. Erosional modification of the chasmas is suggested by progression from chain craters to chasmas, and from narrow plateau segments to intrachasma ridges (1); curvilinear and arcurate chasma walls (1); ridgelike protrusions from walls (3); and widening along curved traces of ancient craters (4). Map about 4000 km wide, north toward top. White area east of Hebes Chasma was not covered by Mariner 9 images. Shaded relief base from U.S. Geological Survey 1:5 000 000 Tharsis, Lunae Palus, Oxia Palus, Phoenicis Lacus, Coprates, Margaritifer Sinus.

CHASMA WALL LANDFORMS

The chasma walls in Valles Marineris are of three major morphologic types, which are locally transitional. The first and most common type—spur-and-gully morphology—consists of walls dissected by steep gullies and intervening spurs that branch downward at acute angles (Sharp, 1973). The second type—tributary canyon morphology—consists of walls dissected by tributary canyons that have characteristic V-shaped cross profiles and blunt canyon heads. The third type—landslide morphology—consists of landslide scars that form broad curved or straight recessed sections of chasma wall with hummocky deposits at the base of these sections. Examples of each type are shown in figure 4, and the distribution of each type in Valles Marineris is shown in figure 5.

Spur-and-gully morphology

Spur-and-gully morphology, which is the most common chasma wall morphology, is well displayed in Coprates Chasma, in Ius Chasma, and on the interior ridges of the chasmas paralleling the chasma walls. Below the plateau surface, the walls commonly have a steep cliff that is dissected into vertical subparallel ribs (*fig. 6A*). Horizontal layering locally shows in the cliff as color bands or as alined, more resistant layers. Lower on the wall, sharp-crested downward-branching spurs descend to the chasma floors, and, locally, the crest of the spur is lined with subparallel

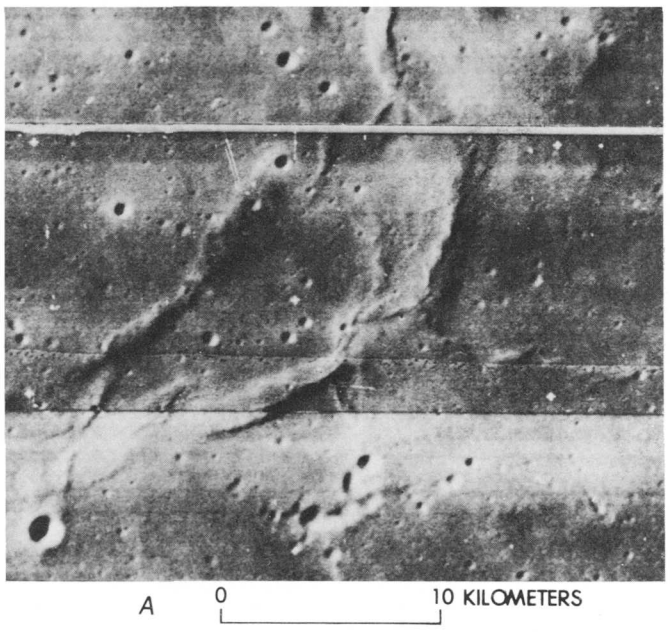

FIGURE 2.—Comparison of lunar and martian wrinkle ridges. *A*, Mare Frigoris, northwest of crater Plato; Lunar Orbiter IV–H–128, north toward bottom. *B*, South of Coprates Chasma, west of crater Lassell; Mariner 9 DAS 7542363N–B, north toward top. Horizontal lines are artifacts of the reconstruction of the images. Both ridges have sharp meandering crests following broad upwarps in mare surface.

vertical ribs. The intervening gullies range from shallow to deeply incised. Spurs on the south wall of Ius Chasma have gradients of 15° to 20°; intervening gullies, as much as 30° (Wu and others, 1973). Lower gradients are common in some gullies that are incised obliquely to the main trend of a trough.

The martian chasma walls, although larger in size, are similar in many respects to some high terrestrial scarps in alpine and desert environments (figs. 6, 7). The dissected cliff face near the top, the steep gradient near the angle of repose, and the straight to slightly concave profiles suggest active scree slope development and downhill motion of loosened material under the influence of gravity (Lehmann, 1933; Rapp, 1960; Sharp, 1973). This wall type appears to be the product of gravity erosion and appears to represent the normal and slow erosion that is developed in the absence of catastrophic events.

The Antarctic scarp (fig. 6*B*; Gunn and Warren, 1962) and the Death Valley scarp (Jennings, 1958) are underlain by fairly homogeneous resistant rocks; the martian scarp may be similarly underlain by fairly resistant homogeneous rock as is indicated by the ribs on spurs that locally descend to near the chasma floors (fig. 6*A*). These ribs are similar to the ribs that line the upper chasma walls below the upper cliff (fig. 6*A*).

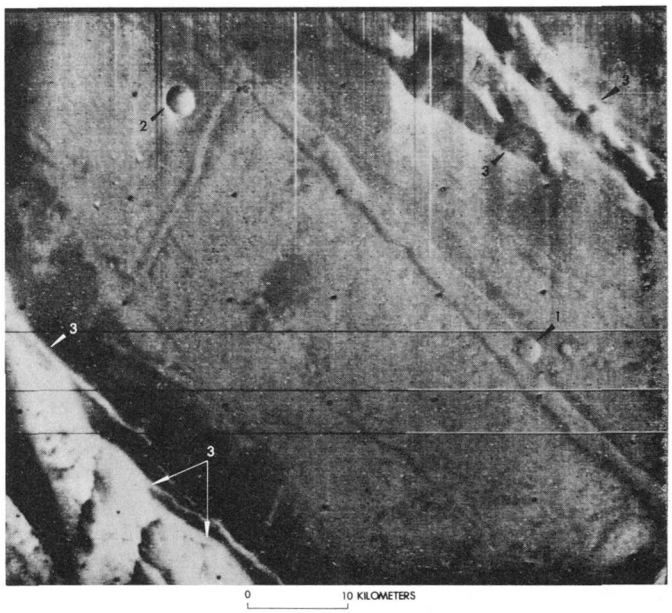

FIGURE 3.—Subdued graben on plateau surface between Tithonium and Ius Chasmas. Graben is cut by old, flat-floored crater (1). By contrast, walls of bowl-shaped crater (2) and of troughs (3) have sharp lips and steep margins. Mariner 9 high-resolution frame DAS 10133069–B. North toward top. Horizontal lines are artifacts.

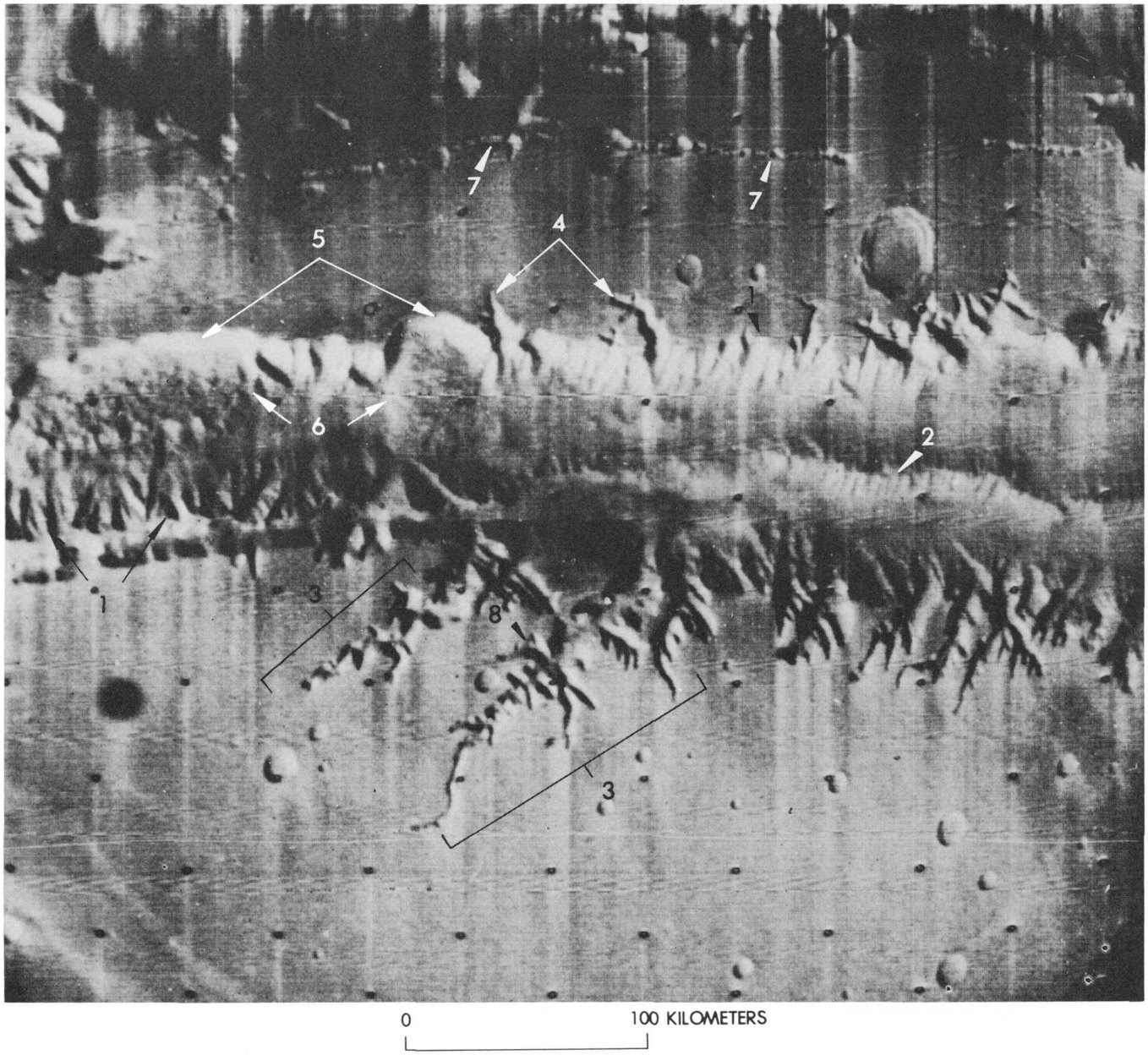

FIGURE 4.—Characteristic chasma wall morphologies (Ius Chasma). Spur-and-gully morpohology is most typical; found on chasma walls (1) and on interior ridges (2). Tributary canyons dissect plateau back from walls of chasmas and occur in groups (3) or more commonly as single valleys (4). Landslide scars form curved or straight recessed sections of chasma wall (5) with hummocky deposits at base (6). Crater chains parallel main trend of trough (7). Note structural control and apparent barbed drainage of tributary canyons (8). Mariner 9 low-resolution frame DAS 5851968–A. North toward top.

A martian debris flow on a segment of chasma wall and a debris flow on a talus-covered slope in the Wright Valley, Antartica, were compared (fig. 8). The martian debris flow resembles the terrestrial one in having a steep gully at the top, a leveed channel in the middle, and flat, overlapping lobate deposits at the base. The similarity between the two debris flows is striking enough to suggest a similar mechanism of origin. Although its origin is not known, the Antarctic debris flow may be a mudflow; debris flows that are interpreted as mudflows occur in the Victoria Valley system nearby (Calkin, 1971), and possible mudflows are found in the lower Wright Valley (Nichols, 1971). If the martian debris flow is a mudflow, the water may have come from the melting of ground ice, whose presence was suggested by Sharp (1973).

Tributary canyon morphology

Groups of tributary canyons dissect the chasma walls in some places, as on the south wall of Ius Chasma (fig. 4), but, in most places, the tributary canyons are solitary valleys. These are 30 to 130 km long and up to 10 km wide and are similar in size to the Grand Canyon of Arizona. Canyon heads typically are blunt, cirquelike bowls, and channels above the canyon heads are mostly absent (fig. 9). The tributary canyons have V-shaped cross profiles with smooth walls (figs. 9–11). The original valley may have been V-shaped, but the shape seems to be intensified through infilling with talus, as suggested by its similarity to talus-covered valleys in Antarctica (Calkin and others, 1970) or in Spitzbergen (Rapp, 1960) (fig. 12). The martian tributary canyons appear to have even gradients of at most a few degrees (U.S. Geological Survey, 1976) and merge with the main trough at the level of its floor. Most side branches merge with the tributary canyons accordantly, but a few intersect the tributary canyon in the form of hanging valleys (figs. 9, 11). Locally, the canyons have hummocky, lobate, or longitudinally streaked deposits on their floors (figs. 10, 13*A*).

Strong structural control during the development of tributary canyons is evident in the alined straight segments, in the near-reticulate pattern of clustered canyons, and in "barbed" side canyons (figs. 4, 9, 10). Locally canyons form smooth curves, possibly eroding along buried craters rather than linear structures (fig. 4).

On the one hand, the overlapping lobate material that can be seen near the head of some side canyons (fig. 13*A*) could be overlapping debris flows of catastrophic origin. On the other hand, the lobate deposit arising from the talus slopes in the cirquelike head of the valley shown in figure 13*A* is remarkably similar in surface details to a rock glacier (Wahrhaftig and Cox, 1959; White, 1976) or a solifluction lobe (Ugolini and Bull, 1965) in Antarctica (fig. 13*B*) and suggests the possibility that the lobate deposits moved by creep and that ground ice (Sharp, 1973) may have facilitated the movement.

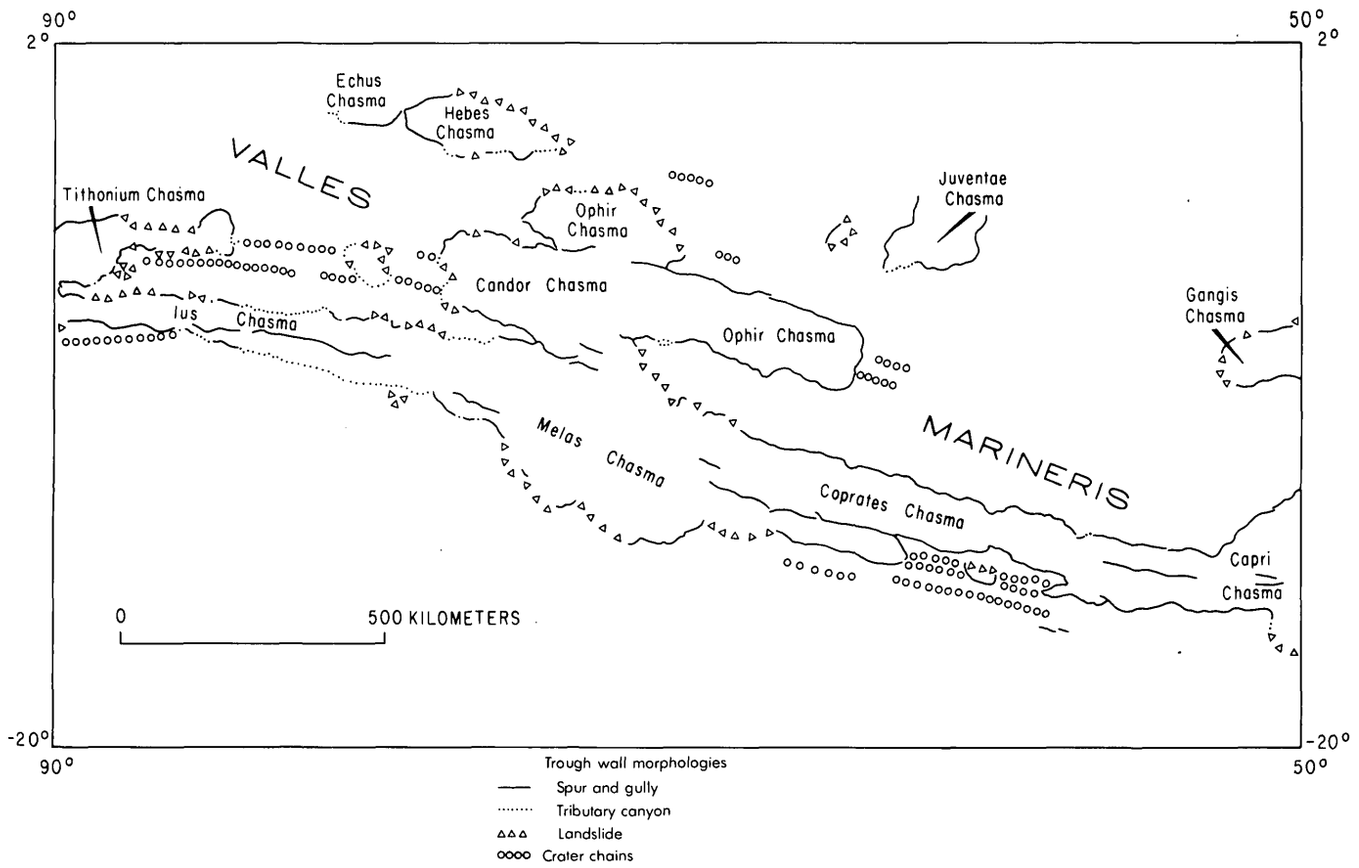

FIGURE 5.—Distribution of characteristic wall morphologies in Valles Marineris.

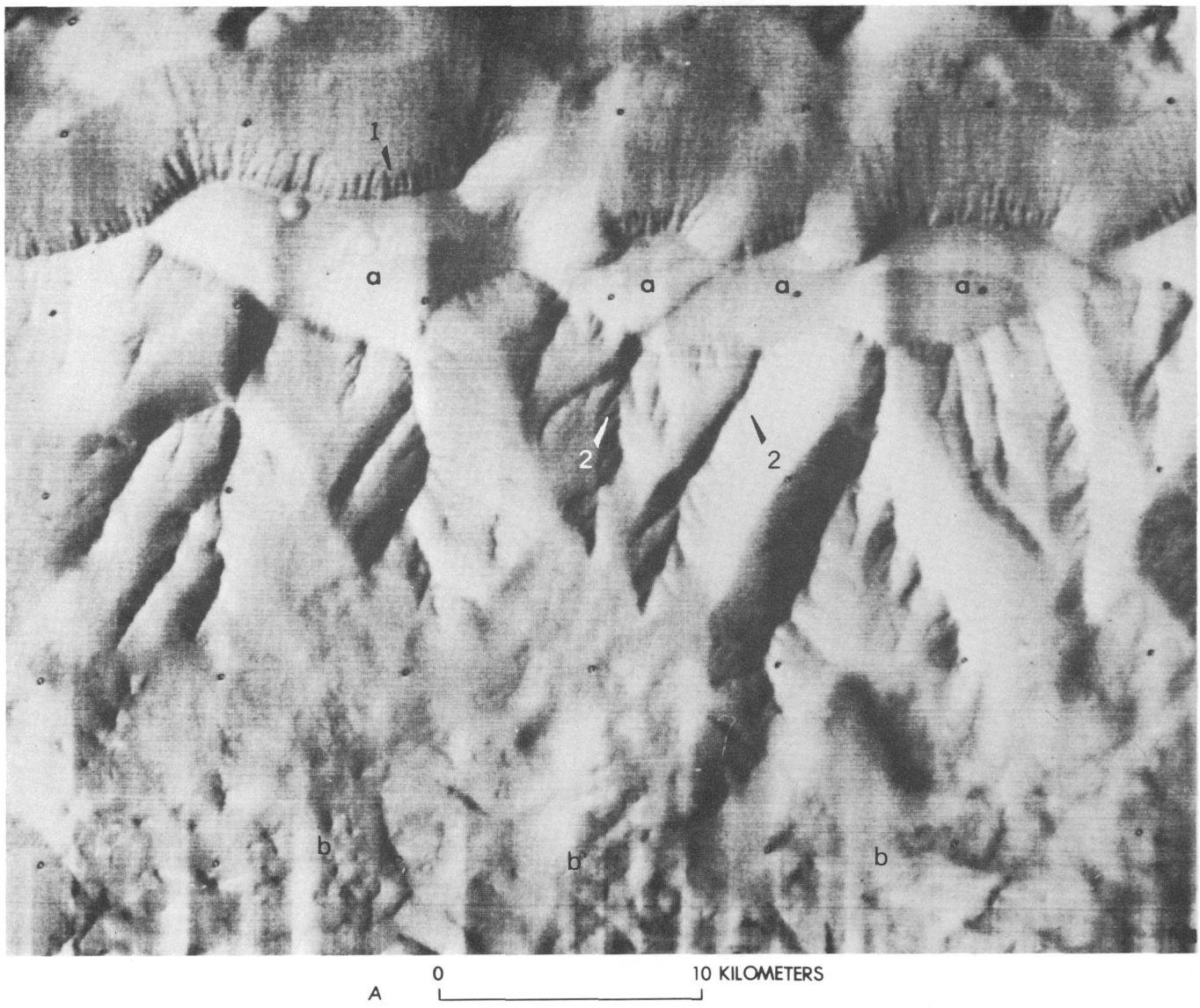

FIGURE 6.—Comparison of martian and terrestrial spur-and-gully morphology. *A*, South wall of Ius Chasma. Mesa of plateau surface across upper middle part of picture (a); chasma floor shown at (b). Below plateau surface, steep cliff is dissected into vertical subparallel ribs (1); below, on main part of slope, are sharp-crested spurs that branch downward at acute angles. Spur crests are locally lined by vertical ribs (2) similar to those in steep cliff near top. Scarp is about 4000 m high. (Mariner 9 frame DAS 7326763–B. North toward bottom. *B*, Wright Valley, Antarctica. Scarp, about 1600 m high, is underlain mostly by metamorphic rock (Gunn and Warren, 1962). Steep, sharp-crested ridges branch downward at acute angles and are locally lined by vertical ribs (3). Intervening gullies and chutes are covered by talus deposits. Channels on fans (4) are evidence of transport by water. Hummocky material near bottom of valley is glacial moraine (5). Valley floor shown at (6). Mount Theseus is in upper middle. View is northwest. Oblique aerial photograph by the U.S. Navy, Wright Valley, January 1958.

Landslide morphology

Broad curved and straight sections of chasma wall that are as long as 100 km and locally recessed 5 to 10 km from the adjoining walls are interpreted as landslide scars (figs. 4, 14). The hummocky material at the base of these recessed sections (figs. 4, 14) shows vague alinement of ridges parallel or perpendicular to the walls and appears to bury the walls locally up to about half their original heights. This material is interpreted as landslide deposits. The straight scar sections tend to be parallel to the preexisting structures.

The walls of the scars are characterized by an upper-

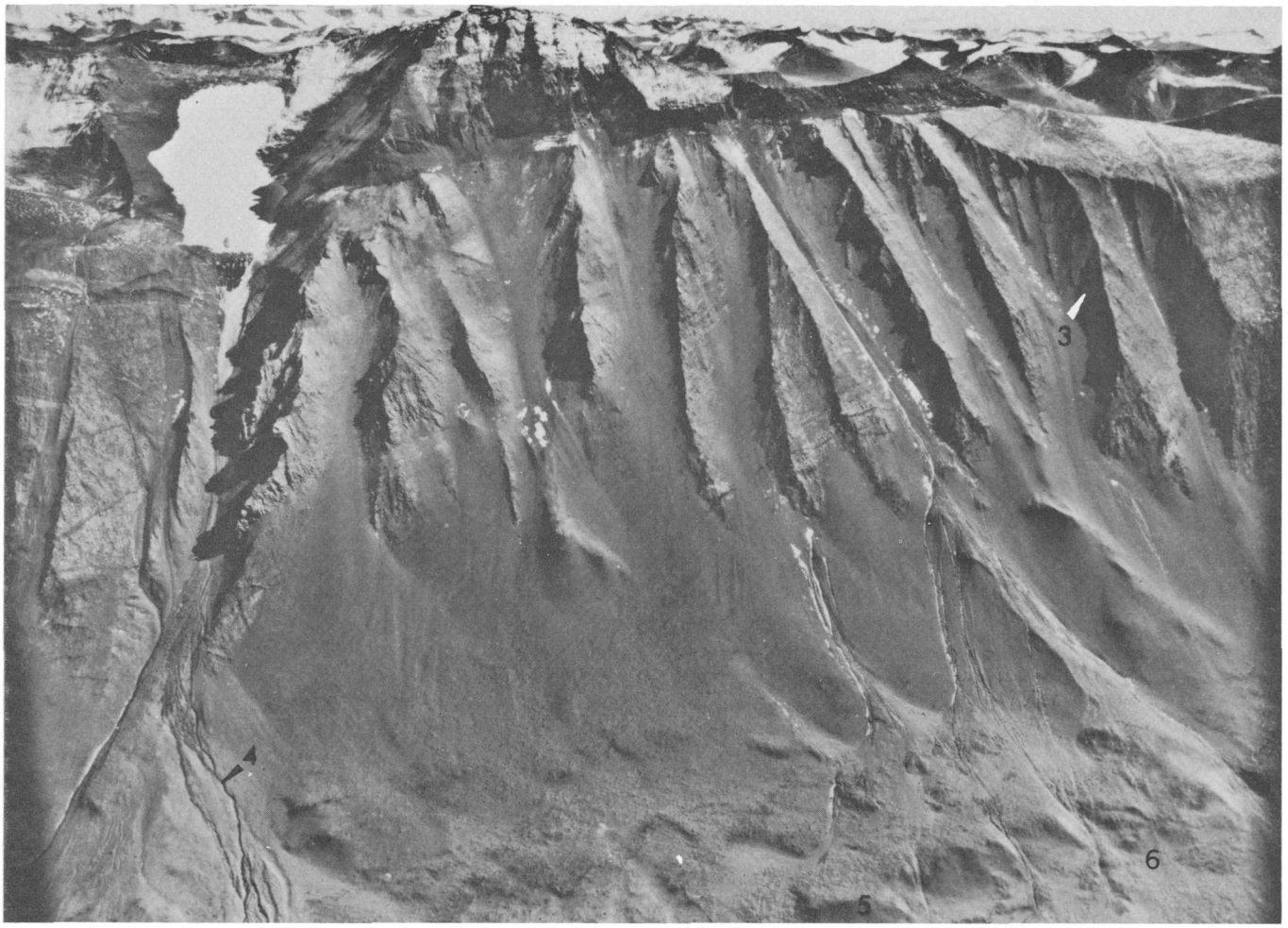

B

FIGURE 6.—Continued.

most layer eroded to evenly spaced knobs that form a cliff immediately below the plateau surface and by coarse stumpy ribs of unequal length and irregular patterns in the upper part of the wall just below that cliff (figs. 11, 14). Horizontal layering in the coarse ribs is evident in crudely alined protrusions and indentations. The stumpy ribs are distinct from the much narrower and nearly parallel vertical ribs found in the cliffs below the plateau surface on the other wall morphologies (figs. 6*A*, 8*B*). On a spur separating a landslide scar from a tributary canyon, these coarse ribs on the scar side are in direct contrast to the finely linear and nearly parallel ribs on the opposite, or tributary-canyon, side of the spur (fig. 11). This indicates that the morphology of the ribs is not caused by the rock type, but by the erosional process. Below the ribs, the walls are smooth talus slopes and display only minor faint vertical straight to sinuous depressions. Terrestrial landslide scars, such as that of the Slumgullion slide in Colorado (Crandell and Varnes, 1961), also have stumpy cliffs occurring at the head of the scar with smooth talus slopes below.

The recession of the walls along the scar segments indicates wall collapse at the expense of other types of wall morphologies that apparently develop more slowly. This is especially true for the spur-and-gully type, which appears to be destroyed periodically by the massive wall collapse through landslides and which then appears to become slowly reestablished on the breakaway scar. Preexisting structures locally seem to have provided the planes of weakness along which collapse occurred.

The number and size of landslides on Mars are larger than those of landslides on Earth. This suggests that the mechanism facilitating wall collapse on Mars is different from that on Earth and that the different circumstances on Mars allowed for a reduction in strength of the materials in the walls. If ground ice

is indeed present in the wall rocks (Sharp, 1973), wall collapse can be explained through melting of the ice along preexisting structures such as fault planes, which is in agreement with an observation by Dobrovol'skiy (1974), who noted increased heat flow underneath such structures in terrestrial permafrost terrain. The massive wall collapse is also consistent with the sudden release of water from clathrate ice in the manner described by Milton (1974).

Chain craters

Irregular-shaped to circular depressions form chains of craters that parallel the main trend of the chasmas (fig. 4). In places, the craters are in lines parallel to and inside grabens on the plateau surface (figs. 4, 5). The depressions commonly have steep, smooth walls locally converging to form V-shaped grooves at the floor or have steep upper walls with shallow bowl-shaped or flat floors (figs. 10, 15). Where the depressions coalesce and are breached towards the main chasmas, they widen and deepen and acquire wall features similar to those of the chasma walls elsewhere.

The chain craters could be of volcanic origin, similar to crater chains found on the Moon (Wilhelms and McCauley, 1971), but the absence of rim deposits makes collapse and removal of material into the subsurface a more likely origin. Removal of material into the subsurface by interior drainage, also called piping (Cooke and Warren, 1973, p. 141–142), could result from opening or widening of fissures at depth or from removal of pore ice through melting of the ice along planes of weakness (fault planes) as discussed in the previous section. In those depressions that are shallow and flat floored (fig. 10), evaporation and deflation may have taken place instead of, or in addition to, subsurface drainage. Where depressions become integrated and are breached, their floors become graded towards the main troughs. Surface transport apparently aided in the enlargement of the depressions. The processes that eroded chasma walls elsewhere apparently became dominant in these integrated depressions because their walls appear to develop similar features.

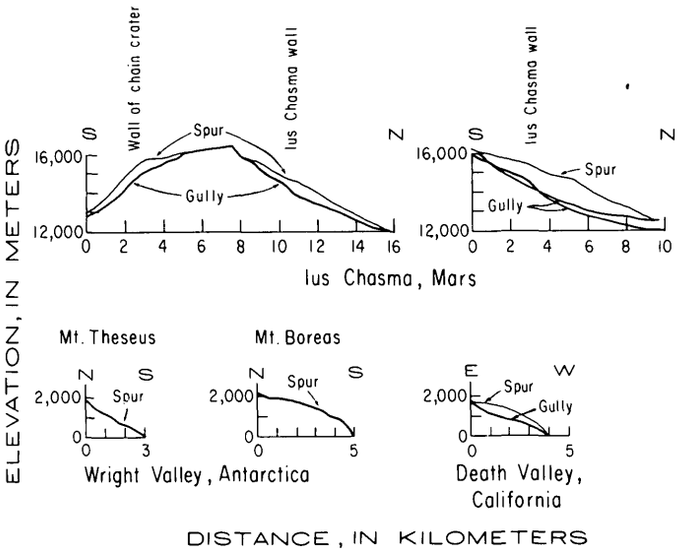

FIGURE 7.—Profiles across martian chasma walls and high terrestrial scarps in desert and alpine environments. No vertical exaggeration. The sections on the wall of Ius Chasma are separated by about 20 km.

SPECULATIONS ON ORIGIN

The origin of the chasmas is conjectural, but, on the basis of morphologic studies, it is suggested that most of the present wall configuration is the result of erosional activity along preexisting structural planes of weakness; structural displacement, however, probably formed the troughs.

The following observations indicate erosional activity on the walls:

(1) The progression from chain craters to chasmas and from narrow plateau segments to intrachasma ridges is clearly erosional (fig. 1). Chain craters enlarge and coalesce to form chasmas, leaving intervening plateau segments that diminish along trend into intrachasma ridges.

(2) Curvilinear and arcuate chasma walls do not have the appearance of fault scarps, especially where caused by massive landslides such as across the entire north side of Hebes Chasma (figs. 1, 5).

(3) Ridgelike protrusions from the walls, as seen in Melas Chasma (fig. 1), are best explained as erosional remnants.

(4) Widening of chasmas near the chaotic terrain follows circular forms (fig. 1), indicating that buried craters exerted a structural control that was enhanced by erosional processes.

A problem of the erosional hypothesis on the origin of the chasmas, as pointed out by other investigators (see, for instance, Sharp, 1973), is the removal of the eroded material to maintain a base level sufficiently low to allow for further erosional widening of the chasmas. Except for Hebes Chasma, the troughs are integrated and have an outlet through the chaotic terrain in the east. Yet the gradient is so low that ponding of any possible drainage in that direction seems very

likely. Indeed, stratified deposits reminiscent of water-laid terrestrial lakebeds or interior basin deposits can be seen in Ophir and Gangis Chasmas (fig. 16), indicating that ponding took place occasionally. Even though some of the material freed by the wall recessions may have been removed through this outlet, much must have been removed by other processes, as is evident from the closed depression of Hebes Chasma (fig. 1). Sharp (1973) could not entirely explain the loss of this material but suggested that it may largely result from evaporation of ground ice and removal of broken-down debris by wind.

All the martian chasma wall features described herein are of much larger size than similar features on

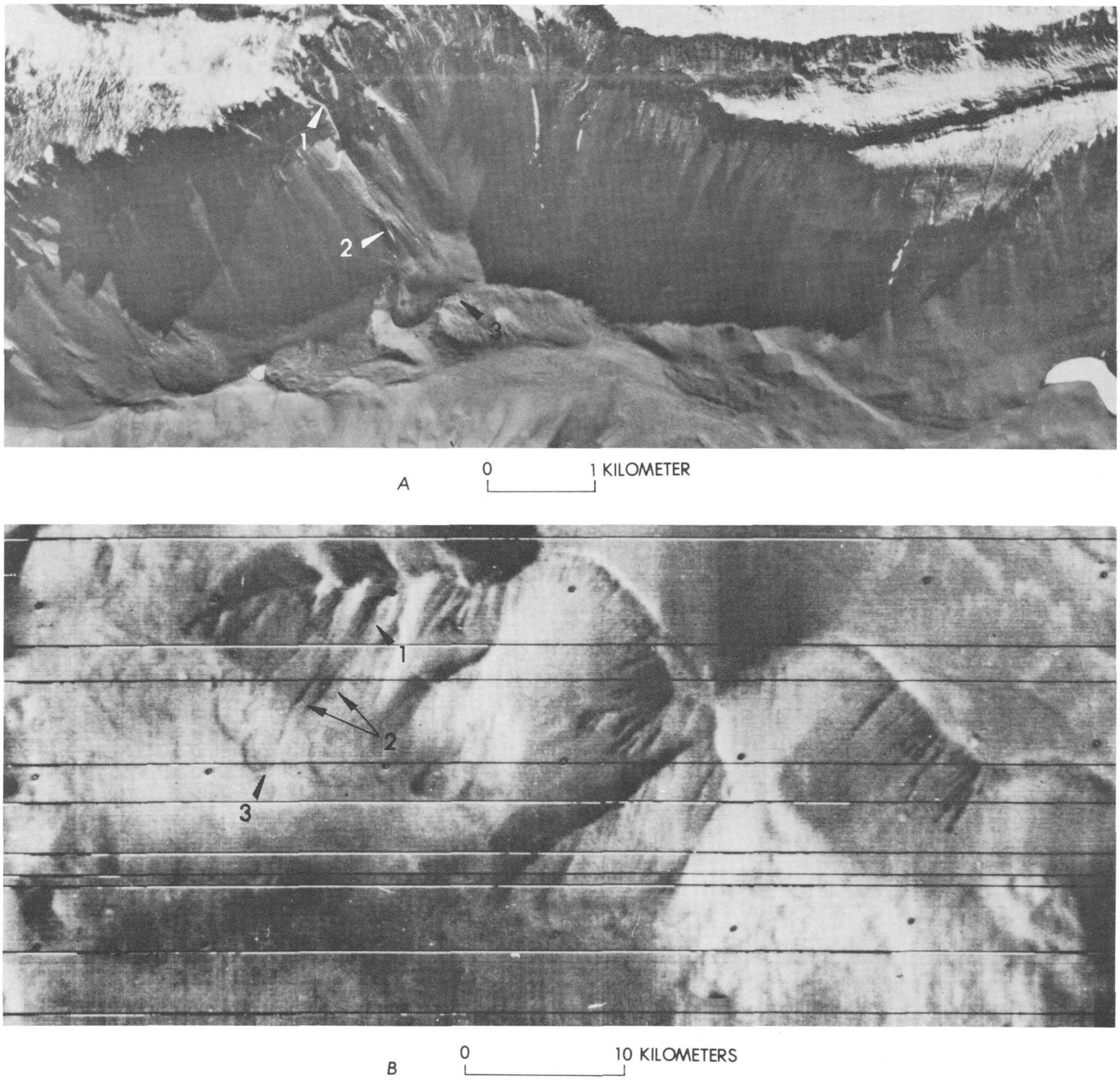

FIGURE 8.—Comparison of martian and terrestrial debris flows. *A*, Wright Valley, Antarctica. Vertical aerial photograph by the U.S. Navy, Wright Valley, January 1956. *B*, South wall of Tithonium Chasma. North toward bottom. Mariner 9 frame DAS 10204959–B. Note similarity in chutes at head of flows (1), raised levees on lower parts of flows (2), and overlapping shallow lobes of deposits at base of flows (3).

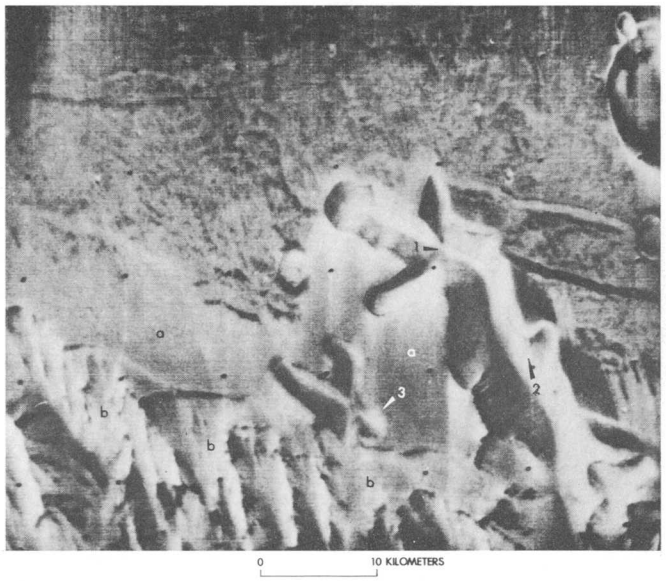

FIGURE 9.—Tributary canyons on north wall of Ius Chasma showing V-shaped cross profiles, blunt, cirquelike canyon-heads and side valleys that merge with the main canyon accordantly (1) or as hanging valleys (2). Canyons appear to develop by headward erosion from gullies. Strong structural control locally results in canyon configuration similar to barbed drainage (3). Plateau surface at (a), chasma walls at (b). Mariner 9 frame DAS 10276639–B. North toward top.

FIGURE 11.—V-shaped tributary canyon on north wall of Ius Chasma (1) separated from landslide reentrant (2) by sharp ridge crest. Stumpy vertical ribs on landslide side (3) are opposite to fine, subparallel vertical ribs at canyon side (4). Hanging valleys (5) merge smoothly with tributary canyon. Stumpy ribs in breakaway scar show layering (6). Landslide deposit has crudely alined roughly perpendicular to wall (7). Mariner 9 frame DAS 10204679–B. North toward top.

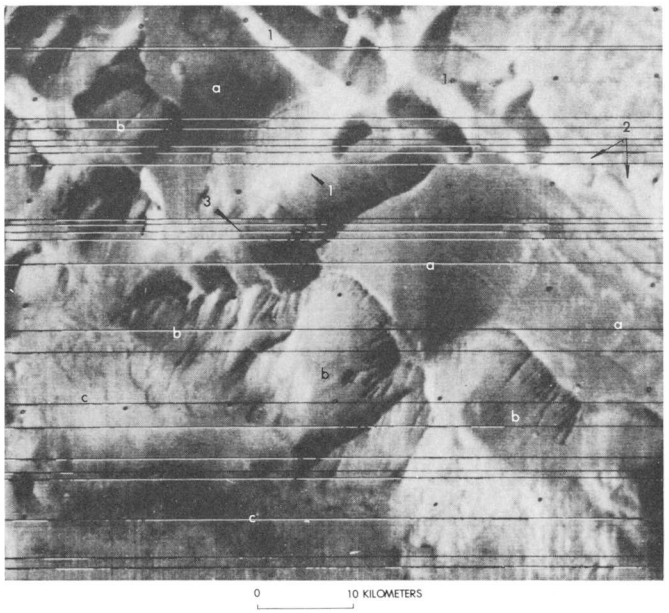

FIGURE 10.—Tributary canyon (1) in south wall of Tithonium Chasma showing evidence of structural control in parallel straight canyon segments, Canyon breaches "crater chain" depression (2). Large canyon (left center) has hummocky floor deposits in lower canyon (3). Plateau surface at (a), chasma walls at (b), chasma floor at (c). Horizontal lines are artifacts. Mariner 9 frame DAS 10204959–B. North toward bottom.

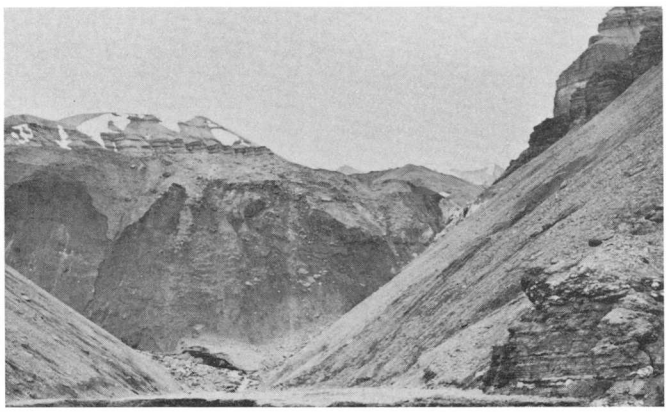

FIGURE 12.—Valley near Tempelfjorden, Spitzbergen. V-shaped cross profile enhanced by talus slopes converging from opposing walls. Large mass in center of valley is glacier terminus. From Rapp (1960, plate VI). Photograph by O. Halldin, 1908, with permission from Rapp.

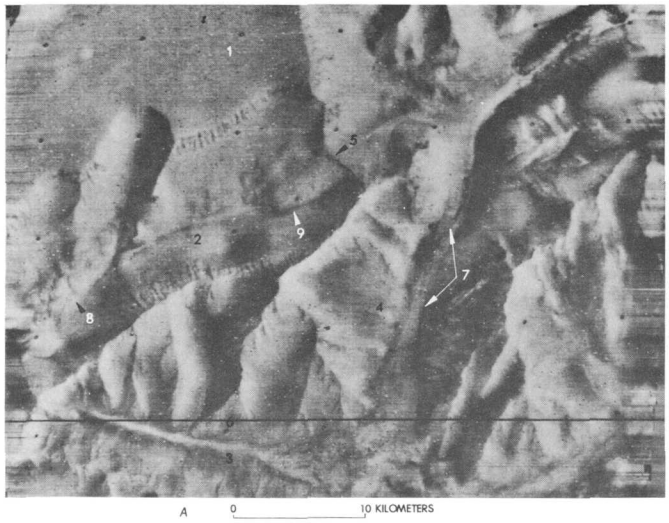

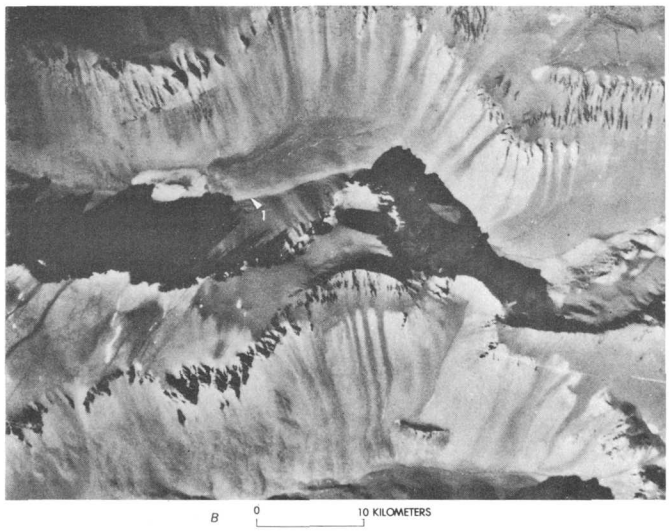

FIGURE 13.—Comparison of martian and terrestrial tributary canyons, *A*, South wall of Ius Chasma. Plateau surface (1) is cut by tributary canyons (2–4), which are locally separated from each other by knife-edge ridge (5). Triangular facet (6) found on spur in deeply incised valley (3). Valley floors have longtiudinally streaked deposit (7) and overlapping lobate (8). Lobate deposit at cirquelike head of valley (9) is smoothly transitional with valley wall on one side, has sharp contact on other side, and terminates in rounded lobes. Small white dots on photograph are artifacts of transmission process. Mariner 9 frame DAS 10204539–B. North toward bottom. *B*, Wright Valley, Antarctica. Lobate feature (1), similar to lobate feature in *A*(g), is smoothly transitional with talus slopes on one valley side, has sharp contact on other valley side, and terminates in rounded lobes. Feature is rock glacier (M. G. Mudrey, oral commun., 1974) or ice-cemented solifluction lobe (Ugolini and Bull, 1965). Vertical aerial photograph, U.S. Navy, Dry Valley, 1970.

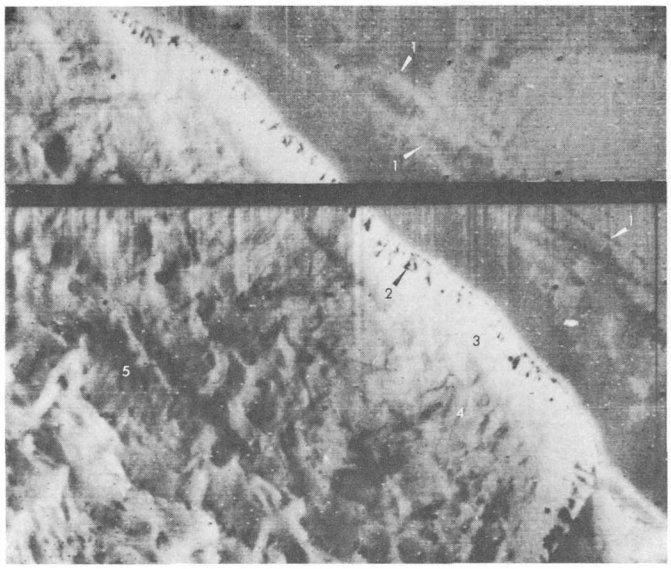

FIGURE 14.—North wall of Ius Chasma showing landslide morphology. Straight scar segments at head of slide parallel preexisting structures (1). Note coarse, stumpy ribs (2) in scar, talus slope (3), and hummocky deposit with vague ridging perpendicular to wall near scarp (4) and ridging parallel to wall farther out (5). Height of wall appears considerably less than that of other types of chasma walls, indicating burial of part of wall by slump deposits. White dots are artifacts. Mariner 9 frame DAS 10132999–B. North toward top.

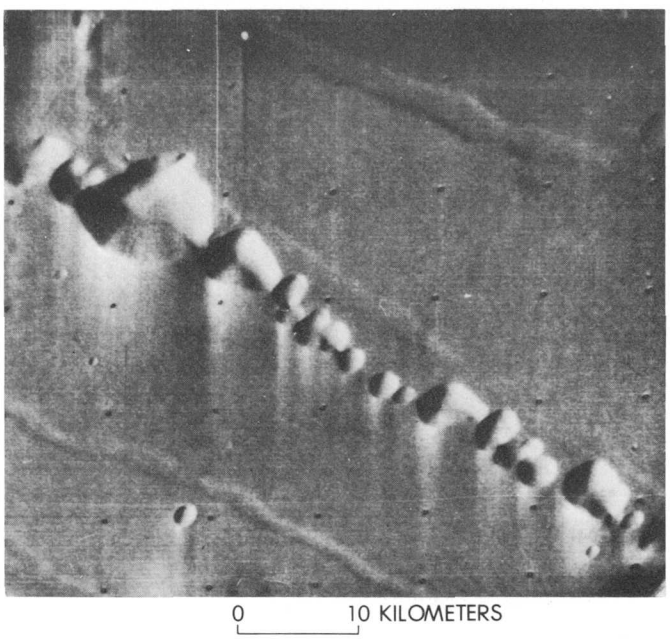

FIGURE 15.—Chain craters on plateau between Ius and Titonium Chasmas. Chains consist of rimless round or irregular shaped depressions, mostly following and truncating older grabens. Mariner 9 frame DAS 58577003–B. North toward top.

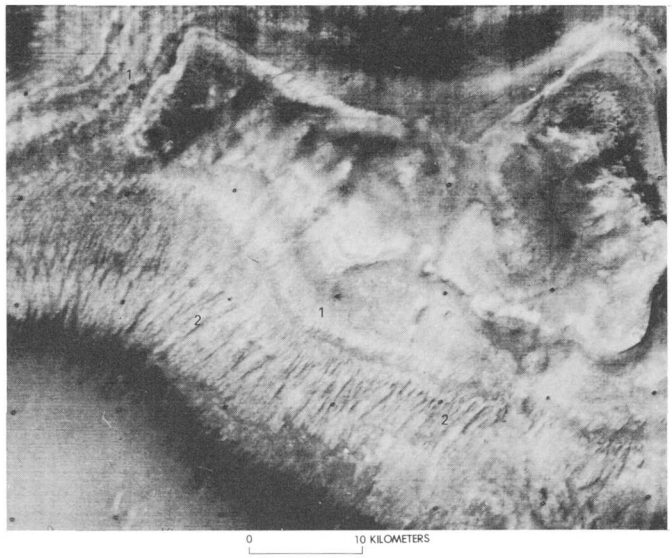

FIGURE 16.—Stratified deposit on floor of Gangis Chasma (1). Deposit is reminiscent of wind-eroded Tertiary sedimentary beds in Peru (J. F. McCauley, oral commun., 1974). Parallel fluting (2) is indicative of wind erosion. Gray area in lower left is featureless terrain on floor of chasma. Mariner 9 frame DAS 9017619–B. North toward top.

Earth. Reasons for this may be the unchanging characteristics of martian environmental conditions; the absence of continuing, active tectonism; and the absence of intense fluvial erosion. Thus, scarps could rise to great heights without being simultaneously worn down by water erosion and without being destroyed by changing tectonic patterns. The erosional and depositional landforms on and below the walls are large in accordance with the height of the scarps and remain distinct because of the stable martian conditions.

REFERENCES CITED

Calkin, P. E., 1971, Glacial geology in the Victoria Valley system, southern Victoria Land, Antarctica, *in* Crary, A. P., ed., Antarctic Research Series, v. 16: Am. Geophys. Union, Washington, D.C. p. 363–412.

Calkin, P. E., Behling, R. E., and Bull, Colin, 1970, Glacial history of Wright Valley, southern Victoria Land: Antarctic Jour., v. 5, p. 22–27.

Carr, M. H., 1974, Tectonism and volcanism of the Tharsis region of Mars: Jour. Geophys. Research, v. 79, no. 26, p. 3943–3949.

Cooke, R. V., and Warren, Andrew, 1973, Geomorphology in deserts: Univ. California Press, Berkeley and Los Angeles, 374 p.

Crandell, D. R., and Varnes, D. J., 1961, Movement of the Slumgullion earthflow near Lake City, Colorado: U. S. Geol. Survey Prof. Paper 424–B, B136–B139.

Dobrovol'skiy, L. A., 1974, Effect of tectonics and subsurface waters on development of permafrost: Internat. Geol. Review, v. 16, no. 7, p. 690–697.

Gunn, B. M., and Warren, Guyon, 1962, Geology of Victoria Land between the Mawson and Mulock Glaciers, Antarctica: New Zealand Geol. Survey, Bull. 71, p. 157.

Hord, C. W., Simmons, K. E., and McLaughlin, L. K., 1974, Mariner 9 ultraviolet spectrometer experiment—Pressure-altitude measurements on Mars: Icarus, v. 21, p. 292–302.

Jennings, C. W., 1958, Geologic atlas of California, Death Valley sheet: California Division of Mines and Geology, scale 1:250 000.

Lehmann, Otto, 1933, Morphologische Theorie de Verwitterung von Steinschlagwänden [Morphological theory concerning the weathering of rock walls]: Viertel Jahresschr. Naturf. Gesell. Zürich, v. 87, no. 3 and 4, p. 3–126.

McCauley, J. F., 1978, Geologic map of the Coprates quadrangle of Mars: U.S. Geol. Survey Misc. Inv. Map I–896. [In press.]

McCauley, J. F., Carr, M. H., Cutts, J. A., Hartmann, W. K., Masursky, Harold, Milton, D. J., Sharp, R. P., and Wilhelms, D. E., 1972, Preliminary Mariner 9 report on the geology of Mars: Icarus, v. 17, no. 2, 289–327.

Milton, D. J., 1974, Carbon dioxide hydrate and floods on Mars: Science, v. 183, p. 654–656.

Nichols, R. L., 1971, Glacial geology of the Wright Valley, McMurdo Sound, *in* Quam, L. D., and Porter, H. D., eds., Research in the Antarctic: Am. Assoc. Adv. Science, Pub. no. 93, p. 293–340.

Rapp, Anders, 1960, Talus slopes and mountain walls at Tempelfjorden, Spitsbergen: Norsk Polarinstitutt Skrifter, n. 119, p. 93.

Sharp, R. P., 1973, Mars—Fretted and chaotic terrains: Jour. Geophys. Research: v. 78, p. 4073–4083.

Soderblom, L. A., Condit, C. D., West, R. A., Herman, B. M., and Kreidler, J. T., 1974, Martian planetwide crater distributions—Implications for geologic history and surface processes: Icarus, v. 22, p. 239–263.

Ugolini, Fiorenzo, and Bull, Colin, 1965, Soil development and glacial events in Antarctica: Quaternaria, v. 7, p. 251–269.

U.S. Geol. Survey, 1976, Topographic map of Mars: U.S. Geol. Survey Misc. Inv. Map I–961, scale 1:25 000 000.

Wahrhaftig, C. A., and Cox, A. V., 1959, Rock glaciers in the Alaska Range: Geol. Soc. America Bull., v. 70, p. 383–436.

White, S. E., 1976, Rock glaciers and block fields, review and new data: Quaternary Research, v. 6, p. 77–97.

Wilhelms, D. E., and McCauley, J. F., 1971, Geologic map of the nearside of the Moon: U.S. Geol. Survey Misc. Geol. Inv. Map I–703, scale 1:5 000 000.

Wu, S. S. C., Schafer, F. J., Nakata, G. M., and Jordan, Raymond, 1973, Photogrammetric evaluation of Mariner 9 photography: Jour. Geophys. Research, v. 78, p. 4405–4410.

Jour. Research U.S. Geol. Survey
Vol. 6, No. 5, Sept.-Oct. 1978, p. 663-676

TRIBOLBINA LATHAM, 1932, AN EARLY CARBONIFEROUS THROUGH PERMIAN PALAEOCOPID OSTRACODE GENUS

By I. G. SOHN, Washington, D.C.

Abstract.—The type-species of *Tribolbina* Latham, 1932, *T. carnegiei*, and *T. gigantea* (Jones, Kirkby, and Brady, 1884) are redefined and reillustrated, and lectotypes for both are designated. *T. permiana* (Kellett, 1933) and *T. tumida* (Scott and Borger, 1941) are also redefined and reillustrated. *Beyrichiana* Kellett, 1933, is considered a junior subjective synonym of *Tribolbina* Latham, 1932. On the basis of abundant silicified specimens from the Permian of Greece, *T. doescheri* n. sp. is described, and *T.* aff. *T. doescheri* and *T.* sp. 1 are illustrated. The stratigraphic range of *Tribolbina* as redefined is lower Carboniferous through Permian, and its known distribution is Europe and North America where representatives lived in shallow seas. Tribolbinidae and Tribolbinecea are established as new suprageneric categories in the Palaeocopida for *Tribolbina* and the Silurian *Kolmodinia* Martinsson, 1962.

This paper is based on silicified specimens from 49 Permian limestone blocks collected by R. E. Grant from 2 localities on the Island of Idhra, Greece; on the holotypes of *Beyrichiana permiana* Kellett, 1933, and *B. tumida* Scott and Borger, 1941; on specimens of *Beyrichia gigantea* Jones, Kirkby, and Brady, 1884; and on a photograph of *Tribolbina carnegiei* Latham, 1932. Both species of *Beyrichiana* are based on imperfectly preserved, unique, single valves. The specimens of *Tribolbina carnegiei* and *Beyrichia gigantea* are also poorly preserved; consequently, both *Tribolbina* and *Beyrichiana* were poorly known.

The holotype of *Beyrichiana permiana* Kellett, 1933, the type-species of *Beyrichiana* Kellett, 1933, was based on a single abraded left valve (USNM 85428) from the Wreford Limestone (Lower Permian) in Chase County, Kans. (Kellett, 1933, p. 74, pl. 13, figs. 21, 22), and is reillustrated here on figures 3*a–d*. The original illustration of the left valve (Kellett, 1933, pl. 13, fig. 22) shows a horizontal groove on the anterior lobe and a circular spot below midheight on the posterior lobe. Kellett (1933, p. 74) interpreted the spot on the posterior lobe as "* * * probably the remains of an attached foraminifer." This spot is the trace of a node as shown on figures 3*a–d* (arrows on figs. 3*b*, *d*) and is present on all the specimens from the Permian of Greece.

Beyrichiana tumida Scott and Borger, 1941, is based on a pyritized broken right valve, obtained by dissolving with dilute hydrochloric acid a thin impure limestone in the Macoupin cyclothem (Upper Pennsylvanian) in Lawrence County, Ill. The illustration of the holotype by Scott and Borger (1941, pl. 49, fig. 1) shows the horizontal groove on the anterior lobe, but not the area of the posterior lobe on which the circular node is present. I am reillustrating the holotype, and, on my photograph (fig. 3 *e*, arrow), part of the node is shown.

The type-species of *Tribolbina* Latham, 1932 (*T. carnegiei* Latham, 1932), was illustrated by a drawing (Latham, 1932, p. 358, fig. 7), reproduced here as figure 2*f*. Latham stated that specimens were rare and recorded the species from only one locality in Scotland. Dr. R. B. Wilson, Institute of Geological Sciences, Edinburgh, furnished me with a photograph of the illustrated specimen, shown here as figure 2*g*. Latham referred only one additional species, *Beyrichia gigantea* Jones, Kirkby, and Brady, 1884, to *Tribolbina*, and I have examined all the specimens in the British Museum of Natural History except the specimen originally illustrated in 1874 by Jones, Kirkby, and Brady on plate 4, figures 27a–c. Photographs of this specimen, which is at the Institute of Geological Sciences, Leeds, were mailed to me by Ms. L. M. Sheppard, British Museum, London (figs. 2*a*, *b*).

Kellett (1935, p. 163) stated that *Beyrichiana* may be a synonym of *Tribolbina*, adding, "However, the members of *Tribolbina* occur much lower in the section in the Mississippian and they are very much larger, ranging in size from 4.5 to 9 mm in length." On the basis of the present study, the genus *Beyrichiana* Kellett, 1933, is considered to be a junior subjective synonym of *Tribolbina* Latham, 1932, which is here redefined and assigned to the Tribolbinacea, new superfamily, in the new family Tribolbinidae. The stratigraphic range of *Tribolbina* is Carboniferous (Upper Mississippian) through Upper Permian, and that of the Tribolbinidae is Middle Silurian through Permian.

Acknowledgments.—I thank Dr. R. E. Grant and

Mr. R. A. Doescher, Department of Paleobiology, U.S. National Museum of Natural History (USNM) for the silicified ostracodes; Dr. R. H. Bate and Ms. Lesley M. Sheppard, British Museum of Natural History, for specimens of *Beyrichia gigantea*, some of which were hand-carried by Dr. Alan Lord, University of London, and for the photograph of the lectotype of *B. gigantea;* Prof. P. Sandberg, Department of Geology, University of Illinois, for the holotype of *Beyrichiana tumida;* and Dr. R. B. Wilson, Institute of Geological Sciences, Edinburgh, for information regarding Latham's collections, as well as for the photograph of *Tribolbina carnegiei.* J. M. Berdan, U.S. Geological Survey, discussed many of the systematic problems with me during this study. Dr. L. S. Kornicker, USNM, reviewed this paper.

COLLECTION LOCALITIES

USNM locality 9260. Southeastern side of the Island of Idhra, just off the Argolian coast, Greece (see Grant, 1972, p. 214, 215, for description), about 0.5 km south of the village of Episkopi. Weathered limestone blocks containing silicified fossils on stratigraphically lower of two benches. Collected by R. E. Grant, Department of Paleobiology, USNM, 1968, 1974, 1975.

USNM locality 9262. Same island as above, about 3 km north-northeast of Episkopi. Limestone blocks and pieces from a bed about 1.2 m thick. Collected by R. E. Grant, 1968, 1974.

SILICIFIED AND OTHER REPLACED OSTRACODES

Ostracodes that have been replaced by acid-insoluble minerals are easily recovered from limestone and may be obtained in abundance, but the process of replacement and recovery may cause problems. The molecular replacement of shell material in rock by silica, pyrite, calcium phosphate, and other insoluble minerals starts on the surface of the shell either from the outside, inside, or on both sides of the shell. A replaced layer of variable thickness that faithfully replicates the original surface structures may seal the shell from further replacement. When both the outer and inner surfaces of the shell are replaced, a variable thickness of the shell between the replaced layers may remain acid soluble. Spectrographic analysis of silicified ostracodes from the Permian of the Glass Mountains, Texas, showed more than 90 percent calcium in the valves. When the outer or inner surface of a valve is incompletely replaced, acid treatment of the enclosing limestone removes the soluble unreplaced parts of the shell, and imperfect replicas of variable thickness are recovered.

Usually, specimens without the outer surface replaced retain the outlines of lobes, nodes, and spines, but may not retain finer surface textures such as reticulations, papillae, pustules, and narrow ribs, and thus have a different surface texture than the original shell. For example, figures 4*a*, *g*, and *j* are all inside views; the specimen shown on figure 4*a* has the inside layer preserved but has a small area missing (indicated by arrow b) below the hinge on top of the sulcus, whereas the specimen shown on figure 4*g* does not have the inside layer preserved, and the inside resembles that part of figure 4*j* below the dorsal margin (indicated by an arrow) where the inside layer is missing. The specimen illustrated on figures 4*m–o* is interpreted as having only the inside layer preserved, the outside surface of the shell having been dissolved. A preserved outside surface is best illustrated on figure 5*c* (arrow) and *d* of a specimen that has part of the outside of the shell missing. Similar shell replacement phenomena in pyritized ostracodes have been described (Sohn, 1977b, p. 44).

CLASSIFICATION

Class *OSTRACODA* Latreille, 1802, emend. 1804

Order *PALAEOCOPIDA* Henningsmoen, 1953

No doubt exists about the ordinal classification of the genera because the specimens from Greece do not have an inner lamella (figs. 4*a*, *j*) and conform in all other respects to the diagnosis of the order (Moore, 1961, p. Q110; Sohn, 1968, p. 12).

Superfamily *TRIBOLBINACEA* Sohn, new superfamily

Diagnosis.—The same as the family.

Family *TRIBOLBINIDAE* Sohn, new family

Diagnosis.—Large, to 9 mm long; straightbacked; tuberculated; bisulcate, sulci meeting at or below midheight to form crude "Y" that curves backwards; horizontal furrow on one or both terminal lobes, dorsal part of all or some of the lobes cuspate, extending above hinge margin. Posterior wider in dorsal outline. Dimorphism unknown.

Genera included.—*Tribolbina* Latham, 1932; *Kolmodinia* Martinsson, 1962.

Discussion.—Latham (1932, p. 358) referred *Tribol-*

bina to the Beyrichiidae which she diagnosed (1932, p. 357) as "Ostracoda with trilobate and quadrilobate valves, deeply sulcated. Brood pouch, when present, subglobular or egg-shaped on the ventral slope." Kellett (1933, p. 69) referred *Beyrichiana* also to the Beyrichiidae without a diagnosis of the family, and Scott and Borger (1941, p. 355) used Kellett's family classification. I (Sohn *in* Moore, 1961, p. Q125) interpreted the rounded spot on the posterior lobe of *Beyrichiana* as the base of a posterior spine; consequently, I questionably placed *Mammoides* Bradfield, 1935, in synonymy and referred the genus group to the Aechminellidae. The family Beyrichiidae as defined by Henningsmoen (1965, p. 387–389) and Sohn (1969, p. C2, C3) has a distinct swelling of the anteroventral, ventral, or posteroventral part of the carapace in heteromorphs, but such a structure is not yet known in *Tribolbina*.

S. A. Levinson (*in* Moore, 1961, p. Q122) questionably referred *Tribolbina* to the Beyrichiidae but did not illustrate the genus. His diagnosis differs from the paraphrased original by the additional sentence, "Female with elongate pouch in anteroventral area. *L. Carb.-L. Perm.*, N. Am.-Eu." I am reillustrating Latham's (1932, p. 358, fig. 7) drawing as well as a photograph of the original carapace (figs. 2*f*, *g*) of *T. carnegiei*. The valves do not have an elongate pouch in the anteroventral area nor is such a pouch present on the silicified specimens of the new species from the Permian of Greece that range in greatest length from 0.63 to 3 mm. I conclude that an elongate pouch, a dimorphic feature in the Beyrichiacea, is not yet known in *Tribolbina*. I assume that Levinson followed Kellett's (1935, p. 163) suggestion that *Beyrichiana* Kellett, 1933, may be a junior synonym of *Tribolbina* and consequently combined the distributions of both genera.

Although *Tribolbina* and *Kolmodinia* have many of the beyrichiacean characteristics, dimorphism is as yet unproved. The uncertainty of beyrichiacean dimorphism and the fact that the sulcation trends backwards in these two genera, whereas, as pointed out to me by J. M. Berdan, the sulci trend towards the anterior in the Beyrichiacea, are the reasons for establishing the new suprageneric categories in the Palaeocopida.

Martinsson (1962, p. 359) stated that *Tribolbina* is not a beyrichiacean. He (1962, p. 354) described *Kolmodinia* Martinsson, 1962, as "?Beyrichiacea incertae sedis" and based *Kolmodinia* on *Beyrichia grandis* Kolmodin, 1879, from the Silurian of Gotland (Martinsson, 1962, p. 23, fig. 7A). Martinsson illustrated one additional specimen as *Kolmodinia* cf. *K. grandis* (1962, fig. 7B), the only representative of this genus in "large quantities of marl surveyed * * *" from the lowermost Eke Beds of Lau Backar, Gotland (1962, p. 57). He stated (1962, p. 355) that *Kolmodinia* cannot be regarded as a beyrichiid, but as a representative of a new family.

Martinsson oriented *Kolmodinia* with the widest lobe anterior, but he had only two poorly preserved specimens which he assumed to represent adults because of their large size (greatest length 5.0 and 2.8 mm). The abundant silicified specimens representing several stages of growth from the Permian of Greece indicate that the node-bearing lobe is not a dimorphic character and that it is located on the posterior of the valve. By analogy with Permian specimens, the orientation of the Silurian *Kolmodinia* shown here in figure 2*k* is reversed 180°.

The posterolateral node on the posterior lobe of *Kolmodinia*, and on all the species of *Tribolbina* except *T. carnegiei*, is similar to a node on the anterodorsal area of the Permian myodocopid genus *Thaumatomma* Kornicker and Sohn, 1976. *Thaumatomma* is present in the same collections from the Permian of Idhra, Greece, from which the new species of *Tribolbina* is here described; the function, however, of the node is at present unknown. Because this node is present also in the Myodocopida, it is not considered to be a suprageneric character in the Tribolbinacea.

Stratigraphic range.—Middle Silurian through Permian.

Genus *TRIBOLBINA* Latham, 1932, emend. Sohn, herein

Tribolbina Latham, 1932, Royal Soc. Edinburgh Trans., v. 57, pt. 2, no. 12, p. 356.

not *Tribolbina* Latham. Levinson *in* Moore, 1961, Treatise on invertebrate paleontology, pt. Q, Arthropoda 3, Ostracoda, p. Q122.

Beyrichiana Kellett, 1933, Jour. Paleontology, v. 7, p. 73.

Beyrichiana Kellett. Sohn, 1977, U.S. Geol. Survey Jour. Research, v. 5, p. 128.

not *Beyrichiana* Kellett. Sohn *in* Moore, 1961, Treatise on invertebrate paleontology, pt. Q, Arthropoda 3, Ostracoda, p. Q125.

Type-species (*original designation*)—*Tribolbina carnegiei* Latham, 1932.

Emended diagnosis.—Valves large, to 9 mm in greatest length, tuberculate, subovate, dorsal margin straight, ventral margin curved, anterior margin sloping towards ventral margin, posterior margin more evenly curved; dorsal part trilobate; anterior lobe narrower, split near top by shallow furrow; central lobe subtriangular, apex generally above midheight; posterior lobe wide, with or without rounded subdued

node near posterior. Two dominant shallow sulci, crudely Y-shaped, start near dorsal margin; anterior sulcus longer, terminates around ventroanterior part of posterior lobe, posterior sulcus trends down and forward, joins anterior sulcus at or below midheight at approximate midlength, trends backwards. Free margins and dorsal parts of end lobes bounded by shallow groove below which is a papillate rim. Valves subequal, right narrowly overlaps left, hinge modified cardiniferellid. Muscle-scar pattern unknown, dimorphism uncertain.

Discussion.—The hinges of the known species of both *Tribolbina* and *Beyrichiana* were neither described nor illustrated. On the bases of silicified material, the hinge of *Tribolbina doescheri* n. sp. is unique in that it is a modification of the palaeocopid cardiniferellid hingement (Sohn, 1953, p. 66) in which the left valve overlaps the right on the free margins, with terminal sockets open to the outside for the reception of rounded terminal knobs on the hinge of the right valve. *T. doescheri* n. sp. has the right valve slightly overlapping the left. The hinge of the left valve consists of a straight groove terminated at each end by sockets that open on the outside of the valve (arrows on fig. 3*f*), and the right valve has thickenings of the overlapping margin that key into open sockets of the opposing valve (figs. 4*j*, 5*a* arrow, *f*, *h*). This type of hingement may explain the presence of open carapaces such as that of *T. doescheri* illustrated on figures 5*a*, *b* and those recorded by Latham (1932, p. 395) for *T. carnegiei*, the type-species. Open carapaces articulated along the dorsum have been recorded in other ostracode genera: Bless and Jordan (1972, pls. 3, 25) illustrated articulated carapaces of *Hollinella* Coryell, 1928, and Scott and Summerson (1943, pl. 1, fig. 19) illustrated this feature in "*Jonesina*? *arcuata* (Bean)."

A poorly preserved right valve 3.1 mm in greatest length from the Permian of Greece (USNM loc. 9262, block 5) is a subinternal mold (inner silicified part of the shell). This valve differs from the other specimens from Greece in lateral outline and in shape of the anterior lobe. It is recorded in open nomenclature as *Tribolbina* sp. 1 (figs. 4*m–o*). I have examined 640 cm^3 of etched material that passed through a Tyler-equivalent 4-mesh (4.76-mm) screen and was retained by a Tyler-equivalent 18-mesh (1.0-mm) screen from the same limestone block (USNM loc. 9262, block 5) and from two additional blocks chosen because they contained the most abundant representatives of this genus (USNM loc. 9260, blocks 62 and 152); I did not find any additional large specimens. One block (USNM loc. 9262, block 18) contained the next largest specimen, a badly preserved, broken right valve (figs. 5*i*, *j*) approximately 1.9 mm in greatest length that is somewhat similar in lateral outline to the largest specimen. Another block (USNM loc. 9260, block 131) contained two similarly shaped left valves (figs. 5*l*, *m*) that are 1.1 and 0.93 mm in greatest length. The anterior lobe of the smaller left valve (fig. 5*m*) differs in size and shape from that of the largest individual (figs. 5*i*, *j*) and also from that of the next largest specimen (figs. 5*k*, *l*). The specimens shown on figures 5*j* and *l* may represent tecnomorphs, with the specimen shown on figure 5*m* being a heteromorph, or they may belong to different species. These are recorded in open nomenclature as *Tribolbina* aff. *T. doescheri* n. sp.

Stratigraphic range.—Carboniferous (Mississippian) through Permian. Figure 1 shows the known stratigraphic positions of species in *Tribolbina*.

Environment.—On the basis of associated faunas and paleogeographic inferences, the genus inhabited shallow marine seas.

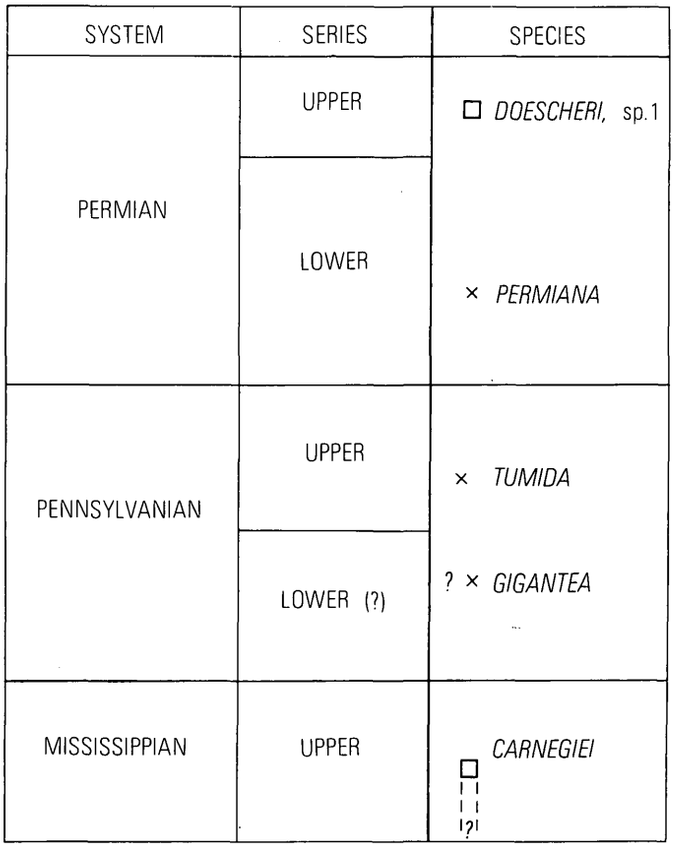

FIGURE 1.—Stratigraphic positions of species in *Tribolbina*.

***Tribolbina carnegiei* Latham, 1932**

Figures 2*d–g, j*

Tribolbina carnegiei Latham, 1932, Royal Soc. Edinburgh Trans., v. 57, pt. 2, no. 12, p. 358, text fig. 7.

Tribolbina gigantea (Jones, Kirkby, and Brady, 1884). Latham, 1932, Royal Soc. Edinburgh Trans., v. 57, pt. 2, no. 12, p. 359.

Beyrichia gigantea Jones, Kirkby, and Brady, 1884 (part), London, Palaeontographical Soc., p. 88 (not pl. 4, figs. 27a–c=*T. gigantea;* not pl. 4, fig. 28 = gen. and sp. indet.)

Beyrichiana gigantea (Jones, Kirkby, and Brady, 1874). Sohn, 1977, U.S. Geol. Survey Jour. Research, v. 5, no. 1, p. 127, figs. 1*d, e*.

Diagnosis (revised)—Central lobe triangular, extends below midheight, no posterolateral node on posterior lobe.

Discussion—The original description by Latham (1932, p. 358–9) does not mention the horizontal sulcus near the top of the anterior lobe, considered here to be a generic character, nor is it shown on the original drawing reproduced here as fig. 2*f* (compare fig. 2*f* with figs. 2*g*, *j*). The photograph of the illustrated specimen (fig. 2*g*) is of a crushed, somewhat distorted, open carapace that is joined along the dorsal margin. No posterolateral node on the posterior lobe is present. That area, shown on the original drawing as a clear area (fig. 2*f*) is covered by tubercles similar to those on the rest of the valve surface.

The specimen that I illustrated (1977a, figs. 1*d*, *e*) as *Beyrichiana gigantea* is reillustrated here (fig. 2*j*) to show that it, and presumably the other specimens from the same locality, belong to *Tribolbina carnegiei*. The specimen from Braidwood mentioned in the discussion of *B. gigantea* by Jones, Kirkby, and Brady (1884, p. 88) is illustrated here as figure 2*d*, to show that this specimen also belongs in *T. carnegiei*. This drawing was among a group obtained by E. O. Ulrich, U.S. Geological Survey, from John M. Clarke, New York Geological Survey, who had inherited them from T. R. Jones. The paper label on which this drawing is pasted has the following notations, "Main Post Limest., Braidwood, J. R. J. Hunter March 1/65 central lobe with a longitudinal furrow apparently done by a knife not shown." A similar original drawing published by Jones, Kirkby, and Brady in 1874 (pl. 4, fig. 28) and here copied (fig. 2*h*) is with the specimen (gen. and sp. indet.) in the British Museum.

According to Dr. Wilson (written commun., May 25, 1977), the illustrated specimen of *T. carnegiei* is one of eight named specimens; the other seven are also open carapaces that are much more poorly preserved. There is a suggestion of a lateromarginal bend, a familial character, but, because of poor preservation, this structure cannot be definitely confirmed.

In a subsequent letter, Dr. Wilson (June 6, 1977) included a sketch of the better preserved of two specimens of *Tribolbina gigantea* (Jones, Kirkby, and Brady, 1884) of Latham, 1932, available in the original collection at the Institute of Geological Sciences, Edinburgh. Wilson's sketch of this specimen, GSE 864–2, is shown in figure 2*e* (this report); the specimen is closer to *T. carnegiei* in shape of central lobe than to *T. gigantea*, compare figure 2*c* with figures 2*a*, *e*. Latham (1932, p. 359) diagnosed *T. gigantea* as differing from *T. carnegiei* in being smaller, 4.5- to 4.9-mm length compared with 7.5- to 9.0-mm length of *T. carnegiei*, and in having a punctate surface. I consider the punctate surface as a fossilization phenomenon and am referring the specimens identified by Latham as *T. gigantea* to *T. carnegiei*.

Although the species is poorly known because of inadequate preservation, nevertheless *T. carnegiei* is the type species of *Tribolbina* Latham, 1932; a holotype of *T. carnegiei* was not designated in the original description. The specimen illustrated here on figure 2*g* is here designated as the lectotype, and the remaining seven specimens in the type-series are paralectotypes. This specimen, only half of which was originally illustrated, was designated by Latham as "Geol. Surv. Edin., M1975."; according to Dr. Wilson, it has been renumbered and is now GSE 6801.

Stratigraphic range.—Middle Viséan Glencartholm Volcanic Beds, River Esk near Langholm; Cementstone Series, Whiteadder Water, Duns; lower Carboniferous shale (fig. 1) from Eskdale, Dufriesshire; and Mainpost Limestone at Braidwood, near Carluke, all in Scotland.

***Tribolbina gigantea* (Jones, Kirkby, and Brady, 1884)**

Figures 2*a–c*

Beyrichia gigantea Jones, Kirkby, and Brady, 1884 (part), London, Palaeontographical Soc., p. 88, pl. 4, figs. 27a–c (not fig. 28 = gen. and sp. indet.; not specimens from Eskdale, Dumfriesshire = *T. carnegiei* Latham, 1932).

not *Tribolbina gigantea* (Jones, Kirkby, and Brady, 1884). Latham, 1932, Royal Soc. Edinburgh Trans. v. 57, pt. 2, no. 12, p. 359 = *T. carnegiei* Latham, 1932.

Beyrichiana? gigantea (Jones, Kirkby, and Brady).

a

b

c

d

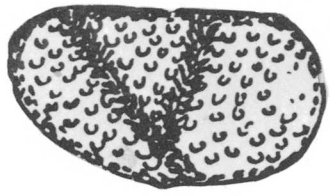

f

h

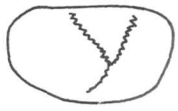

e

j

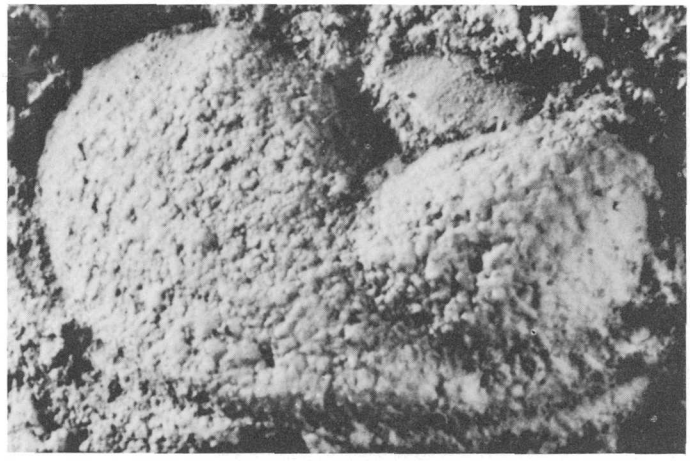

i

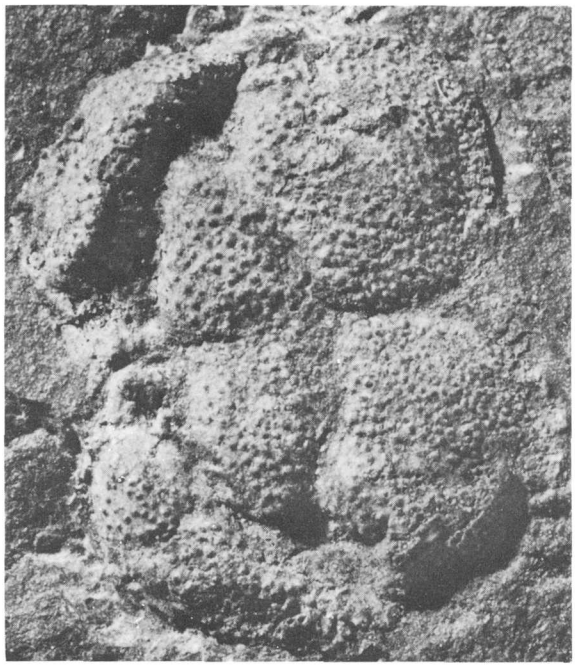

g

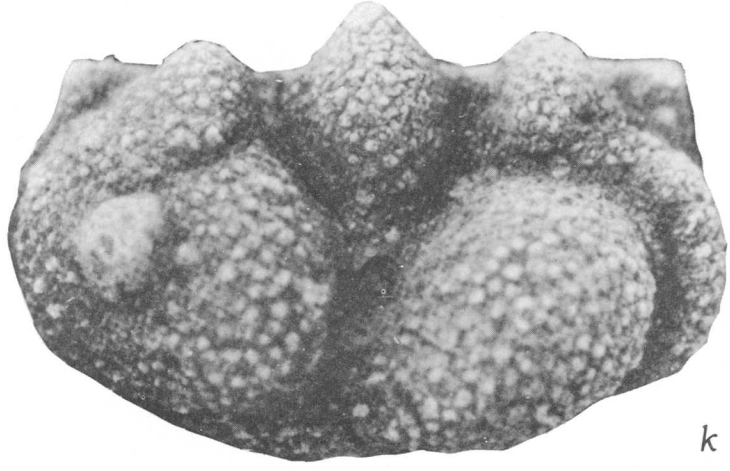

k

Bassler and Kellett, 1934, Bibliographic index of Paleozoic Ostracoda: Geol. Soc. America Spec. Papers 1, p. 211 (list).

not *Beyrichiana gigantea* (Jones, Kirkby, and Brady, 1874). Sohn, 1977a, U.S. Geol. Survey Jour. Research, v. 5, no. 1, p. 127, figs. 1*d*, *e* = *Tribolbina carnegiei* Latham, 1932.

Diagnosis.—Posterior sulcus starts at posterior third of greatest length; bottom of anterior lobe distinctly outlined; posterolateral node on posterior lobe above midheight.

Discussion.—Jones, Kirkby, and Brady illustrated *Beyrichia gigantea* on plate 4, figures 27a–c, 28, published in 1874, and their discussion of this species was printed in 1884 (p. 88). The partly exfoliated left valve from the upper Carboniferous limestone (Pennsylvanian), from Parkhill, near Longnor, Derbyshire, was referred to as being on tablet 38/14 in the Museum of the Geological Survey at Jermyn Street, London, and was illustrated as plate 4, figures 27a–c (Jones and others, 1874); the shell of a right valve from the Carboniferous of Cork, Ireland, was illustrated as plate 4, figure 28 (Jones and others, 1874). I have not seen the original specimen shown on plate 4, figure 27 (Jones and others, 1874), but Ms. Lesley M. Sheppard mailed me four photographs of the specimen (two of which are reproduced here as figs. 2*a*, *b*). I have seen the Irish specimen, which I am reillustrating as figures 2*h*, *i*. I agree with Latham (1932, p. 359), who stated regarding the specimen shown by Jones, Kirkby, and Brady (1874) on plate 4, figure 28, "If this specimen is figured correctly it is certainly not *T. gigantea* and it probably does not even belong to the same genus." As can be seen on figure 2*i*, the middle lobe is of a different texture than the rest of the specimen, and it represents a fragment superposed on the valve. This specimen is here referred to as genus and species indet.

One of the specimens from the lower Carboniferous shale from Eskdale, Dumfriesshire, mentioned by Jones, Kirkby, and Brady (1884) on p. 88 was illustrated by me (Sohn, 1977a, figs. 1*d*, *e*) and is reillustrated here as fig. 2*j* to show that it belongs to *T. carnegiei* Latham, 1932. The imperfect cast found by J. R. J. Hunter in the Mainpost Limestone at Braidwood, near Carluke, and also mentioned by Jones, Kirkby, and Brady (1884) on p. 88, likewise belongs to *T. carnegiei* (this report, fig. 2*d*). I have examined 18 poorly preserved specimens on fragments of calciferous sandstone in the British Museum of Natural History; the specimens were labelled as *Beyrichia gigantea* under no. I–885, and these also do not have a posterolateral node on the posterior lobe. They very likely belong to *T. carnegiei*. As a result, this leaves only the originally illustrated (Jones and others, 1874, pl. 4, figs. 27a–c) late Carboniferous specimen (this report, figs. 2*a–c*) as the name bearer of *T. gigantea*, and it is here designated as the lectotype. This specimen is a left valve on matrix; the outer surface of the shell has been removed. The lobes and the ventral part of the valve represent a surface on the inner part of the shell. Compare the surface texture (fig. 2*a*) with that of *Tribolbina* sp. 1 (figs. 4*m–o*). The area of the adductor muscle attachment scar and the deeper parts of the sulci

FIGURE 2.—*Tribolbina gigantea*, *T. carnegiei*, gen. and sp. indet., and *Kolmodinia* cf. *K. grandis*

a–c. *Tribolbina gigantea* (Jones, Kirkby, and Brady, 1884).
a, *b*. Left valve and ventral oblique view of posterior lobe to show remnant of posterolateral node approx. × 18. Photographs from British Museum of Natural History, London, of specimen on which fig. 2*c* is based.
c. Left valve × 4, copy of original drawing in Jones, Kirkby, and Brady (1874, pl. 4, fig. 27a). Note adductor muscle scar, split anterior lobe, and suggestion of posterolateral node on posterior lobe. Lectotype, Inst. Geol. Sci. Leeds, GSL 884. Upper Carboniferous limestone (Pennsylvanian), Derbyshire, England.

d–g. *Tribolbina carnegiei* Latham, 1932.
d. Imperfect cast of right valve mentioned by Jones, Kirkby, and Brady (1884, p. 88) in original discussion of *T. gigantea*. Unpublished drawing (obtained from T. R. Jones, see p. 6), magnification unknown. Note subtriangular central lobe reaching below midheight. Mainpost Limestone at Braidwood, near Carluke, Scotland.
e. Sketch by R. B. Wilson of right valve of *T. gigantea* approx. × 5. Hypotype, GSE 864–2. Cementstone Series, Whiteadder Water, Duns, Scotland.
f. Original drawing by Latham (1932, p. 358, fig. 7). Left valve × 5.
g. Photographs of specimen on which fig. 2*f* is based approx. × 9. Photograph from Inst. Geol. Sci. Edinburgh. Lectotype, Inst. Geol. Sci. Edinburgh, GSE 6801. Calciferous sandstone, Dumfries District, Scotland.

h, *i*. Gen. and sp. indet.
Copy of Jones, Kirkby, and Brady, 1874, pl. 4, fig. 28, × 4, and photograph of the same right valve approx. × 16, illustrated as *Beyrichia gigantea* from light grey limestone of Cork, Ireland. Note difference in surface texture of central lobe which represents a superposed fragment of shell.

j. *Tribolbina carnegiei* Latham, 1932.
Photograph published as *Beyrichiana gigantea* by Sohn (1977a, p. 127, fig. 1*d*) approx. × 6. Figured specimen British Museum I–6219. Lower Carboniferous shale from Eskdale, Dumfriesshire, Scotland.

k. *Kolmodinia* cf. *K. grandis* (Kolmodin, 1879). Martinsson, 1962.
Left valve approx. × 30. Copy of Martinsson, 1962, fig. 7B. Eke Beds (Silurian), Lau Backar, Gotland.

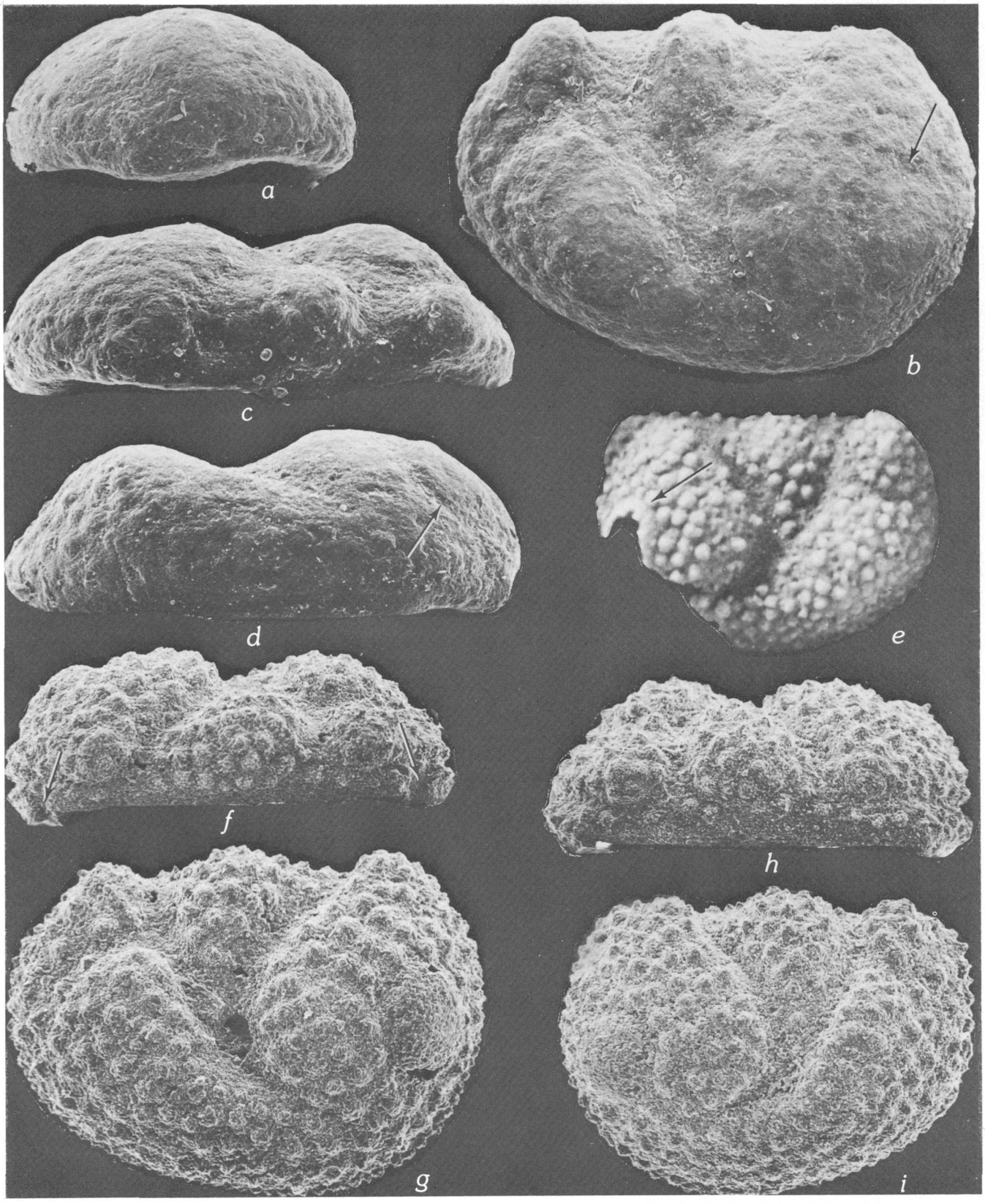
a
b
c
d
e
f
h
g
i

on the lectotype appear to be represented by the middle part of the shell, equivalent to the void indicated by an arrow on figure 5*c*. The adductor muscle scar consists of a subrounded area with minute flecks, a type common in many Paleozoic ostracodes. The early Carboniferous specimens of *T. gigantea* discussed by Latham (1932, p. 359) cannot be borrowed from the Institute of Geological Sciences, Edinburgh (Dr. R. B. Wilson, written commun., May 1977), but on the basis of a sketch supplied by Dr. Wilson (this report fig. 2*e*), they are here transferred to *T. carnegiei*.

Stratigraphic range—Known only from the upper Carboniferous limestone (Pennsylvanian) (fig. 1) from Parkhill, near Longnor, Derbyshire.

Tribolbina permiana (Kellett, 1933)

Figures 3*a–d*

Beyrichiana permiana Kellett, 1933, Jour. Paleontology, v. 7, p. 74, pl. 13, figs. 21, 22; Kellett, 1935, Jour. Paleontology, v. 9, p. 163 (discussion).

Diagnosis.—Has posterolateral node on posterior lobe; posterior sulcus starts at approximate posterior quarter of dorsal margin, makes acute angle with dorsal margin; dorsal part of posterior margin makes about 45° angle with dorsal margin.

Discussion.—The posterolateral node on the posterior lobe that was interpreted by Kellett (1933, p. 74) as an attached foraminifer is visible on all four views (this report, figs. 3*a–d*); it is indicated by arrows on figures 3*b*, *d*. Comparison of fig. 3*b* with the outside view of the holotype of *T. doescheri* (fig. 3*g*), as well as with the other illustrations of the species, clearly shows the congeneric affinities. Unfortunately, the inside of the valve does not show the hinge and other interior features and that view is not illustrated.

Stratigraphic range.—Known only from the Wreford Limestone (Lower Permian = upper Sakmarian) (fig. 1) of Kansas.

Tribolbina tumida (Scott and Borger, 1941)

Figure 3*e*

Beyrichiana tumida Scott and Borger, 1941, Jour. Paleontology, v. 15, p. 355, pl. 49, fig. 1.

Diagnosis.—Has posterolateral node on posterior lobe; posterior sulcus at approximate posterior third of dorsal margin; central lobe almost circular; dorsal part of posterior margin approximately perpendicular to hingeline.

Discussion.—The holotype is a pyritized broken right valve, and the original illustration does not show the part of the posterolateral node still preserved, which is indicated by an arrow on figure 3*e* (this report). Because the specimen is probably fragile, I did not remove it from the slide and did not obtain SEM (scanning electron microscrope) micrographs of the inside and dorsal views; it was photographed by R. H. McKinney, U.S. Geological Survey.

Stratigraphic range.—Known only from the Macoupin cyclothem (Upper Pennsylvanian=lower Stephanian) (fig. 1) of Illinois.

Tribolbina doescheri Sohn, n. sp.

Figures 3*f–i*; 4*a–l*; 5*a–h*, *n*

Name.—In honor of R. A. Doescher, Smithsonian Institution, who processed most of the limestone blocks and picked most of the silicified ostracodes.

Holotype.—USNM 248121

Paratypes.—USNM 248122–248179

Material.—Several hundred valves

Type-locality.—USNM loc. 9262

Other localities.—USNM loc. 9260

Type-level.—"Lyttonienkalk," Permian (see Grant, 1972, p. 215 for discussion of age). According to R. E. Grant (oral commun., March 1977), Dr. Merlynd Nestell, Univ. Texas at Arlington, has suggested a Dzhulfian (Late Permian) Age, on the basis of fusulines.

Diagnosis.—*Tribolbina* with shallow furrow splitting upper part of anterior lobe closer to dorsal margin and lobe split less well defined than in *T. permiana* and *T. tumida*.

Description.—The valves are thick shelled and straight backed and have rounded free margins; the

FIGURE 3.—*Tribolbina permiana*, *T. tumida*, and *T. doescheri*; all SEM micrographs except *c*.

a–d. Tribolbina permiana (Kellett, 1933).
Posterior (dorsal to right), outside, dorsal (anterior to right), and ventral (anterior to left) views of *Beyrichiana permiana* Kellett, 1933, approx. × 90. Holotype, USNM 85428, abraded left valve, arrows on figs. 3*b*, *d* point to posterior node. Wreford Limestone (Lower Permian), Chase County, Kans.

c. Tribolbina tumida (Scott and Borger, 1941).
Outside view of *Beyrichiana tumida* Scott and Borger, 1941, approx. × 60. Holotype, Illinois Univ. Pal. coll. no. X–1226, broken right valve, arrow points to remnant of posterior node. (Upper Pennsylvanian) Macoupin cyclothem (Wanless, 1931, p. 811), Lawrence County, Ill.

f–i. Tribolbina doescheri Sohn, n. sp.
f, *g*. Dorsal (anterior to right), and outside views of left valve approx. × 60. Holotype, USNM 248121, greatest length 1.4 mm, arrows on fig. 3*f* point to open terminal sockets. Permian, Greece, USNM loc. 9262, block 25.
h, *i*. Dorsal (anterior to left), and outside views of right valve approx. × 60. Paratype, USNM 248122, greatest length 1.2 mm. Permian, Greece, USNM loc. 9260, block 152.

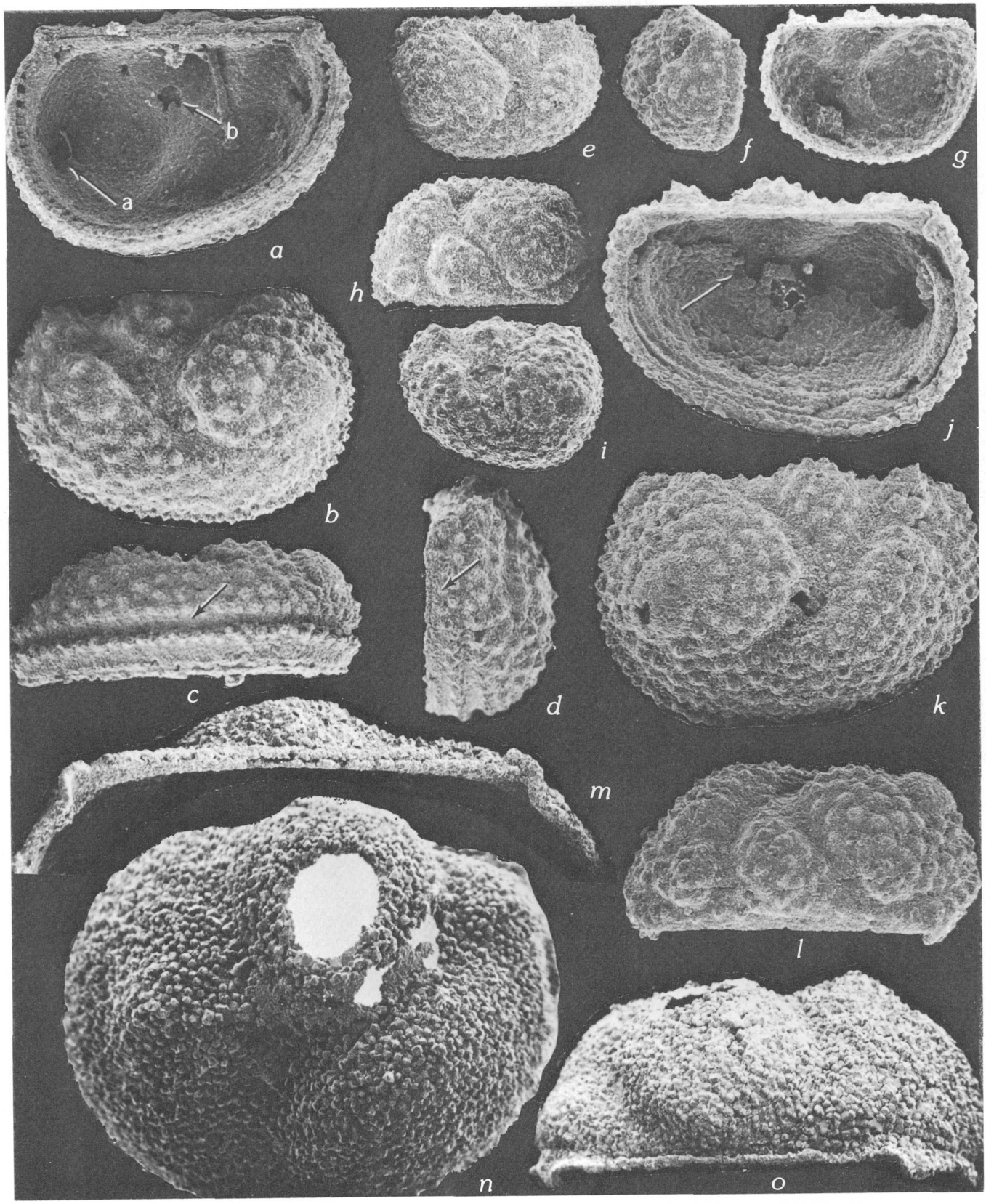
a
b
a
e
f
g
h
i
j
b
c
d
k
m
l
n
o

posterior margin is more broadly rounded than the anterior margin; the ventral margin curves gently backward so that the greatest height is behind the approximate midlength. On the left, smaller valve, the greatest curvature of the posterior margin is at the approximate midheight, that of the anterior margin is slightly higher, and the greatest curvatures of the end margins of the right valve are approximately at the same height, at, or slightly below midheight. The greatest width is slightly below midheight (figs. 4*d*; 5*g*). The lobation is distinct in dorsal view; the anterior slope is more angular than the posterior. The surface is coarsely tuberculate, except that of the posterolateral node, which appears to be bare of tubercles. The posterolateral node is hollow on the inside of the valve (figs. 4*a* arrow a, *j*; 5*f*, *h*). The hingement, sulcation, and lobation are like those described for the genus (figs. 4*a*, *j*; 5*a*, *f*, *h*). The dorsal part of the anterior lobe above the separating sulcus is narrower, more pointed, and less well defined than in *T. permiana* (fig. 3*b*) and *T. tumida* (fig. 3*e*). The greatest height is closer to the approximate midlength than in *T. permiana;* the greatest length of *T. tumida* is unknown because the posteroventral part of the holotype, and only known specimen, is broken. The free margins (velar bend?) of both valves are bounded by a deep groove that is bordered on both sides by closely spaced tubercles (figs. 4*c* arrow, *d* arrow, *f*; 5*g*).

Discussion.—The specimen illustrated on figure 5*n* differs in lateral outline from those illustrated on figures 3*f–i*, 4*a–l*, and 5*a–h* because the valve is bent inward along the central part of the ventral margin; it is illustrated to show variation due to artificial causes. The presence of the posterolateral node on a specimen of *T. doescheri*, representing a young growth stage and having a greatest length of 0.63 mm (figs. 4*e–h*); on a specimen of *T. doescheri* having a greatest length of 1.4 mm (figs. 3*f*, *g*); and on the largest specimen of *Tribolbina* from the Permian, *T.* sp. 1, having a greatest length of 3.1 mm (figs. 4*m–o*) indicates that this node is probably not a dimorphic feature. Dimorphism in ostracodes develops in the adult, or in the stage before the adult (A−1), and the range in size definitely represents more than two growth stages. I chose one of the largest specimens in the type-series as the holotype, but I have no evidence that this size represents the adult stage. In addition to the 10 illustrated specimens, 445 individuals were recovered from 49 limestone blocks at USNM localities 9260 and 9262. Because Dr. R. E. Grant is recording all the fossils obtained from each limestone block, specimens from each block were segregated on slides, USNM nos. 248131–248179.

Habitat.—Associated ostracode taxa were listed by Kornicker and Sohn (1976, p. 107). They, and the associated fossils in other phyla, suggest a shallow-water environment.

Stratigraphic range.—Known only from the Upper Permian (fig. 1) of Idhra Island. Greece.

FIGURE 4.—*Tribolbina doescheri* Sohn, n. sp. and *Tribolbina* sp. 1; all SEM micrographs.

a–l. Tribolbina doescheri Sohn, n. sp.

a–d. Inside, outside, ventral (anterior to left), and anterior views of left valve approx. × 55. Paratype, USNM 248123, greatest length 1.15 mm. Permian, Greece, USNM loc. 9260, block 62.

e–h. Outside, anterior oblique, inside, and dorsal oblique (anterior to left) views of right valve approx. × 62. Paratype USNM 248124, greatest length 0.63 mm. Permian, Greece, USNM loc. 9260, block 62.

i. Outside view of left valve approx. × 57. Paratype, USNM 248125, greatest length 0.65 mm. Permian, Greece, USNM loc. 9260, block 100.

j–l. Inside, outside, and dorsal oblique (anterior to left) views of right valve approx. × 64. Paratype, USNM 248126, greatest length 1.1 mm. Permian, Greece, USNM loc. 9260, block 62.

m–o. Tribolbina sp. 1

Hinge approx. × 36, outside and dorsal (anterior to left) views of right valve, approx. × 30, represented by the outer surface of the inner silicified part of the shell. Figured specimen, USNM 248180, greatest length 3.1 mm. Permian, Greece, USNM loc. 9262, block 5.

***Tribolbina* aff. *T. doescheri* n. sp.**

Figures 5*i–m*

Discussion.—Three specimens, differing in lateral outline, in shape of Y-shaped sulci, and possibly also in type of papillae, were recovered from two limestone blocks; two from USNM locality 9260, block 131, the third from USNM loc. 9262, block 18, field coll. 7–4–74–5. The broken poorly preserved valve illustrated in figure 5*j* has a greatest length of approximately 1.9 mm and is the second largest specimen in the collections. The arrow on figure 5*j* points to the thickness of that part of the shell that is above the silicified inner part of the valve. The three specimens range in greatest length from 0.93 to 1.9 mm, but, as far as I can interpret, the variation in the anterior lobe does not indicate dimorphism. The specimen illustrated in figure 5*m* is slightly higher in relation to length, and similar variability was noted in specimens of *T. doescheri* (USNM 248175). This variation in length-height proportions is assumed to be due to individual variability within the population.

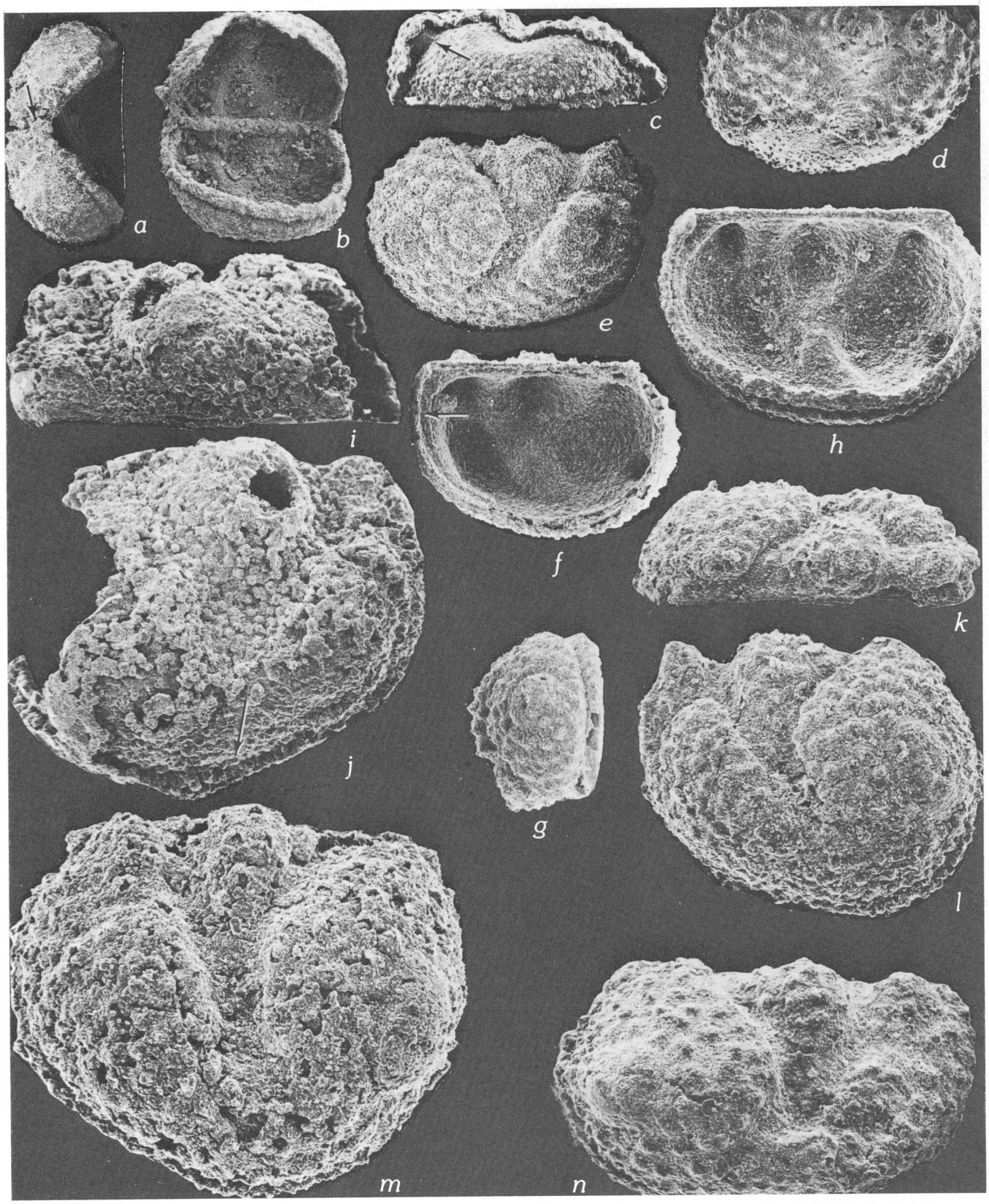
a
b
c
d
e
h
i
f
k
j
g
l
m
n

***Tribolbina* sp. 1**

Figures 4*m–o*

Discussion.—One poorly preserved right valve that represents the inner silicified part of the shell was recovered from USNM loc. 9262, block 5. The greatest length of the valve is 3.1 mm. This specimen differs from *T. doescheri* n. sp. and also from *T.* aff. *T. doescheri* in lateral and dorsal outlines and possibly also in shape and size of lobation. It is recorded in open nomenclature.

REFERENCES CITED

Bassler, R. S., and Kellett, Betty, 1934, Bibliographic index of Paleozoic Ostracoda: Geol. Soc. America Spec. Papers 1, 500 p.

Bless, M. J. M., and Jordan, Hanspeter, 1972, Ostracodes of the family Hollinellidae: [Netherlands] Rijks Geol. Dienst Med. Ser. C., v. 3, no. 1, 154 p., 35 pls.

Grant, R. E., 1972, The lophophore and feeding mechanism of the Productidina (Brachiopoda): Jour. Paleontology, v. 46, p. 213–248, 9 pls.

Henningsmoen, Gunnar, 1965, On certain features of palaeocope ostracodes: Geol. Fören. Stockholm Förhandlingar, v. 86, pt. 4, no. 519, p. 329–394, 16 figs.

Jones, T. R., Kirkby, J. W., and Brady, G. S., 1874–84, A monograph of the British fossil bivalved Entomostraca from the Carboniferous formations, pt. 1, The Cypridinadae and their allies: London, Palaeontographical Soc., 92 p., 7 pls.

Kellett, Betty, 1933, Ostracodes of the Upper Pennsylvanian and the Lower Permian strata of Kansas. I. The Aparchitidae, Beyrichiidae, Glyptopleuridae, Kloedenellidae, Kirkbyidae, and Youngiellidae: Jour. Paleontology, v. 7, p. 59–108, pls. 13–16.

——— 1935, Ostracodes of the Upper Pennsylvanian and the Lower Permian strata of Kansas. III. Bairdiidae (concluded), Cytherellidae, Cypridinidae, Entomoconchidae, Cytheridae, and Cypridae: Jour. Paleontology, v. 9, p. 132–166, pls. 16–18.

Kornicker, L. S., and Sohn, I. G., 1976, Phylogeny, ontogeny, and morphology of living and fossil Thaumatocypridacea (Myodocopa, Ostracoda): Smithsonian Contr. Zoology, 219, 124 p., 93 figs.

Latham, M. H., 1932, Scottish Carboniferous Ostracoda: Royal Soc. Edinburgh Trans., v. 57, pt. 2, no. 12, p. 351–395, 24 figs.

Martinsson, Anders, 1962, Ostracodes of the family Beyrichiidae from the Silurian of Gotland: Uppsala Univ. Geol. Inst. Bull., v. 41, 369 p., 203 figs.

Moore, R. C., ed., 1961, Treatise on invertebrate paleontology pt. Q, Arthropoda 3, Crustacea, Ostracoda: New York, N.Y., and Lawrence, Kans., Geol. Soc. America and Kansas Univ. Press. p. Q1–Q442, 334 figs.

Scott, H. W., and Borger, H. D., 1941, Pennsylvanian ostracodes from Lawrence County, Illinois: Jour. Paleontology, v. 15, p. 354–358, pls. 49, 50.

Scott, H. W., and Summerson, C. H., 1943, Non-marine Ostracoda from the Lower Pennsylvanian in the southern Appalachians, and their bearing on inter-continental correlation: Am. Jour. Sci., v. 241, no. 11, p. 654–675, 2 pls.

Sohn, I. G., 1953, *Cardiniferella* n. gen., the type of a new family of Carboniferous Ostracoda: Washington Acad. Sci. Jour., v. 43, no. 3, p. 66–68, 12 figs.

——— 1968, Triassic ostracodes from Makhtesh Ramon, Israel: Israel Geol. Survey Bull. 44, 71 p., 4 pls.

——— 1969, *Pseudoleperditia* Schneider, 1956 (Ostracoda, Crustacea), an Early Mississippian genus from southwestern Nevada: U.S. Geol. Survey Prof. Paper 643–C, p. C1–C6, 1 pl.

——— 1977a, Radiate shell structures in Paleozoic myodocopid and palaeocopid ostracodes are epigenetic: U.S. Geol. Survey Jour. Research, v. 5, no. 1, p. 125–133, 2 figs.

——— 1977b, *Paraparchites mazonensis* n. sp. (Ostracoda) from middle Pennsylvanian ironstone concretions of Illinois: Fieldiana—Geology, v. 37, no. 2, p. 43–59, 10 figs.

Wanless, H. R., 1931, Pennsylvanian section in western Illinois: Geol. Soc. America Bull., v. 42, no. 3, p. 801–812, 7 figs.

FIGURE 5.—*Tribolbina doescheri* Sohn, n. sp.; all SEM micrographs.

a–h. *Tribolbina doescheri* Sohn, n. sp.

a, b. Anterior and inside views of gaping carapace joined along dorsal margin approximately × 50. Paratype, USNM 248127, greatest length 0.7 mm. Permian, Greece, USNM loc. 9260, block 17.

c, d. Ventral and outside views of right valve with outer part of shell missing along venter showing ornament on the outer silicified surface of the shell and also on outer surface of inner silicified part of the shell approx. × 50. Paratype, USNM 168187, greatest length 1.05 mm. Permian, Greece, USNM loc. 9260, block 62.

e–g. Outside, inside, and posterior views of right valve approx. × 60. Arrow on fig. 5*f* indicates overlap. Paratype, USNM 248128, greatest length 0.8 mm. Permian, Greece, USNM loc. 9260, block 62.

h. Inside view of right valve approx. × 60. Paratype, USNM 248129, greatest length 1.0 mm. Permian, Greece, USNM loc. 9260, block 62.

i–m. *Tribolbina* aff. *T. doescheri* n. sp.

i, j. Dorsal (anterior to left) and outside views of a broken and poorly preserved right valve showing ornament on both the outer silicified surface and outer surface of the inner silicified part of the shell approx. × 42. Figured specimen, USNM 248181, greatest length 1.9 mm. Permian, Greece, USNM loc. 9262, block 18.

k, l. Dorsal (anterior to right) and outside views of left valve approx. × 60. Figured specimen, USNM 248182, greatest length 1.1 mm. Permian, Greece, USNM loc. 9260, block 131.

m. Outside view of left valve approx. × 90. Figured specimen, USNM 248183, greatest length 0.93 mm. Permian, Greece, USNM loc. 9260, block 131.

n. *Tribolbina doescheri* Sohn, n. sp.

Outside view of right valve bent inward along ventral margin, approx. × 60. Paratype, USNM 248130, greatest length 1.2 mm. Permian, Greece, USNM loc. 9260, block 152.

Jour. Research U.S. Geol. Survey
Vol. 6, No. 5, Sept.–Oct. 1978, p. 677–690

LATE MIOCENE MOLLUSKS FROM THE QUEEN CHARLOTTE ISLANDS, BRITISH COLUMBIA, CANADA

By WARREN O. ADDICOTT, Menlo Park, Calif.

Abstract.—A fauna of bivalve mollusks, scattered gastropods, and an echinoid from exposures of the Skonun Formation in the northeastern part of Graham Island is indicative of an early late Miocene age and correlation with the provincial Wishkahan Stage. The molluscan assemblages are from the upper 600 of the 1800-m-thick marine and nonmarine formation, which appears to be entirely of late Miocene age. The Skonun Formation is the strandline facies of marginal marine and nonmarine deposits of the northwestern part of the Queen Charlotte basin, a Neogene embayment paralleling the modern mainland coast. The molluscan fauna and associated lignite beds are known from a few widely scattered outcrops; they are indicative of alternating marine and nonmarine to brackish-water environments in the upper part of the formation. The Skonun fauna occurs near the northern boundary of the Pacific Northwest Neogene molluscan province. It is the only marine Neogene molluscan fauna known from the British Columbia coast. The fauna has strong taxonomic ties with the fauna of the Empire Formation of southwestern Oregon and has several species in common with the upper Miocene of the Lituya district, southeastern Alaska, implying that these three faunas are coeval.

Nearshore marine and nonmarine sandstones of the Skonun Formation in the northeastern part of Graham Island, Queen Charlotte Islands, British Columbia (fig. 1), represent the only marine Neogene strata exposed along the Pacific coast of Canda. The age and correlation of these sedimentary rocks have been speculative owing to the lack of definitive paleontologic determinations. Age determinations have been based, for the most part, on generalized molluscan data published nearly 100 years ago (Whiteaves *in* Dawson, 1880). Because this early work predated the definitive description of Neogene molluscan faunas of the eastern North Pacific, the determinations were mostly of genera and, therefore, do not permit accurate correlation with the subsequently developed provincial molluscan chronology (Arnold and Hannibal, 1913; Weaver, 1916; Weaver and others, 1944; Addicott, 1976).

This report is based upon both new and previously unreported collections from the type locality of the Skonun Formation about 6 km northeast of Masset (fig. 2) as well as upon other collections from the

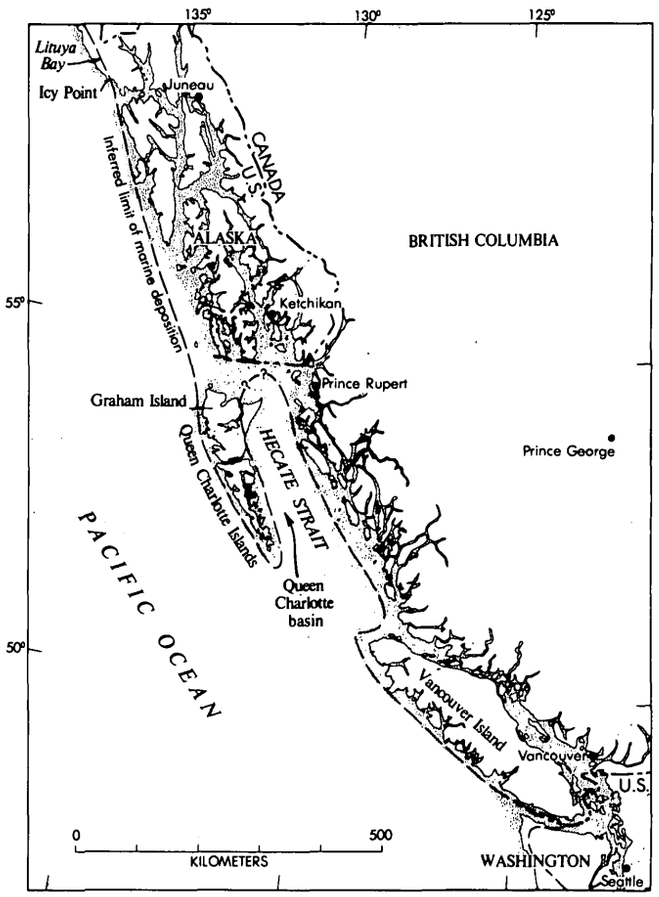

FIGURE 1.—Location and paleogeographic setting of northeastern part of Graham Island, Queen Charlotte Islands, British Columbia, with respect to Neogene Queen Charlotte basin of Shouldice (1971).

northeastern part of Graham Island. The initial collection from the Skonun, made by Dawson in 1878, has been reexamined and the new identifications are listed herein. The larger invertebrate fauna of about 30 taxa is clearly referable to the early late Miocene Wishkahan Stage of western Washington.

This report documents the molluscan fauna and discusses the age and correlation of the containing strata

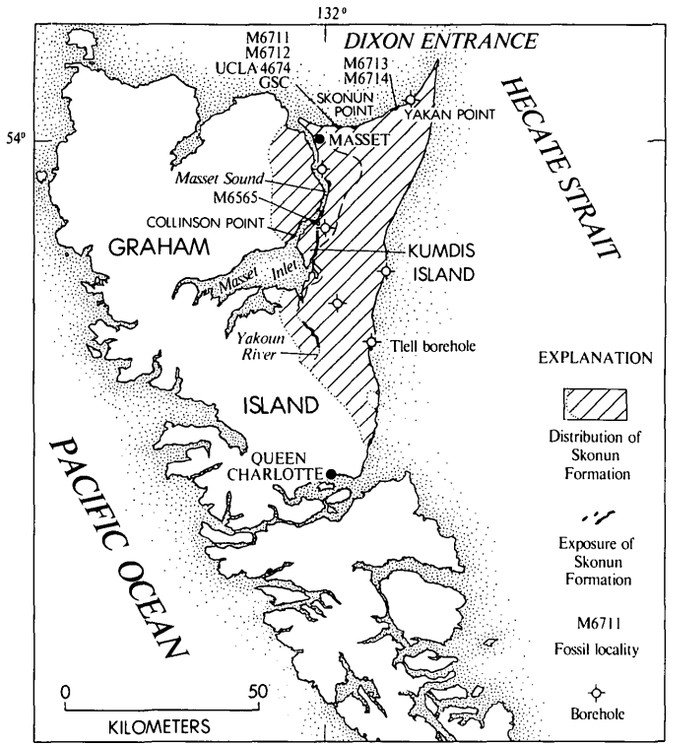

FIGURE 2.—Inferred distribution of Skonun Formation, surface exposures, and macrofossil localities in northeastern part of Graham Island (from Sutherland Brown, 1968).

in the context of the Pacific Northwest Neogene molluscan province. The Skonun molluscan fauna is of palebiogeographic interest as it links coeval cool temperate faunas from the Gulf of Alaska near Icy Point (lat 58° N.) with warm-temperate or temperate faunas in western Washington (lat 48° N.), well to the south of the Skonun localities (lat 54° N.).

Most of the fossil material upon which this report is based was collected in September 1976, during a field conference with Donald Tiffin and Christopher Yorath of the Geological Survey of Canada and P. D. Snavely, Jr., of the U.S. Geological Survey.

Acknowledgments.—I am indebted to Tiffin and Snavely for making arrangements that enabled me to secure the fossil material. M. J. Copeland, Geological Survey of Canada, arranged the loan of the original material from Skonun Point identified by Whiteaves (*in* Dawson, 1880). Louella Saul, University of California, Los Angeles, kindly lent collections from the Skonun Formation made during the 1950's by Richfield Oil Co. that were subsequently donated to the University. J. Wyatt Durham, University of California, Berkeley, identified the echinoid collected from exposures at Yakan Point. Druid Wilson searched the fossil mollusk collections in the U.S. National Museum for specimens reportedly collected from Skonun Point by J. C. Swan (Dall, 1896). I was assisted in the preparation of fossil specimens by John W. Miller. Kenji Sakamoto photographed the mollusk specimens ilustrated in this study.

PREVIOUS WORK

Neogene mollusks from Skonun Point were first noted by Dawson (1880) who included a list of 17 molluscan taxa identified by J. F. Whiteaves. Until now, this list has formed the basis for nearly all subsequent comments on the age of the formation. A few reports list or describe additional mollusks from the Skonun Point exposures: Dall (1896), Arnold *in* MacKenzie, 1916), Addicott (1965), MacNeil (1967), and Wagner (*in* Sutherland Brown, 1968). Martin and Rouse (1966) determined 50 species of plant microfossils of apparent late Miocene to early Pliocene age from five localities in the Skonun Formation including the type locality. Estimates of the age of the mollusk-bearing strata of the Skonun Formation range from middle Miocene (Arnold and Hannibal, 1913; Addicott, 1970a) to Pliocene (see Sutherland Brown, 1968, p. 127; Shouldice, 1971).

The Skonun Formation was named by MacKenzie (1916, p. 73) from exposures at Skonun Point, about 6 km northeast of Masset. An important reference section on the lower Yakoun River figured prominently in the original description, and four other isolated exposures on the northeastern part of Graham Island were noted.

The definitive description and the lithogenetic interpretation of the Skonun Formation were by Sutherland Brown (1968, p. 118–127), who observed that the stratigraphy of this 1800-m-thick formation is best defined by borehole data.

STRATIGRAPHY AND GEOLOGIC SETTING

The Skonun Formation of eastern Graham Island forms the northwestern part of the Queen Charlotte Tertiary basin of Shouldice (1971). These predominantly nonmarine rocks of late Neogene age grade southeastward into a 3000-m-thick section of marine sandstone and siltstone in the southern part of the basin as determined from a series of offshore boreholes (Shouldice, 1971, fig. 11). Subsurface stratigraphic data (Sutherland Brown, 1968) indicate that the brackish water to nearshore marine strata exposed at places along the northern coast of Graham Island and along Masset Sound (fig. 2) occur at or near the top of the Skonun Formation; stratigraphically, lower

units seem to be entirely or almost entirely of nonmarine origin.

Mackenzie (1916) named and described the Skonun Formation from fossiliferous calcareous sandstone with minor conglomerate and lignite beds and lenses of gray limestone typically exposed at Skonun Point about 10 km east of Masset Sound. There are very few exposures of the Skonun Formation although it underlies most of the eastern one-third of Graham Island (Sutherland Brown, 1968, fig. 18). Probably the best outcrops occur in, or just above, the intertidal zone near Skonun Point and Yakan Point (fig. 3) on

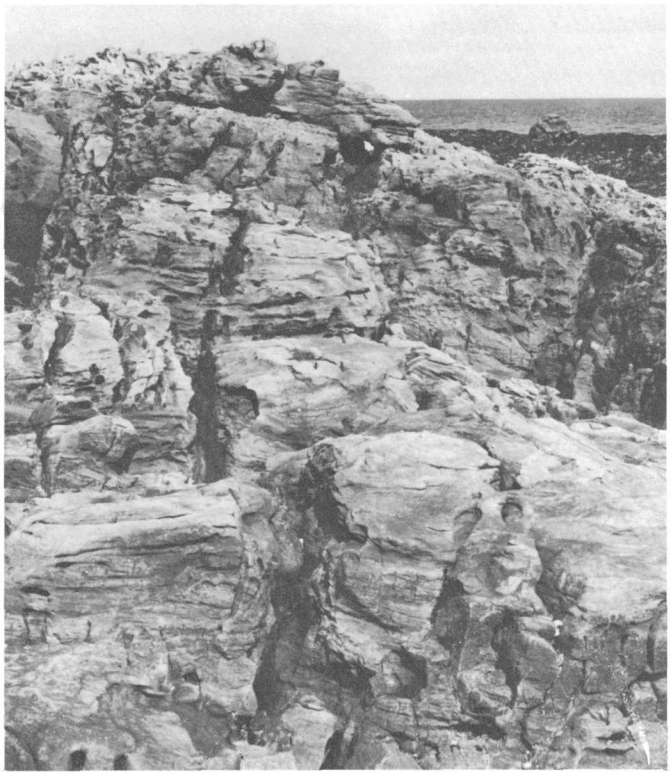

FIGURE 3.—Massive crossbedded sandstone of Skonun Formation exposed at Yakan Point. Scattered specimens of small sand dollar echinoid *Remondella* n. sp.? occur in lower part of this sandstone. View northeast.

the southern shore of Dixon Entrance. Other exposures occur along the shore of Masset Sound as far south as Kumdis Island (USGS loc. M6565) and Collinson Point. All known occurrences of marine macrofossils are from these two areas.

The Skonun Formation unconformably overlies the Masset Formation, a thick (8000 m) volcanic unit of early Tertiary age that may be coeval with Metchosin Volcanics as used by Sutherland Brown (1968, p. 118) on southern Vancouver Island. The Skonun is as much as 1800 m thick in borehole sections, according to Sutherland Brown (1968); it consists of calcareous sandstone and shaly mudstone with minor amounts of conglomerate and lignite. Inasmuch as the greatest thickness of the formation at Skonun Point is only 100 to 150 m, a series of six boreholes drilled by Richfield Oil Co. during the 1950's (fig. 2) best defines the lithology and stratigraphic sequence of the formation (Sutherland Brown, 1968); at Skonun Point marine mollusks occur in beds in the upper 25 m, and interbedded lignite and nonmarine silty shale occur in the lower 70 m of the exposed section.

Interpretation of data from the Richfield boreholes (Sutherland Brown, 1968, p. 123) indicates that marine shell-bearing strata are limited to the upper 70 to 600 m of these wells but are not present in all of them. Stratigraphically, lower parts of the section are of nonmarine origin and, apparently, have been successfully subdivided and correlated by palynological data (Shouldice, 1971, fig. 9).

The relationship of the marine strata exposed at Skonun Point and Yakan Point with the subsurface sections is not clear. Both of the surface exposures are in gently folded anticlinal structures, which makes it very difficult to relate them to the nearest borehole sections. Judging by the occurrence of marine shells in the uppermost 70 to 600 m of these borehole sections (Sutherland Brown, 1968, p. 123), it seems that the mollusk-bearing beds must be in the upper part of the Skonun Formation.

PALEONTOLOGY

The fauna of the Skonun Formation consists of 29 molluscan taxa and an echinoid (table 1). Most of the species have not previously been reported from the Skonun Formation, although many of the early generic determinations of Whiteaves (*in* Dawson, 1880) can be correlated with species recognized in this report, as shown in table 2.

Prior to this writing only nine species of larger marine invertebrates had been identified in collections from the Skonun Formation, mostly by Whiteaves (*in* Dawson, 1880) [*Crypta adunca*, *Arca microdonta*, *Macoma nasuta*, and *Tapes staminea*] and Arnold (*in* MacKenzie, 1916) [*Cryptonatica clausa* and *Hemimactra* cf. *H. albaria*]. Other species were recorded by Addicott (1965), MacNeil (1967), and Frances Wagner (*in* Sutherland Brown, 1968). Seven of the mollusks listed by Dall (1896, p. 844–845) from his Astoria Group of Alaska were shown to occur in the Miocene of British Columbia. It is possible that these species (table 3) are from the Skonun Formation as Dall

TABLE 1.—*Mollusks from the Skonun Formation northeastern Graham Island*

[x, present as identified; cf., similar form; ?, doubtful identification]

Localities	M6711	M6712	M6713	M6714	M6565	UCLA 4676	GSC 6111-6129
Gastropods:							
Eulima washingtoni Reagan (fig. 5h-5j)	x	-	-	-	-	-	-
Trochita n. sp. Moore (1963) (fig. 7e)	-	-	-	-	-	-	x
Calyptraea sp. (fig. 5k)	x	-	-	-	-	-	-
Crepidula adunca (Sowerby) (fig. 5a, 5f)	x	-	-	-	-	-	x
Tectonatica janthostoma (Deshayes) (fig. 5b)	x	-	-	-	-	x	?
Undetermined naticid	-	x	-	-	x	-	-
Fusitriton sp. (fig. 5g)	-	-	-	-	-	x	-
Nucella?	-	-	-	-	-	x	-
Molopophorus bogachieli (Reagan) (fig. 5c-5e)	x	-	-	-	-	-	-
Searlesia sp. (fig. 5n)	x	-	-	-	-	-	-
Nassarius whitneyi (Trask) (fig. 5m)	x	x	-	-	-	-	x
Megasurcula gabbiana (Dall) (fig. 5o, 5p)	-	-	-	-	-	x	-
Bivalves:							
Anadara trilineata (Conrad) (fig. 7a)	-	-	-	-	-	-	x
Glycymeris gabbi Dall (fig. 6c, 6f, 6h)	x	x	-	x	-	-	x
Patinopecten oregonensis (Howe) (fig. 7f)	-	-	-	-	-	x	-
Lucinoma sp. (fig. 6o)	x	-	-	-	-	-	-
Clinocardium coosense (Dall) (fig. 5t-5v, 5x, 5y)	cf.	?	-	-	x	x	x
Spisula praecursor Dall (fig. 6a, 6i, 6m, 6r)	x	cf.	-	-	-	-	x
Pseudocardium cf. *P. densatum* (Gabb) (fig. 6p)	-	x	x	-	-	-	-
Solen conradi Dall (fig. 6l)	-	x	-	-	-	-	-
Solen cf. *S. sicarius* Gould	-	-	-	-	-	-	x
Siliqua lucida (Conrad) (fig. 5r)	x	-	-	-	-	-	x
Siliqua oregonia Dall (fig. 5s, 5w)	?	cf.	-	-	-	-	-
Macoma cf. *M. calcarea* Gmelin (fig. 6n)	x	-	-	-	-	-	-
Macoma nasuta (Conrad) (fig. 6d, 6j; fig. 7d)	x	-	-	-	-	-	x
Corbicula sp. (fig. 5l, 5q)	-	-	-	x	-	-	-
Saxidomus giganteus Deshayes (fig. 6q; fig. 7b)	x	?	-	-	-	-	x
Protothaca montesanoensis (Weaver) (fig. 6g, 6k; fig. 7c)	x	x	-	-	-	-	x
Securella securis (Shumard) (fig. 6b, 6e, 6s)	x	x	-	-	-	x	x
Echinoid:							
Remondella n. sp.?	-	-	x	-	-	-	-

(1896, p. 843) stated earlier; "On the south side of Dixon's entrance at Skookum Point, near Massett [SIC], Queen Charlotte Islands, Hon. J. G. Swan collected specimens, now in the National Museum, showing the presence of these [Astoria Group] beds." These specimens, however, are not now in the Tertiary

TABLE 2.—*Correlation of mollusk identifications from earlier reports with names used in this report*

Whiteaves (in Dawson, 1880)	Arnold (in MacKenzie, 1916)	This report
Gastropods:		
Trochita or *Galerus*		*Trochita* n. sp. Moore (1963)
Crypta adunca Sowerby		*Crepidula adunca* Sowerby
Lunatia? sp.	*Cryptonatica clausa* Broderip and Sowerby	*Tectonatica janthostoma* (Deshayes)
Nassa sp.	*Caesia* sp. K	*Nassarius whitneyi* (Trask)
Mangelia? sp. undet.		*Nassarius whitneyi* (Trask)
Bivalves:		
Arca microdonta Conrad		*Anadara trilineata* (Conrad)
Axinaea		*Glycymeris gabbi* Dall
Cardium [cf.] *C. islandicum*		*Clinocardium coosense* (Dall)
Cardium [cf.] *C. blandum* Gould		*Clinocardium coosense* (Dall)
Standella	*Hemimactra* cf. *albaria* Conrad	*Spisula praecursor* Dall
Solen sp.		*Solen* cf. *S. sicarius* Gould
Siliqua		*Siliqua lucida* (Conrad)
Macoma nasuta Conrad		*Macoma nasuta* (Conrad)
Saxodomus		*Saxidomus giganteus* Deshayes
Chione sp. undet.		*Securella securis* (Shumard)
Tapes staminea Conrad	*Paphia* sp. C.	*Protothaca montesanoensis* (Weaver)
Mercenaria		*Securella securis* (Shumard)

mollusk collections in the U.S. National Museum (Druid Wilson, oral commun., March, 1977).

The molluscan fauna consists principally of bivalves. Even though gastropods make up one-third of the known taxa, they are rarely found in the field, and the taxa identified herein are represented by few specimens. The mollusk shells are generally well preserved. Most of the bivalves in the coarse-grained sandstone exposed at Yakan Point (USGS locs. M6713, M6714), however, are represnted by internal and external molds (fig. 4).

Nearly all of the macrofossils listed in table 1 occur at Skonun Point. Only the echinoid *Remondella* n. sp.? and the brackish- or fresh-water bivalve *Corbicula*, from assemblages collected at Yakan Point, have not been found in the type area of the Skonun Formation. The Yakan Point assemblages and those from Kumdis Island near the south end of Masset Sound (fig. 2) are all of very low taxonomic diversity.

An effort has been made to illustrate as much of the Skonun molluscan fauna as possible (figs. 5–7). Until now only two mollusks from the Skonun Formation, *Patinopecten oregonensis* (Howe) [as *P. skonunesis* MacNeil (1967, pl. 4, fig. 2, pl. 6, fig. 7)] and *Nassarius whitneyi* (Trask) (Addicott, 1965, pl. 2, figs. 19–22) have been illustrated.

TABLE 3.—*Miocene mollusks from British Columbia listed by Dall (1896, p. 844–845)*

[These specimens are lost; only *Macoma nasuta* is known to occur in the Skonun Formation]

Gastropods :
Crepidula praerupta Conrad
Neverita saxea Conrad

Bivalves:
Cardium decoratum Grewingk
Serripes gronlandicus Beck
Tellina carlottensis Whiteaves
Macoma inconspicua Broderip and Sowerby
Macoma nasuta Conrad

AGE AND CORRELATION

The molluscan fauna of the Skonun Formation is inferred to be of late Miocene age. Eighteen of the 22 specifically identified taxa occur in the fauna of the early late Miocene Wishkahan Stage of Addicott (1976); another, *Nassarius whitneyi* (Trask), occurs in coeval strata in central California. Correlation with the Wishkahan Stage, the type section of

FIGURE 4.—Poorly preserved internal molds of bivalve *Pseudocardium* cf. *P. densatum* (Gabb) in coarse-grained cross-bedded sandstone at Yakan Point. Chisel is 15 cm long.

which is in southwestern Washington, is indicated by the presence of the stratigraphically restricted species *Protothaca montesanoensis* (Weaver) and *Patinopecten oregonesis* (Howe) (table 1). The cooccurrence in the Skonun of the distinctive gastropod *N. whitneyi*, which occurs in strata of late middle Miocene and early late Miocene age in California (Addicott, 1965), and the gastropod *Trochita* n. sp. Moore (1963), which occurs in strata of early to late Miocene age in Oregon and Washington, with several species that range from the Wishkahan Stage to the Graysian Stage [*Molopophorus bogachieli* (Reagan), *Glycymeris gabbi* Dall, *Clinocardium coosense* (Dall), and *Pseudocardium* cf. *P. densatum* (Gabb)], also suggests assignment to the Wishkahan Stage.

The echinoid *Remondella* further suggests a late Miocene age. The known occurrences of this genus are from strata of late Miocene age in Baja California, northern California, southwestern Washington, and the Alaska Peninsula (Grant and Hertlein, 1938; Wagner, 1974). The Alaska occurrence, once thought to be of Pliocene age, is now assigned to the late Miocene (Allison, 1976).

A middle Miocene age, suggested by some earlier workers (Arnold and Hannibal, 1913; Durham, 1950; Addicott, 1970a), can be ruled out by the fact that two genera in the Skonun Formation, *Protothaca* and *Remondella*, do not appear in the Neogene record of the eastern North Pacific margin until after the middle Miocene, that is, are not known to occur in the faunas of the Temblor Stage of Weaver and others (1944) or the Newportian Stage.

FIGURE 5.—Mollusks from Skonun Formation. Localities M6711, M6712, and UCLA 4674 are at Skonun Point. Locality M6565 is at north end of Kumdis Island; M6714 is at Yakan Point. Specimens natural size unless otherwise indicated in parentheses.

a, f. *Crepidula adunca* Sowerby. USNM 245654, USGS loc. M6711. (× 2).
b. *Tectonatica janthostoma* (Deshayes). USNM 245655, USGS loc. M6711. (× 2½).
c. *Molopophorus bogachieli* (Reagan). USNM 245656, USGS loc. M6711. (× 3).
d. *Molopophorus bogachieli* (Reagan). USNM 245657, USGS loc. M6711. (× 2).
e. *Molopophorus bogachieli* (Reagan). USNM 245658, USGS loc. M6711 (× 2).
g. *Fusitriton* sp. UCLA 57585, UCLA loc. 4674. loc. M6711. (× 3).
h, i. *Eulima washingtoni* (Reagan). USNM 245659, USGS loc. M6711. (× 4), a rubber cast.
j. *Eulima washingtoni* (Reagan). USNM 245660, USGS loc. M6711. (× 4).
k. *Calyptraea* sp. USNM 245661, USGS loc. M6711.
l. *Corbicula* sp. USNM 245662, USGS loc. M6714, a rubber cast.
m. *Nassarius whitneyi* (Trask). USNM 245663, USGS loc. M6711. (× 4).
n. *Searlesia* sp. USNM 245664, USGS loc. M6711. (× 2).
o, p. *Megasurcula gabbiana* (Dall). UCLA 57586, UCLA loc. 4674. (× 3).
q. *Corbicula* sp. USNM 245665, USGS loc. M6714. (× 1½), a rubber cast.
r. *Siliqua lucida* (Conrad). USNM 245666, USGS loc. M6711.
s. *Siliqua* cf. *S. oregonia* Dall. USNM 245667, USGS loc. M6712, (× 1½).
t. *Clinocardium coosense* (Dall). USNM 245668, USGS loc. M6712, a rubber cast.
u. *Clinocardium coosense* (Dall). USNM 245669, USGS loc. M6711.
v. *Clinocardium coosense* (Dall). USNM 245670, USGS loc. M6711. (× 3).
w. *Siliqua* cf. *S. oregonia* Dall. USNM 245671, USGS loc. M6711.
x. *Clinocardium coosense* (Dall). USNM 245672, USGS loc. M6711. (× 1½), a rubber cast.
y. *Clinocardium coosense.* (Dall). USNM 245673, USGS loc. M6565, a rubber cast.

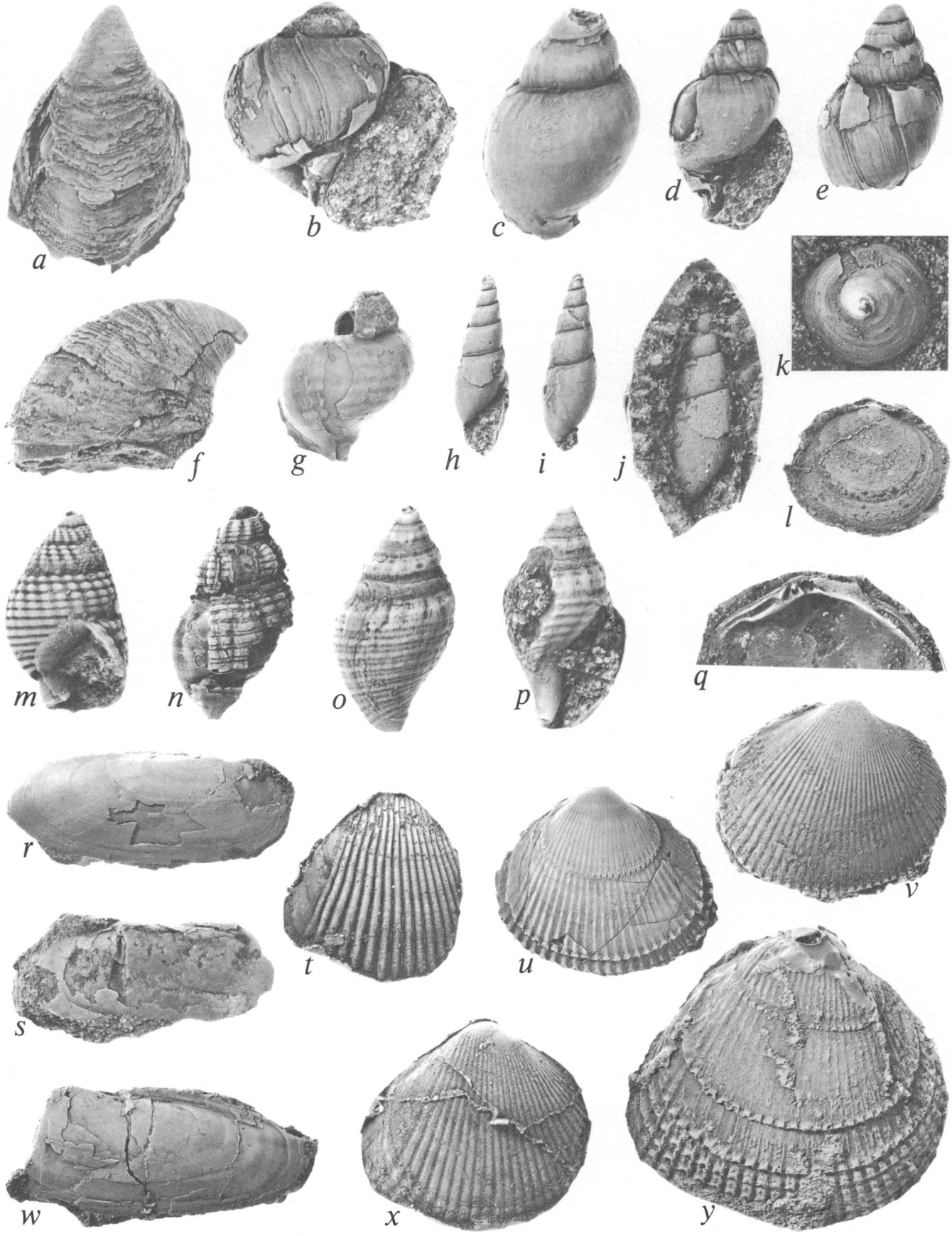
a
b
c
d
e
f
g
h
i
j
k
l
m
n
o
p
q
r
s
t
u
v
w
x
y

The Pliocene age for these marine strata suggested by Shouldice (1971, fig. 9) can be ruled out, at least in the context of the marine macrofossil chronology, by the fact that several species in the Skonun Formation are not known to occur in the provincial Pliocene as indicated earlier in this section. It should be noted here that the Pliocene of most earlier reports on the Pacific coast Neogene sequence was based upon recognition of the Miocene-Pliocene boundary at about 10 m.y. (million years) rather than at the currently recognized 5 to 5.5 m.y. boundary (Addicott, 1977).

A more general means of determining the age of the mollusk-bearing strata of the Skonun Formation also suggests assignment to the provincial early late Miocene. Three of the 23 (13 percent) molluscan genera in the Skonun are either extinct (*Molopophorus* and *Securella*) or are no longer living in the eastern North Pacific (*Pseudocardium*); *Nucella?* and *Corbicula* are excluded from this count. This percentage compares favorably with late Miocene values on a curve showing the percentage of extinct genera in Eocene to Pliocene molluscan faunas of the San Joaquin basin of central California (fig. 8). A Pliocene (1.8 to 5 or 5.5 m.y.) age seems unlikely on the basis of these criteria which indicate that the expected percentage of extinct genera would be 5 percent or less.

The percentage of living species in the fauna is also strongly suggestive of late Miocene age when compared with values from the well-known Neogene sequence of central California (fig. 9). Seven of the 22 (31 percent) specifically identified mollusks in the Skonun fauna are still living. This percentage compares very closely with values from the early late Miocene faunas of the Margaritan Stage of Corey (1954) from the Santa Margarita Formation of the Coalinga area and the Cierbo Sandstone and the Neroly Formation of the Mount Diablo area, both in California. The percentage of living species in the former is 33 and in the latter is 36, on the basis of analysis of faunal lists compiled by Hall (1960, p. 290–293, 294–295). The late late Miocene faunas of the Jacalitos Stage of Weaver and others (1944) of California have appreciably higher percentages of living species, suggesting that the Skonun fauna is not to be assigned to the late late Miocene. The Pancho Rico Formation of the Salinas Valley area contains 49 percent living species, the *Turritella nova* Zone of the Jacalitos Formation contains 45 percent living species, and the *Chione elsmerensis* Zone of the same formation contains 44 percent living species. These figures are based upon analysis of data in Durham and Addicott (1965) and Nomland (1917). The older faunas of the Tremblor Stage of California have significantly lower percentages of living species: 9 percent in the Kern River area and 12 percent in the San Juan district (fig. 9), on the basis of data from Loel and Corey (1932, p. 167–174) and Addicott (1970c, p. 25–27).

Plant microfossils from five localities in the Skonun Formation, including Skonun Point and Yakan Point, were judged by Martin and Rouse (1966, p. 171) to be "apparently late Miocene to early Pliocene in age." Pollen from near the bottom of the 1250-m borehole near Tlell (fig. 2) "is essentially identical to that from outcrops" (Sutherland Brown, 1968, p. 118) suggesting no appreciable difference in age. However, microfloral data by which the six Skonun borehole sections in northeastern Graham Island are correlated by Shouldice (1971, figs. 8, 9) suggest that both early

FIGURE 6.—Mollusks from Skonun Formation. Localities M6711 and M6712 are at Skonun Point. Specimens natural size unless otherwise indicated in parentheses.

a. *Spisula praecursor* Dall. USNM 245674, USGS loc. M6711. (× 1½).
b. *Securella securis* (Shumard). USNM 245675, USGS loc. M6711. (× 1½).
c. *Glycymeris gabbi* Dall. USNM 245676, USGS loc. M6711. (× 1½).
d. *Macoma nasuta* (Conrad). USNM 245677, USGS loc. M6711.
e. *Securella securis* (Shumard). USNM 245678, USGS loc. M6711.
f. *Glycymeris gabbi* Dall. USNM 245679, USGS loc. M6711. (× 1½).
g. *Protothaca montesanoensis* (Weaver). USNM 245680, USGS loc. M6712.
h. *Glycymeris gabbi* Dall. USNM 245681, USGS loc. M6711. (× 1½).
i. *Spisula praecursor* Dall. USNM 245682, USGS loc. M6711. (× 1½).
j. *Macoma nasuta* (Conrad). USNM 245683, USGS loc. M6711.
k. *Protothaca montesanoensis* (Weaver). USNM 245684, USGS loc. M6712.
l. *Solen conradi* Dall. USNM 245685, USGS loc. M6712, a rubber cast.
m. *Spisula praecursor* Dall. USNM 245686, USGS loc. M6711. (× 1½).
n. *Macoma* cf. *M. calcarea* Gmelin. USNM 245687, USGS loc. M6711. (× 1½).
o. *Lucinoma* sp. USNM 245688, USGS loc. M6711.
p. *Pseudocardium* cf. *P. densatum* (Gabb). USNM 245689, USGS loc. M6712.
q. *Saxidomus giganteus* Deshayes. USNM 245690, USGS loc. M6711.
r. *Spisula praecursor* Dall. USNM 245691, USGS loc. M6711. (× 3).
s. *Securella securis* (Shumard). USNM 245692, USGS loc. M6711.

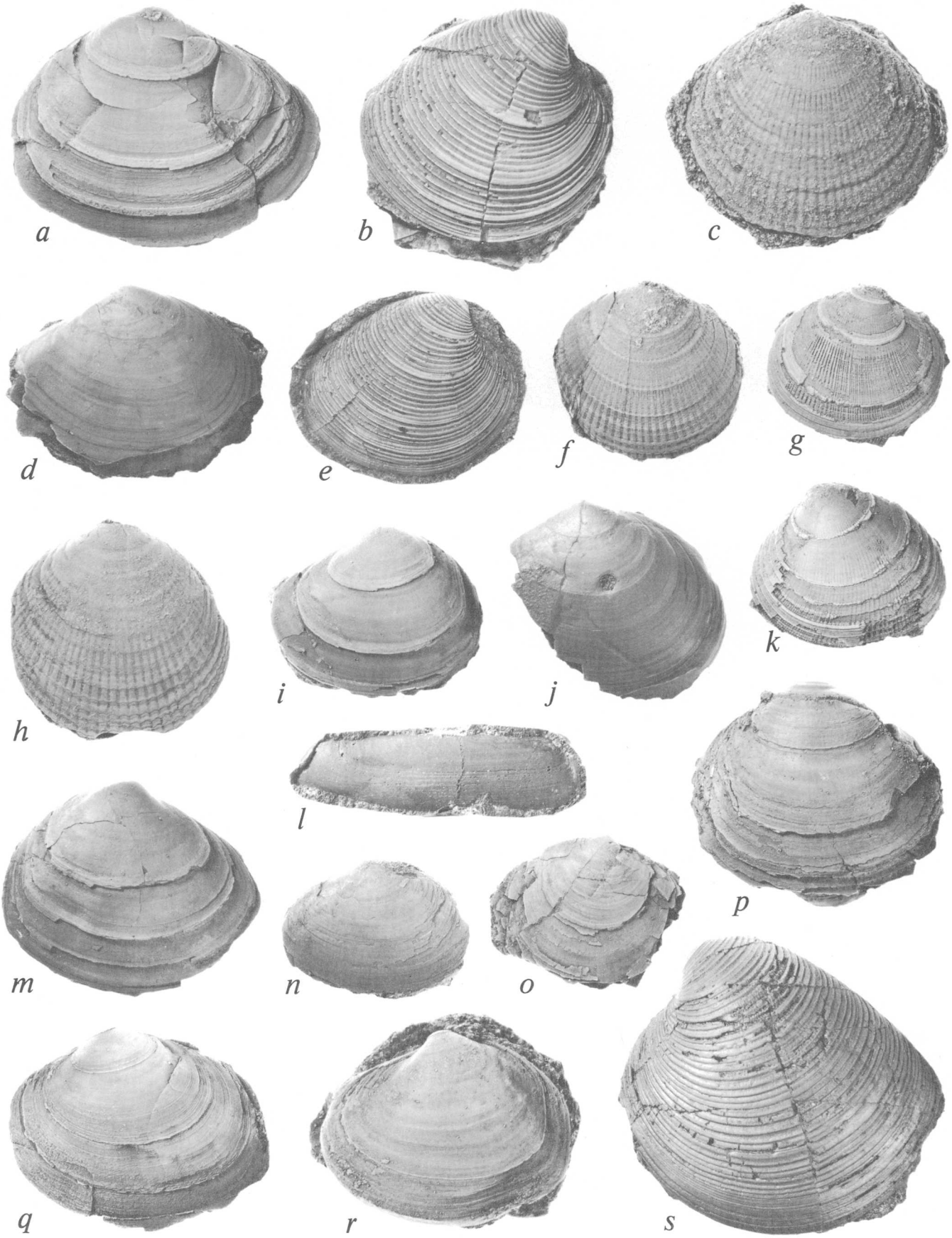
a
b
c
d
e
f
g
h
i
j
k
l
m
n
o
p
q
r
s

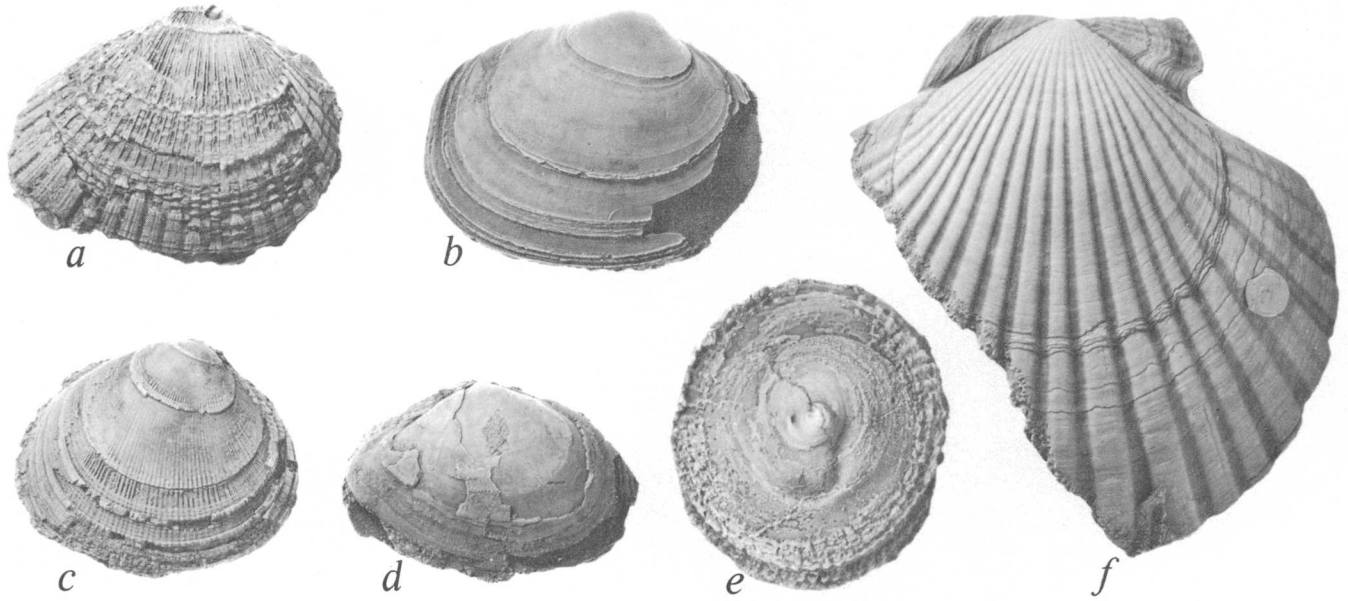

FIGURE 7.—Mollusks from type area of Skonun Formation at Skonun Point. GSC specimens are from Dawson's (1880) collection. Views are natural size unless otherwise indicated in parentheses.

a. *Anadara trilineata* (Conrad). GSC 49813. GSC loc. 6122.
b. *Saxidomus giganteus* Deshayes. GSC 49814. GSC loc. 6116.
c. *Protothaca montesanoensis* (Weaver). GSC 49876. GSC loc. 6115.
d. *Macoma nasuta* (Conrad). GSC 49877. GSC loc. 6111a.
e. *Trochita* n. sp. Moore. GSC 49878. GSC loc. 6123a. (× 3), a rubber cast.
f. *Patinopecten oregonensis* (Howe). UCLA 39474. UCLA loc. 4674.

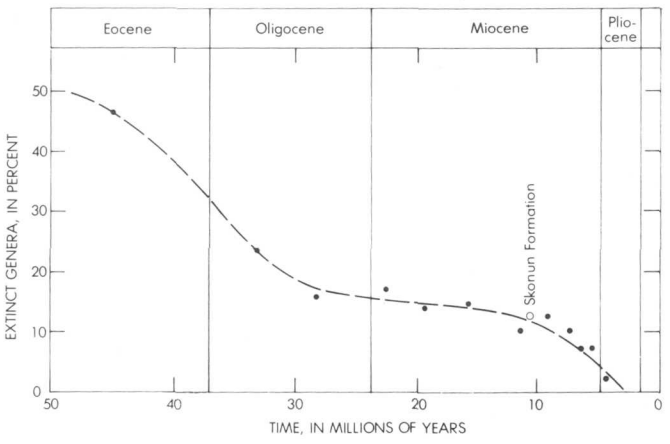

FIGURE. 8.—Comparison of percentage of extinct genera in molluscan fauna of Skonun Formation with Eocene to Pilocene extinction curve for San Joaquin basin, central California Data points (•) are from Addicott (1970b).

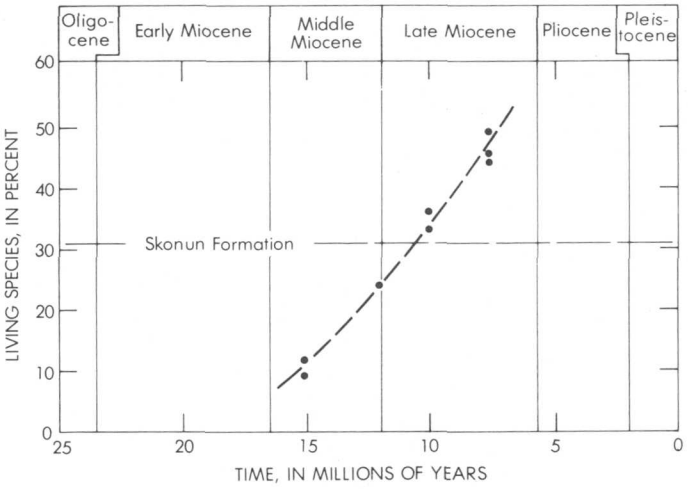

FIGURE 9.—Comparison of percentage of living species in fauna from Skonun Formation with data from Miocene faunas from central California. Sources for data points (•) are indicated in text.

Pliocene and late Miocene microfloras can be recognized. In at least two boreholes, the late Miocene floras are from the lower of Sutherland Brown's (1968) two subsurface units—nonmarine sand, shale and lignite. The occurrences of marine shelly sands are from stratigraphically higher beds in this upper unit. Shouldice (1971) assigns this upper unit to the lower Pliocene.

Taken together, the marine macrofaunal data considered herein and the microfloral correlations (Shouldice, 1971) suggest that most, if not all, of the Skonun Formation is of late Miocene age.

Some of the outcrops of the Skonun Formation along Masset Sound (fig. 2) contain faunas of

modern aspect (GSC localities 48562, 48567, 44746), according to Sutherland Brown (1968), and may belong to a Pleistocene unit distinct from the Skonun. However, at least one of the exposures in this area (USGS M6565, fig. 2) is of late Miocene age and is clearly a part of the Skonun Formation.

The Skonun fauna has many species in common with the lower part of the Montesano Formation as used by Fowler (1965), exposed on the southern side of the Olympic Mountains in western Washington. Fourteen of the 20 specifically identified mollusks in the Skonun collections have been reported from the lower part of the Montesano (Weaver, 1916) or occur in U.S. Geological Survey collections now in Menlo Park, Calif. The same number of species occurs in common with the much better known late Miocene fauna of the Empire Formation (Dall, 1909; Weaver, 1945) at Coos Bay, southwestern Oregon.

Upper Miocene strata in the Lituya district, southeastern Alaska, contain a few age-diagnostic species of mollusks in common with the Skonun Formation, but the faunal similarities are not nearly so strong as those with Wishkahan faunas from Washington and Oregon. Conspecific bivalves in U.S. Geological Survey collections identified by F. S. MacNeil (unpublished list which includes the late Miocene collections reported by Mertie, 1931, p. 129–130) are *Clinocardium* cf. *C. coosense* (Dall), *Securella* cf. *S. securis* (Shumard), *Pseudocardium* cf. *P. densatum* (Gabb), and *Spisula* cf. *S. praecursor* Dall. Gastropods in these collections are of cooler, and apparently deeper, water aspect than those of the Skonun Formation. Still, the presence of shallow-water late Miocene assemblages in the Lituya district is indicated by such bivalve genera as *Mya*, *Pseudocardium*, *Protothaca*, and *Securella*.

ZOOGEOGRAPHY AND PALEOCOLOGY

The molluscan fauna of the Skonun Formation is the only marine Neogene fauna known from the Pacific coast of Canada. It links the extensive mollusk-bearing strata of the late Miocene part of the Yakataga Formation on the Gulf of Alaska margin (Plafker, 1971), about 600 km to the northwest, with the late Miocene faunas of western Washington, about 900 km to the southeast. The fauna of the Sooke Formation on the southwestern coast of Vancouver Island (Clark and Arnold, 1923), formerly assigned to the early Miocene, is now believed to be of late Oligocene age according to recent recalibration of the molluscan chronology with European series-epoch boundaries (Addicott, 1977).

The Skonun fauna is referable to the Pacific Northwest molluscan Neogene province (Addicott, 1977) on the basis of the previously mentioned high percentage of species in common with the late Miocene Wishkahan Stage of western Washington. The northern boundary of this province was between lat 54° N. and the Lituya district (lat 58° N.), the closest late Miocene section to the north. The late Miocene fauna of the Lituya district is of cooler water aspect and, thus, is referable to the Gulf of Alaska Neogene molluscan province. The occurrence of the cool- to cold-water gastropods *Neptunea* and *Buccinum* and the bivalve *Serripes* place the Lituya district fauna in the more northern province.

A temperature marine climate is indicated by the modern distribution of molluscan genera that make up the Skonun fauna. One of the 21 still-living marine genera (*Megasurcula*) extends no farther north than the central California coast (lat 38° N.) (Burch, 1944–46); two others (*Anadara s.s.* and *Trochita*) now live in subtropical and tropical latitudes even farther to the south. The modern ranges of the other molluscan genera include the latitude of the fossil localities on Graham Island. These distributions suggest that the shallow-water marine climate was probably somewhat warmer than that which occurs off this coast today, possibly analogous to that of protected embayments along the central California coast about 2000 km to the south. The two warm-water taxa, *Anadara s.s.* and *Trochita*, are represented by solitary specimens suggesting that normal populations were not present at this site during the late Miocene. These taxa could represent holdovers from warm-water middle Miocene populations or stray individuals recruited via northward-flowing inshore countercurrents from warm-water populations living to the south. In any event, the presence of *Anadara s.s.* in the Skonun fauna cannot be taken, by itself, as an index of the subtropical to warm temperate faunas to which it is limited today because the subgenus seems to have been more tolerant of cooler water conditions during the Neogene (Kern, 1973, p. 38). The early and middle Miocene climatic warming that brought *Anadara s.s.* and its warm-water congeners northward into the Pacific Northwest molluscan province (Addicott, 1969, 1970a) was followed by a rapid withdrawal of these taxa during the post-middle Miocene cooling. During this retreat, however, *Anadara s.s.* consistently lagged far behind the other warm-water genera. The late Neogene distributional pattern of *Trochita*, however, suggests that it did not undergo a comparable change in temperature tolerance and that it is a more faithful index of shal-

low water marine temperatures than *Anadara s.s.*

The microflora from the Skonun Formation has similar paleoclimatic implications, according to Martin and Rouse (1966, p. 179) who postulated "relatively humid, and probably somewhat more temperate [conditions] than those of the region today." The plant associations suggested a higher mean annual temperature with little or no frost during the year.

Mollusk-bearing strata of the Skonun Formation, apparently at or near the top of the 1800-m-thick sequence (Sutherland Brown, 1968; Shouldice, 1971), are indicative of fully marine to brackish-water conditions. At Skonun Point, the molluscan associations (locs. M6711, M6712, UCLA 4674) contain marine species indicative of very shallow water depositional environments. Subtidal depths, possibly in the range of about 0 to 15 m, are suggested by the association of *Clinocardium*, *Spisula*, *Pseudocardium*, *Macoma*, *Protothaca*, and *Securella* at localities M6711 and M6712. This kind of bivalve association is characteristic of shallow-water bay environments. The occurrence of *Patinopecten* and *Megasurcula* in the collection from UCLA loc. 4674 implies somewhat greater depth on the basis of their modern occurrences in the Oregonian Molluscan Province of Hall (1964). Comparison is made with bathymetric distributions off central and northern California because the marine climate inferred from the Skonun molluscan fauna most closely approximates this present-day coastal area. *Patinopecten* and *Megasurcula* live at depths of about 35 m or greater in a mild temperate marine climatic belt (Hall, 1964) off the central California coast (Grau, 1959; Addicott, 1969). However, the common occurrence of isolated specimens of these two genera with shallower water assemblages in the late Neogene (Durham and Addicott, 1965; Addicott, 1969) indicates that they cannot be used inflexibly in bathymetric interpretations. The bathymetric range of *Patinopecten* in the modern cool temperate fauna off British Columbia is appreciably shallower; the shallowest records are 5 m according to Bernard (1970) and about 18 m according to Quayle (1973).

Brackish-water to nonmarine environments are indicated by the very low diversity assemblage of *Corbicula* and *Glycymeris* in sandstone beds at Yakan Point (loc. M6713). Stratigraphically higher crossbedded sandstone containing *Pseudocardium* and *Remondella* was deposited under more normal marine conditions.

At both Yakan Point and Skonun Point, the marine to brackish-water units are underlain by nonmarine beds that contain lignite (Sutherland Brown, 1968); these strata appear to form all but the highest part of the formation (Shouldice, 1971). Martin and Rouse (1966) recognized three coastal communities on the basis of plant microfossils, including dinoflagellates: a coastal, blackish-water association; a forest-swamp association; and an everglades or fairly open-water association.

The Skonun fauna, together with the microflora and lignites, seems to represent a basin-margin environment in the northernmost part of the Queen Charlotte Neogene basin of Shouldice (1971, fig. 1). As such, these biostratigraphic data tend to confirm the postulated northward closure of this basin at the head of Hecate Strait (fig. 1).

The preponderance of bivalves over gastropods, both quantitatively and taxonomically, seems to indicate a protected bay environment. This disparity between gastropod and bivalve specimens can be explained by reference to quantitative ecological studies of San Francisco Bay by Packard (1918a). His studies indicate that about five species of bivalves for each gastropod species are found in dredgings within this central California bay. Also, only 1 gastropod (*Nucella*) occurs among the 13 most commonly found mollusk species in the bay (Packard, 1918b). Packard (1918a) infers that the numerical abundance of bivalves seems to be characteristic of enclosed, protected water because quantitative sampling for modern mollusks along the open coast outside of San Francisco Bay recovered almost equal numbers of bivalves and gastropods. Similar abundances of bivalves occur in late Pleistocene fossiliferous terraces at Bay Center, Wash. (lat 47° N.) (Addicott, 1966, p. C19), which clearly represent a protected, strongly embayed environment (Clifton and Phillips, 1976; Mallory and others, 1977). It seems, therefore, that the bivalve-rich molluscan associations of the Skonun Formation do indeed reflect a highly protected bay or baylike depositional environment.

REFERENCES CITED

Addicott W. O., 1965, Some western gastropods of the genus *Nassarius:* U.S. Geol. Survey Prof. Paper 503–B, p. B1–B24, 3 pls.

——— 1966, Late Pleistocene marine paleoecology and zoogeography in central California: U.S. Geol. Survey Prof. Paper 523–C, p. C1–C21, 4 pls.

——— 1969, Tertiary climatic change in the marginal northeastern Pacific Ocean: Science, v. 165, no. 3893, p. 583–586.

——— 1970a, Latitudinal gradients in Tertiary molluscan faunas of the Pacific coast: Palaeogeography, Palaeoclimatology, Palaeoecology, v. 8, n. 4, p. 287–312.

——— 1970b, Tertiary paleoclimatic trends in the San Joaquin basin, California: U.S. Geol. Survey Prof. Paper 644–D, p. D1–D19.

——— 1970c, Miocene gastropods and biostratigraphy of the Kern River area, California: U.S. Geol. Survey Prof. Paper 642, 174 p., 21 pls.

——— 1976, Neogene molluscan stages of Oregon and Washington, *in* Neogene Symposium: Soc. Econ. Paleontologists and Mineralogists, Pacific Sec., San Francisco, April 1976, p. 95–115, pls. 1–5.

——— 1977, Neogene chronostratigraphy of nearshore marine basins of the eastern North Pacific—northwestern Mexico to Canada: Internat. Cong. Pacific Neogene Stratigraphy, 1st, Tokyo, May 1976, Proc., p. 151–175.

Allison, R. C., 1976, Late Oligocene through Pleistocene molluscan faunas in the Gulf of Alaska region: Internat. Cong. Pacific Neogene Stratigraphy, 1st Tokyo, May 1976, Abs. of Papers, p. 10–13.

Arnold, Ralph, and Hannibal, Harold, 1913, The marine Tertiary stratigraphy of the north Pacific Coast of America: Am. Philos. Soc. Proc., v. 52, no. 212, p. 559–605.

Bernard, F. R., 1970, A distributional checklist of marine mollusks of British Columbia [Canada]—Based on faunistic surveys since 1950: Syesis, v. 3, p. 75–94.

Burch, J. Q., ed., 1944–46, Distributional list of the west American marine mollusks from San Diego, California, to the Polar Sea: Concholog. Club. Southern California Minutes Nos. 33–63.

Clark, B. L., and Arnold, Ralph, 1923, Fauna of the Sooke Formation, Vancouver Island, with description of a new coral by T. Wayland Vaughan: California Univ. Pubs., Dept. Geol. Sci. Bull., v. 14, no. 5, p. 123–234, pls. 15–42.

Clifton, H. E., and Phillips, R. L., 1976, Pleistocene estuaries on the southern Washington coast: Geol. Soc. America Abs. with Programs, v. 8, no. 3, p. 362.

Corey, W. H., 1954, Tertiary basins of southern California, pt. 8 *in* Chapter 3 *of* Jahns, R. H., ed., Geology of southern California: California Div. Mines Bull. 170, p. 73–83.

Dall., W. H., 1896, Report on coal and lignite of Alaska: U.S. Geol. Survey 17th Ann. Rept., pt. 1, p. 763–875.

——— 1909, Contributions to the Tertiary paleontology of the Pacific Coast, pt. 1, the Miocene of Astoria and Coos Bay, Oregon: U.S. Geol. Survey Prof. Paper 59, 278, p., 23 pls.

Dawson, G. M., 1880, Report on the Queen Charlotte Islands: Canada Geol. Survey Rept. Prog. for 1878–79, p. 1–239.

Durham, D. L., and Addicott, W. O., 1965, Pancho Rico Formation, Salinas Valley, California: U.S. Geol. Survey Prof. Paper 524–A, p. A1–A22, 5 pls.

Durham, J. W., 1950, Cenozoic marine climates of the Pacific Coast: Geol. Soc. America Bull., v. 61, no. 11, p. 1243–1264.

Fowler, G. A., 1965, The stratigraphy, foraminifera, and paleoecology of the Montesano formation, Grays Harbor County, Washington: Los Angeles, Southern California Univ., Ph.D. thesis. Ann Arbor, Mich., University Microfilms, Inc., 354 p.

Grant, U. S., 4th, and Hertlein, L. G., 1938, The West American Cenozoic Echinoidea: Los Angeles, California Univ., Pub. Math. Phys. Sci., v. 2, 225 p., 30 pls., 17 figs.

Grau, G., 1959, Pectinidae of the Eastern Pacific: Allan Hancock Pacific Exped., v. 23, p. 1–308, pls. 1–57.

Hall, C. A., Jr., 1960, Displaced Miocene molluscan provinces along the San Andreas fault, California: California Univ. Pubs. Geol. Sci., v. 34, no. 6, p. 281–308.

——— 1964, Shallow-water marine climates and molluscan provinces: Ecology, v. 45, no. 2, p. 226–234.

Kern, J. P., 1973, Early Pliocene marine climate and environment of the eastern Ventura basin, southern California: California Univ. Pubs. Geol. Sci., v. 96, 117 p.

Loel, Wayne, and Corey, W. W., 1932, The Vaqueros formation, lower Miocene of California, pt. 1, Paleontology: California Univ. Pubs., Dept. Geol. Sci. Bull., v. 22, no. 3, p. 31–140, pls. 4–65.

MacKenzie, J. D., 1916, Geology of Graham Island, British Columbia: Canada Geol. Survey Mem. 88, 221 p.

MacNeil, F. S., 1967, Cenozoic pectinids of Alaska, Iceland, and other northern regions: U.S. Geol. Survey Prof. Paper 553, 57 p., 25 pls.

Mallory, V. S., Whitney, B. L., Crandall, Robert, Jayaraman, J. K., Leo, S. R., Petrarcha, Daryl, and Wiley, B. H., 1977, Pre-Wisconsin biostratigraphy, paleoecologly, and sedimentation at Bay Center, southwestern Washington: Geol. Soc. American Abs. with Programs, v. 9, no. 4, p. 458.

Martin, H. A., and Rouse, G. E., 1966, Palynology of late Tertiary sediments from Queen Charlotte Islands, British Columbia: Canadian Jour. Botany, v. 44, p. 171–208.

Mertie, J. B., Jr., 1931, Notes on the geography and geology of Lituya Bay, Alaska: U.S. Geol. Survey Bull. 836–B, p. B117–B135.

Moore, E. J., 1963, Miocene mollusks from the Astoria formation in Oregon: U.S. Geol. Survey Prof. Paper 419, 109 p., 33 pls. [1964].

Nomland, J. O., 1917, The Etchegoin Pliocene of middle California: California Univ. Pubs., Dept. Geology Bull., v. 10, no. 14, p. 191–254, pls. 6–12.

Packard, E. L., 1918a, A quantitative analysis of the molluscan fauna of San Francisco Bay: California Univ. Pubs. Zoology, v. 19, no. 13, p. 299–336.

——— 1918b, Molluscan fauna from San Francisco Bay: California Univ. Pubs. Zoology, v. 14, no. 2, p. 199–452, pls. 14–60.

Plafker, George, 1971, Possible future petroleum resources of Pacific-margin Tertiary basin, Alaska: Am. Assoc. Petroleum Geologists Mem. 15, p. 120–135.

Quayle, D. B., 1973, Intertidal bivalves of British Columbia: British Columbia Prov. Mus. Handbook no. 17, 104 p., illus.

Shouldice, D. H., 1971, Geology of the western Canadian continental shelf: Canadian Petroleum Geology Bull., v. 19, no. 2, p. 405–436.

Sutherland Brown, A., 1968, Geology of the Queen Charlotte Islands, British Columbia: British Columbia Dept. Mines and Petroleum Resources, Bull. 54, 226 p.

Wagner, C. D., 1974, Fossil and recent sand dollar echinoids of Alaska: Jour. Paleontology, v. 48, no. 1, p. 105–124.

Weaver, C. E., 1916, The Tertiary formations of western Washington: Washington Geol. Survey Bull. 13, 327 p.

——— 1945, Stratigraphy and paleontology of the Tertiary formations at Coos Bay, Oregon: Washington Univ. [Seattle] Pubs. Geology, v. 6, p. 31–62.

Weaver, C. E., Chm., and others, 1944, Correlation of the marine Cenozoic formations of western North America: Geol. Soc. America Bull., v. 55, no. 5, p. 569–598.

Jour. Research U.S. Geol. Survey
Vol. 6, No. 5, Sept.-Oct. 1978, p. 691–696

NEW PALEOGENE POLLEN SPECIES FROM THE GULF AND ATLANTIC COASTAL PLAINS

By NORMAN O. FREDERIKSEN, Reston, Va.

Abstract.—Four new pollen species are described on the basis of specimens from the Paleocene to early middle Eocene interval of the Gulf and Atlantic Coastal Plains. The species and their known geologic and geographic ranges are *Trivestibulopollenites fissuratus* (Midwayan to early Sabinian, Claibornian?; gulf coast?, Georgia to South Carolina); *Pseudoplicapollis limitata* (Midwayan to late Sabinian; gulf coast to Massachusetts), *Tricolpites asper* (early Midwayan to early Claibornian; gulf coast to Massachusetts), and *Tricolpites redactus* (early Midwayan to early Sabinian; South Carolina to Massachusetts).

Drilling of the U.S. Geological Survey Clubhouse Crossroads corehole 1 in South Carolina has provided abundant material for the study of Paleogene sporomorphs (spores and pollen grains). Dating of the cored section by using a variety of marine microfossils and megafossils (Hazel and others, 1976, 1977; Bybell and others, 1976) has allowed comparison of the sporomorph ranges in the core with the sporomorph ranges on the gulf coast. Four new pollen species are described in this paper. All four have been observed in material from the South Carolina corehole; two or three of the species are also known from the gulf coast, two from Virginia, and three from Massachusetts. Information on occurrences of the species in Virginia and Massachusetts is from unpublished data of the writer.

LOCATION AND STRATIGRAPHY OF COREHOLE

The U.S.G.S. Clubhouse Crossroads corehole 1 is located at lat 32°53.25′ N., long 80°21.41′ W., Dorchester County, S.C. The hole was completed in March 1975, and its total depth was 792 m. The cored section includes rocks of Cenomanian to late Oligocene age; the Cretaceous-Tertiary boundary is at 244 m. Lower Tertiary formations in the core are the Beaufort(?) (244–192 m; lower and middle Midwayan; lower Paleocene), Black Mingo (192–125 m; upper Midwayan to upper Sabinian; upper Paleocene to lower Eocene), Santee (125–69 m; upper Claibornian to Jacksonian; upper middle Eocene to upper Eocene), and Cooper (69–5 m; Jacksonian, and upper Vicksburgian to Chickasawhayan; upper Eocene and upper Oligocene). Principal disconformities within the Paleogene sequence of the core are at the base of the Tertiary, where the basal Midwayan is missing; between the Black Mingo Formation and Santee Limestone, where the uppermost Sabinian and the lower and middle Claibornian are missing; and within the Cooper Formation, where the lower and middle Vicksburgian are missing (Hazel and others, 1976, 1977; Bybell and others, 1976). In this paper, the informal terms "lower" and "upper" Sabinian are used to designate the upper Paleocene and lower Eocene parts, respectively, of the Sabinian Provincial Stage.

SPECIMEN LOCATIONS AND RELATIVE FREQUENCIES

Slides of the Clubhouse Crossroads core material are on file at the U.S. Geological Survey, Reston Palynological Laboratory. The coordinates listed in the holotype descriptions and in table 1 give the locations of the specimens on Leitz microscope 871956 in this laboratory. The coordinates for the center point of a standard-sized 2.5×7.6-cm microscope slide are 38.2×102.9 mm (horizontal × vertical axes); the slide label is to the left, and the horizontal coordinates increase toward the right edge of the stage, whereas the vertical coordinates increase toward the front edge.

Relative frequency terms used in this paper are "infrequent" (less than 1 percent of total sporomorphs), "occasional" (1–5 percent), and "common" (6–20 percent); the sporomorph counts on which the relative frequencies were based ranged from 71 to 157 grains per sample. The counts included all sporomorphs except most of the reticulate tricolpates and tricolporates, which are so difficult to classify to species level that I did not attempt to tabulate them.

SYSTEMATIC DESCRIPTIONS

Genus *TRIVESTIBULOPOLLENITES* Pflug *in* Thomson and Pflug 1953

Trivestibulopollenites fissuratus n. sp.

Figure 1*a–e*

Description.—Size 16–25 μm, mean 19 μm (12 measured specimens), holotype 19 μm. Oblate, outline tri-

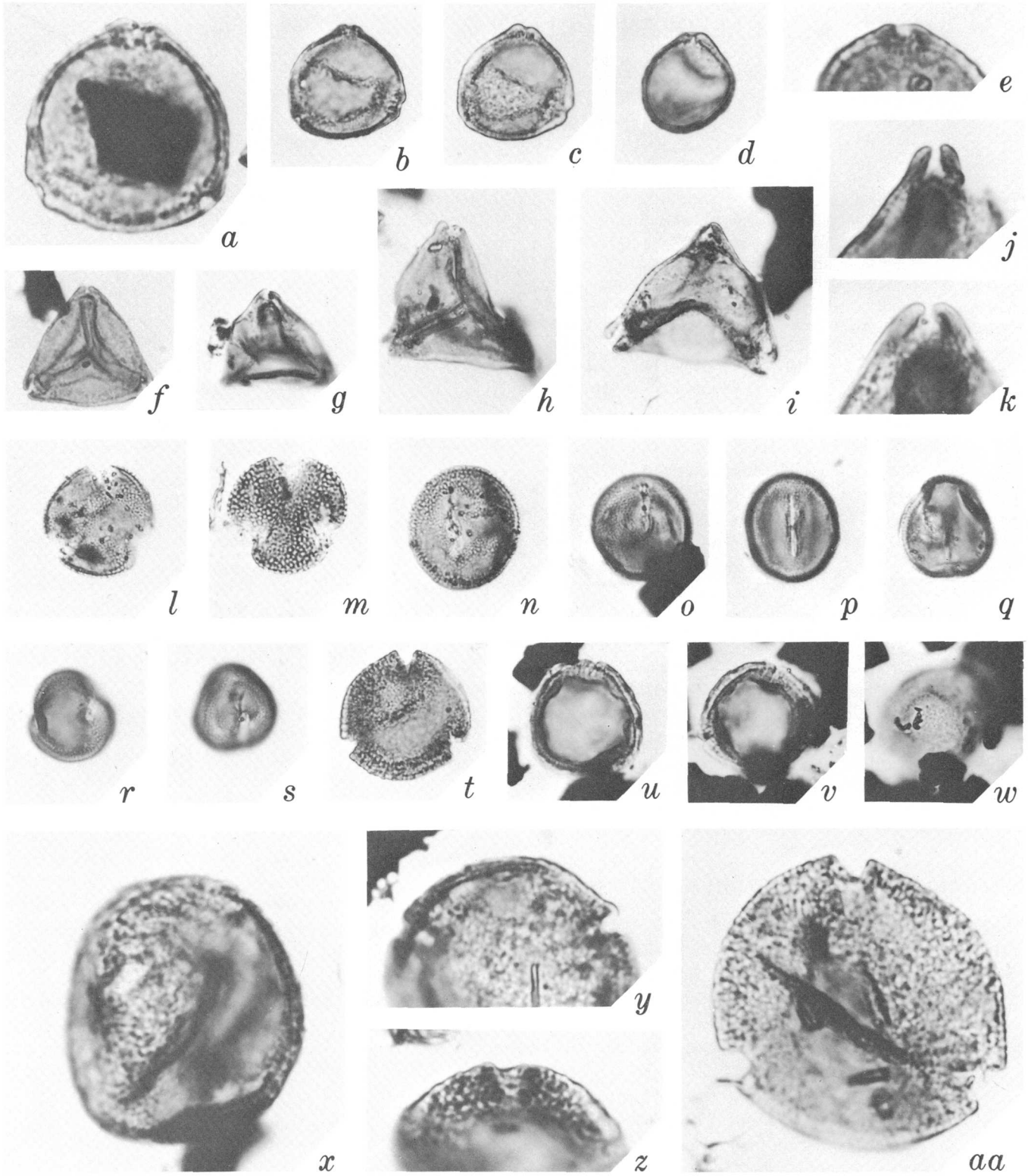

FIGURE 1.—*Trivestibulopollenites fissuratus, Pseudoplicapollis limitata, Tricolpites asper,* and *Tricolpites redactus.* Magnification × 1000 unless otherwise stated.

a–e. Trivestibulopollenites fissuratus n. sp.

a. Holotype, × 2000. Black Mingo Formation, lower Sabinian, depth 160.0 m.

b, c. A specimen showing the granulate ornamentation of the species and the indistinct columellae present at the apertures in some specimens. Beaufort(?) Formation, Midwayan, depth 225.9 m.

d, e. Specimens with scarcely any separation present between the sexine and nexine at the aper-

FIGURE 1.—Continued

tures. Magnification of specimen *e*, × 2000. Midwayan, depth 225.9 m.

f–k. Pseudoplicapollis limitata n. sp.

f. Holotype. Black Mingo Formation, lower Sabinian, 152.4 m.

g. Black Mingo Formation, lower Sabinian, 152.4 m.

h. Black Mingo Formation, lower Sabinian, depth 160.0 m.

i. Beaufort(?) Formation, Midwayan, depth 213.1 m.

j. Detail of aperture structure showing weak columellae in the sexine. Magnification × 2000. Black Mingo Formation, Midwayan, depth 182.9 m.

k. Detail of aperture, columellae appear to be lacking. Magnification × 2000. Black Mingo Formation, lower Sabinian, depth 160.0 m.

l–s. Tricolpites asper n. sp.

l. Holotype showing the shallow, ragged colpi typical of the species. Black Mingo Formation, lower Sabinian, depth 160.0 m.

m. A specimen with slightly deeper colpi and slightly coarser reticulation, transitional to other species of *Tricolpites*. Beaufort(?) Formation, Midwayan, depth 196.0 m.

n–s. Specimens in equatorial view, having very narrow colpi, sometimes bordered by narrow margines. Specimens *n–p*, Black Mingo Formation, lower Sabinian, depth 160.0 m; specimens *q–s*, Beaufort(?) Formation, Midwayan, depth 225.9 m.

t–aa. Tricolpites redactus n. sp.

t. Holotype. Note the shallow colpi and the granulate-microreticulate appearance of the exine in plan view, characteristics of the species. Beaufort(?) Formation, Midwayan, depth 196.0 m.

u. A specimen showing distinct columellae in optical section and folds parallel to the outline. Black Mingo Formation, lower Sabinian, depth 165.5 m.

v, w. A specimen showing columellae and folds parallel to the outline (*v*) and the granulate-microreticulate exine (*w*). Black Mingo Formation, lower Sabinian, depth 165.5 m.

x. A specimen in equatorial view, showing short colpi that lack margines. Magnification × 2000. Beaufort(?) Formation, Midwayan, depth 225.9 m.

y–aa. Specimens magnified × 2000, showing details of apertures and appearance of exine. Specimen *y*, Black Mingo Formation, lower Sabinian, depth 160.0 m; specimen *z*, Beaufort(?) Formation, Midwayan, depth 213.1 m; specimen *aa*, Beaufort(?) Formation, Midwayan, depth 225.9 m.

angular with convex sides. Exine between apertures 1–3 μm thick; sexine:nexine is 2–3:1. Sexine tegillate and indistinctly columellate. Surface smooth; exine appears coarsely granulate to verrucate in plan view. Exopores round, 1–1.5 μm in diameter; endopores, 2–2.5 μm in diameter, or else ragged; irregularly discontinuous nexine may extend across the aperture. Sexine slightly thickened at the pores; slight labra are present. Vestibulum very shallow, may be indistinct, 0.5×4 μm in optical section; indistinct columellae may hang down into the vestibulum.

Holotype.—Figure 1*a*, slide DC–13(4), coordinates 36.9×98.2, Clubhouse Crossroads core at 160.0 m, Black Mingo Formation, lower Sabinian (upper Paleocene).

Remarks.—In this species the sexine and nexine are only slightly separated from each other at the pores (*fissuratus*, Latin for "split"); the coarsely granulate appearance of the exine in plan view is also characteristic. In some respects, the species is intermediate between *Betula infrequens* Stanley 1965 and *Casuarinidites*. *Betula infrequens* has a more distinct labrum and annulus and is less coarsely granulate. *Casuarinidites* is triatriate rather than trivestibulate and is more distinctly columellate.

Occurrence.—"Infrequent" to "common" in four samples from the Midwayan to the lower Sabinian of the Clubhouse Crossroads core (225.9–160.0 m). Possible specimens of this species have been seen in the Clayton Formation or Porters Creek Clay (Midwayan) and Nanafalia Formation (lower Sabinian) of the gulf coast (R. H. Tschudy, written commun., 1977). I have also seen a specimen of *T. fissuratus* in the Tallahatta Formation (lower Claibornian) of Georgia, but it is not clear whether this specimen was reworked or whether the species actually ranges this high in the section.

Genus *PSEUDOPLICAPOLLIS* Krutzsch *in* Góczán and others 1967

Pseudoplicapollis limitata, n. sp.

Figure 1*f–k*

Triatriopollenites sp. Groot and Groot, 1962, p. 166, pl. 30, figs. 11, 12.

Plicapollis sp. Fairchild and Elsik, 1969, pl. 38, fig. 60.

Pseudoplicapollis sp. A. Tschudy, 1975, p. 22–23, pl. 13, figs. 13–17; text fig. 22.

Description.—Size 21–36 μm (25 measured specimens from South Carolina and the gulf coast), mean 26 μm, holotype 21 μm. Oblate; outline triangular with straight to slightly convex sides and narrowly rounded corners. Exine 0.5–1 μm thick between apertures; tegillate and distinctly columellate; nexine thin. Surface of exine slightly rough, granulate to finely verrucate. Plicae usually distinct but narrow, only 2–5 μm wide, with broadly rounded ends near the bases of the apertures; occasionally the plicae are vague or even lack-

ing. Annulus 1–2 μm thick on most specimens, occasionally as much as 3 μm; endosexine coarsely and distinctly to indistinctly columellate at the apertures. A slight labrum is often present. Exogerminal is a lolongate, equatorial slit 0.5–2 μm wide and 2–5 μm deep. Atrium indistinct, endogerminal about 4–9 μm wide, nexine ending approximately at the base of the annulus; or, a deep vestibulum may be present.

Holotype.—Figure 1*f*, slide DC–12(3), coordinates 46.1×97.0, Clubhouse Crossroads core at 152.4 m, Black Mingo Formation, lower Sabinian (upper Paleocene).

Remarks.—This species is characterized by the granulate appearance of the exine, the nearly straight sides, narrow plicae, and thin annulus. The name is derived from the limited stratigraphic range of the species. *Sporopollis elaeagnoides* Zaklinskaya 1963 is larger (35–45 μm) and apparently less distinctly tegillate and columellate.

Occurrence.—"Infrequent" to "occasional" from the middle Midwayan to the top of the Sabinian in the Clubhouse Crossroads core (213.1–125.9 m); the maximum relative frequencies are in the Midwayan. Elsewhere on the Atlantic Coastal Plain, the species occurs in the Brightseat Formation (Midwayan) of Maryland (Groot and Groot, 1962); in the Aquia Formation (lower Sabinian) and the Marlboro Clay Member of the Nanjemoy Formation (lower and upper? Sabinian) of northern Virginia, and as reworked specimens in Neogene strata of Plymouth County and Martha's Vineyard, Mass. On the gulf coast the known range is from the Nanafalia Formation (lowermost Sabinian; Tschudy, 1975) to the Wilcox Formation (upper lower Sabinian; Tschudy, 1975).

Genus *TRICOLPITES* Couper 1953 emend. Potonié 1960

Tricolpites asper n. sp.

Figure 1*l–s*

Tricolpopollenites hians (Stanley 1965). Elsik, 1968, p. 622, 625, pl. 24, figs. 3, 5, 6, 9 only.

Tricolpites n. sp. A (microreticulate). Tschudy, 1973, p. B13, pl. 2, figs. 9, 10 only.

Description.—Length 16–18 μm, diameter in polar view 17–25 μm (14 measured specimens), holotype 19.5 μm. Prolate spheroidal to subprolate. Tricolpate, with short, shallow, colpi 1–1.5 μm wide and 6–10 μm long in equatorial view and gaping, 2–6 μm deep in polar view, edges typically rough, sometimes with dark, presumably thickened margines up to 1 μm wide and (or) with small granules along the edges. In equatorial view, irregular "ora" as much as 4 μm wide may be present in the colpi in optical section. Exine 1.25–1.5 μm thick, consisting of a dark layer overlain by the reticulum; ratio of dark layer to reticulum is 1:1 to 2:3. Both the dark layer and the reticulum thin to about half their normal thicknesses near the colpi, but the size of the lumina does not diminish there. Reticulum clavate in optical section; lumina about 0.25 μm in diameter.

Holotype.—Figure 1*l*, slide DC–13(4), coordinates 29.5 × 93.0, Clubhouse Crossroads core at 160.0 m, Black Mingo Formation, lower Sabinian (upper Paleocene).

Remarks.—This species is distinguished by its short, shallow colpi with rough edges (*asper*, Latin for "rough"). *Tricolpites hians* Stanley 1965 and *T. parvus* Stanley 1965 have deeper colpi with smoother edges. *Platanus* pollen types are larger.

Occurrence.—One of the most abundant species in every sample from the lower Midwayan to the lower Sabinian (225.9–152.5 m); "occasional" occurrence in the upper Sabinian (132.3 m) of the Clubhouse Crossroads core. The species also occurs in the Aquia Formation (lower Sabinian) and the Nanjemoy Formation (upper Sabinian) of northern Virginia, and as reworked specimens in Neogene strata of Plymouth County and Martha's Vineyard, Mass. On the gulf coast, the known range is from the Rockdale Formation (upper lower Sabinian; Elsik, 1968) to the Tallahatta Formation (lower Claibornian; Tschudy, 1973).

Tricolpites redactus n. sp.

Figure 1*t–aa*

Description.—Size 19–25 μm, mean 22 μm (21 measured specimens), holotype 25 μm. Suboblate; outline round to rounded triangular in polar view. Exine 1–1.5 μm thick; sexine distinctly columellate; nexine very thin. Exine sharply and finely granulate to microreticulate; surface minutely rough. Many specimens have a fold completely around the grain just inside the equator and parallel to it. Colpi in equatorial view are short and boat shaped, with pointed ends, to slitlike, measuring about 0.5–1.5 × 4–5 μm; in polar view, the colpi are V-shaped, 2–4.5 μm wide and 1.5–4 μm deep. A very small labrum and (or) annulus may be present, producing a darkened margo about the colpus about 1 μm wide in equatorial view. Apparently no ora are present.

Holotype.—Figure 1*t*, slide DC–17(3), coordinates 53.4 × 100.1, Clubhouse Crossroads core at 196.0 m, Beaufort(?) Formation, Midwayan (lower Paleocene).

Remarks.—*Tricolpites redactus* is characterized by its suboblate shape, strongly convex sides, and shallow colpi (*redactus*, Latin for "reduced").

Occurrence.—"Infrequent" to "common" in every sample from the lower Midwayan to the middle of the lower Sabinian (225.9–160.0 m) of the Clubhouse Crossroads core. The species also occurs as reworked specimens in Neogene strata of Plymouth County, Mass. It has not been reported from the gulf coast.

TABLE 1.—*Locations of specimens illustrated in figure 1*

[Stratigraphic data on the samples are given in the figure explanations. All samples are from the Clubhouse Crossroads core]

Specimen	*Slide*	*Coordinates*
a	DC–13(4)	36.9 × 98.2
b, c	DC–19(4)	58.0 × 107.8
d	DC–19(4)	58.3 × 98.1
e	DC–19(3)	52.5 × 104.9
f	DC–12(3)	46.1 × 97.0
g	DC–12(3)	44.1 × 95.5
h	DC–13(4)	33.4 × 97.0
i	DC–18(4)	34.0 × 99.9
j	DC–16(4)	38.1 × 100.2
k	DC–13(4)	33.5 × 111.3
l	DC–13(4)	29.5 × 93.0
m	DC–17(3)	50.1 × 107.1
n	DC–13(4)	34.0 × 104.3
o	DC–13(4)	28.5 × 93.0
p	DC–13(4)	36.0 × 105.8
q	DC–19(4)	61.8 × 101.4
r, s	DC–19(4)	56.4 × 103.2
t	DC–17(3)	53.4 × 100.1
u	DC–15(5)	45.6 × 105.6
v, w	DC–15(5)	51.0 × 104.0
x	DC–19(3)	52.4 × 95.5
y	DC–13(4)	37.4 × 93.8
z	DC–18(4)	58.5 × 98.9
aa	DC–19(2)	50.7 × 92.6

REFERENCES CITED

[Bybell, L., Christopher, R. A., Frederiksen, N. O., Hazel, J. E., May, F. E., McLean, D. W., Poore, R. Z., Smith, C. C., Sohl, N. F., and Valentine, P. C.], 1976, Unconformities in a South Carolina core, *in* Geological Survey Research 1976: U.S. Geol. Survey Prof. Paper 1000, p. 193–194.

Couper, R. A., 1953, Upper Mesozoic and Cainozoic spores and pollen grains from New Zealand: New Zealand Geol. Survey Paleont. Bull. 22, 77 p.

Elsik, W. C., 1968, Palynology of a Paleocene Rockdale lignite, Milam County, Texas. II. Morphology and taxonomy (end): Pollen et Spores, v. 10, no. 3, p. 599–664.

Fairchild, W. W., and Elsik, W. C., 1969, Characteristic palynomorphs of the Lower Tertiary in the Gulf Coast: Palaeontographica, Abt. B, v. 128, p. 81–89.

Góczán, Ferenc, Groot, J. J., Krutzsch, Wilfried and Pacltová, Blanka, 1967, Die Gattungen des "Stemma Normapolles Pflug, 1953b" (Angiospermae); Neubeschreibungen und Revision europäischer Formen (Oberkreide bis Eozän): Paläont. Abhandlungen, Abt. B, v. 2, no. 3, p. 429–539.

Groot, J. J. and Groot, C. R., 1962, Some plant microfossils from the Brightseat Formation (Paleocene) of Maryland: Palaeontographica, Abt. B, v. 111, pts. 4–6, p. 161–171.

Hazel, J. E., Bybell, L. M., Christopher, R. A., Frederiksen, N. O., May, F. E., McLean, D. W., Poore, R. Z., Smith, C. C., Sohl, N. F., and Valentine, P. C., 1976, Biostratigraphy and paleoenvironmental analysis of a 2500-foot core in Dorchester County, South Carolina [abs.]: Geol. Soc. America Abs. with Programs, v. 8, no. 2, p. 193–194.

Hazel, J. E., Bybell, Laurel, Christopher, R. A., Frederiksen, N. O., May, F. E., McLean, D. W., Poore, R. Z., Smith, C. C., Sohl, N. F., Valentine, P. C., and Witmer, R. J., 1977, Biostratigraphy of the deep corehole (Clubhouse Crossroads corehole 1) near Charleston, South Carolina: U.S. Geol. Survey Prof. Paper 1028–F, p. 71–89.

Potonié, Robert, 1960, Synopsis der Gattungen der Sporae dispersae. III. Teil—Nachträge Sporites, Fortsetzung Pollenites mit Generalregister zu Teil I–III: Geol. Jahrb. Beihefte 39, 189 p.

Stanley, E. A., 1965, Upper Cretaceous and Paleocene plant microfossils and Paleocene dinoflagellates and hystrichosphaerids from northwestern South Dakota: Bulls. Am. Paleontology, v. 49, no. 222, p. 175–384.

Thomson, P. W., and Pflug, Hans, 1953, Pollen und Sporen des mitteleuropäischen Tertiärs: Palaeontographica, Abt. B, v. 94, p. 1–138.

Tschudy, R. H., 1973, Stratigraphic distribution of significant Eocene palynomorphs of the Mississippi embayment: U.S. Geol. Survey Prof. Paper 743–B, 24 p.

Tschudy, R. H., 1975, Normapolles pollen from the Mississippi embayment: U.S. Geol. Survey Prof. Paper 865, 42 p.

Zaklinskaya, E. D., 1963 [Pollen of angiosperms and its significance for the substantiation of the stratigraphy of the Upper Cretaceous and Paleogene]: Akad. Nauk SSSR Geol. Inst. Trudy, v. 74, 256 p. (In Russian.)

CHANGE OF ADDRESS FORM

NAME—FIRST, LAST

COMPANY NAME OR ADDITIONAL ADDRESS LINE

STREET ADDRESS

CITY | STATE | ZIP CODE

PLEASE PRINT OR TYPE

(or) COUNTRY

Mail this form to:

NEW ADDRESS
Journal of Research of the
U.S. Geological Survey
Superintendent of Documents
Government Printing Office SSOM
Washington, DC 20402

Attach last subscription label here.

(please detach here)

SUBSCRIPTION ORDER FORM

SUBSCRIPTION ORDER FORM

Enter my subscription to "Journal of Research of the U.S. Geological Survey" at $18.90 (domestic) or $23.65 (foreign). Domestic remittance should be made by money order or check. Foreign remittance should be made by international money order, draft on an American bank, or UNESCO coupons.

NAME—FIRST, LAST

COMPANY NAME OR ADDITIONAL ADDRESS LINE

STREET ADDRESS

CITY | STATE | ZIP CODE

PLEASE PRINT OR TYPE

(or) COUNTRY

☐ Remittance Enclosed (Make checks payable to Superintendent of Documents)

☐ Charge to my deposit Account No.....

MAIL ORDER FORMS TO:
Superintendent of Documents
Government Printing Office
Washington, DC 20402

ANNOUNCEMENT

DIRECT-MAIL SALES OF USGS OPEN-FILE REPORTS By the U.S. Geological Survey

Purpose of Program

- To furnish microfiche or paper-duplicate copies of open-file reports from a single, centrally located facility.
- To provide faster order-filling service to the public for copies of open-file reports.
- To increase the availability of earth-science information to the scientific community.

Order USGS Open-File Reports From:

Open-File Services Section, Branch of Distribution, U.S. Geological Survey, Box 25425, Federal Center, Denver, CO 80225. (Telephone: 303-234-5888.)

Price information will be published in the monthly listing "New Publications of the Geological Survey."

This facility will stock open-file reports only. Please do not mix orders for open-file reports with orders for any other USGS products. Checks or money orders, in exact amount for open-file reports ordered, should be made payable to U.S. Geological Survey. Prepayment is required.

Order by series and number (such as Open-File Report 77-123) and complete title.

Inquiries concerning this new program should be sent to the address given above.

☆U.S.GOVERNMENT PRINTING OFFICE: 1978--261-198/15

RECENT PUBLICATIONS OF THE U.S. GEOLOGICAL SURVEY

The following books may be ordered from the Branch of Distribution, U.S. Geological Survey, 1200 South Eads Street, Arlington, VA 22202 (an authorized agent of the Superintendent of Documents, Government Printing Office). Prepayment is required. Remittances should be sent by check or money order payable to U.S. Geological Survey. Give series designation and number, such as Bulletin 1368–A, and the full title. Prices of Government publications are subject to change. Increases in costs make it necessary for the Superintendent of Documents to increase the selling prices of many publications offered. As it is not feasible for the Superintendent of Documents to correct the prices manually in all the previous announcements and publications stocked, the prices charged on your order may differ from the prices printed in the announcements and publications.

In addition to the publications mentioned below, other professional papers, water-supply papers, bulletins, circulars, single copies of the periodical "Earthquake Information Bulletin," maps, and items of general interest, such as leaflets, pamphlets, and booklets, are available at the above address. All new Survey publications are listed in a free monthly catalog, "New Publications of the Geological Survey"; to subscribe, send name and address to U.S. Geological Survey, 329 National Center, Reston, VA 22092. (Some reports that are now out of print at the Superintendent of Documents can also be obtained at the Branch of Distribution address.)

Professional Papers

P 641–C. Metamorphic rocks of the Quadrilatero Ferrifero, Minas Gerais, Brazil, by Norman Herz. 1978. p. C1–C81; plate in pocket. $2.75.

P 745. Geology and uranium deposits, Shirley Basin area, Wyoming, by E. N. Harshman. 1972. 82 p. $2.75. (Reprint.)

P 813–M. Summary appraisals of the Nation's ground-water resources—Hawaii region, by K. J. Takasaki. 1978. p. M1–M29. $1.50. (Supersedes Open-File Report 77–825.)

P 849. Carboniferous microfacies, microfossils, and corals, Lisburne Group, Arctic Alaska, by A. K. Armstrong and B. L. Mamet. 1977 (1978). 144 p., 39 plates; additional plates in pocket. $6.50.

P 899. The karst landforms of Puerto Rico, by W. H. Monroe. 1976. 69 p.; plate in pocket. $3.25. (Reprint.)

P 904. The Cenozoic rocks; a discussion to accompany the geologic map of the United States, by P. B. King and H. M. Beikman. 1978. 82 p. $2.75.

P 935–B. Cooling and vesiculation of Alae lava lake, Hawaii, by D. L. Peck. 1978. 59 p. $2.50.

P 993. Historic ground failures in northern California triggered by earthquakes, by T. L. Youd and S. N. Hoose. 1978. 177 p.; plates in pocket. $5.25.

P 1003. Effects of urbanization on streamflow and sediment transport in the Rock Creek and Anacostia River basins, Montgomery County, Maryland, 1962–74, by T. H. Yorke and W. J. Herb. 1978. 71 p.; plates in pocket. $2.50.

P 1029. Hydraulic geometry of river cross sections—theory of minimum variance, by G. P. Williams. 1978. 47 p. $2.30.

P 1045. Computer-aided estimates of concentrating-grade iron resources in the Negaunee iron-formation, Marquette district, Michigan, by W. F. Cannon, S. L. Powers, and N. A. Wright. 1978. 21 p. $1.30.

P 1050. Geological Survey research 1977. 1977 (1978). 411 p. $6.

P 1054–A. Hydrothermal alteration and self-sealing in Y–7 and Y–8 drill holes in northern part of Upper Geyser Basin, Yellowstone National Park, Wyoming, by T. E. C. Keith, D. E. White, and M. H. Beeson. 1978. p. A1–A26. $1.40.

Bulletins

B 1131. Geology and mineral deposits of the Turtle Lake quadrangle, Washington, by G. E. Becraft and P. L. Weis. 1963. 73 p.; plates in pocket. $3.50 (Reprint.)

B 1448. Geology of the Juazohn quadrangle, Liberia, by R. G. Tysdal. 1978. 39 p. $1.60.

B 1452. Thermodynamic properties of minerals and related substances at 298.15 K and 1 bar (10^5 pascals) pressure and at higher temperatures, by R. A. Robie, B. S. Hemingway, and J. R. Fisher. 1978. 456 p. $4.75.

Water Supply Papers

W 1849. Roughness characteristics of natural channels, by H. H. Barnes, Jr. 1967. 213 p. $6.25. (Reprint.)

W 2046. Calibration of a mathematical model of the Antelope Valley ground-water basin, California, by T. J. Durbin. 1978. 51 p.; plates in pocket. $7.25. (Supersedes Open-File Report 76–833.)

W 2051. Relation of urban land-use and land-surface characteristics to quantity and quality of storm runoff in two basins in California, by M. A. Sylvester and W. M. Brown III. 1978. 49 p. $2. (Supersedes Open-File Report 77–288.)

W 2053. Evaporation and radiation measurements at Salton Sea, California, by A. M. Sturrock, Jr. 1978. 26 p. $1.30. Supersedes Open-File Report 77–74.)

W 2055. Stress and recovery of aquatic organisms as related to highway construction along Turtle Creek, Boone County, West Virginia, by J. L. Chisholm and S. C. Downs. 1978. 40 p. $1.60.

U.S. GOVERNMENT
PRINTING OFFICE
PUBLIC DOCUMENTS DEPARTMENT
WASHINGTON, D C 20402
OFFICIAL BUSINESS
PENALTY FOR PRIVATE USE $300

FOURTH-CLASS MAIL
POSTAGE & FEES PAID
USGS
PERMIT No. G23

BR OF PLANNING
OFFICE OF PLANS & PLANS DEV
USGS NATL CENTER STOP 512
RESTON VA 22092